The northern piedmont of Tian Shan : a case study of immature range front

Ke Chen

ÉCOLE DOCTORALE SCIENCES ET TECHNOLOGIE

INSTITUT DES SCIENCES DE LA TERRE D'ORLEANS
INSTITUE OF GEOLOGY AND GEOPHYSICS (CAS)

THÈSE EN COTUTELLE INTERNATIONALE présentée par :

Ke CHEN

soutenue le 1er décembre 2010
pour obtenir le grade de :

Docteur de l'Université d'Orléans
et de l'Institute of Geology and Geophysics
Discipline : Sciences de la Terre et de l'Univers

LE PIÉDMONT NORD DU TIAN SHAN : CAS D'ÉCOLE D'UN FRONT DE CHAÎNE IMMATURE

THÈSE dirigée par :

M. Yan CHEN	Professeur, ISTO, Université d'Orléans-CNRS, France
M. Qingchen WANG	Professeur, IGG, CAS, Chine

RAPPORTEURS :

M. Marc JOLIVET	CR, CNRS, Géosciences Rennes, France
M. Bihong FU	Professeur, KLEDI, CAS, Chine

JURY :

M. Romain AUGIER	MCF, ISTO, Université d'Orléans-CNRS, France
M. Bihong FU	Professeur, KLEDI, CAS, Chine
M. Charles GUMIAUX	MCF, ISTO, Université d'Orléans-CNRS, France
M. Marc JOLIVET	CR, CNRS, Géosciences Rennes, France
M. Wei LIN	Professeur, IGG, CAS, Chine
M. Guillaume MARTELET	Ingénieur, BRGM, Orléans, France
M. Qingchen WANG	Professeur, IGG, CAS, Chine
M. Rixiang ZHU	Professeur, IGG, CAS, Chine

INVITÉ :

M. Yan CHEN	Professeur, ISTO, Université d'Orléans-CNRS, France
M. Julien CHARREAU	MCF, INPL, CRPG, France

Table of contents

Chapter 1

Intracontinental orogens

1.1 Basic concepts of intracontinental orogen

The term “orogeny” appeared in the middle of the 19th century. It refers to forces and events leading to build mountains on continents. Its meaning and content have been developed with the whole geosciences, and constantly formed new hotspots and new arguments. During 1857-1960s, most geologists took the orogenesis as the results of the closure of geosynclines (Schuchert. 1925). After that, in early 1960s, it was considered as the results of subduction and collision at the margin of plates, associated with the development of the “Plate tectonics” (Dewey and Bird, 1970; Sengör，1991). The orogenesis is often related to the subduction and collision of plates in the marginal area to form the intercontinental orogeny. However, the rigid plate characteristic was challenged by extensive deformation in plates interior (Molnar, 1988). Simply stated, interaction at plate boundaries could produce deformation, magmatic activity, and metamorphism for a considerable distance from those boundaries (Molnar, 1975; Tapponnier, 1979). For example, the Atlas in Morocco, northern Africa, the Pyrenees between France and Spain, in southwest of Europe, Canadian Rocky mountain, located in the America.

A wide variety of tectonic models have been suggested to explain the intracontinental orogeny. These models assume that much of the contemporary tectonic activity is controlled by pre-existing geological features. The crustal homogeneities serve to localize in a passive manner the deformation resulting from stresses generated by a variety of tectonic forces. These forces may be and probably are completely alien to those initially responsible for the features, and, therefore, these models are grouped under the general term “resurgent tectonics” (Hinze et al., 1990; Figure 1-1).

(1) *Crustal Rifting.* Rifting of the continental crust and its commonly associated igneous events are a major source of large-scale crustal disturbance and are therefore particularly susceptible to resurgent tectonics. It has become increasingly clear that rifting of the crust has played a major role in the geological history of central North

America and the Pyrenees.

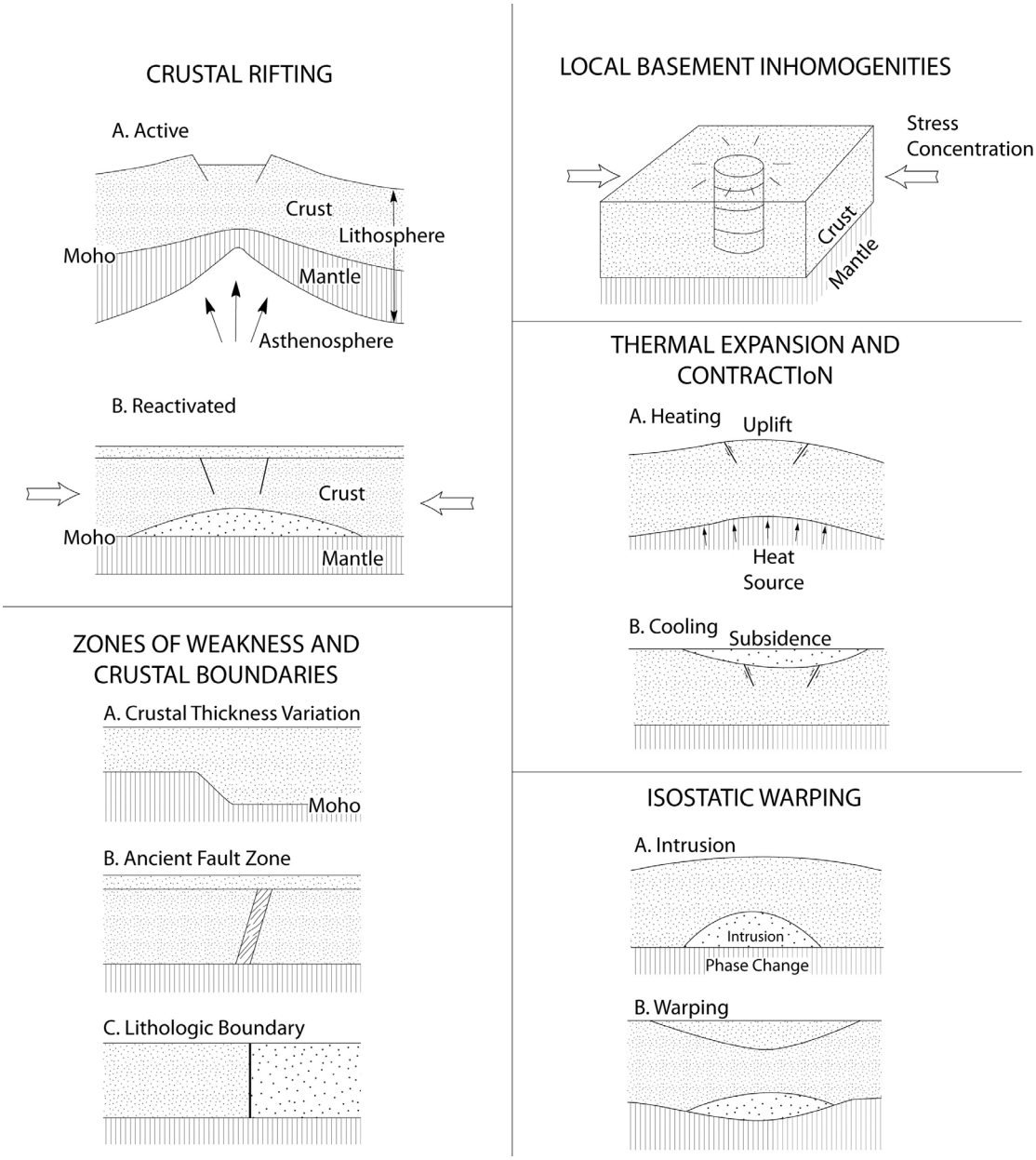

Figure 1-1. *Some possible mechanical models for the intraplate orogen (Hinze et al., 1990).*

(2) *Zones of weakness and crustal boundaries.* Old zones of weakness are widespread in many plates, such as crustal thickness variation, ancient fault zone or lithologic boundary. They may have significant influences on subsequent structural development.

(3) *Local basement heterogeneities.* Mafic or ultramafic intrusive bodies which are probable sources of major gravity and magnetic anomalies have been suggested to

be some influence of the intraplate orogeny.

(4) *Thermal expansion and contraction.* Thermally induced forces are generally recognized as an origin of stress within the earth. A major method of translating thermal energy into stress is by thermal expansion and contraction. Thus, it is to be expected that this mechanism could be used to explain the geodynamics of plate interiors. It could be the results of igneous intrusions or the mantle penetrative convection.

(5) *Isostatic warping.* Regional variations in loading or unloading of the crust cause isostatic deviations, leading to crustal warping and the possibility of relatd crustal rupture and earthquake activity.

1.2 Some examples of intracontinental orogens

An early hypothesis of plate tectonics was that plates moved as rigid pieces of lithosphere and that the relative motion between plates was taken up at narrow zones along their boundaries. However, intraplate deformation is universal in the world. For example, the Atlas in Morocco, northern Africa; the Pyrenees between France and Spain, in southwest of Europe; Canadian Rocky mountain, located in the America.

(a) Atlas

The High Atlas and part of the Middle Atlas correspond to an intracontinental mountainous system that developed on a former set of WSW–ENE and NE–SW striking Mesozoic grabens.

These grabens were approximately initiated contemporaneously with the Trias to Lias rifting (Laville et al., 2004) that led to the opening of the Atlantic and Tethys Oceans. This graben-related thinned crust appears then to have behaved as a weakened lithosphere that has subsequently localized the compressional deformations during the Cenozoic inversion resulting from the Africa–Eurasia convergence. The major High Atlas inversion occurred during Neogene and Quaternary and developed a

bi-vergent mountain chain (Jacobshagen et al., 1988; Gomez et al., 2000; Teixell et al, 2003; Sébrier et al., 2004).

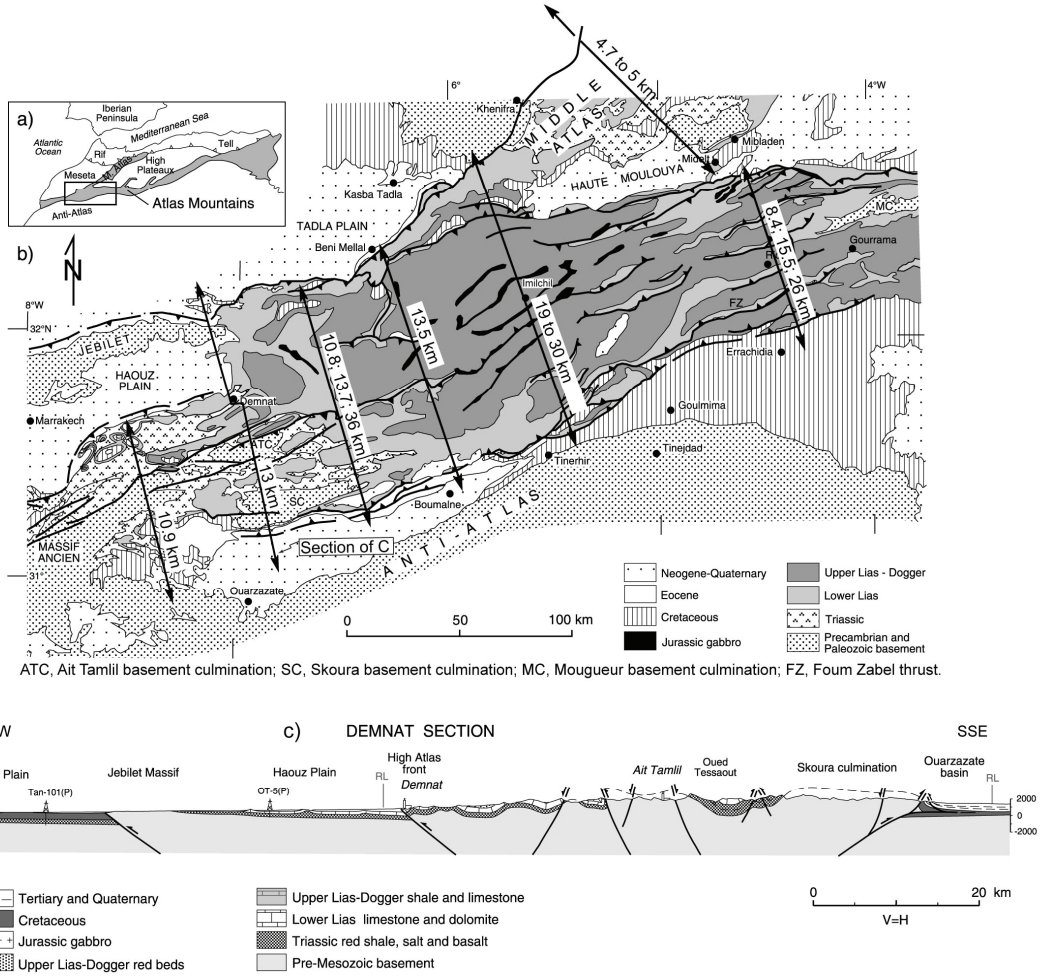

ATC, Ait Tamlil basement culmination; SC, Skoura basement culmination; MC, Mougueur basement culmination; FZ, Foum Zabel thrust.

Figure 1-2. *(a) Location sketch map of the Atlas Mountains in the North African foreland. (b) Geological map of the central High Atlas. (c) Geological cross sections through the High Atlas of Morocco (location in Figure b) (Modified after Teixell et al., 2003; Missenard 2006).*

In the core of the chain, the basement uplift is triggered by a fan of steep reverse faults, most of which are inherited from Triassic-Liassic rifting. Deformation propagated to the proximal basins by four different décollement levels (Missenard et al., 2007). The Shortening in the High Atlas, which is mainly localized on its southern and northern border faults, is overall small and ranges between 10 and 25% (Figure 1-2) (Teixell et al., 2003; Missenard 2006). The deformation style varies laterally along the two northern and southern fronts, which caused by the competition of

different rocks, the thickness of Mes-Cenozoic sediments and the inherited structures (Missenard et al., 2007). However, section restoration indicates that shortening decreases along strike from east to west in the High Atlas (Fig 1-1a), while topographic elevation generally increases. This inverse correlation suggests that crustal thickening does not fully explain the observed topography and suggests a mantle contribution to uplift (Teixell et al., 2003).

(b) Pyrenees

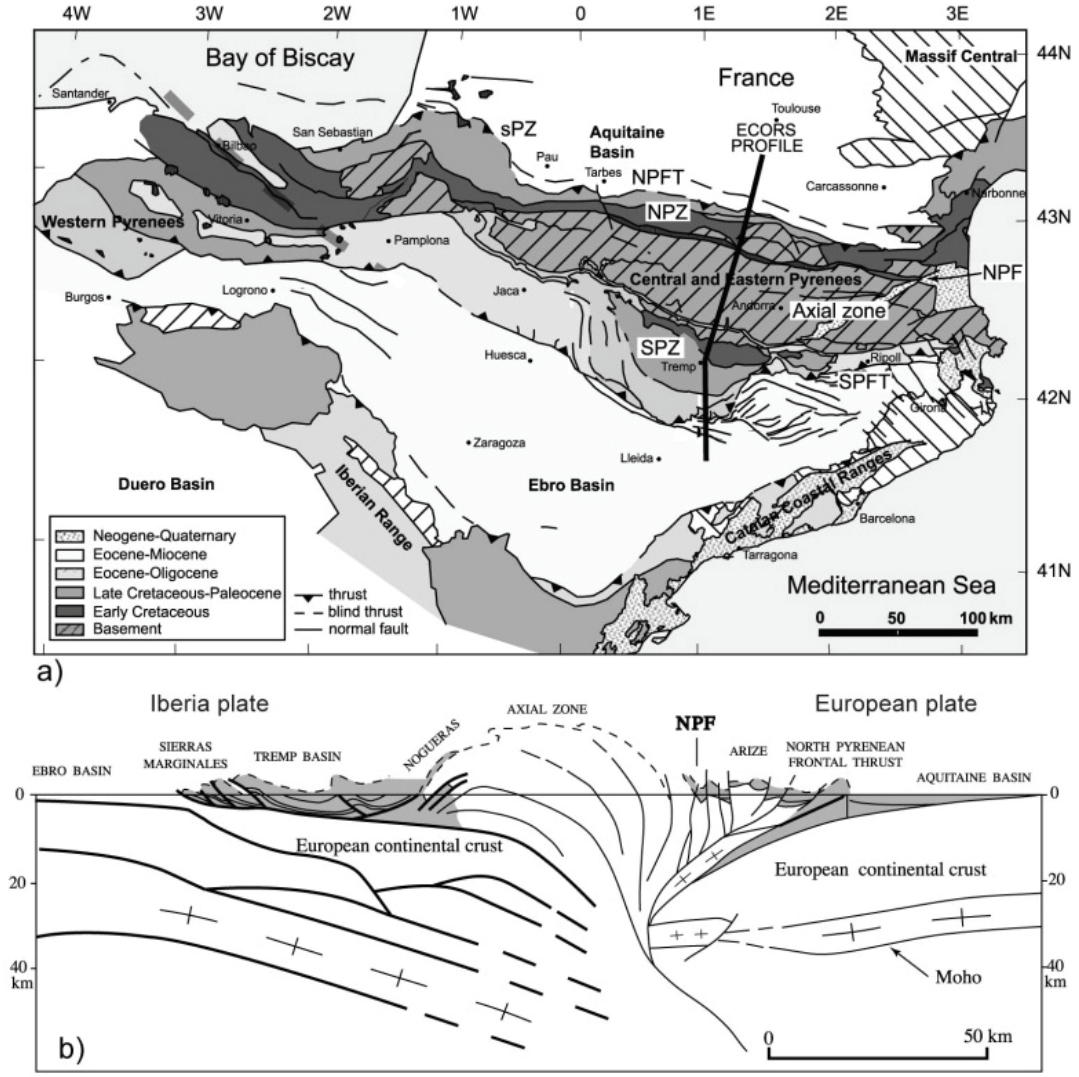

Figure 1-3. *(a) Structural map of the Pyrenees and its main tectonic units (Sibuet et al., 2004). Also shown are the locations of the ECORS (Choukroune and ECORS Team, 1989) deep seismic reflection profiles. NPF, north Pyrenean fault; NPFT, north*

Pyrenean frontal thrust; NPZ, north Pyrenean zone; SPFT, south Pyrenean frontal thrust; SPZ, south Pyrenean units; sPZ, sub-Pyrenean zone. (b) Interpretation (on depth section) without vertical exaggeration based on the ECORS profile (Roure et al., 1989; Sibuet et al., 2004).

The Pyrenees is a 400-km-long but relatively narrow (~150 km) trending fold belt located between France (part of European plate) in the north and Spain (part of Iberia plate) in the south (Figure 1-3). It formed in Late Cretaceous–Eocene times in response to the collision between the European plate and the Iberian-Sardinian-Corsican block (Arthaud and Séguret, 1981; Choukroune et al., 1989). The deep seismic ECORS (Etude Continentale et Océanique par Réflexion et réfraction Sismique) profile suggests that Iberia plate subducted beneath the Europeen plate (Roure et al., 1989). Above, the chain interior is composed by an antiform of Variscan basement and the thrust propagate to the foreland basins, Aquitaine basin to the north and Ebro basin to the south. The amount of shortening cross the total Pyrenees is considered in the order of 100 to 150 km (Déramond et al., 1985; Roure et al., 1989; Specht, 1989; Muñoz, 1992).

(c) Rocky Mountain

The Rocky Mountains stretch more than 4800 km from the northernmost part of British Columbia, in western Canada, to New Mexico, in the southwestern United States. They were formed in the late Cretaceous, by the Laramide orogeny (English et al., 2004). The structural styles are very diverse along the front of the Rcoky Mountains (Erslev et al., 2004). In the southern part, located in USA, the high-angle dipping basin-bounding faults separate the core basement and adjacent basins (Figure 1-4a). The basement-cored uplift by these reverses faults, caused by intraplate compression. In contrast, the Canadian Rocky Mountains display asymmetry structures, with much uplifted Paleozoic basement in the western and less uplifted with cretaceous sedimentary in the east. The crust-scale thrusts propagate up to upper

crust by a ramp, forming a décollement in the base of sediments (Figure 1-4b). Delaminations with up-concave thrusts were indicated by seismic profiles and drilled wells (Debelmas et al., 2008).

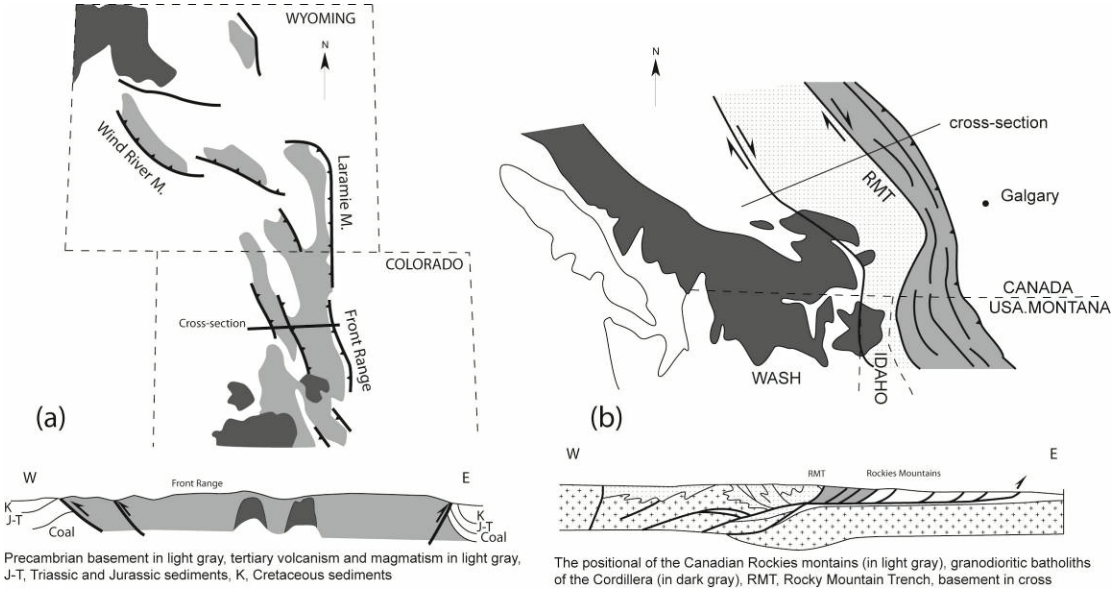

Figure 1-4. *(a) Simplified geological map of the rocky mountain in USA and the geological cross-section traverse the mountain. (b) Canadian Rocky Mountains with cross-section (After Debelmas et al., 2008).*

There are some characteristics of the chains intracontinental as presented above. First, they reactive in the weak place of lithosphere, where may be the ancient suture or rifts. For example, the Pyrenees and the Atlas were built by the inverted structural in the ancient rifts. Second, the driving force probably is the far-effect of the plate margin, e.g. subduction and collision. The objective of above brief introductions is to compare attributes of different kinds of intraplate mountains with the Tian Shan Mountain, which will be described in the following (Discussion see chapter 6).

1.3 Deformation in fold-and-thrust belts

As discussed above, Fold-and-thrust belt is one of the characteristic in the fronts of almost of the compressional orogens, also in these intracontinental orogens. They are commonly strongly deformed and the key to understand the characteristics and evolutions of the intracontinental orogens. Here, the discussion of crustal deformation

was limited to the surface scale (~15 km in depth) deformation in the fold-and-thrust belts. Therefore, the mainly deformation types in this area are of faults and folds. Many studies in thrust belts have shown that most folds are ultimately generated by fault movement at depth (Rich, 1943; Dahlstrom, 1969; Fail, 1973; Dahlstrom, 1990). Thus, we can use the geometry of an exposed fold to infer the position and geometry of a fault at depth. The kink-like character of folds in thrust belts can be generalized in cross-section construction by used of the "kink-fold" method developed in the early 1980s by Suppe (1983). This method assumes that the folds are produced by a flexure-slip mechanism so that bed thickness does not change, and the footwall remains undeformed during the formation of folds in the hanging wall. There are several kinds of structures as described below.

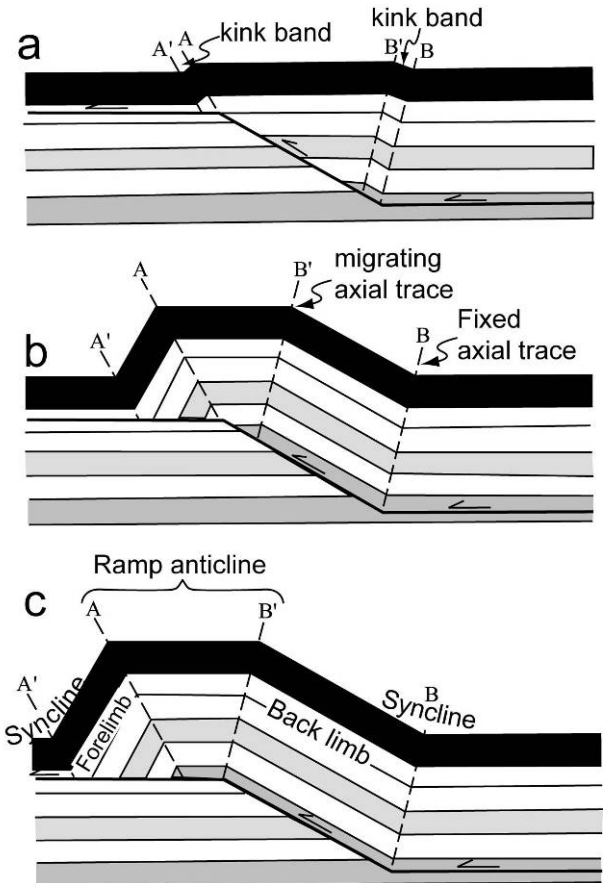

Figure 1-5. *Progressive development of a fault-bend fold as the thrust sheet moves over a ramp in a decollement (after Suppe, 1983). Letters A, A', B, and B' denote the axial traces.*

(a) Fault-bend folds

Fault-bend folds occur where a thrust fault steps up from a structurally lower flat to a higher flat. Two kink bands form in the hanging wall, one above the base of the ramp, and the other above the top of the ramp (Figure 1-5a). With continued slip on the fault, these two kink bands grow in width (Figure 1-5b). As the truncated hanging wall moves up the ramp, and the two kink bands widen, an anticline forms at the top of the ramp. This anticline terminates downward into the upper flat (Figure 1-5b and c).

(b) Fault-propagation folds

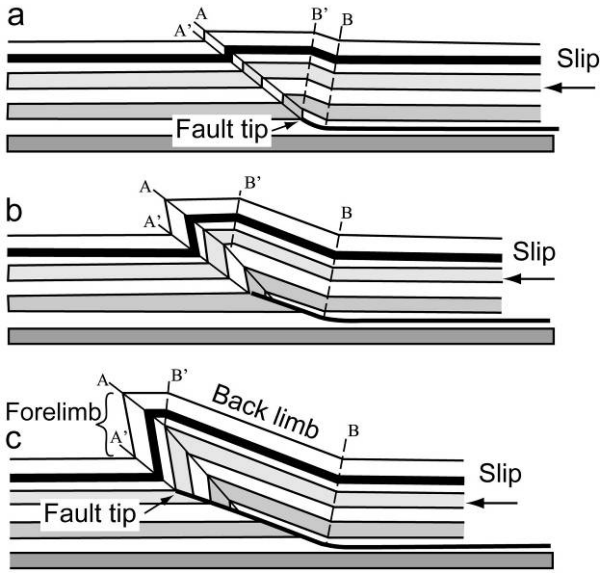

Figure 1-6. *Progressive development of a fault-propagation fold at the tip of a thrust, as the thrust sheet moves over a ramp in a decollement (after Supper, 1983). Letters A, A', B and B' denote the axial surfaces. Note that the fault tip coincides with the hinge of an asymmetric syncline.*

Fault-propagation folding occurs when a propagating thrust fault loses slip and terminates upsection by transferring its shortening to a fold developing at its tip (Mitra, 1990; Figure 1-6). This model is developed by Suppe and Medwedeff (1990), keeping the constant thickness and fixed axis fault propagation folding. However, several other modes are built: trishear folding (Erslev, 1991; Hardy and Ford, 1997; Allmendinger, 1998); and basement-involved (triple junction) folding (Narr and Suppe, 1994).

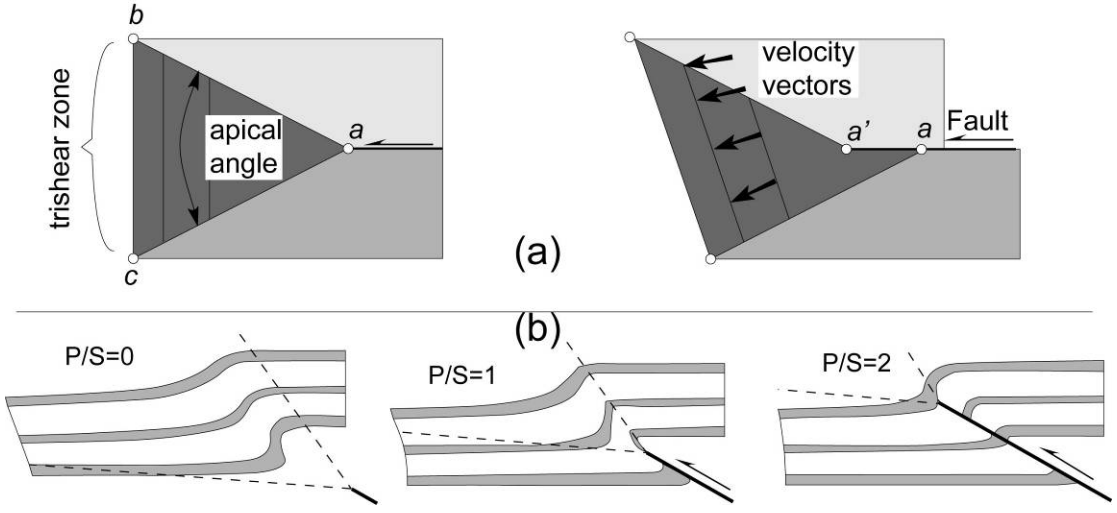

Figure 1-7. *(a) The geometry of trishearing (after Shaw et al., 2003). The dark area (a-b-c) indicates trishear zone. (b) Influence of propagation/ slip ratio on fold configuration (after Shaw et al., 2003; Allmendinger, 2004).*

Trishear folds form by distributed shear within a triangular (trishear) zone that expands outward from a fault tip (Erslev, 1991; Figure 1-7 a). Folds develop in the trishear zone, the bed thickness or lengths are not preserved during deformation. The geometry of the structure is a function of the apical angle, the fault dip, and the fault propagation to slip (P/S) ration (Figure 1-7 b).

Narr and Suppe (1994) proposed another kinematic theory: fault-fault-fold triple junction, in which fold growth is governed by the migration of fault-fold triple junction (Figure 1-8). The main monocline in the stratified cover forms as a drape fold over a triple junction in the basement. The development stages are composed by: i) layer-parallel shortening in the early time and ii) extension in the cover sequence later.

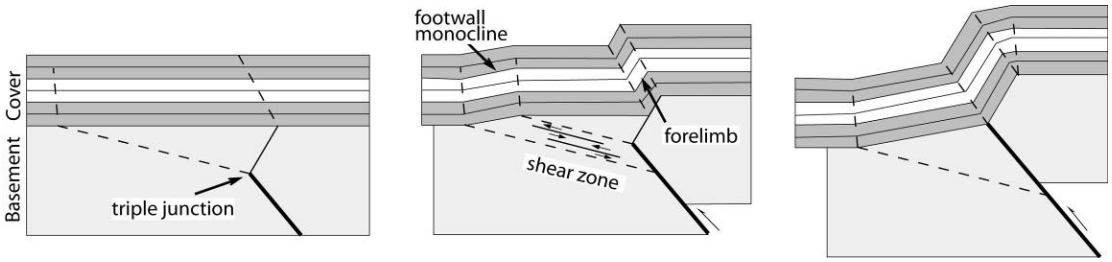

Figure 1-8. *The evolution stages of basement-involved model (after Shaw et al., 2003).*

Forced-folding has also been proposed as the mechanism for some of these structures (Johnson and Johnson, 2002). Forced folding defined by Stearns (1978) as 'folding in which the final overall shape and trend of the fold are dominated by the shape of some forcing member below'. This is different from the normal buckle folds by layer-parallel compression. The essential features of the mechanism are a sedimentary cover deformed more or less passively and the rigid basement blocks that are displaced along planar or listic faults. The main deformation mechanism is 'bending', defined as the flexuring of a layer or surface by a compression at a high angle to the layering. However, many folds in nature will compose components of compression both parallel to (viz. bulking) and normal to the layering (viz. bending) (Mohammed and Ameen, 2000).

(c) Detachment folds

Detachment folds form when a thrust fault contines to displace above a bedding-parallel detachment and transferred into folding of the hanging wall layers. They are different from fault-bend and fault-propagation folds, because they are not directly related to thrust ramps but rather to distributed deformation above detachments. In the core of fold, an incompetent and ductile basal unit is thickened. Growth units, if present, will thin onto the fold crest and exhibit a fanning of limb dips (Shaw et al., 2003). They generally occur above a good detachment such as the gyps or coal. Poblet et al., (1997) proposed three kinematic models to account for the geometry and kinematics of detachment folds involving a homogeneous competent layer detached over a ductile unite: 1) variable limb dip-constant limb length, 2) constant limb dip-variable limb length, and 3) variable limb dip- variable limb length (Figure 1-9).

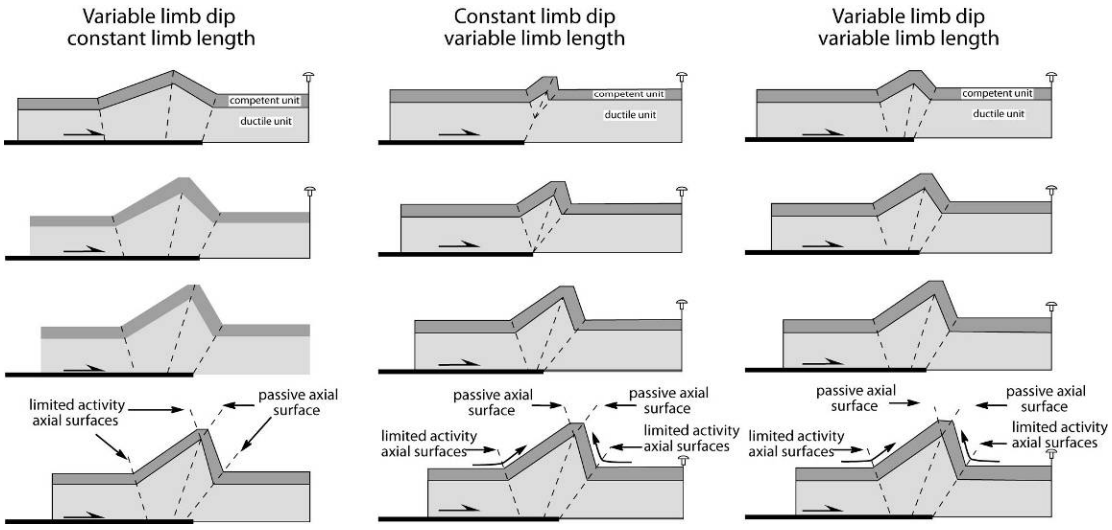

Figure 1-9. *Three different models for asymmetric kink detachment folds. A homogeneous competent layer has preserved the length and the ductile unite shorted in the core of the anticline (after Shaw et al., 2003).*

(d) Shear fault-bend folds

Shear fault-bend folds are similar with the normal fault-bend folding, but it is distinguished by a long back-limb that dips less than the fault ramp (Figure 1-10). It was developed by Suppe et al., (2004), reflecting the significant non-flexural slip component to the deformation. This structure is also characteristic by a significant stratigraphic section covered the back limb during fold growth, moreover the front limbs are quite narrow relative to their long back limbs.

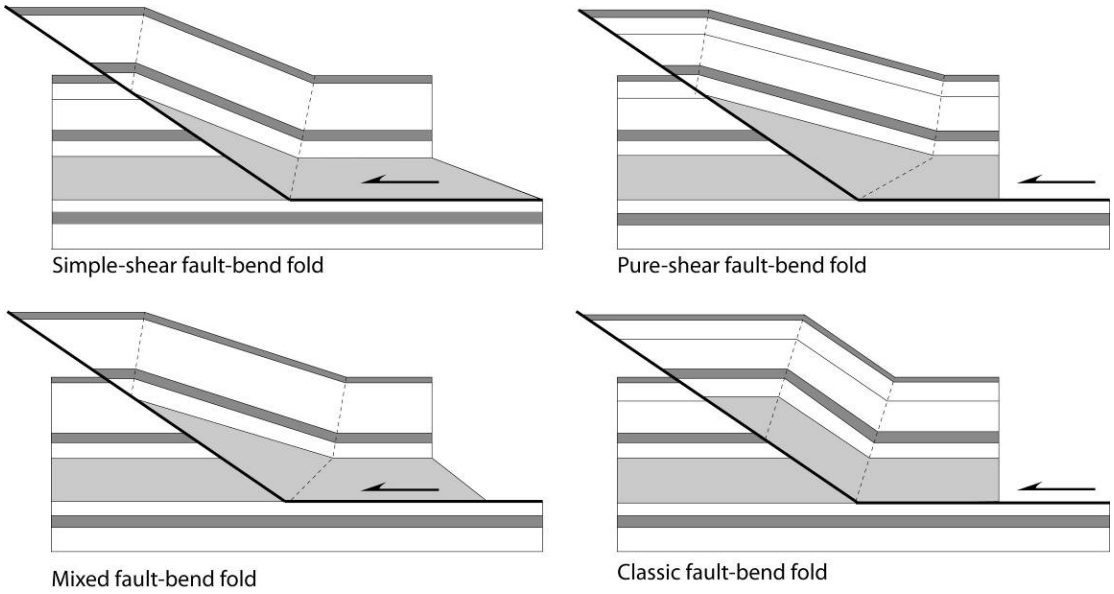

Figure 1-10. *The models of shear fault-bend folds, two end-member of simple-shear and pure-shear, mixed model of the two end-member above, the classic normal fault-bend fold (after supper et al., 2004).*

Two end-member theories are used to explain the structure, simple-shear and pure-shear (Figure 1-10). In the simple-shear member, the décollement layer undergoes bedding-parallel simple shear with no actual basal fault, just a distributed zone of shear. In the contrast of the pure-shear member, the décollement layer slides above a basal fault and shortens and thickens in a triangular area above the ramp. The mixtures between these are possible as well, shown in Figure 1-10. The model becomes to classic fault-bend fold when the ductile unite (gray light) is competent with thickness preserved.

(e) Imbricate structures

When thrust structure is characterized by the stacking of two or more thrust sheets, they are referred as the imbricate fault-bend folds. Two types of this structure are proposed, the break-forward propagation and break-backward thrusting, or with coeval motion on both deep and shallow faults (Shaw et al., 1999; Figure 1-11).

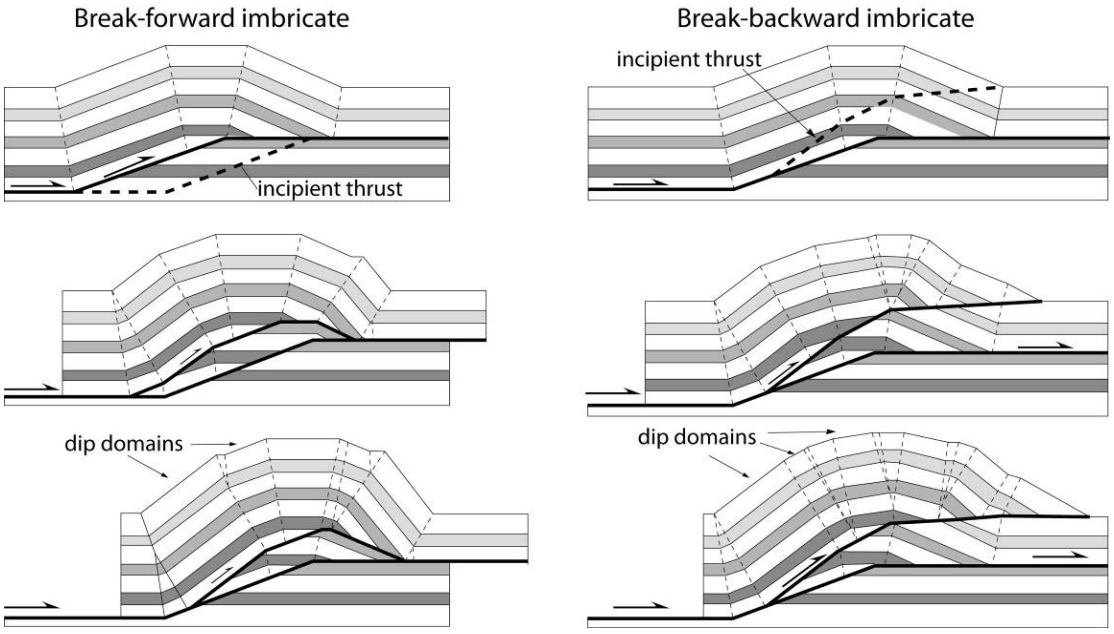

Figure 1-11. *The evolution models of break-forward imbricate and break-backward imbricate fault-bend folds (after Shaw et al., 2003).*

(f) Structural wedges

Structural wedges could occur at a variety of scales. It is often associated with mountain fronts in large scale or decameter fault and fold belt in small scale. Here, we limited the structural in the hectometer geological sections. Structural wedges composed by two connected fault segments that bound a triangular fault block. Folding developed in the wedge zone pin to the wedge tip (shaw et al., 2003; Figure 1-12).

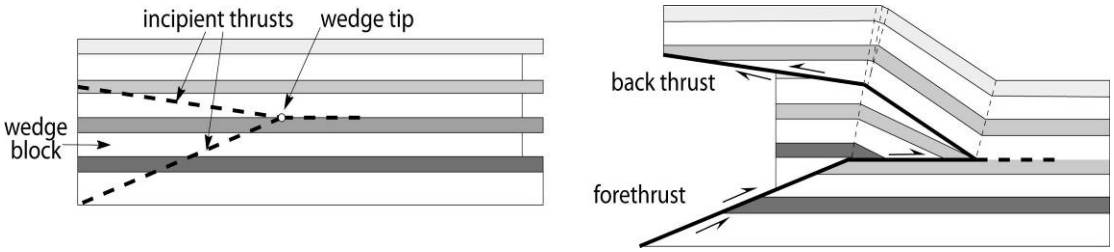

Figure 1-12. *The structural wedges contain two faults, forethrust and back thrust.*

(g) interference structures

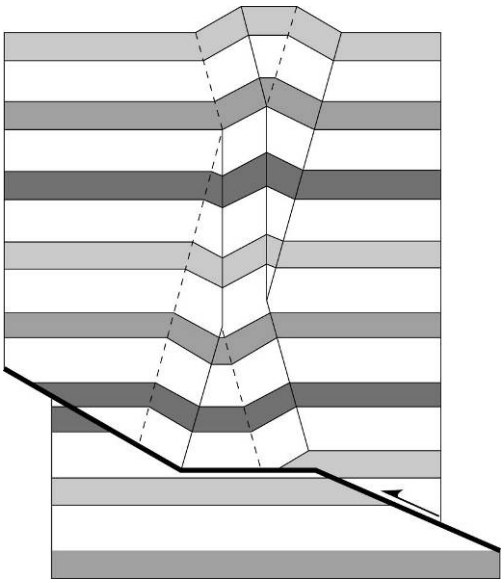

Figure 1-13. *Interference structures by two bends above a bended fault (Shaw et al. 2003).*

Interference structures have been studied since several decades (e.g. Dewey, 1965; Paterson and Weiss, 1966; Stewart and Alvarez, 1991) and they are considered as the origin of structure in seismic profiles interpretations (e.g. Novoa et al., 1998; Shaw et al., 2003).

Interference structure refers a typical geometry when two or more monoclinal kink bands intersect and yied distinctive paterns in cross section with anticlines perched above synclines (Shaw et al., 2003). Interference structure can induce complex structures, which sometimes are difficult to explain. Here we present a simple example, interfering developed above two bends in the same fault (Figure 1-13).

In a summary, these structures could help us to understand the geometry in depth and the deformation processes. However, it is worthy to notice that these models are based on two basic assumptions. First, folds are produced by a flexure-slip mechanism so that bed thickness is constant. Second, the footwall remains undeformed during the formation of folds in the hanging wall. Moreover, the deformation in fold-and-thrust belts is always complex and affected by variety kinds of factors. It forces us to analysis local structure with considering every local

characteristic and obtain as much as data in depth, such as seismic profiles and drilled wells.

Chapter 2

Geological setting and history of Tian Shan

2.1 Cenozoic tectonics in Asia

Asia constitutes two broad Cenozoic deformation zones: the India-Asia collision zone in the east and the Arabia-Asia collision zone in the west (Yin et al., 2010).

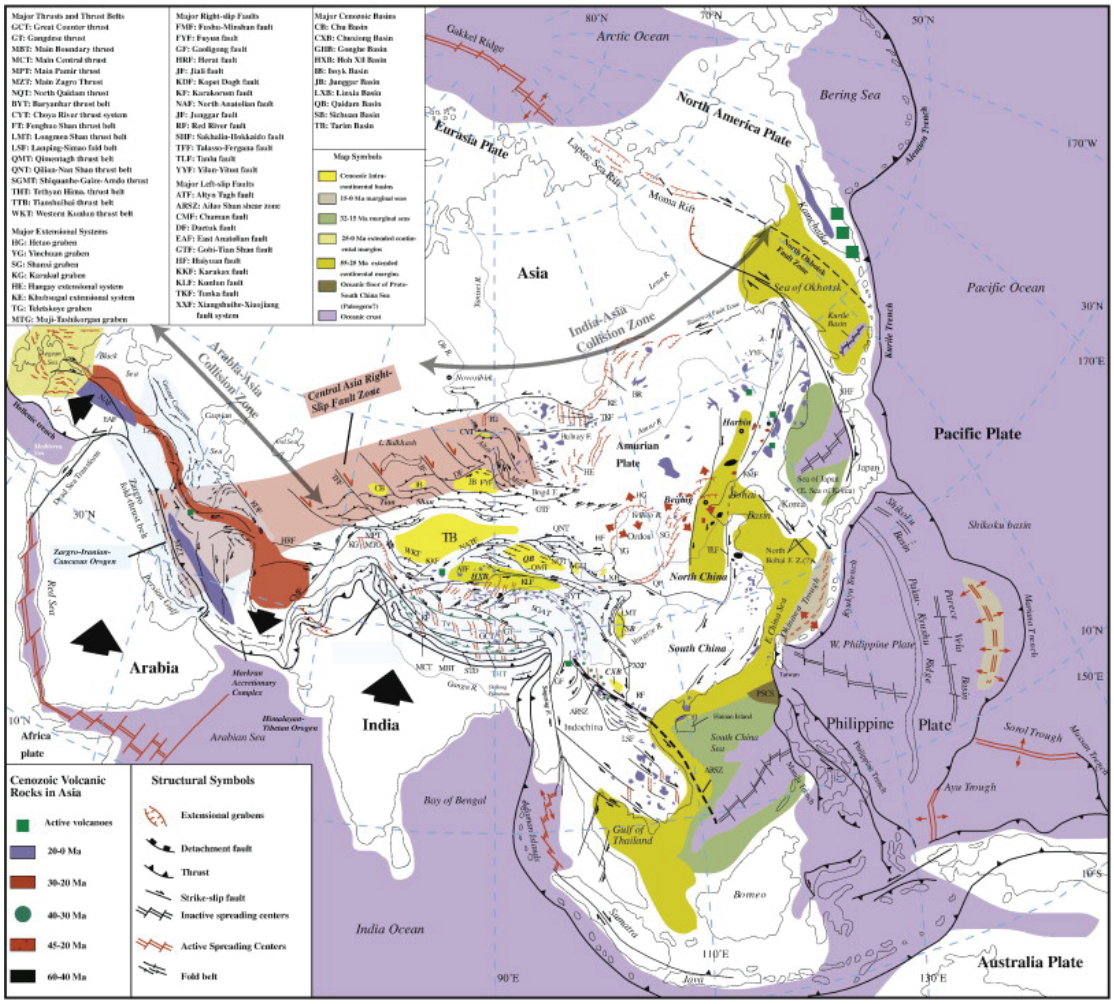

Figure 2-1. *Cenozoic structures and distribution of volcanic rocks (Yin et al., 2010).*

The India-Asia collision zone consists of the following major tectonic domains: 1) the Himalayan orogen, 2) the Tibetan Plateau, 3) the southeast Asia extrusion system, 4) the Central Asia deformation domain stretching from the Tian Shan in the south to the Baikal rift zone in the North, 5) the North China deformation domain, and 6) the eastern Asia margin deformation domain extending from the eastern continental margin of Asia to the western Pacific trench system in the E-W direction and from the Sea of Okhotsk in the north to South China Sea in the south in the N-S direction (Yin et al., 2010; Figure 2-1). The Arabia-Asia collision zone will not be discussed here in

details.

2.1.1 The collision of the India-Asia

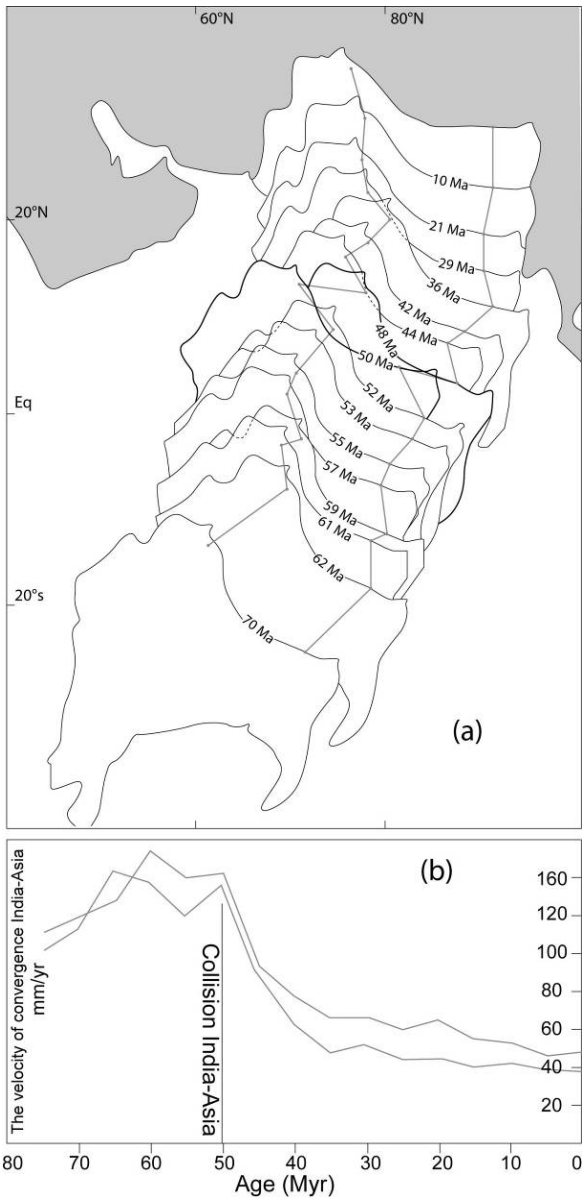

Figure 2-2. *(a) Cenozoic northward drift of India, relative motion of India with respect to Eurasia, kept arbitrarily fixed in its present position. The two traces indicate two points located on the Indian continent near the northern margin. Black-bold outlines indicate the initiation of India-Asia collision. (b) The velocity of the two points above move toward the Asia plate. India-Asia collision time was suggested by the sudden decrease (~ 50 Ma) (Patriat and Achache, 1984; Avouac and DeWver, 2002).*

The most recent dramatic structure in the earth is the development of the Tibetan plateau resulting from the India-Asia collision, which is firstly documented by paleomagnetic study of Patriat and Achache. (1984; Figure 2-2). The Himalya belt isolates the Indian subcontinent from the rest of Eurasia, with the world's highest mountain Mount Everest (8844.43 meter in altitude). It is among the youngest mountains of the world, and it is still undergoing structural changes and growing (Sorkhabi, 2003).

However, the onset age of collision India-Asia is still in debates. Stratigraphic research suggested that the western part of Himalayan region the collision age is well constrained as starting in the Late Ypresian (~ <52 Ma). However, the most eastern sections are younger than Lutetian (< 48 Ma) (Rowley, 1996).

Yet, Beck et al. (1995) report that accretionary-prism and trench strata were first thrust onto the northwest Indian passive margin after 66 Myr but before 55.5 Myr, and suggest that suturing was complete by 49 Myr. Yin and Harrison. (2000) reviewed the stratigraphic, paleontologic evidences and age of the Gangdest batholiths, suggesting that the initial collision between India and Asia could have stated as early as the latest Cretaceous time (~ 70 Ma). However, Aitchison et al., (2007) recently suggested by stratigraphic study that the India-Asia collision did not start until about 35 Ma, which is not consistent with most of the geologic observations (Garzanti, 2007).

Though, the exact onset age of the collision remains debated and as it is out of scope of this study, most acceptable range from 65 Ma to ~ 50 Ma (e.g., Rowley, 1996, 1998; Najman et al., 2001; Zhu et al., 2005; Yin, 2010) is referred in this dissertation. Regardless of this uncertainty, the deformation review on the Cenozoic will discussed below.

2.1.2 The deformation by the India-Asia collision

The India-Eurasia collision caused a high stress to be transmitted over a broad area (Molnar et al., 1973). Two end member models of how the high elevations in Tibet formed are (i) continuous thickening and widespread viscous flow of the crust

and the mantle of the entire plateau and (ii) time-dependent, localized shear between coherent lithospheric blocks (Tapponnier et al., 1982).

The crustal shortening amount due to the India-Asia collision is mainly controlled by the paleomagnetic studies. Besse et al. (1984) reported that order of 550 km and 400 km convergence amounts were found in suture and intracontinental thrusting respectively between the major Himalayan thrusts and the india-Tibet suture zone. Chen et al. (1993) estimated ~ 2700 km of crustal shortening between India and Siberia and documented that the Tibetan plateau has probably experienced the internal deformation of different scales from 1 to 1000 km. Pozzi and Feinberg. (1991) proposed that the post-collision continental shortening of the north of the Tajik basin did not exceed a few hundred kilometers and was probably between 100 and 300 km. This displacement amounts were absorbed not only by intracontinental thrusting and internal deformation but also by subduction of continental crust and lateral extrusion (Patriat and Achache, 1984). Reconstruction of the initial geometry of the Indian crust shows that at least 670 km of shortening have been accommodated at the scale of the Himalayan belt (e.g., DeCelles et al., 2002).

The crustal shortening due to the India-Asia collision are essentially absorbed by reactivation of the ancient suture zones, such as Kunlun, and Tian Shan ranges (Chen et al., 1993). Quaternary faulting and seismicity show that most of the active deformation of Central Asia is partitioned between thrusting in mountain belts and sliding along great strike-slip faults (Tapponnier and Molnar, 1977; 1979). Avouac and Tapponnier (1993) modeled the velocity field of present-day deformation in Central Asia by four rotating blocks: Siberia, Tarim, Tibet and India on a spherical earth. It implies that nearly all the present convergence between India and Asia can be accounted for by slip-partitioning on these four zones, with as much as 50% absorbed by northeastwards extrusion of Tibet. The resulting deformation of Asia apparently occurred in several discrete phase. Harrison et al. (1992) suggest that rapid uplift and unroofing of southern Tibet began about 20 million years ago and that the present elevation of much of the Tibetan plateau was attained by about 8 million years ago.

Zhong and Ding (1996) proposed four stages of uplift from the onset of the collision: 45-38 Ma; 25-17 Ma; 13-8 Ma and 3 Ma-today. A fundamental switch in the latest Oligocene-early Miocene in the tectonic style of the collisional system is suggested by multidisciplinary studies from the collision zone (Hendrix et al., 1994). Numereous studies of the Himalyaya and Tibet suggest a major shift from extrusion-dominated to crustal thickening-dominated tectonics occurred in that time, which is approximaltely coincident with the start of unroofing in the Tian Shan. For example, major left-lateral movement on the Red River fault system of Southeast Asia ceased at ~23 Ma (Tapponnier et al., 1990). Exhumation rates within the Trans-Himalayan batholiths (Copeland et al., 1987; Richter et al., 1991) and parts of the western Himalaya (Zeitler, 1985) increased in that time.

2.2 Geological setting and history of Tian Shan

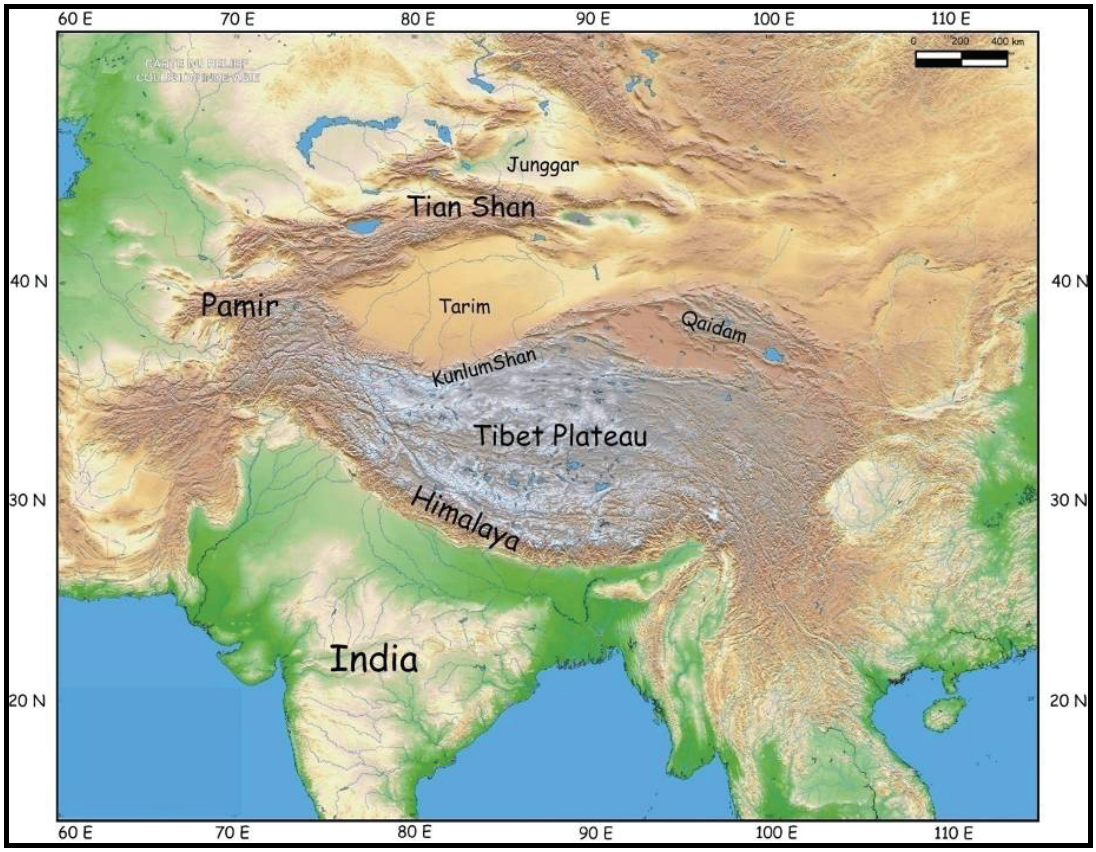

Figure 2-3. *The topography of the central and southern Asia. MNT (NASA).*

Tian Shan (Shan is Chinese for mountain) is the pre-eminent mountain range of

Central Asia, over 2500 kilometers in length, with peaks in excess of 7000 meters in elevation. The range locates in the border region of Kazakhstan, Kyrgyzstan and the Xinjiang Uyghur Autonomous Region of western China (Figure 2-3).The highest peak in Tian Shan is the Victory Peak up to 7,439 meters, on the Kyrgyzstan-China border. The eastern part of Tian Shan is bounded by the Junggar basin to the north and Tarim basin to the south.

2.2.1 The origin of basement and Paleozoic assembly of Tian Shan

The Paleozoic Tian Shan is a major orogenic domain within the Central Asian Orogenic Belt (CAOB) (e.g. Jahn et al., 2000; 2004a; 2004b; Xiao et al., 2004; Kröner et al., 2007; Windley et al., 2007) or Altaid orogenic collage (Sengör et al., 1993; Sengör and Natal'in 1996). It is bounded by the Kazakhstan microcontinent to the northwest, the Junggar basin to the northeast, and the Tarim basin to the south (Coleman 1989; Xiao et al., 1992; Konopelko et al., 2007; Kröner et al., 2008 错误！未找到引用源。). It extends east-west for over 2500 km and exhibits the highest relief in Central Asia. The present topography is due to the Tertiary Asia-India collision (Tapponnier et al., 1986; Nelson et al., 1987; Avouac et al., 1993; Sobel and Dumitru 1997). In addition, the Cenozoic tectonism is responsible for the recent northward underthrusting of Tarim below South Chinese Tian Shan, and for the southward underthrusting of Junggar below North Tian Shan (Windley et al., 1990; Avouac et al., 1993; Hendrix et al., 1994; Burchfiel et al., 1999; Allen et al., 1999; Li et al., 2009). From the Neoproterozoic to Paleozoic, accretion of several continental blocks, island arcs and accretionary complexes to the southern margin of Eurasia formed the CAOB, within which the Tian Shan Belt resulted from amalgamation of the Tarim, Junggar and Kazakhstan-Yili blocks and intervening microcontinents (Wang et al., 1994; Gao et al., 1998; Chen et al., 1999; Charvet et al., 2007; Wang et al., 2007; Windley et al., 2007).

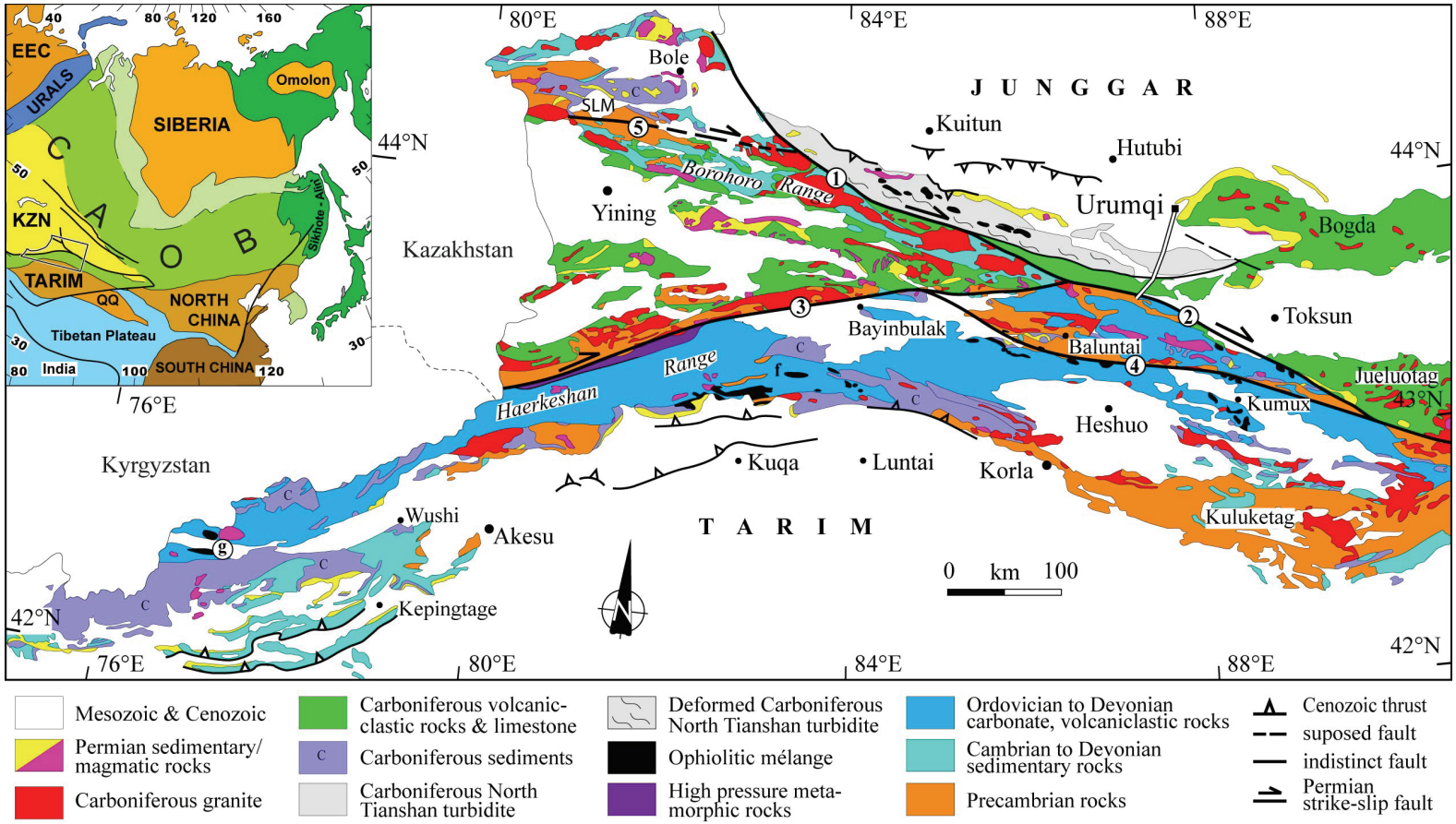

Figure 2-4. *Geological map of the Chinese western Tian Shan belt (after Wang et al., 2008). Numbers in circle refer to the main faults: 1, North Tian Shan fault (NTF); 2, Main Tian Shan shear zone (MTSZ); 3, Qingbulak-Nalati fault (QNF); 4, Sangshuyuanzi fault; 5, Jinghe fault. Inset shows location of the Tian Shan Belt in Central Asia (modified from Jahn, 2004). Abbreviations: CAOB, Central Asian Orogenic Belt; EEC, Eastern European Craton; KZN, Kazakhstan; QQ, Qaidam-Qinling.*

According to previous works (e.g. Windley et al., 1990; Allen et al., 1993; Gao et al., 1998; Chen et al., 1999), several ophiolitic belts have been used to define an Early Paleozoic South Tian Shan Suture (STSS, corresponding to faults 3 and 4 in 错误！未找到引用源。) and a Late Paleozoic North Tian Shan suture (NTSS, corresponding to faults 1 and 2 in 错误！未找到引用源。), dividing the Chinese Tian Shan belt into North Tian Shan, Central Tian Shan and South Tian Shan zones. In the literature, there is often a confusion on the suture zone that represents an initial plate boundary and also the strike-slip fault resulted from a reworking of the plate boundaries during Permian, i.e. after accretion and collision.

In addition, the tectonic evolution of this complex orogen remains controversial, and numerous geodynamic models have been proposed since the last two decades. According to Coleman (1989), the Tian Shan resulted from the closure of an oceanic basin during the early Paleozoic. Ma et al. (1993) suggested that the southern Tian Shan evolved from a back-arc basin that formed by southward subduction of the Paleo-Junggar Oceanic lithosphere, whereas Cao et al. (1992) considered that the southern Tian Shan represents oceanic crust thrust to the south upon the Tarim Block during the late Paleozoic. According to Windley et al. (1990) and Allen et al. (1993), in the eastern Chinese Tian Shan, the north-directed subduction occurred during the late Devonian-early Carboniferous along the STSS and the south-directed subduction occurred in late Carboniferous-early Permian time along the NTSS. In western Tian Shan, Gao et al. (1995, 1998) proposed a north-directed subduction along the southern Tian Shan suture zone. According to Chen et al. (1999), the southern Tian Shan was originated from the closure of an early Paleozoic ocean located between Tarim and the Central Tian Shan and subsequent late Paleozoic oblique collision. More recently, Charvet et al. (2007), Wang et al. (2008) argued that the Paleozoic Chinese Tian Shan is a polyorogenic belt formed by the closure of three oceanic basins that separated four continental blocks, namely from north to south, Junggar, Yili-North Tian Shan, Central Tian Shan, and Tarim. The three subduction systems were not coeval, but all directed to the south. However, these models are often controversies, many of them

are still in debates.

(a) The Altaid tectonic collage

Sengor (1993) suggested that all the independent orogens within the Altaid edifice, including Tian Shan, have evolved dominantly along a single subduction zone that developed during the Cambrian along the eastern margin of a unified Baltico-Siberian continent. Most units are bounded by large strike-slip faults. Passive consolidation of the southern margin of Paleo-Asia is marked by accretion and subduction of the Paleo-Tethys oceanic basins and by development of volcanic arcs. It highlighted the function of strike-slips and the continental growth in the evolution processes, which is different from Alps and in the Himalaya belts (Sengor and Natal'in, 1996; Figure 2-5).

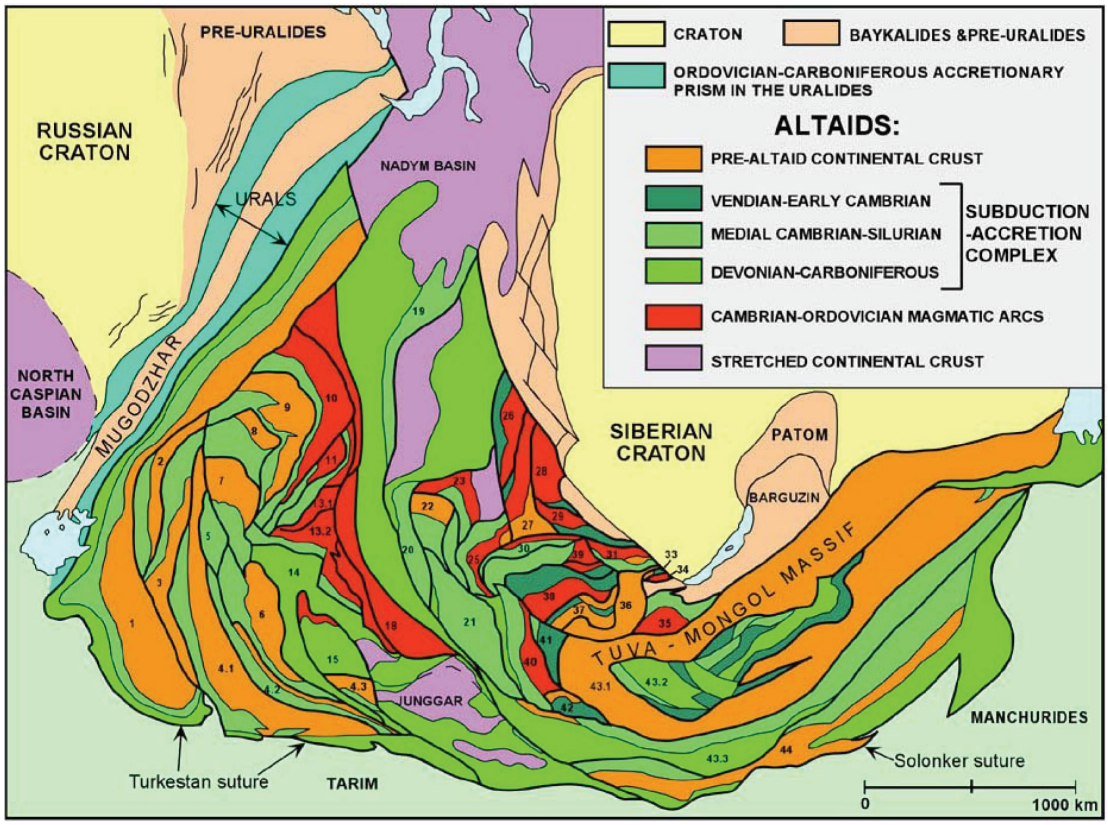

Figure 2-5. *Simplified and generalized tectonic map of the Altaids and related surrounding units. Numbers refer to different geological units (see reference Sengor and Natal'in, 1996).*

(b) Multi-subduction and collision

An alternative model of with the Altaid model concerns multi-subduction and collision ones are proposed by different authors based on different evidences (Windley et la., 1990; Allen et al., 1993; Gao et al., 1998; Laurent-Charvet, 2001; Xiao et al., 2004; Wang et al., 2008). The all highlight the function of multi-subductions, arcs and collisions in the evolution of the Paleozoic Tian Shan. However, several important issues are still under debate, such as the suture locations, the age of (U) HP metamorphism and the polarity of subduction and so on. A recent geodynamic model seems to be commonly recognized during the international field excursion and workshop in Urumqi, China on the Paleozoic Tian Shan evolution (September 9-18, 2009, Wang et al., 2010 错误！未找到引用源。). It may be briefly described as follows.

(1) Early Paleozoic closure of the Central Tian Shan Ocean.

The oceanic basin separating the Tarim and Kazakh-Yili-North Tian Shan block began to close in the Ordovician. The closure was due to a south-directed subduction below the Tarim block. Later, the northern margin of the Tarim block suffered extensional tectonism that resulted in the formation of the South Tian Shan back-arc basin during Late Silurian-Middle Devonian (Figure 2-6 (1)).

(2) Devonian-Early Carboniferous collision between the Kazakh-Yili-North Tian Shan and Central Tian Shan blocks.

This early collision in the evolution of the Tian Shan orogen was responsible for the development of the high to ultra-high pressure metamorphism along the Central Tian Shan suture. The collision was followed by oceanic lithosphere consumption, deep subduction and coeval with top-to-the-North ductile shearing (Figure 2-6 (2)).

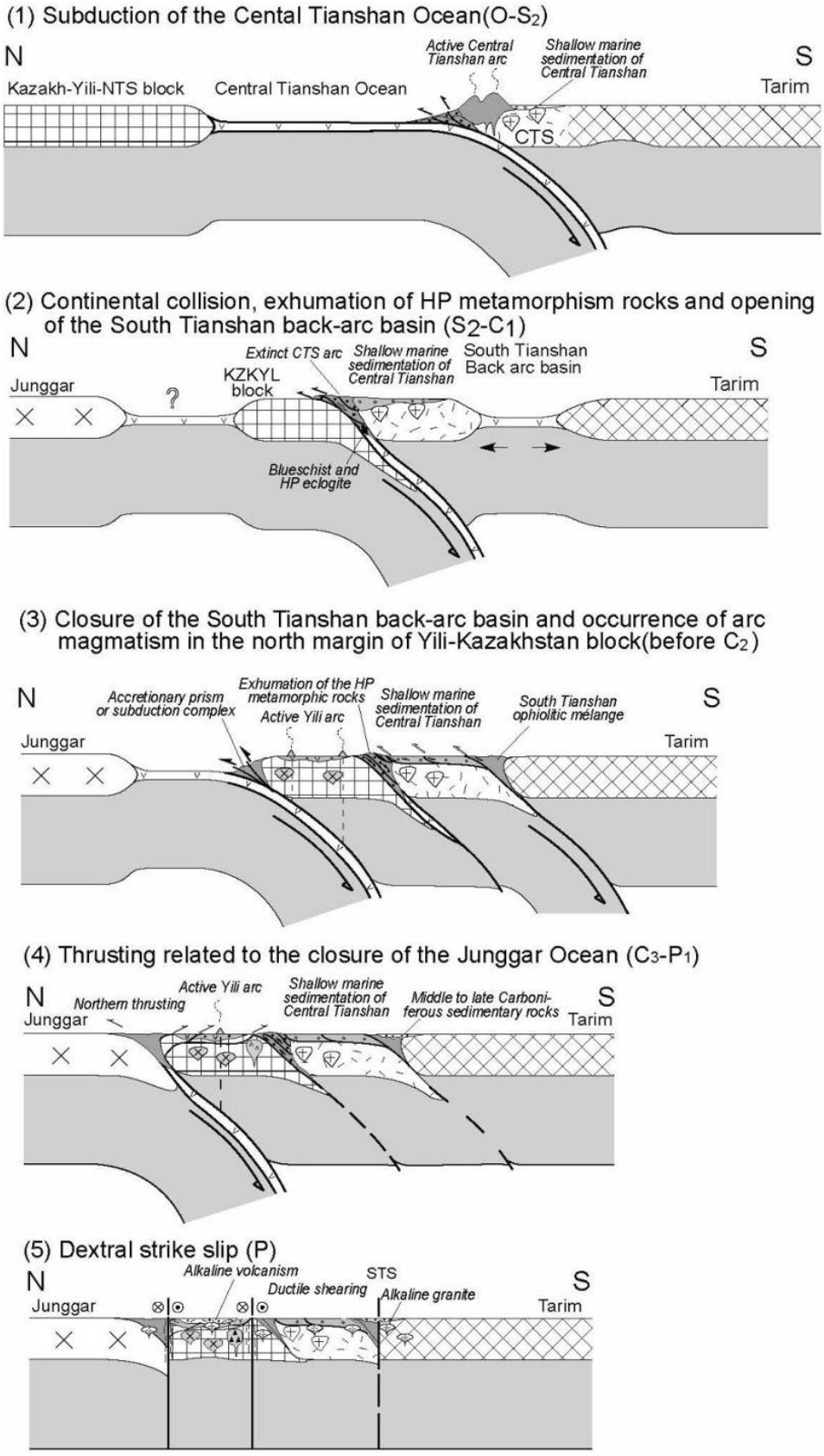

Figure 2-6. *A multi-subductins and collisions geodynamic evolution model for the Paleozoic Chinese Tian Shan (after wang et al., 2008; Wang et al, 2010).*

(3) Early Carboniferous closure of the South Tian Shan back-arc basin, and formation of the North Tian Shan magmatic arc.

The welding of the Kazakh-Yili-North Tian Shan and Central Tian Shan blocks collided with the Tarim block and induced closure of the South Tian Shan back-arc basin. Southern Tian Shan ophiolitic mélange formed by sedimentary rocks (chert, siliceous mudstone, limestone), remnants the oceanic crust (pillow lava, diabase, gabbro), and the underlying mantle (serpentinized peridotite) of the South Tian Shan back-arc basin mixed together with sedimentary rocks of the Tarim block. This unit crops out as klippes emplaced from South to North upon the Central Tian Shan block in the current Tian Shan. Furthern north, high pressure eclogitic rocks along the Central Tian Shan suture are retrogressed into greenschist facies during their exhumation. Finally, the northern boundary of the Kazakh-Yili-North Tian Shan became an active margin along the North Tian Shan accretionary complex, coeval with the North Tian Shan ophiolitic melange, and the North Tian Shan magmatic arc developed (Figure 2-6 (3)).

(4) Late Carboniferous tectonics in the Kazakh-Yili-North Tian Shan block.

During this period, Most of the tectonic activity was located in the Kazakh-Yili-North Tian Shan block. The end of North Tian Shan arc magmatism is probably the consequence of subduction of the continental part of the Junggar basement. Late Carboniferous sedimentation was characterised by shallow marine terrigeneous and carbonated rocks in the Central Tian Shan. South-directed thrusts and folds that developed in the Kazakh-Yili-North Tian Shan and Central Tian Shan blocks can be considered as back-folding and back-thrusting due to the north Tian Shan subduction (Figure 2-6 (4)).

(5) Permian dextral strike-slip faulting.

During the end of the Carboniferous, the various tectonic elements, including magmatic arcs, continental blocks, and ophiolitic melanges, were already welded together. Later in Permian, all these units experienced major dextral wrenching parallel to the strike of the orogen. The Altai Fold Belt underwent sinistral strike-slip

faulting to the norther. The two strike-slip systems accommodated an opposite motion of Tarim and Siberia as suggested by paleomagnetism studies. This strike-slip tectonics was accompanied by pull-apart basin opening and post-tectonic magmatism expressed by volcanic rocks and granitic plutons. The coeval emplacement of Permian calc-alkaline and alkaline suites suggest the influence of the mantle metasomatism during the Carboniferous subduction (Figure 2-6 (5)).

During the Mesozoic, deformation resumed, as documented by Triassic and Jurassic unconformities. But these tectonic events were purely intracontinental, like the Cenozoic event responding to the Asia-India collision.

2.2.2 Mesozoic activity and inactivity

Up to now, most of the previous studies in Tian Shan focused on either the Paleozoic evolution of the range linked to the agglomeration of Central Asia and the accretion of Central Asia Orogenic Belt or its Cenozoic intracontinental evolution linked with the India-Asia collision. Few studies found in the literature essentially concern the sedimentological studies on Mesozoic sediments of these basins adjacent to the Tian Shan (Hendrix et al., 1992, 2000; Li et al., 2004, 2010). The Mesozoic of the Tian Shan are poorly studied. Explanation for the regional Jurassic sedimentation is at odds. Some Chinese geologists have the hypothesis of a Mesozoic Tian Shan (Huang 1978; 1949) with long time. They proposed that the Mesozoic-Tian Shan was the remains of eugeosynclinal variscides and less lofty by erosion, associated by intermountain basins interior. Watson et al. (1987) proposed that the Tarim and Junggar Basins were flexural, foreland basins in the Jurassic, loaded by thrusts originating within the orogenic belts at their margins.

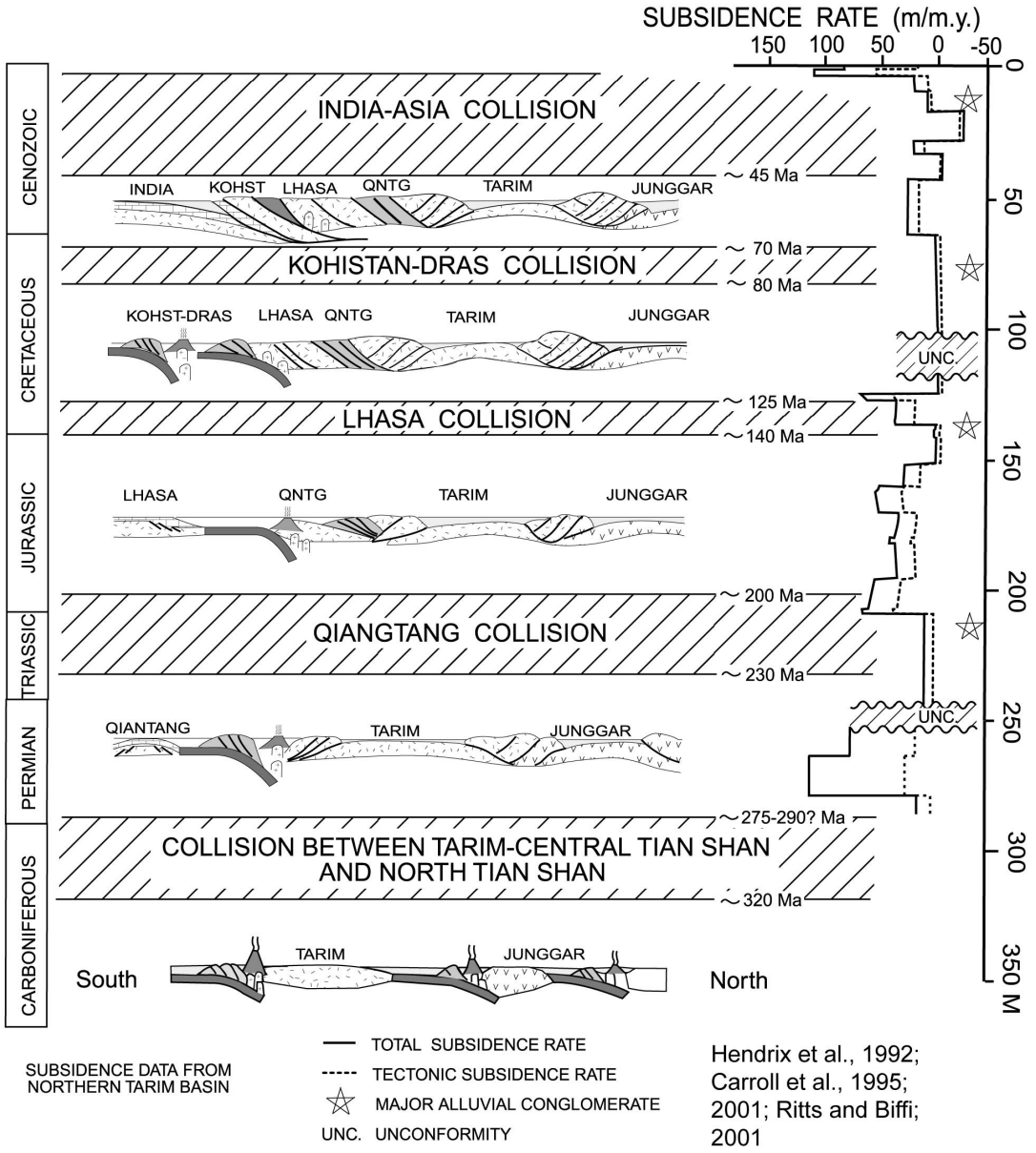

Figure 2-7. *Summary diagram of indicators of timing of deformation in Chinese Tian shan. Subsidence history in northern Tarim basin shows rapid subsidence during collisions at southern margin of Asia (After Dumitru et al., 2001).*

Several stratigraphic evidences suggest that the Junggar and Tarim basins continued to be physiographically separated by the ancestral Tian Shan during Mesozoic contractile deformation (Hendrix et al., 1992; Figure 2-7). However, basing on Jurassic basins without fault control, Allen et al. (1991) suggested that it was proceeded a phase of thermal subsidence associate with fluvial and lacustrine sedimentation throughout the Jurassic, Cretaceous and early Tertiary. Shu et al. (2004)

take notice of the coaly Jurassic deposited widely even in the Tian Shan without molasse of marginal facies. He proposed that in the interval of Jurassic-Paleogene, extensional tectonic activity within plate split the peneplaned Tian Shan region into a series of sub-E-W-striking extensional basins. Jia et al. (1997) related the Chinese northwest basins to the evolution of the Tethyan orogenic belt. He proposed the extension in early to middle Jurassic, whereas compression in latest later Jurassic to Cretaceous.

Low temperature thermochronology approach (fission tracks and (U-Th)/He) is widely used to constrain the Triassic to present history of the range. The thermochronolgy ages distributed in various periods during Mesozoic and Cenozoic (Dumitru et al., 2001; Wang et al., 2009; Jolivet et al., in press). These ages indicate the multiphase uplifting in the Tian Shan area. It is noteworthy that the ages vary along the orogen strike in the Tian Shan and difference between the northern and southern sides along faults (Figure 2-8).

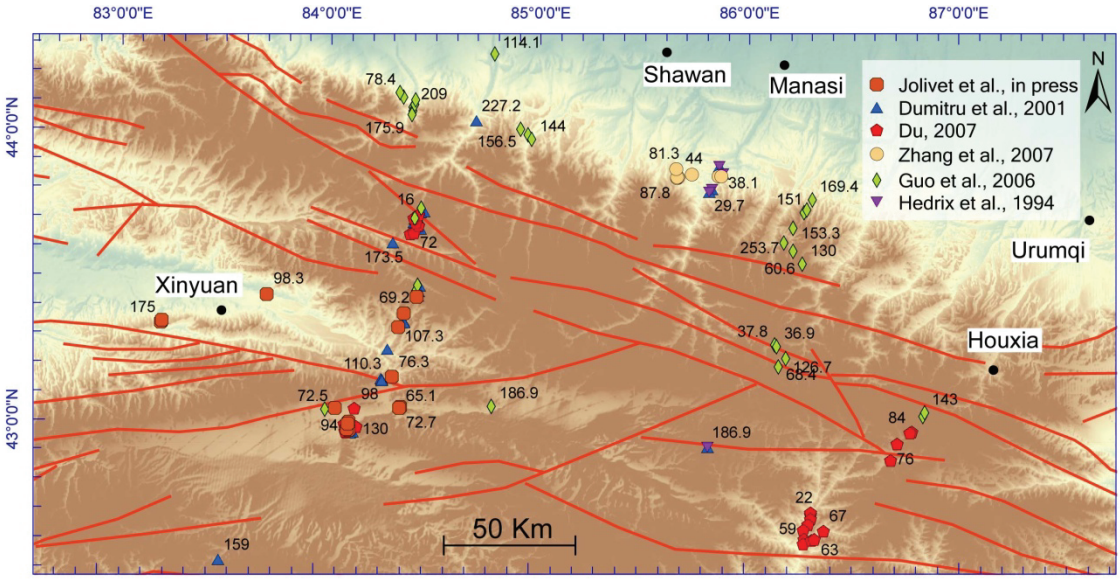

Figure 2-8. *Low temperature thermochronology ages in the Tian Shan area. The numbers denote the cooling ages (Ma). Red lines are the faults in the mountain basement (faults from XBGMR, 1993).*

2.2.3 The current Tian Shan

(a) Seism

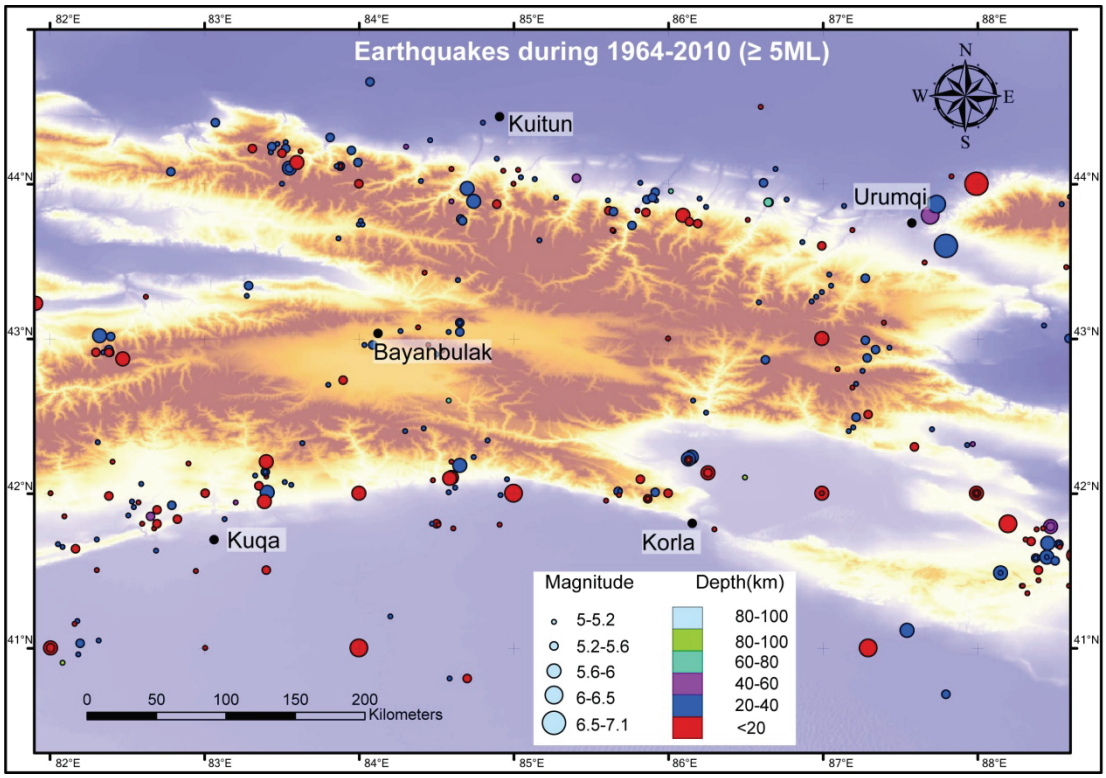

Figure 2-9. *Seismicity map of the Tian Shan (IRIS).*

The biggest documented earthquakes in Tian Shan took place on Decembre 3rd, 1906, with M≈8, in Manasi area, north piedmont of Tian Shan (Molnar and Deng, 1984; Avouac et al., 1993; Wang et al., 2004). Field investigations indicate that this earthquake occurred along a blind thrust fault (Deng et al., 2004).

Figure 2-9. presents about 500 seisms in Tian Shan area science 1965 (M≥5; 82°-88.5°E in longitude; 40.5°-45°N in Latitude; http://www.iris.edu/data/event/eventsearch.htm). This map show that the deformation in the Tian Shan is mainly located in both the northern and southern fronts. Seismic moment tensors of major earthquakes in this century suggest an average shortening rate of 7 (± 2) mm yr^{-1} across the Tian Shan (Molnar and Ghose, 2000).

(b) GPS measurement

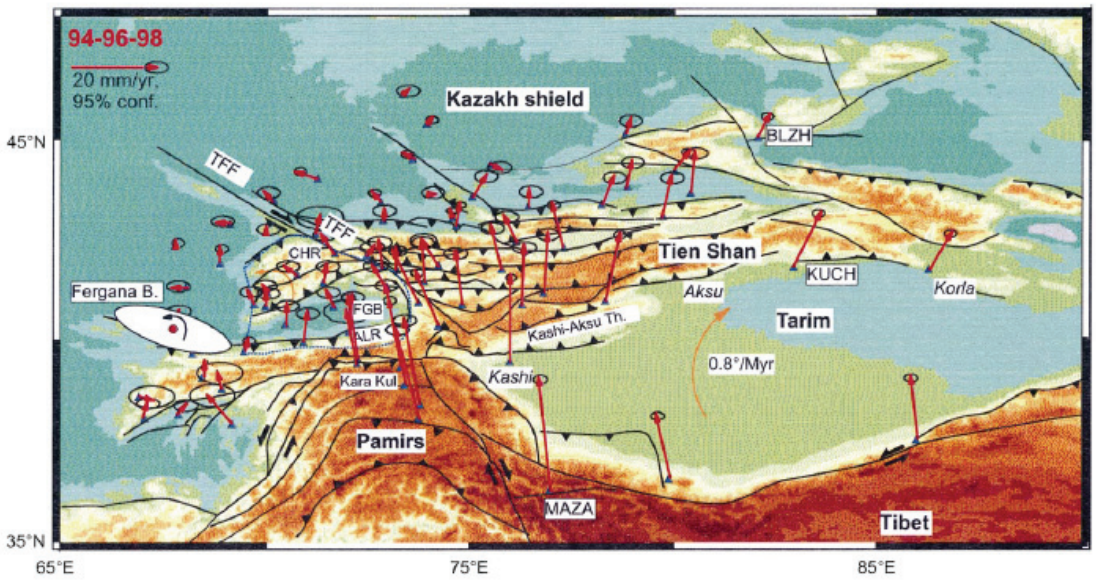

Figure 2-10. *GPS vectors with respect to stable Eurasia. Fergana B.: Rotation pole of FGB, TFF: Talas Fergana Fault, CHR: Chatkal range, ALR: Alai range (Reigber et al., 2001).*

GPS (Global Positioning System) is used to measure the present-day kinematics of deformation on the surface of earth. The results of GPS network in the Republics of Kyrgyzstan and Kazakhstan suggest that the total shortening of Tian Shan is approximately 20 mm yr^{-1}. This result also indicates that most of Tian Shan has been constructed during the past 10 Myr (Abdrakhmatov et al., 1996). Later, more dense GPS network measurement suggested 20 mm/yr N-S shorting rate in the west of Tian Shan and 10 mm/yr in Chinese Tian Shan (Reigber et al., 2001; Figure 2-10). Chinese GPS measurements taken from 1992 to 2006 in the Tian Shan mountains and their adjacent areas show that slip rates on east-west trending detachment vary from 10-13 mm/yr in the southwest of Chinese Tian Shan to 2-5 mm/yr in western Chinese Tian Shan (Yang et al., 2008). The rotation clockwise of Tarim basin was proposed by paleomagnetic results and structural analyses with the pole in the west of Tian Shan (Chen et al., 1991; Avouac et al., 1993), which is corresponding to the GPS results (Reigber et al., 2001).

(c) The deformation along the piedmont.

Based on fault scarp offsets (10.2±0.7m) and the Holocene age (10±2 kyr) for highest terrace surface, Avouac et al., (1993) proposed the surface shortening rate is about 1.25±0.5 mm/yr and the mean depth shortening rate have been 3.0±1.5 mm/yr. They also estimated the Cenozic shortening amount was the order of 30 km in the northern piedmont Cenozoic shortening, assuming with an imaged antiformal stacking in the front. The differences of relative heights between two terraces could reach 100 to 120 m over the crests of anticlines in the northern piedmont, Morlnar et al., (1994) infer that this spacing is due to alternating stages of valley widening and rapid incision associated with climate changes with a periodicity of 100 kyr. Hence, the average vertical rate of is about 1 mm/yr. Burchfiel et al., (1999) constructed four cross-sections in the northern piedmont of Tian Shan, the southern part of the Hutubi River, Tugulu anticline, Tuositai anticline and Dushanzi anticline. The balanced cross-sections show that the shortening amounts are 6.2km, 5.5km, 4.6-5.0 km and 2.12-2.35 km respectively. Calculating large-scale shortening rate is difficult, because the four profiles are spare and not lined. Moreover, their structures are active and laterally vary significantly. The range interior is poorly studied as well. A minimum shortening rate of >5.7 to 7.2 mm/yr was proposed assuming the time of initiation of deformation is 2.5 Ma (Burchfiel et al., 1999).

Along the southern piedmont, at least 20-40 km of crustal shortening with a hozizontal shortening strain of 20-30% was proposed by Yin et al. (1998). It was suggested that these estimates are minimum because of both conservative extrapolation of the thrust geometries and partial coverage of the thrust belt by the cross sections. A shortening strain of 1.0-1.9 mm yr-1 was obtained, assuming the initiation thrust begin about 21-24 Ma (Yin et al., 1998). Burchfiel et al. (1999) constructed cross-sections of Kalasu River, Qiulitage anticline in the west part and Boston Tokar in the east and suggested the shortening of 12-14 km, 6-7 km and 10.3-13.0 km, respectively. Deng et al (2000) applied system studies in the Tian Shan area on the active tectonics. Based on geological mapping and technique of balanced

cross-section, the amounts of shortening in Tulufan, Urumqi and Kuche foreland basins are calculated with 10-12 km, 17 km and 23 km respectively.

The reason of these diversity values of shortening amounts and rate are due to lacking of reliable geometry data in depth, such as seismic profiles or other geophysics data. Most of the cross-sections are constructed by surface observations, combining with theoretical models.

2.3 Problems and methodology

The northern and southern piedmonts of Tian Shan are characterized by foreland thrust-and-fold belts, which are the key areas to understand the multiphase mountain building. Geodesic measurement shows the decrease GPS velocity from the southern Tibet plateau, to the northern Tian Shan area (Reigber et al., 2001; Wang et al., 2001; Niu et al., 2007; Figure 2-10). The northern piedmont of Tian Shan has been proposed to be the north end of the far-effect by India-Asia collision (Tapponnier and Molnar., 1977; Avouac et al., 1993; Tapponnier, 2001). Within the northern piedmont depression of Tian Shan, three sub-parallel fold belts prolong along east-west strikes due to the north-south convergence. North-flowing rivers incise the anticlines perpendicular to strike where they expose successions of deposited series. Magnetostratigraphy studies have been carried out in the Cenozoic series of some of these anticlines to find out the sedimentary rates and defined the growth strata ages (Charreau et al., 2005; 2006; 2008; 2009; Sun et al., 2004; Huang et al., 2006; Ji et al., 2008; Li et al., 2010; Lu et al., 2010). Numerous petroleum seismic profiles and drilled wells are located in this area by profit-driven. Furthermore, the structural and the sedimentary characteristics in the northern piedmont of Tian Shan may offer direct evidences of the far-effect by India-Asia collision and the Cenozoic tectonic evolution history of Central Asia. This is the the reason why we chose the northern piedmont of Tian Shan as the study area. Up to now, structural studies along the northern front of Tian Shan are mostly modern–driven than data-driven (Avouac et al., 1993; Burchfiel et al., 1999), which were essentially based on surface studies. The structural profile

published from seismic profiles lack often surface constraints and, moreover, with limited extent to the piedmont of Tian Shan that may make missing of information on the contact between the range basement and basin cover (Wang et al., 2005; Chen et al., 2007; Lu et al., 2007). The results from previous studies by different methods are often therefore contradictory, such as shortening rates along the northern piedmont (Avouac et al., 1993; Burchfiel et al., 1999; Deng et al., 2000). This study focuses on the field observations along the northern front of Tian Shan, especially in the contact zones between the mountain basement and basin sediments, to define their tectonic and geometric relationships. Following major problematic subjects are evoked in this study:

1, What are the relationships between the Paleozoic mountain basement and the Meso-Cenozoic basin sediments in the northern front of Tian Shan?

2, What is the nature of Tian Shan during Mesozoic as most of previous studies are concentrated on its Paleozoic and Cenozoic histories? Moreover, a good understanding on its Mesozoic nature will help to recognize better the Cenozoic evolution of Tian Shan;

3, Consequently, how much the deformation has occurred due to the Cenozoic tectonics along the northern piedmont of Tian Shan?

4, What is the mechanism of the Cenozoic deformation in the northern piedmont of Tian Shan?

To answer these questions, multidisciplinary studies are carried out in the northern piedmont of Tian Shan. Two types of the data are obtained, the surface and subsurface data (Figure 2-11). The surface data consist of (1) available geological maps, which were digitized in Arcgis (ESRI) with geological limits, faults, strikes and dip angles. (2) detailed geological observations made in the northern front of Tian Shan. Subsurface data consist of available seismic profiles and drilled wells. For following reasons, the gravity measurements have been carried out along certain profiles and then integrated into subsurface data, (1) Outcrops cannot be continuously observed in the field because of the important Cenozoic cover; (2) Seismic profiles

are often limited in the basin and there is no any data available on the depth close to the mountain; (3). Seismic method becomes less sensitive to the strongly deformed zone. These gravimetric data are treated to Bouguer anomaly and two dimensional (2D) forward gravity modeling has been performed using the Geosoft-GM-SYS software. With these surface and sub-surface data, a 3D model of the northern piedmont of Tian Shan is possible to construct with Geomodeller or Gocad softwares (Figure 2-11， see Annexes).

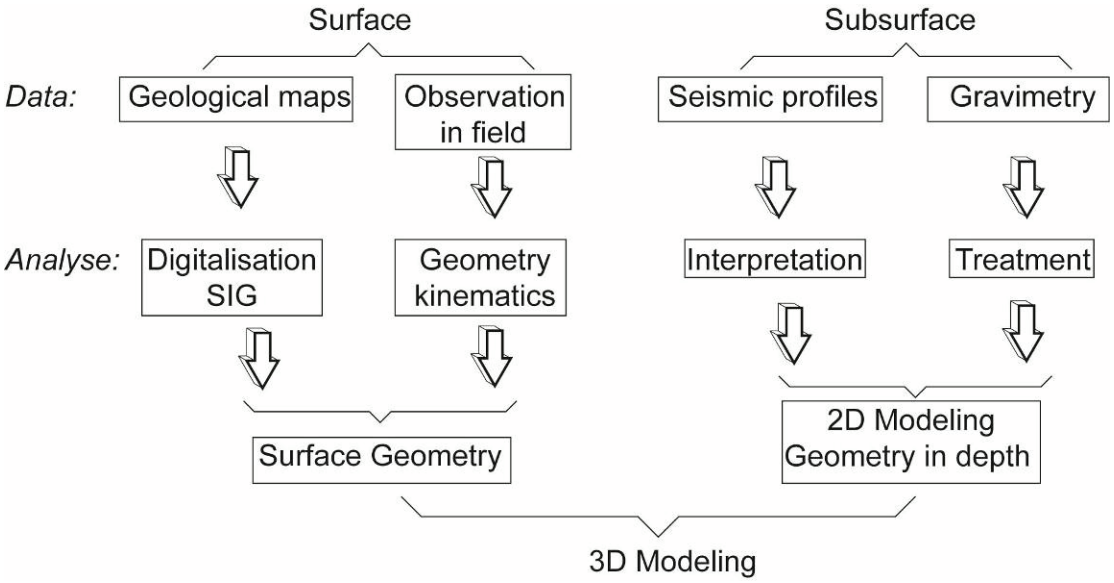

Figure 2-11. *The methods applied in this study and the processes.*

Chapter 3

The Mesozoic paleo-relief of the northern Tian Shan - submitted manuscript

The Mesozoic Paleo-relief of the Northern Tian Shan – submitted manuscript

Ke CHEN[1,2], Charles GUMIAUX[1], Romain AUGIER[1], Yan CHEN[1], Qingchen WANG [2], Wei LIN[2] , Shengli WANG[3] ,

1 Université d'Orléans, CNRS/INSU, Université François Rabelais - Tours, Institut des Sciences de la Terre d'Orléans - UMR6113, Campus Géosciences, 1A rue de la Férollerie, 45071 Orléans cedex2, France

3 State Key Laboratory of Lithospheric Evolution, Institute of Geology and Geophysics, Chinese Academy of Sciences, P.O. 9825, Beijing 100029, China

3 Department of Earth Sciences, Nanjing University, 210093, Nanjing, China

3.1 Abstract

The Tian Shan mountain range offers a natural laboratory to study orogenic processes. Most of the previous studies focused on either the Paleozoic evolution of the range or its Cenozoic intracontinental evolution linked with the India-Asia collision. In this study, detailed stratigraphic and structural investigations on the relationship between sedimentary cover and basement allow to constrain the Mesozoic evolution of Northern Tian Shan. Stratigraphic field observations argue for Jurassic sedimentation with very limited transport in certain places of the range front. Sections presented in this paper show that, in some locations, Triassic to Jurassic sedimentary series present a continuous onlap type sedimentary unconformity on the top of the basement. At different scales, observations clearly evidence the existence of a major paleo-relief during Mesozoic. According to the present study, the actual Tian Shan nature and the associated movements along its northern front structures cannot be considered as the consequence of Cenozoic reactivation alone.

3.2 Introduction

The modern Tian Shan is one of the Major mountain range in Central Asia belt.

The current structure of the Tian Shan results from two principal tectonic phases: i) subductions, arc-accretions and continental collision during Paleozoic (e.g. Windley et al., 1990; Söngor et al., 1993; Gao et al., 1998; Laurent-Charvet et al., 2002; Charvet et al., 2007; Wang et al., 2007) and ii) intracontinental reactivation linked with the India-Asia collision, during Cenozoic (e.g. Tapponnier and Molnar, 1977; Avouac et al., 1993). At first order, this finite structure displays a remarkable uprising of Paleozoic 'basement' rocks – as a crustal-scale 'pop-up' – surrounded by two closed intracontinental basins (Figure 3-1). The present-day high topography of the Tian Shan, with a mean altitude of ~2500m and summit of more than 7000m, is traditionally related to the latest intracontinental reactivation of the range (e.g. Tapponnier and Molnar, 1977; Avouac et al., 1993). Ages constraints for the onset of this intracontinental reactivation range from 10 Ma to 24Ma (Avouac et al., 1993; Hendrix et al., 1994; Abdrakhmatov et al., 1996; Métivier and Gaudemer, 1997; Sobel et al., 1997; Dumitru et al., 2001; Charreau et al., 2009). In spite of this relative age discrepancies mostly related to the method applied, all ages estimated for the deformation and the associated relief erosion suggest that the mountain range reactivation and relief creation began during Early Miocene at oldest.

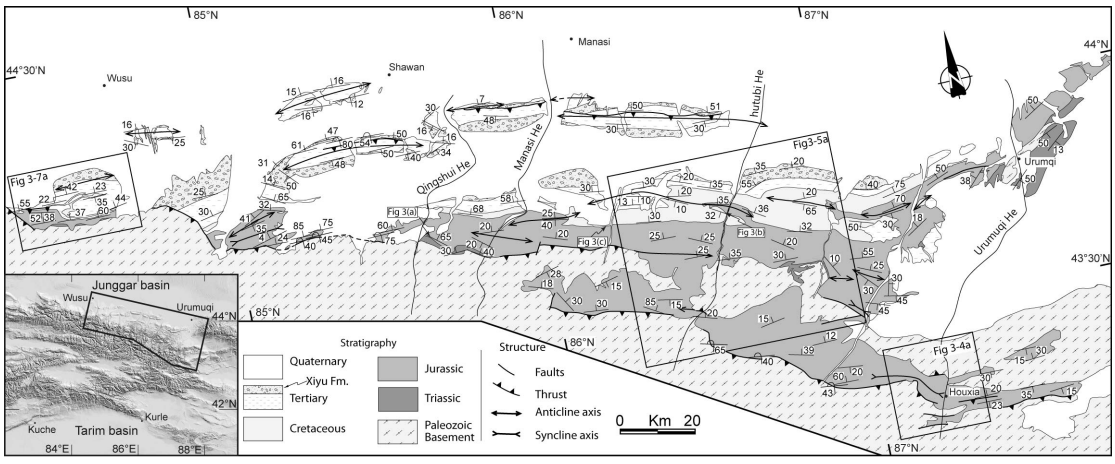

Figure 3-1. *Simplified geological map of the northern Tian Shan from Wusu to Urumqi area. Mesozoic series are most exposed in the southernmost parts of the Junggar basin along the adjacent Tian Shan range. 'He' indicates river in Chinese (geological map modified after He et al., 2005).*

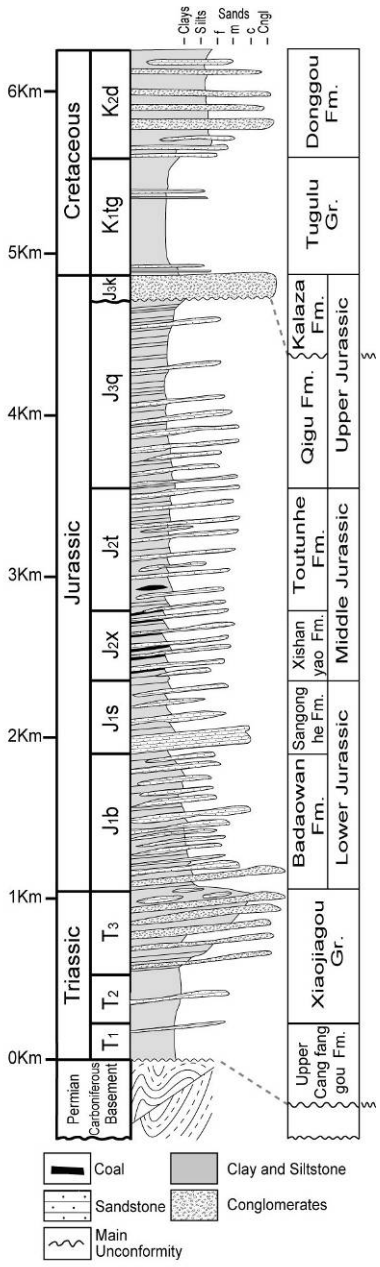

Figure 3-2. *Synthetic stratigraphic log of the study area (Modified after Hendrix et al., 1992). The Mesozoic lie unconformably over the Paleozoic basement.*

However, recent fission track analyses suggest that uplifting may have existed well before the onset of the Tertiary reactivation through Tian Shan, with exhumation ages as: 160-120Ma in central Tian Shan, 200-250 Ma detritus cooling age in the Manasi River valley (Dumitru et al., 2001) or 140-120Ma from Bayanbulak intracontinental basin, in the southern Tian Shan (Wang et al., 2009). Moreover, Triassic to Cretaceous sediments are composed of thick series often coarse grained continental sediments within both foreland basins, suggesting rather high erosion rate at that time (Hendrix et al., 2000; Carroll et al., 2010).

This study considers the Mesozoic tectonic and morphologic evolution of Tian Shan through a combined stratigraphic and structural analysis of Mesozoic deposits. It focuses on the northern piedmont of the range, along a ~280Km west-east trending segment (Figure 3-1); thanks to deep incisions of seasonal rivers, contacts between Paleozoic basement and Mesozoic-Cenozoic sedimentary cover are particularly well exposed along several north trending sections in this region (Figure 3-1). A better understanding of the Mesozoic Tian Shan would lead to highlight the real role of Cenozoic tectonics and the relative contribution of the paleo-topographic remained in the mountain range building.

3.3 Stratigraphy of Mesozoic sediments within the study area

Sedimentary series can be extensively observed and have already been studied within the Junggar basin, as summarized below (Figure 3-1 and Figure 3-2; Hendrix et al., 1992 and references therein; XBGMR, 1993). Basement units of the north Tian Shan mainly consist of Paleozoic volcanic and sedimentary rocks. From bottom to top, the entire Mesozoic series is composed of continental clastic deposits (Figure 3- 2). In the study area, the Triassic series is mostly missing along the piedmont though locally exposed (Figure 3-1). Where it crops out Triassic displays alluvial or braided-fluvial sandstone and siltstone intercalated with conglomerate and mudstone.

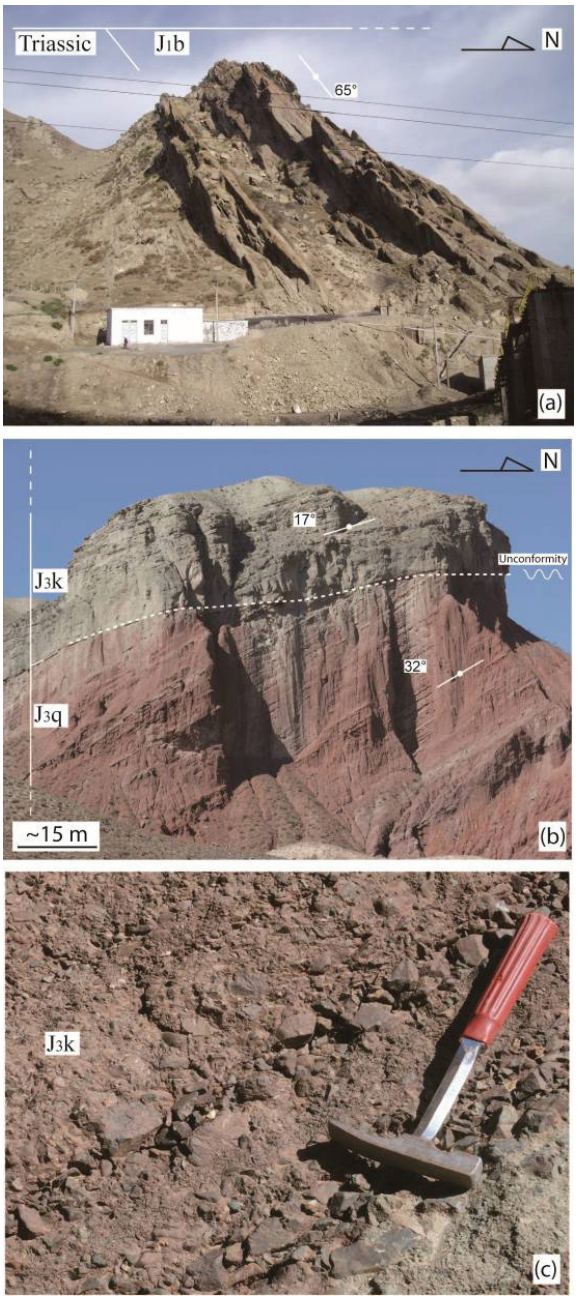

Figure 3-3. *Landscape pictures of representative features of the Mesozoic series (see position in the Fig.1) (a) Coarse-grained conglomerate bars in the lowermost Jurassic (southern Qingshui He area); (b) Uppermost Jurassic breccias (J3k) unconformably overlie the Upper Jurassic Qigu formation (Hutubi He area); (c) Detailed view of the Uppermost Jurassic breccias (west to Hutubi He area).*

Lowermost Jurassic layers are characterized by thick and coarse conglomeratic layers which can be observed in numerous places along the northern front of Tian Shan, as to the south of Qingshui He (Figure 3-3a). Lower Jurassic thickness reaches 1000m over an area extending from Manasi to Urumuqi, and decreases westwardly and eastwardly. Series become finer upward, grading into a very thick series of Lower/Middle Jurassic gray sandstone, siltstone and shale (Figure 3-2). Middle Jurassic sandstone and mudstone locally contains very rich coal layers consistent with a lacustrine environment deposit (Hendrix et al., 1992). Upper Jurassic comprises typical fine-grained red beds. Transition from Jurassic to Cretaceous series is marked by up to 800m thick breccias (Kalaza formation; Figure 3-3b). Clasts forming these particular layers are dark, 5 to 30 cm in width and display highly angular shapes (Figure3-3c) suggesting very short transport distances of material before deposition. The basal contact of this formation is sharp and often presents unconformity on top of the finer-grained Upper Jurassic red beds (Fig3-3b). The Kalaza formation laterally grades to finer deposits and is exclusively made of sandstone within the Junggar basin itself.

In this study, Mesozoic sediments have also been extensively observed within internal parts of the range, and more particularly in the eastern half part of the study area (Figure 3-1). Triassic to Jurassic sediments lying in direct contact with the Paleozoic basement can be found at rather high altitudes (2000 to 3000 m) in comparison with the mean altitude of the foreland fold-and-thrust belts (1000 to 1500 m high). In the Houxia valley – 65km SSW of Urumuqi – a Lower to Upper Jurassic continuous sedimentary series is preserved in a syncline structure (Figure 1-4a). According to the map (Figure 4-4a; XBGMR, 1993), a south verging thrust developed along one limited central segment of the northern limb of the fold while, elsewhere, sediments unconformably rest on top of the Carboniferous volcanic sediments. Besides, according to the geological map, Lower Jurassic formations directly lie on top of basement units to the northwest, with no preserved sediments owning to Triassic or to the lowermost Jurassic formation (Figure 3-4a). Along a

section made to the north of the syncline, in a small south trending valley, sedimentary

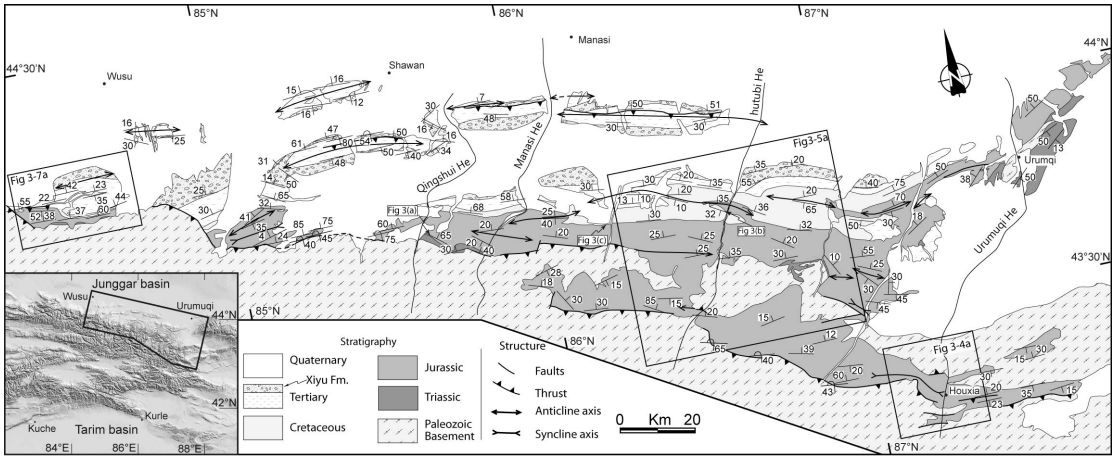

series can be continuously observed with no internal structural contact. To the south, its upper and main part is composed of fine grained sandstone with mudstone layers with a constant stratification dip-angle of about 30˚ to the south. To the north, stratifications progressively straighten up and overturned below the thrust displayed on the map (Figure 3-4a, b).

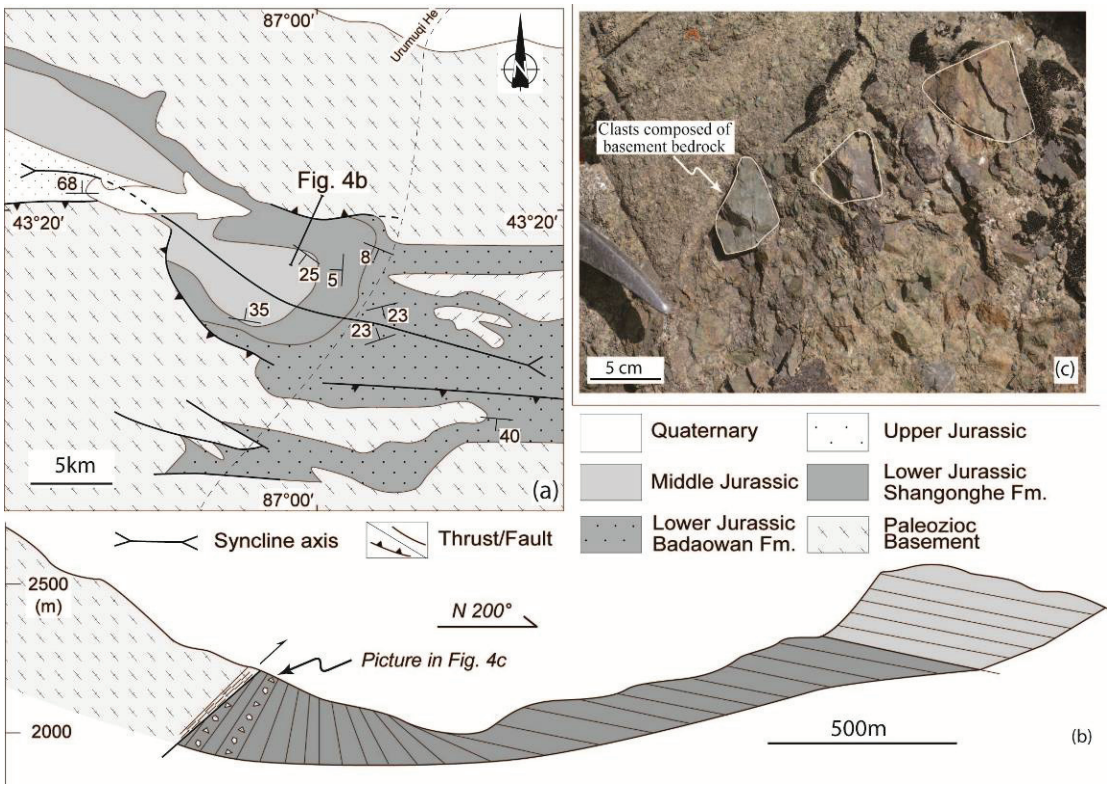

Figure 3-4. *Structural and sedimentological features of the Houxia area (a) Simplified geological map of Houxia area. (b) Geological cross-section of Houxia. (c)*

Close-up view of the Lower Jurassic breccias, here mainly composed of carboniferous basement detritus (see location on the cross-section).

There, the lowermost deposits of the series comprise interbedded levels of sedimentary breccias with coarse grained conglomerates and both rich in highly angular clasts of Carboniferous tuffaceous sandstone (Figure 3-4c). Local abundance of these breccias and the common lithological nature of the clasts with the adjacent basement unit strongly suggest a very small distance transport.

3.4 Structural analysis of the Mesozoic basal contact

Deformation of northern Tian Shan has already been studied through the structural analysis of sedimentary series, within the proximal foreland basin (Avouac, 1993; Deng, 1996; Burchfiel et al., 1999). Yet, as described above, Mesozoic series restricted to the piedmont fold-and-thrust belts are also widely preserved on top of the basement units, within range (Figure 3-1). As shown on the map (Figure 3-1), classical frontal thrust structures can be pointed out over some segments of the piedmont. In that case, the structure marks out the boundary between the uplifted basement Paleozoic units and the relatively subsiding proximal foreland basin. For other segments, following Mesozoic layers, structural continuity of the sedimentary series can be observed from basin until more internal and higher parts of the range (Figure 3-1). Structural analysis of such unstrained basal contact of Mesozoic series is presented for two of the studied sections constructed from field work, seismic profiles and drill-holes data: the Hutubi He and the Wusu sections.

At first order, to the north of the Hutubi He area, Triassic to Neogene sedimentary series forms a rather simple monocline structure, dipping 15-20° to the north (Figure 3-5a). The first fold-and-thrust belt is composed of one gentle upright anticline and associated syncline with only very limited thrusts developed (Figure 3-5a). These are second order structures which can be regarded as a fault propagation fold structure according to the available seismic data (Figure 3-5b). Further south, entering within the interior parts of the range, sub-horizontal Lower Jurassic strata lie on top of the

Carboniferous units (Figure 3-5b). While basement is strongly deformed as evidenced by sub-vertical cleavage, overlying sedimentary layers form very gentle upright folds as marked by the curved outline of the Mesozoic series bottom, few kilometers west of the river (Figure 3-5a). No décollement structure has been observed between the basement top and the sedimentary cover. Besides, a southward backthrust of basement rocks above sediments can be observed to the south of the section, but the net slip must be limited as it rapidly dies out and fault westwardly transforms to a fold (Figure 3-5a).

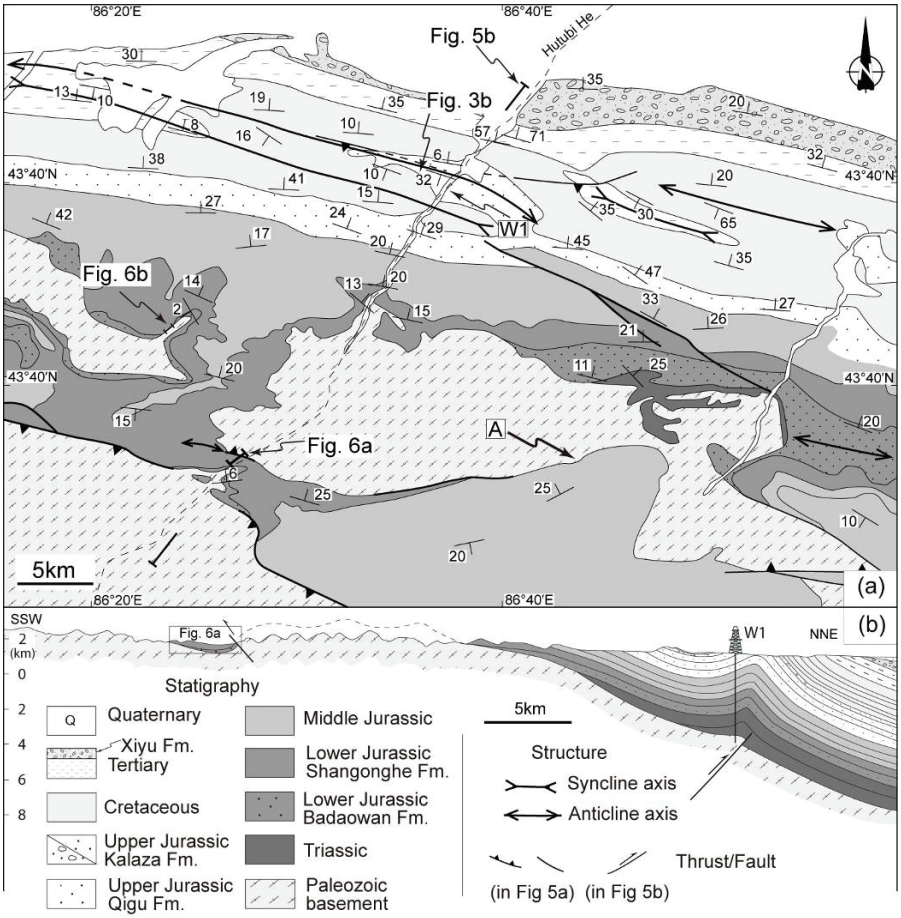

Figure 3-5. *(a) Simplified geological map of the Hutubi He area. 'A' indicates the unconformity between Middle Jurassic and Carboniferous basement. There, Triassic and Lower Jurassic are apparently lacking. (b) Geological cross-section of along the Hutubi He constrained by field data, seismic profile and drill well W1.*

Unconformity of the basal contact of Mesozoic sediments on top of basement units is observed to the southernmost part of the section (Figure 3-5a and Figure 3-6a). As a whole, the successive sub-horizontal and monocline segments draw a hinge fold

at regional scale (Figure 3-5b). Nevertheless, while ~900m thick of Triassic sediments have been drilled along the W1 well (Figure 3-5b), in the basin, no series of Triassic exist further south, toward the range (Figure 3-5a). Similarly, Jurassic of contrasted ages have been observed and mapped on top of the basement units (Figure 3-5a). In a similar situation to that of the Houxia area, basal contact of the Mesozoic series suggests its onlap deposit, from basin to range, at least during Triassic and Lower-Middle Jurassic.

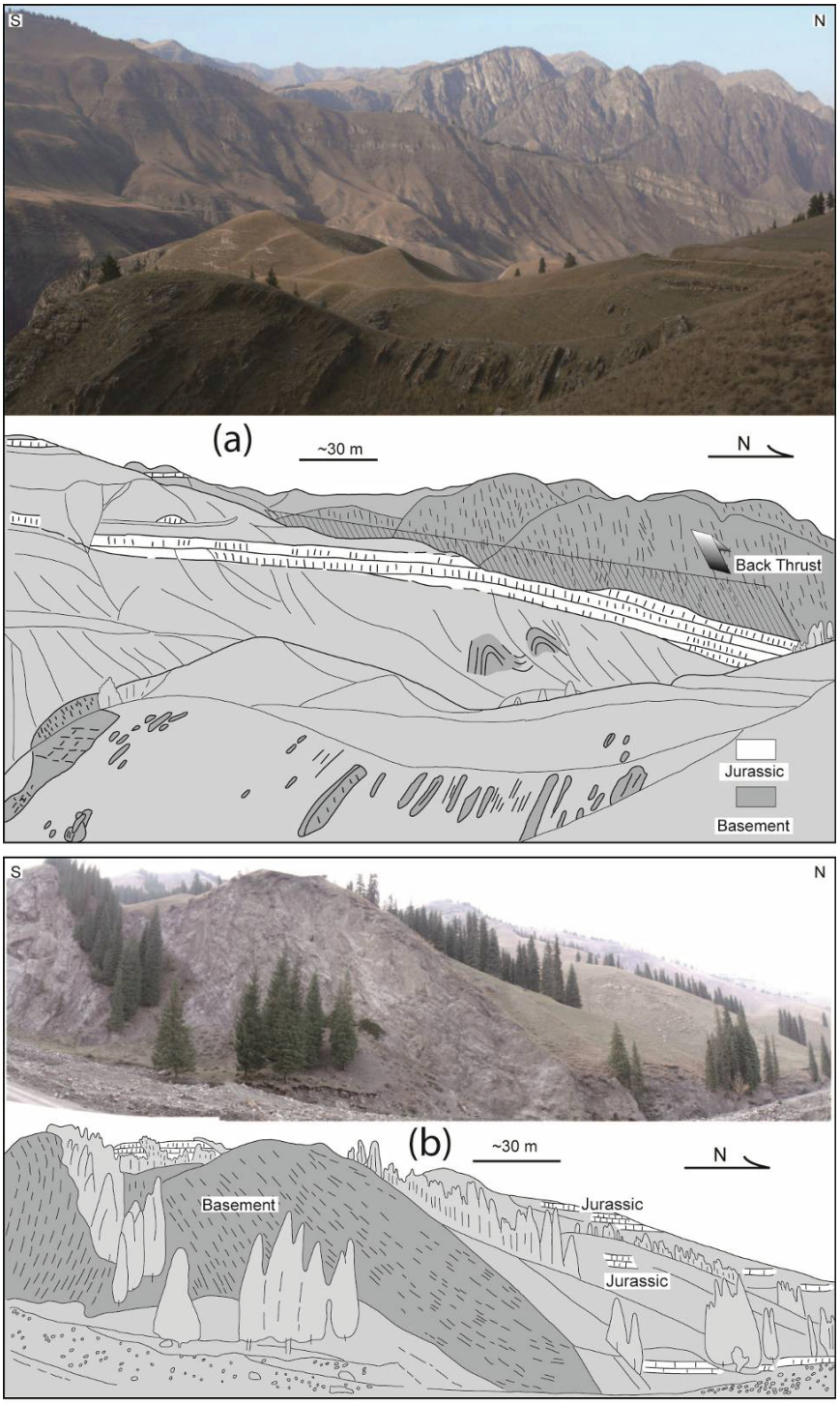

Figure 3-6. *Landscape pictures (corresponding field sketches) of the contacts between the Jurassic series and the basement. (a) General southward onlap of the Jurassic sediments over the folded basement. In the North, a basement block is back thrusted over the sediments (see Fig. 5b). (b) Meso-scale basement relief coved by Jurassic sandstones as evidenced by onlaps over a steep inherited ~150 m high basement paleo-relief. Basement rocks are deformed with a large inclined Paleozoic fold.*

More local-scale evidences for onlap sedimentation can be observed in the Hutubi He area. First, to the south end of the section, Lower Jurassic strata display a kilometer scale onlap type structure on top of basement units, i.e. with younger sediments progressively covering basement, from north to south (Figure 3-5a and Figure 3-6a). Second, ~10 km west of the Hutubi river, subhorizontal layers of the Lower Jurassic formation, which can be continuously followed all along few kilometers in this small valley, structurally die on deformed Paleozoic basement units (Figure 3- 6b).

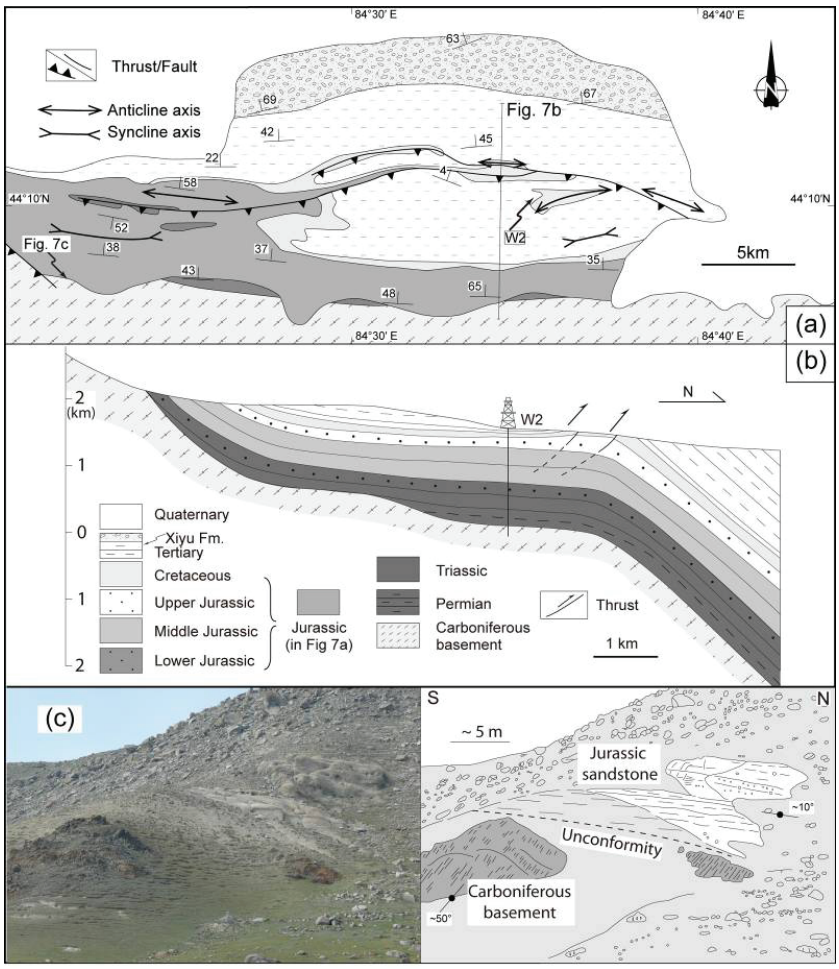

Figure 3-7. *Structural and sedimentological features of the Wusu area. (a) Simplified geological map of the Wusu area. (b) Geological cross-section constrained by field data, seismic profile and drill well W2 (location see Figure 3- 7a). (c) Picture and the corresponding field sketch of the unconformable contact between Jurassic layers and the carboniferous basement.*

There, stratification planes are markedly oblique with the top of the Paleozoic units and no deformation has been observed along this contact. In the landscape, younger Jurassic sediments progressively extend southwardly, on top of the Carboniferous units. From bottom to top, sediments progressively overlie and cover a ~150 m high drop of the basement units that was forming a relief when Jurassic sediments deposited.

To the north of the Wusu section, first order structure of the Mesozoic-Cenozoic series displays as a 40-45° north dipping monocline (Figure 3-7a, b). To the south, stratification is sub-horizontal and structure of the sedimentary series displays as a large hinge fold. As drawn on the geological map, thrust faults are observed at surface but seismic data show that these do not extend down in the Mesozoic series, which is compatible with the limited throw they display (Figure 3-7a, b). While ~400 meters of Triassic sediments have been found along a well drilled, in the basin, close to the section (see W2 on Figure 3-7a), Triassic series becomes much thinner to the south and Jurassic sandstones sometimes directly lie on top of the Carboniferous rocks thought an erosional unstrained contact (Figure 3-7c). On the map, the curvilinear shape of the outline of the top of the basement units results from their southward progressive covering by Triassic and Jurassic sediments.

3.5 Discussion and conclusions

In parallel to rather classical view of frontal forward thrust systems, this study highlights that the northern piedmont of Tian Shan is also characterized by full segments where Mesozoic series are preserved unconformably on the basement though onlap-type relationships. Such features are pointed out along two distant cross-sections and have also been clearly shown at outcrop-scale. Sedimentary breccias showing very limited transport distances have been found within Lower Jurassic sediments of the internal parts of the range. Whatever the scale, all these observations argue for the existence of proximal relieves when Triassic/Jurassic sediments deposited in this area.

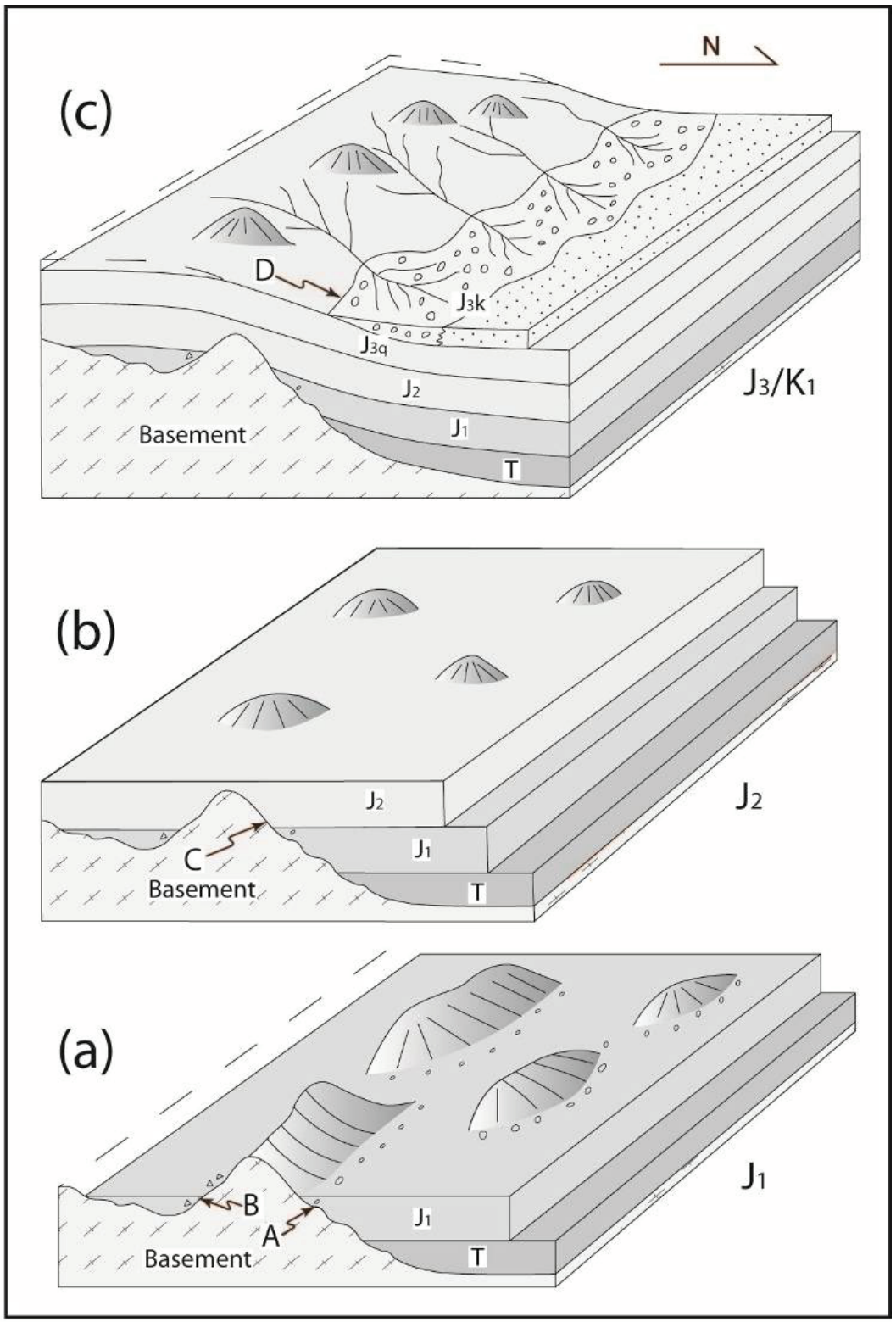

Figure 3-8. *Conceptual models of the paleo-relief evolution in the Northern piedmont of Tian Shan during the Early, Middle and Late Jurassic times. 'A' indicates the locality of Figure 3-3a; 'B' indicates Figure 3-4c; 'C' indicates Figure 3-5a-A; 'D' indicates Figure 3-3b, c.*

Our direct observations are consistent with previously published indirect ones, such as paleocurrent measurements, heavy mineral composition and sedimentological source analyseswithin sediments of the Junggar and Tarim basins show that Tian Shan could already have existed as a positive physiographic feature during Mesozoic times (Hendrix et al., 1992, Graham et al., 1993; Hendrix, 2000; Li et al., 2004).

At outcrop scale, the studied onlap architecture reveals that the paleo-altitude difference can be as important as 100-150m in a hectometer horizontal distance highlighting local steep slope see cliffs (cf. Figure 3-6c). This and the sedimentological observations within the Houxia valley suggest that small-scale ridges with intercalated intramountainous basins probably have existed during Mesozoic (Figure 3-8a).

The drill well W1 (Figure 3-4a, b) displays ~1300m of Lower Jurassic sediments. A comparable J_1 thickness has also been observed in the Manasi area, 50km west of the Hutubi section (Figure 3-2). In the southern part of the Hutubi River, the geological map shows that the Middle Jurassic directly rest unconformably onto the Carboniferous basement, with no Triassic or Lower Jurassic sediments preserved (see location A in Figure 3-4a). The thickness difference of Jurassic sediments achieves 1300 m between the location A and the drill well position, for a horizontal distance of about 50 km (Figure 3-4a). Such thicknesses difference may result from three distinct mechanisms: thermal subsidence, tectonic subsidence or relief infilling.

If considering thermal subsidence, the latest regional tectono-magmatic event occurring before Mesozoic is dated around 240 Ma (Han et al., 1999), which is about 100 Ma earlier than Jurassic sedimentation. Moreover, wavelength of the subsidence, as highlighted by the altitude difference calculation, is not large enough to be properly explained by a thermal type subsidence. Therefore, following Hendrix et al. (1992) it seems that thermal driving mechanism for Early and Middle Jurassic subsidence may play a weak role for the Jurassic sedimentation. If considering tectonic subsidence, as described above, Jurassic strata often overlie directly on Carboniferous by onlap, without fault or others syn-sedimentary deformations observed. Seismic profiles

across the southern margin of the Junggar basin do not show any fault controlling sedimentation for the Early Jurassic period (Allen et al., 1991; Wang et al., 2005). Furthermore, compressional flexure subsidence may also be negligible as lithosphere buckling process would result in much larger wavelength (~100 km) than observed in this study (~50 km). Finally, in the Kuqa sub-basin, south of the Tian Shan, mineralogical maturities of conglomerate and sandstone increase from Triassic to Middle Jurassic (Li et al., 2004; 2010), indicating that the tectonics is relatively calm at that time. In other words, Jurassic sedimentation could not be considered as controlled by tectonic processes across northern Tian Shan.

Accordingly, the 1300m thickness difference may be principally produced by infilling of a relatively high lasting relief of ~1300 m high in this region, during Triassic/early Jurassic times (Figure 3-8a). During Middle Jurassic times, finer grained sediments conformably deposited on top of the Lower Jurassic strata, within the basin, and deposited onlap of the Paleozoic basement toward the mountain interior (Figure 3-5a and Figure 3-8b). Middle Jurassic sediments extend to a larger area with respect to the Lower Jurassic and the paleo-relief lateral extension was certainly less important during Middle Jurassic than during Triassic/Early Jurassic (Figure 3-8b). During uppermost Jurassic to Lower Cretaceous, conglomerates and breccias deposited onto the Middle Jurassic sediments with a weak angular discordance. These conglomerates are geographically confined along the front of Tian Shan and this particular formation becomes finer toward the basin. This behaves as very thick alluvial fans deposited down of a major relief rising to the south, as the ones currently deposited along the modern Tian Shan range, with limited northward transport of sediments (Figure 3-8c). This uplifting movement is also recorded by AFT chronology studies: fission-track modeling indicates ca. 160 and 120 Ma cooling age along a Dushanzi-Kuqa corridor, in the mountain interior (Dumitru et al., 2001). Apatite sampled from Bayanbulak in the northern part yield the earliest cooling ages of Early Cretaceous (Dumitru et al., 2001; Wang et al., 2009). Finally, the main morphological front of the current Tian Shan range would correspond to an ancient

one that might be stable from early Cretaceous.

Results from this study show that the topography of the current Tian Shan can probably not be considered only as the consequence of the Cenozoic intracontinental reactivation alone. Physiography of the range actually results from a combination of Cenozoic deformations superimposed on a reminiscent Mesozoic paleo-range. These new results question on the total amplitude of the movements along the northern front structures that could be attributed to the Cenozoic India-Asia collision.

Chapter 4

Structural pattern along the northern piedmont of Tian Shan

In the previous chapter, field observations and geological maps evidence that a significant relief existed, during Mesozoic times, through northern Tian Shan. Such a paleo-relief has probably significantly contributed to the presently observed topography of the Tian Shan range; in other words, the Mesozoic relief influence cannot be ignored when considering the morphologic and tectonic evolution when Cenozoic reactivation occurred. As the whole present day topography can not be solely attributed to Cenozoic tectonic history, our observations and interpretations also imply that the Cenozoic deformation along Tian Shan front may be less important than what has been estimated in previous studies (Avouac et al., 1993; Burchfiel et al., 1999).

In northern Tian Shan region, most of the structural analyses have been performed within the folded and thrusted foreland Junggar basin and the "front" contact zone in-between basement Paleozoic units and Mesozoic to Cenozoic sedimentary series has only been poorly studied. As shown by seismic activity (Figure 2-9) modern deformation likely concentrates along this front of the range. On another hand, our new field observations, has presented in chapter 3, highlight unconformity structures, in some places of the range front, with a strict structural prolongation of sedimentary layers from basin to more internal parts of the range onward. This suggests only limited movement along this zone. In order to clarify this point and misunderstanding, detailed geological observations have been made on the contact between the range basement and basin cover along the northern front of Tian Shan (Figure 4-1). Mesozoic sediments are widely exposed and the Jurassic to Cretaceous strata, in particular, make very good markers for qualifying and quantifying post-Mesozoic deformations. The structural analysis which is presented in this chapter has been applied thanks to several river valleys crossing the contact zone of the northern front of Tian Shan and, also, thanks to newly open roads which facilitate access and rather continuous observations of outcrops from west of Wusu to the east of Urumqi (Figure 4-1a). Structural field work has been performed during three field trips (Sept.-Oct. 2007, 2008, 2009) and more than 800 outcrops have been visited

(Figure 4-1).

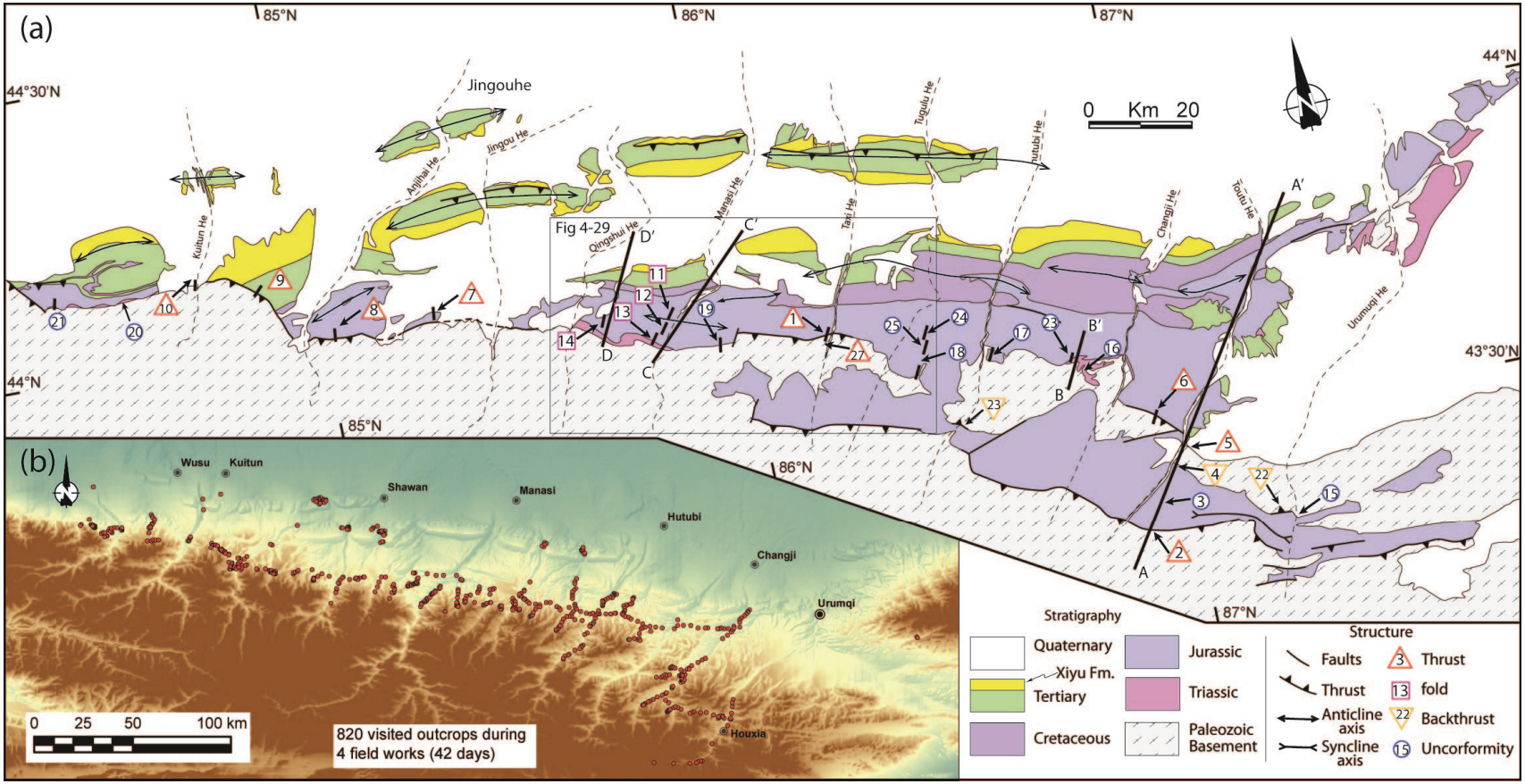

Figure 4-1. *Geological map of the northern piedmont of Tian Shan with locations of field observations along the front. The upper map (a) shows the observed locations of cross-sections and outcrops (modified after He et al., 2005). Red triangles with numbers: thrust contact outcrops, purple squares: fold-type contact outcrops, orange reversed triangle: backthrusts in the mountain and blue circles: unconformity contact between range basement and basin sediments. All the numbers will be found in the pictures displayed and presented in this chapter.Lower framed map (b) is the DEM of the northern piedmont of Tian Shan with red circles points indicating 820 visited outcrops during 3 field trips.*

As detailed below, rather classical forward thrusts have been identified for some segments of the piedmont, delineating the boundary between the uplifted basement units and the relatively subsiding proximal foreland basin.

On the contrary, for other segments, Mesozoic series display as structural continuous layers from basin to higher parts of the range, showing regional scale unconformity on top of the Paleozoic basement units. Synthesizing the numerous structural observations made during this work, four types of contact can be drawn along the northern front of Tian Shan: thrust, unconformity, large fold and backthrust types. Based on the most representative and the most comprehensive data that could be used among hundreds observation points, sections corresponding to each one of these types of contact are detailed and interpreted in the following four parts of this chapter.

4.1 Thrust contact

Thrust type contacts have been observed in several localities and are presented in detail, as follows. These observations are located along rivers flowing down the mountain: Taxi He, Toutoun He and its western sector, Anjihai He, Jingou He, Kuitun He and its eastern section (Figure 4-1).

4.1.1 Taxi He

The southern end of the Taxi He section shows a typical thrust fault between the basement and the Jurassic series of the Junggar basin (Figure 4-1 and Figure 4-2, N°1). As shown on the panoramic picture of Figure 4-3, the boundary can be easily drawn in between the Paleozoic basement, to the south and the Jurassic basin sediments, to the north. From north to south, the roughly east striking Jurassic strata become steeper (from 30° north to vertical), and even overturned (55° south) close to the Carboniferous basement rocks. This fan shape like structure is preserved for a horizontal distance of about 500 to 1000 meters.

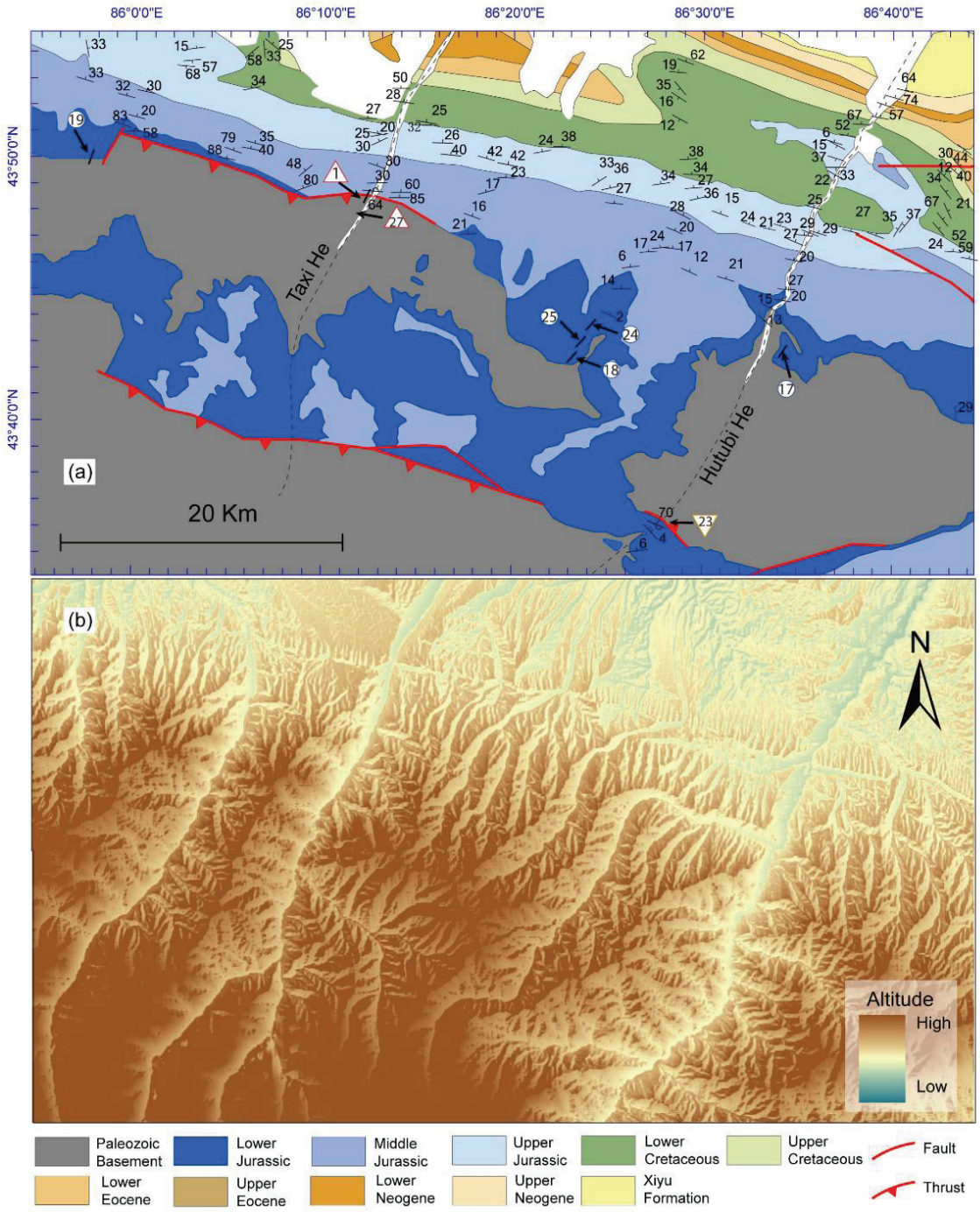

Figure 4-2. *(a) Geological map (b) DEM of the Taxi He and Hutubi He area.*

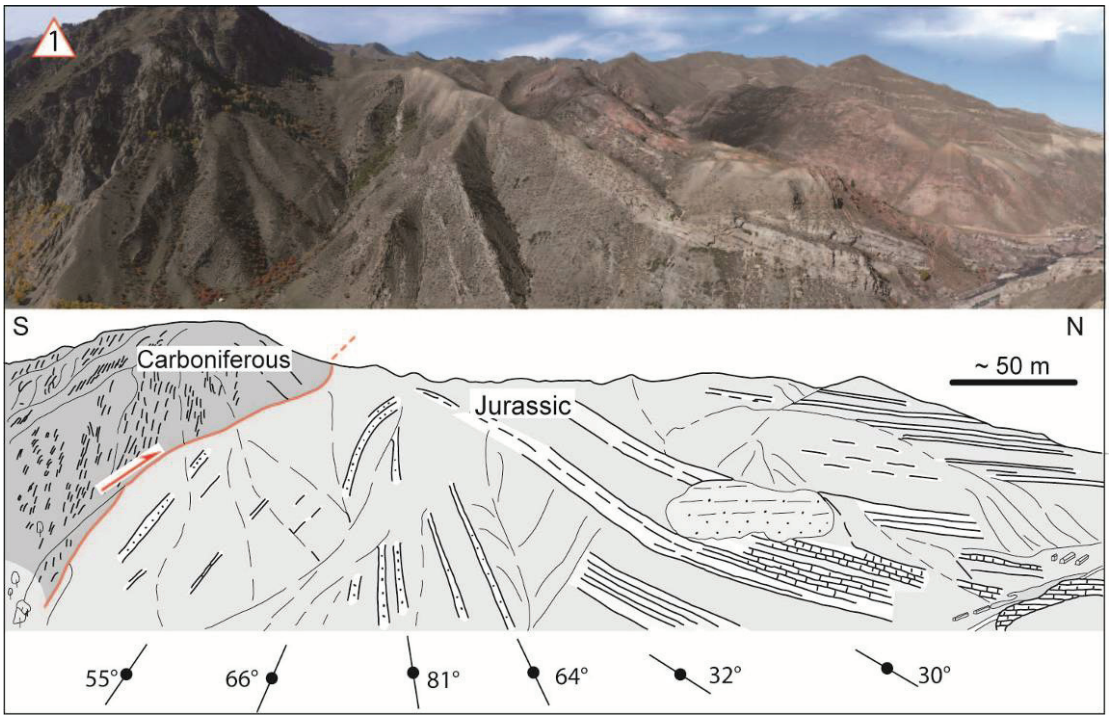

Figure 4-3. *The Carboniferous basement thrusts onto the Jurassic series. The dip angles of Jurassic sediment strata are overturned adjacent to the basement, to the south.*

Here, the structure exposed along the Taxi He section obviously shows deformation associated with the development of a forward, south directed thrust of the basement units on the foreland basin domain. The particular structure within the sedimentary series suggests a significant net slip associated with. However, the deep structure along such a thrust fault contact can be questioned. If considering overturned series in front of the thrust, two alternative models could be proposed for the kilometer-scale structure in this contact zone. In the first model, a concentric type folding is considered with the sedimentary series keeping parallel strata under and adjacent to the thrust fault (Figure 4-4a). In contrast, a second model type shows a similar fold type development in front of the thrust, with thickening of the layer strata in the hinge and thinning in the limb, along the adjacent thrust fault (Figure 4-4b). The first type model is typical of nappes stacking and implies much more net slip than for the second model type. As shown on our structural interpretation (Figure 4-4b),

the Taxi He section displays clear variable Jurassic sediment thickness adjacent to the thrust fault, which is compatible with the second model type for the deep structure of the frontal thrust contact (Figure 4-4b, c). The superficial pattern of such structure within the sediment strata (Figure 4-4c) has been observed along several sections in front of the range and is a typical deformation pattern for this kind of front contact in north Tian Shan. This will be detailed and discussed below.

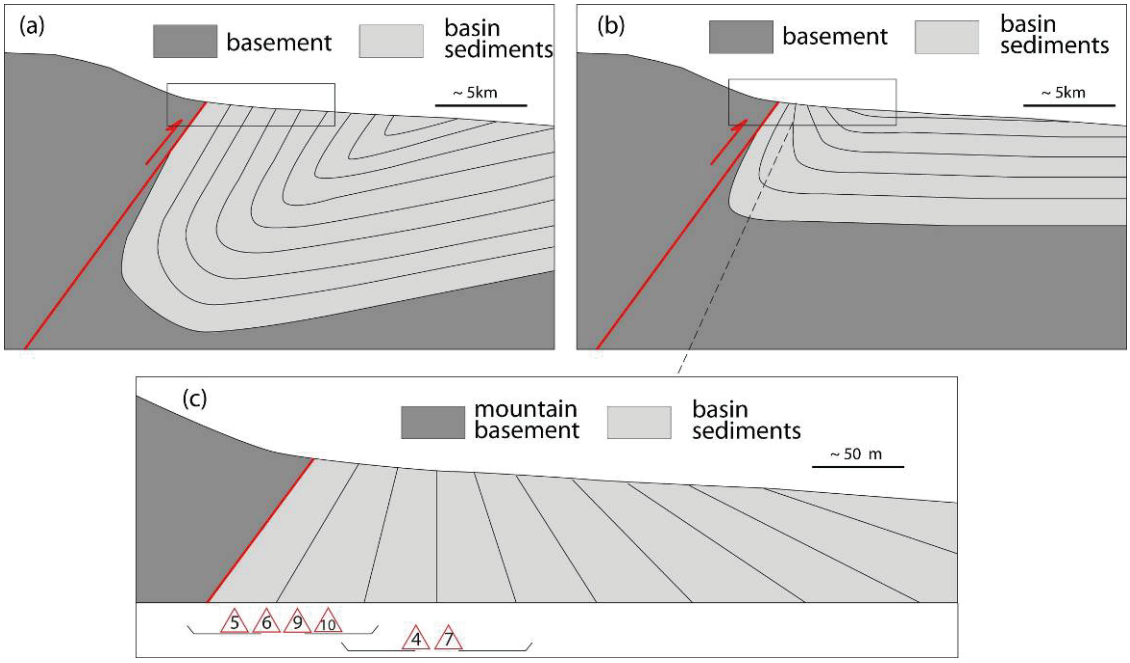

Figure 4-4. *Deep structure of a range basement thrusting on a basin sediment cover. (a). In the first model, the frontal sedimentary series keeps parallel strata under the thrust and adjacent to it, (b) the second model type displays variable thickness of strata, thicker in the drag fold axis area and thinner in the limb, close and along the thrust fault. (c) Close-up on the surface structure of the second model (b), which is displayed by several examples along the northern Tian Shan front. Numbers refer to locations where such deformation pattern has been observed (see Figure 4-1a and 4-2 for location).*

4.1.2 Toutun He West

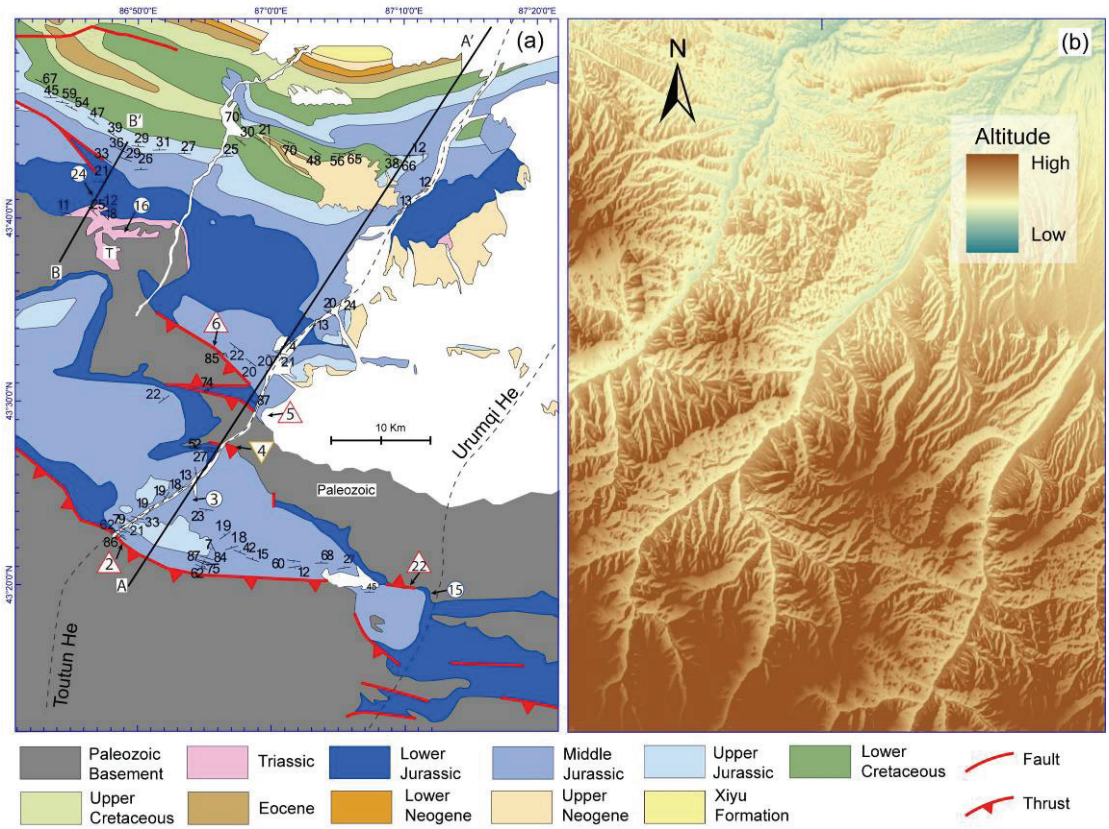

Figure 4-5. *(a) Geological map (b) DEM of the Toutun He and Urumqi He area.*

This section is located about 5 km west of the Toutun He valley (Figure 4-1, Figure 4-5, N°6). In its middle segment, this section displays a sharp and straighten up contact in-between the Paleozoic rock units, to the south, and the Mesozoic sediments, to the north (Figure 4-6a). To its southernmost part, Paleozoic rocks are well layered Carboniferous turbidites with no or only limited deformation observed (Figure 4-6a and b). When approaching the contact, these sediments become deformed with cleavage and associated shear planes developed inside. These planes form sigmoid-shapes indicating top to the north shearing within this contact zone (Figure 4-6c and e).

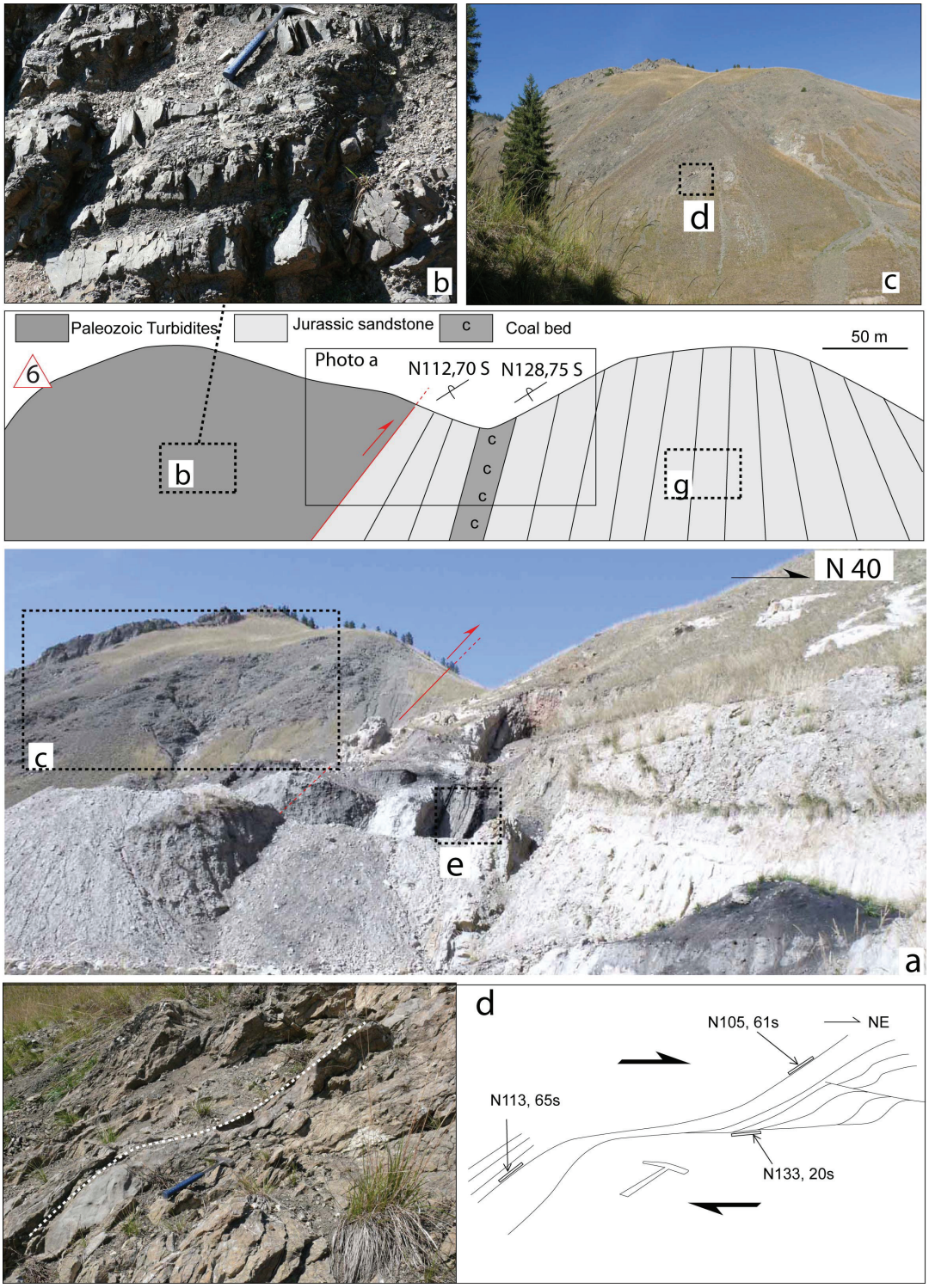

Figure 4-6. *Structural analysis along the "west" Toutun He section. (a) Panoramic view of the section, (b) undeformed Carboniferous turbidites of the basement units, (c) and (d)different scaled pictures and drawings of the ductilely deformed basement rocks, along the thrust zone, (f) overturned Jurassic sandstone evidenced by crossbeding geometry, (g) straighten up sheared coal bed.*

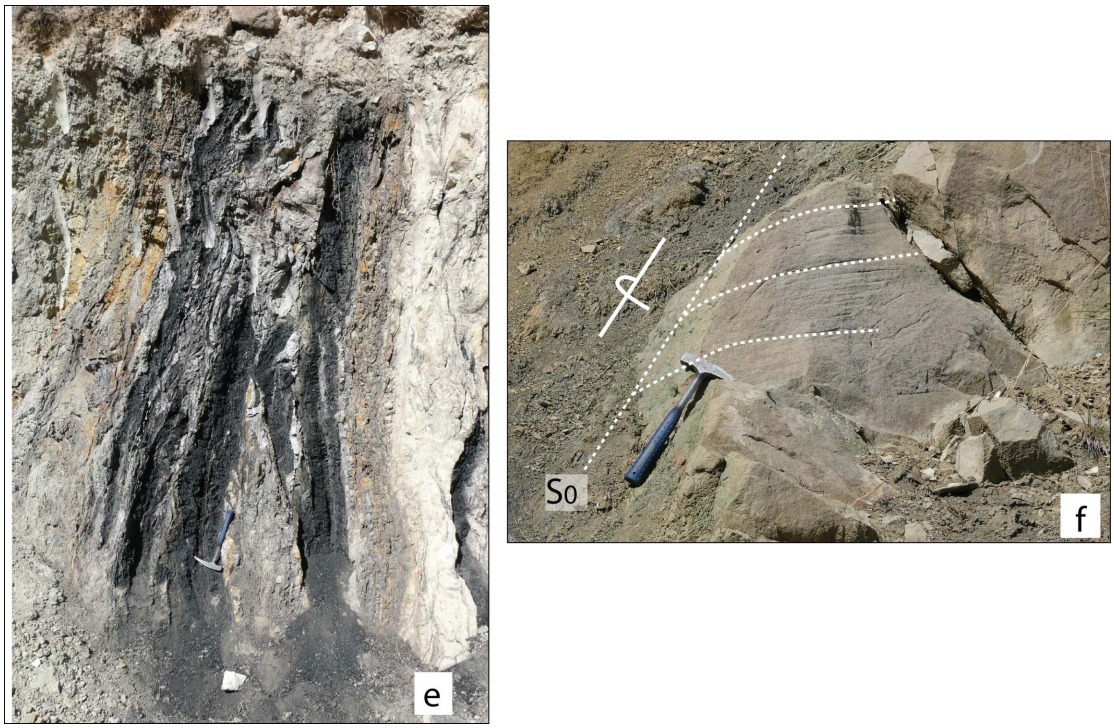

Figure 4-6 (Continued)

Due to a topographic depression formed in the landscape, the Paleozoic/Mesozoic contact is only poorly exposed along the section but scarce outcrops display highly brecciated rocks. Northeast, close to the contact, Jurassic sandstone and conglomerate layers display straighten up stratification planes, along ~300m long, and clear overturning as evidenced by cross-bedding attitude within thick sandstone layers (Figure 4-6f). Northward, beyond limits of the section presented here, the bedding progressively flattened within this series, displaying "fan like" geometry. Here again, the "west" Toutoun He section highlight a clear north- to northeastward thrusting of Paleozoic basement units on Mesozoic sedimentary series (cf. Figure 4-1. and Figure 4-5). Hence, the thrust contact can be well characterized here: it is in fact composed of a ~50m thick deformation band with development of rather "cold" ductile structures within the upper basement unit to more brittle type ones toward lower unit.

Moreover, several coal beds are interstratified in between coarse grain white/yellow-colored Jurassic sandstones for a ~5m cumulated thickness (Figure 4-6a). Coal display strong breccias and cleavage planes developed (Figure 4-6e) while on both sides, Jurassic clastic layers are not deformed at all (Figure 4-6a and f). This

deformation analysis is well compatible with the model of similar/drag fold presented on Figure 4-6c; the contrasted mechanical behavior of sedimentary layers allows the development of internal décollements necessary to form similar folds, in front of the thrust, within the Jurassic series.

4.1.3 Toutun He

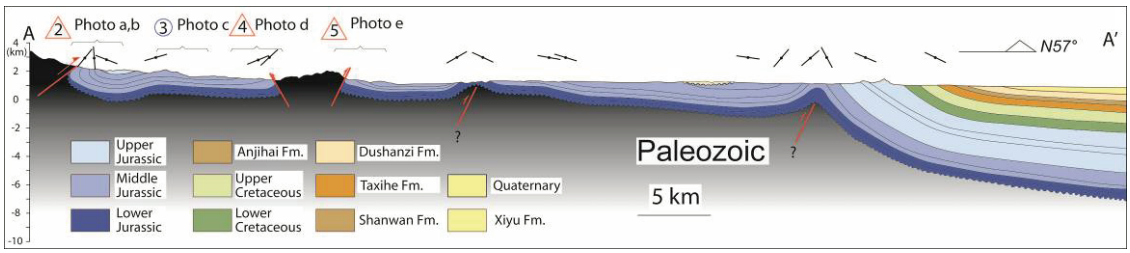

Figure 4-7. *Geological cross section of the Toutun He based on the geological observations. Bar symbols on the top of the section indicate the dip direction. See photos in Figure 4-8. Continued.8 for 2 to 5 and Figure 4-1 for the section location*.

The Toutun He flows about 20 km west of Urumqi and trends North-South parallel to the Urumqi He (N° 2 to 5, *Figure 4-1* and Figure 4-5). Lower- to Upper-Jurassic series are widely exposed all along this section. At first order, layers display as sub-horizontal ones to gentle upright open folds, which explains how the sedimentary layers of the same age could be observed and followed along tens of kilometers in this particular sector of the north piedmont (Figure 4-7 and Figure 4-5). This section also exposes several contacts in-between Mesozoic sediments and Paleozoic basement units. Contact studied to the southernmost end of the section looks sharp and upright even if not strictly exposed there (Figure 4-8a).

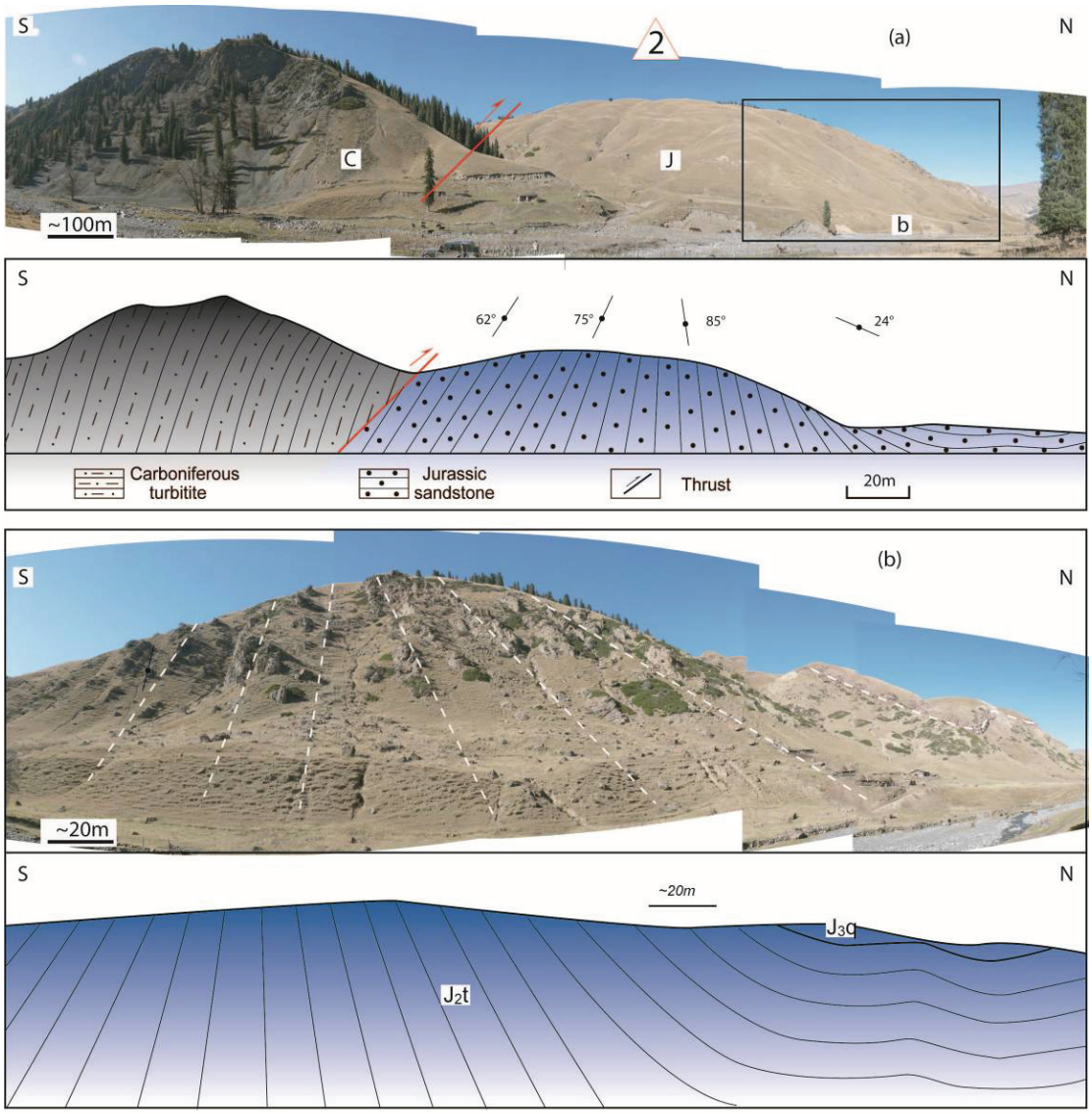

Figure 4-8. *Pictures of several outcrops all along the Toutoun He and the corresponding interpretation drawings. (a) Carboniferous basement thrusts northwards onto the Jurassic deposits, (b) deformed Jurassic series showing steep dip angle to overturned stratification planes, (c) horizontal Jurassic deposits resting on the basement rocks and showing neither internal deformation nor basal décollement, (d) backthrust within the mountain internal parts at the southern margin of a basement "pop-up", (e) tectonic breccias along the northern boundary of the basement "pop-up". See* ***错误！未找到引用源。*** *locations in Figure 4-7.*

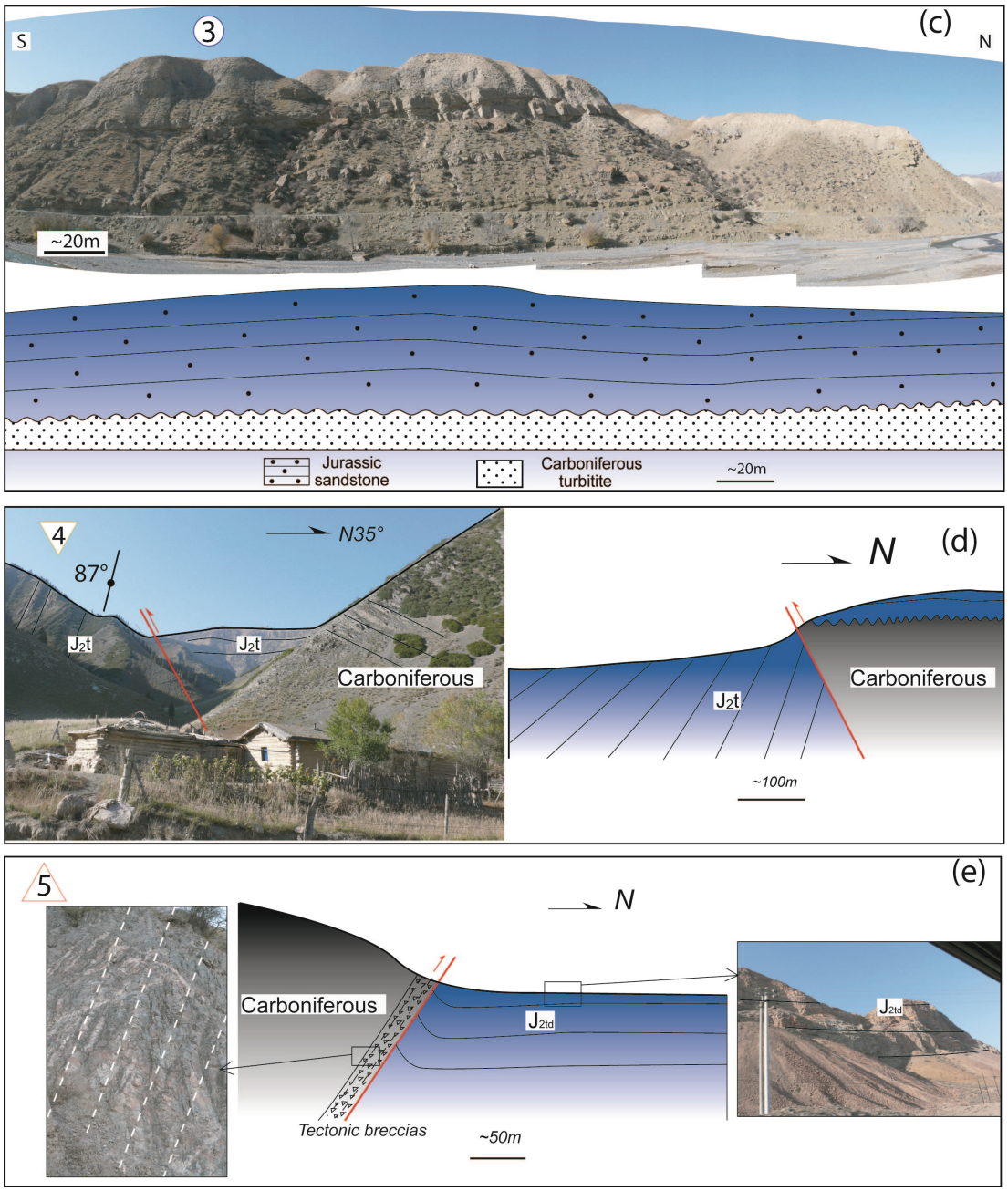

Figure 4-8. *Continued.*

However, Jurassic sediments show local vertical to overturned strata just north of the contact zone (Figure 4-8. *Continued.*8a and b) while bedding progressively flatten northward to become horizontal few kilometers north of the contact (Figure 4-8. *Continued.*8c and see n°3 on Fig.4-1a). The deformed zone which extends 1 to 2 kilometers north of the Paleozoic rocks and, in particular, the straightening up and overturning of Jurassic sedimentary layers close to the contact argue for a thrust movement developed along this southernmost extension boundary of Jurassic

sediments (see Figure 4-1). Forming local summits, Paleozoic units also outcrop at about one third south of the Toutoun He section on about 5 km long (Figure 4-5 and Figure 4-7). Here again, the Jurassic strata becomes steeper on both sides of the basement. Along the northern contact, tectonic breccias in a ~30m thick deformation band were observed in the basement turbidites (Figure 4-8. *Continued.*8d) and this kilometer scale structure as been analysed as a "pop-up" of basement units limited by two steep WNW striking thrust faults (Figure 4-5). As said before, the rest of the section highlights only gentle deformation within sedimentary series. Hundreds of meters north of the Paleozoic pop-up, Jurassic strata rest horizontally (Figure 4-8e).

Summarizing, the structure of the north half of the section is characterized by two principal anticlines (Figure 错误！未找到引用源。4-7): the southern one is a gentle and upright anticline with both limbs dipping about 25-30° to the north and south, respectively. The northern one is an asymmetrical one with about 40° dip angle of stratification along the southern limb and 60° in the northern limb (Figure 错误!未找到引用源。4-7). We proposed a northward thrust under the anticline developed in the Paleozoic basement (Figure 4-7).

4.1.4 Jingou He

Thanks to deep incision two major and well studied anticlines, the Anjihai (north) and Huoerguosi (south) anticlines are exposed along the Anjihai He and Jingou He (Charreau et al., 2008; Figure 4-1 and Figure 4-9). However, Quaternary alluvial terraces and loess deposits cover a large area of this studied segment of the north Tian Shan piedmont (see white color on geological map, Figure 4-9a). When accessible, stratification planes orientations have been measured along those valley. In the contact area in between the Paleozoic units and the basin series, outcrops are very scarce within the river bed of the Jingou He and the range "front" can not be directly studied there.

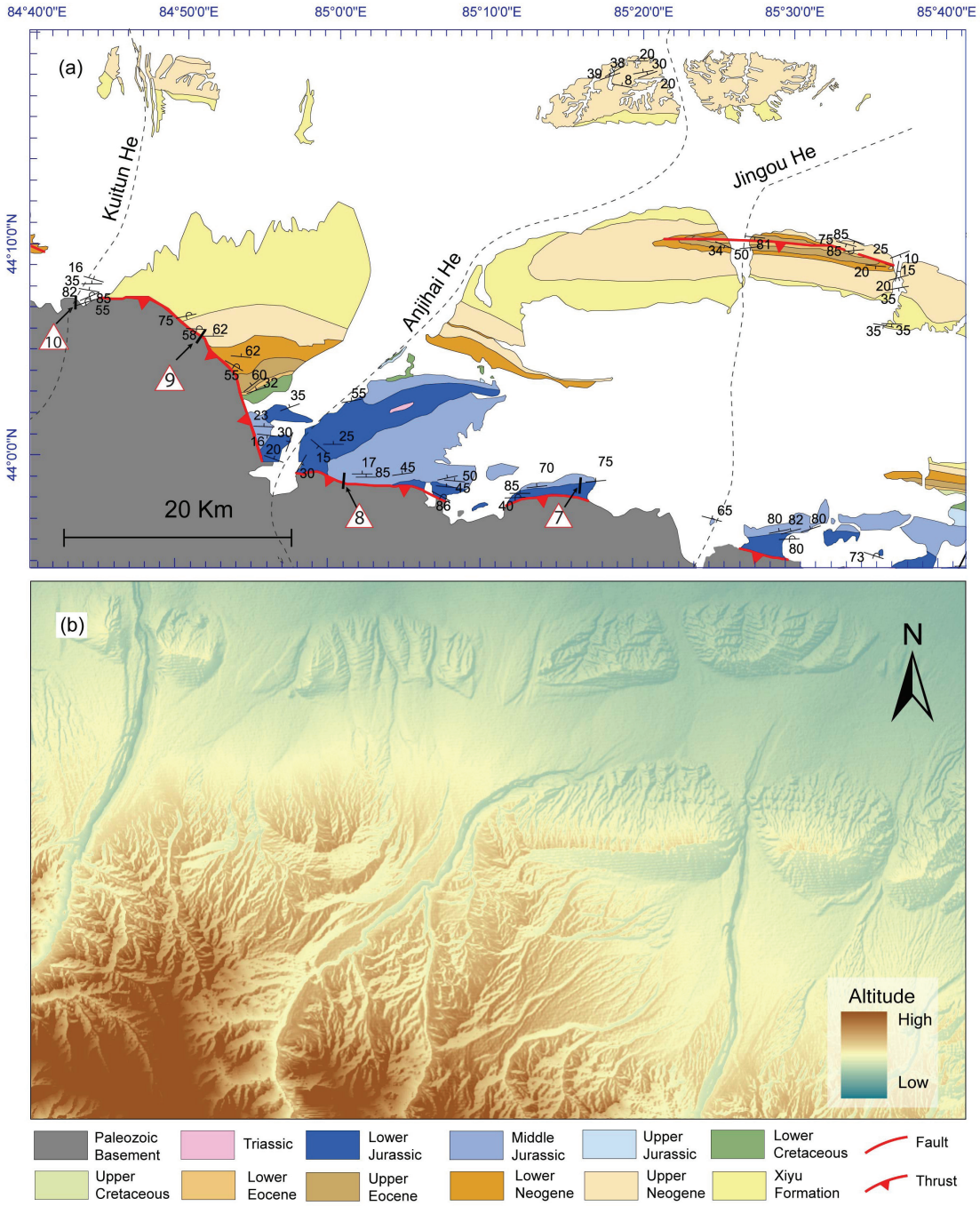

Figure 4-9. *(a) Geological map (b) DEM of the Jingou He, Anjihai He and Kuitun He area.*

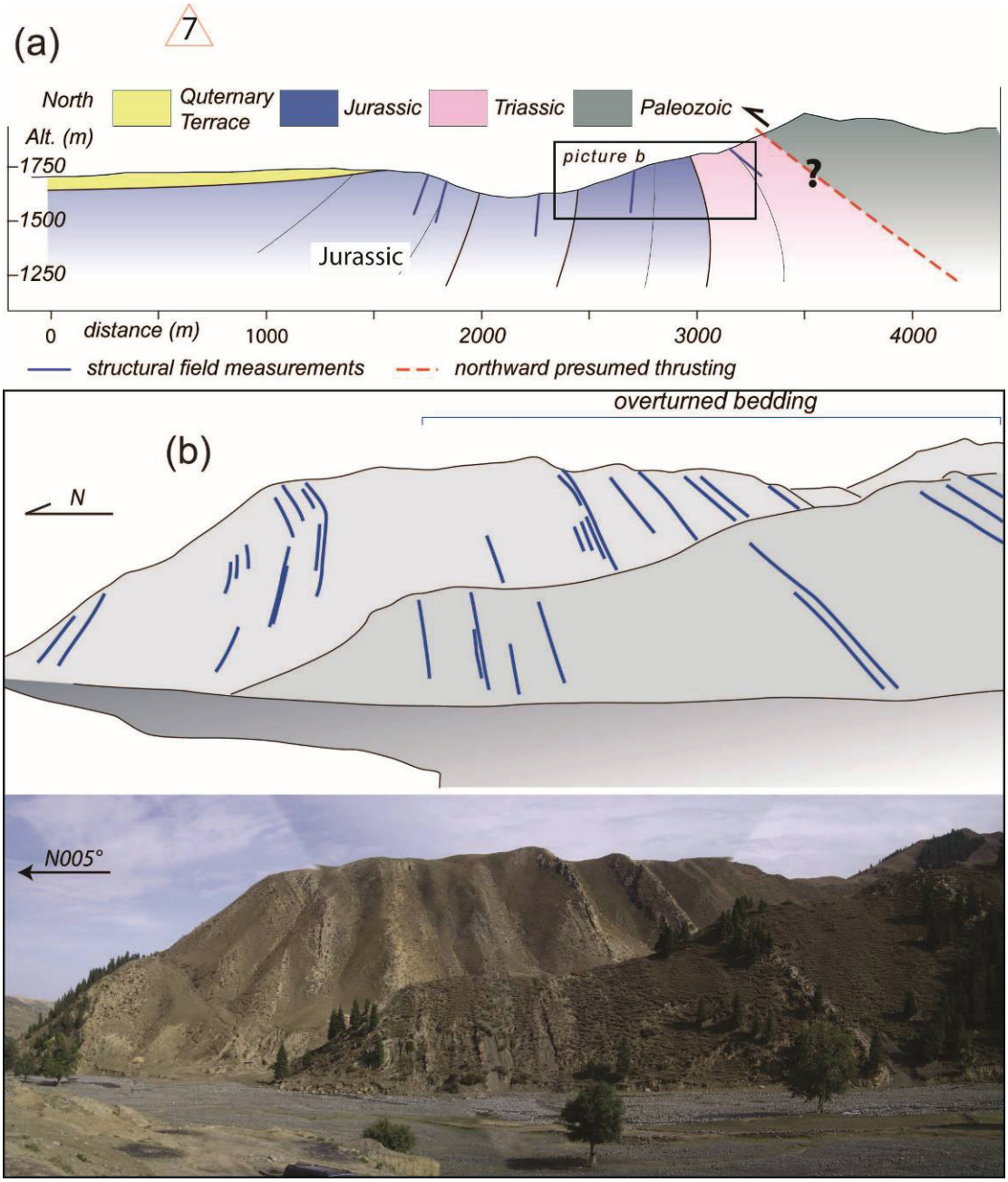

Figure 4-10. *Structure of the Jurassic and Triassic sedimentary strata of the basin along the main contact with the Paleozoic units along a N-S oriented small valley, west of the Jingou He: (a) Geological cross section and (b) field structural observations.*

However, ~10 km west to the main valley, a second order river valley allows analyzing this contact area (see N° 7 in Figure 4-1 and Figure 4-9). Along the right bank of this river, Triassic to Jurassic strata display a continuous evolution of bedding orientation from steep, north oriented dip angle, to the north, through vertical and to

overturned strata, in the southernmost part of the section (Figure 4-10). There, Jurassic series is made of a rhythmic alternation of coarse grain thick sandstone layers with shales (see differential erosion of layers on the picture of Figure 4-10b). To the south, Paleozoic meta-sedimentary units are in direct contact with an overturned thick layer of Triassic purple shales and marls. In addition, second order chevron folds can be observed within the sedimentary series as the one shown on the top hill of Figure 4-10b. These folds well underline a northward dragging of the sedimentary layers compatible with a northward thrust movement. Even not exposed, though, the front contact can be identified here as a northward thrust of the basement Paleozoic units onto Mesozoic sedimentary series; again, strata display a typical fan like type deformation in front of the thrust that can be developed in favor of the contrast in competency of the layers forming the series (cf. Figure 4-4 and discussion before).

4.1.5 Anjihai He

The Anjihai He flows north-northeast in the eastern part of the studied area (Figure 4-1). The contact area in-between basement rock units and foreland sedimentary basin is marked by a strong slope break of the topography (Figure 4-9, N°8). Close to the contact, the western side of the valley highlight a dragging type structure within the Jurassic sediments: bedding dip angles increase rapidly from basin toward the northern boundary of the basement, on about 1.5 km distance along the section (Figure 4-9). The sharp and straight contact in-between the basement rocks and the Mesozoic sediments combined with the internal deformation of the strata most probably result from a northward thrusting of the Paleozoic units (Figure 4-11). On the other hand, the east bank section display a similar dragging structure of the Jurassic strata showing a continuous increase of the bedding dip angle, from north to south (Figure 4-11, bottom). It must be pointed out here that i) both pictures/drawings have been strictly made perpendicular with the bedding ~east striking direction and ii) both valley sides display the same segment of the Jurassic sedimentary section which mean that one section, as illustrated on Figure 4-11, is expected to be the strict lateral

prolongation of the other one. However, both sections do not exactly display the same structure as, along strike of the sedimentary layers, bedding systematically dips more along the western bank than along the eastern one (compare the two pictures and drawings of Figure 4-11). To be more precise, structures are in fact comparable on both sides of the valley but do not present the same amplitude in their development. Finally, the thrust occurring in-between basement and sedimentary rocks as identified along the western bank (see above) do neither extend further east; the basement/sedimentary rocks contact is mapped a few hundred meters further south along the eastern bank section and is not visible on the corresponding picture of Figure 4-11.

The Anjihai He section displays a dragging type structure, as presented on Figure 4-4b and c, within the Jurassic sedimentary series and this can be regarded as resulting from a forward thrust developed in front of the uprising basement units of the range. The particularity of the Anjihai He section is that the structure is not cylindrical at local scale. Thrust fault map trace as well as the bedding attitude can not be extended from one side to the other of this ~north oriented valley. As far as the valley is only ~500 m wide, it seems difficult to envisage a continuous transition from one side to the other; better, a strike slip fault must have developed perpendicularly with the thrust contact and sub-parallel with the local principal shortening direction, acting as a small transform zone during deformation in front of the range (Figure 4-12). Nowadays, the trace of this right lateral transform fault does correspond to the one of the river bed and/or associated terraces. Such structural local observations can highlight modes of deformation within the specific segments of the piedmont where frontal forward thrust display curved shape at map scale.

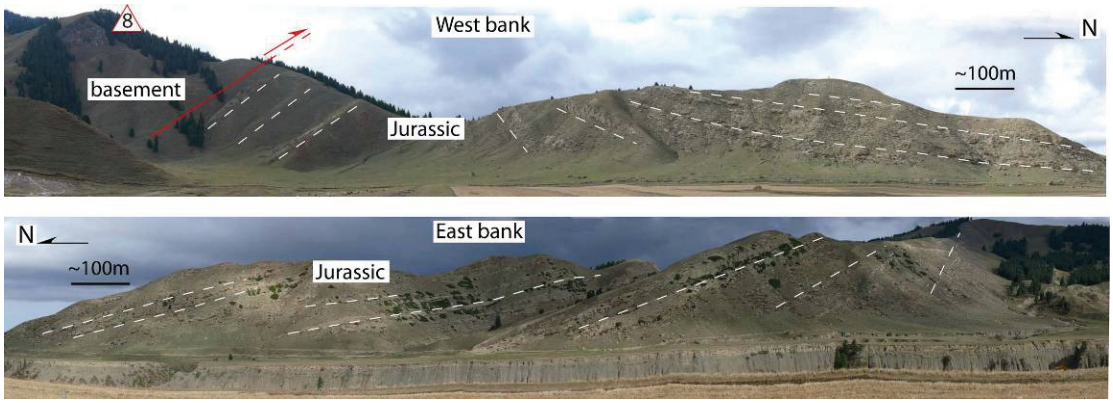

Figure 4-11. *Panoramic views of the Anjihai He banks. Along the western bank (top picture) the Jurassic strata displays as a "fan like" type structure; on about 1.5 km long, gently northward dipping bedding become vertical and even overturned close to the contact with basement units. The eastern bank of Anjihai He (bottom picture) displays a similar and compatible structure within the Jurassic sediments. Pictures have been made perpendicularly to the strike of the bedding orientation and both correspond to the same section segment within the stratigraphic column; note that, however, the two banks do not display strictly the same structural pattern.*

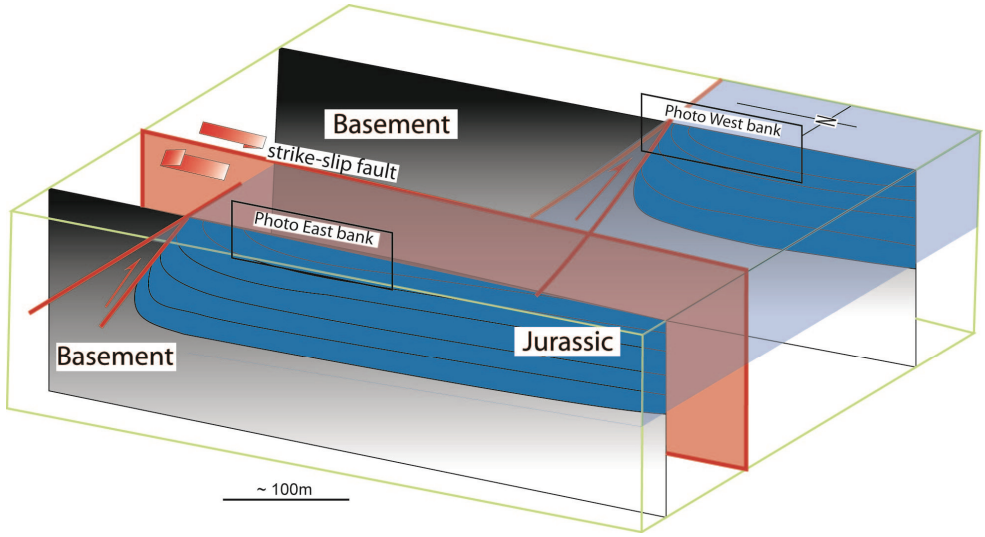

Figure 4-12. *Block-diagram illustrating the structural pattern within the Anjihai He valley, in the contact area in-between the basement units, to the south, and the Jurassic sediment, to the north. A strike-slip transform fault developed in-between the western and eastern bank, perpendicular with the structures (i.e. main thrust and associated drag fold structure, in front of this one). See* ***错误！未找到引用源。*** *for the corresponding photographs and interpretation drawings.*

4.1.6 Kuitun He

In the area comprised in-between the Kuitun and the Anjihai rivers, the contact between the Paleozoic basement units and the basin sediments displays a great northward convex arc shape in map view (Figure 4-9). Going from south-southeast to north-northwest along this front, Paleozoic rock units are observed in contact with sediments of younger and younger age, from lower Jurassic to upper Neogene series, as clearly shown on the geological map (Figure 4-9). Field structural measurements highlight overturning of the sedimentary layers in several locations, all along and just at the contact with Paleozoic rocks (Figure 4-9). Moreover, note that, along this peculiar arc shape in front of the basement units, the bedding measurements strike oblique to the map direction of the contact (Figure 4-9).

The first structural observations detailed here for this sector are located at mid distance in-between the Kuitun and Anjihai rivers (13 km east of Kuitun He, N°9 in Figure 4-1 and Figure 4-9). Strictly speaking, the contact between the Paleozoic basement rocks and the sediments is not outcropping there but the contact area displays as a rather thin corridor with a steep attitude (Figure 4-13). The Tertiary green shale of the Taxihe formation is overturned along the contact itself (see southward dipping layers on Figure 4-13) and the red shale and silt clastic sediments of the Dushanzi formation steeply dips to the north (see measurements displayed on Figure 4-9 for this particular location) which, once again, is compatible with a northward thrusting of the basement on the basin sedimentary series. As said before, it must be pointed out that bedding planes strike N90° while the thrust contact at the base of the basement units strikes ~southeast.

Figure 4-13. *Northward thrusting of the Paleozoic basement on Cenozoic sediments observed ~13km east of the Kuitun river, along the northern front of the Tian Shan.*

In the same area, geological observations have also been carried out along the Kuitun He valley. In the basin, the Northern part of this section exposes the Dushanzi anticline which has been already extensively studied (Charreau et al., 2005; He et al., 2005) and which belongs to the third and more external belt of the northern Tian Shan piedmont (N°10 in (Figure 4-1 and Figure 4-9). At front of the mountain green–brown-colored upper Neogene taxi He fromation mudstone layers are straightened up and overturned along the contact with basement Carboniferous turbidites (Figure 4-14). Few hundreds meters north of the contact, toward the basin, Tertiary series displays normal strata (Figure 4-14) and bedding becomes even horizontal about 1 to 2 km apart from this studied location. Note that thick dark and coarse conglomerates of the Xiyu formation rest horizontally on top of the straight Neogene series, with a clear angular unconformity surface at the base (see Figure 4-14 and geological map on Figure 4-9). This geometrical configuration shows that Cenozoic thrusting and associated deformation in front of the range must have occurred before the local age for onset of the Xiyu formation deposit.

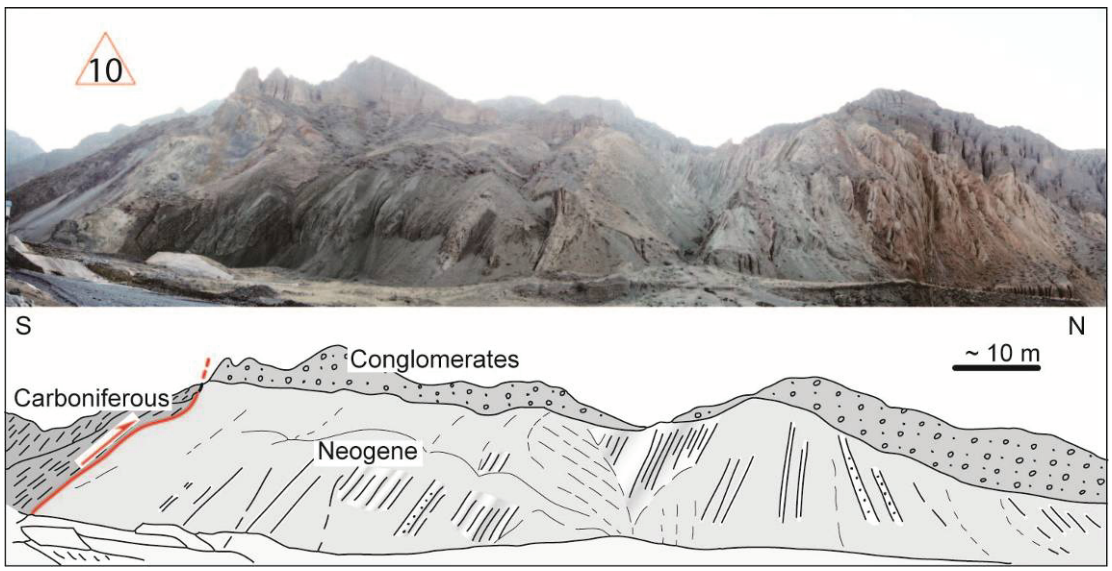

Figure 4-14. *Carboniferous basement turibidites thrusting onto Neogene sediments along the Kuitun river. Close to the contact, basin sedimentary strata are overturned and progressively flatten northward.*

4.2 Unconformity contact

As detailed in the first part of this chapter, forward thrusting of Paleozoic basement has been observed at numerous locations along the northern Piedmont of the Tian Shan range. This systematic northward thrusting is associated with the development of large-scale drag folds which results in “fan like” type typical structures within the underlying sedimentary series of the Jungar basin (see Figure 4-4 and the relative discussion in the text). Most of such northward thrusting has been observed at the boundary contact in-between Paleozoic rocks and sediments of Jurassic age but certain front geometrical configurations, like the “arc” shape in the Kuitun/Anjihai He area, display younger sediments of the basin in direct thrust contact with the basement. As shown before, clastic sedimentary series are composed of alternations of rather coarse grained and thick sandstone and conglomerate layers with shale and/or marls sediments. Such layering configuration and competency contrast certainly allows the initiation and amplification of the “drag folds” structures in the sedimentary series, below the thrust contact. Finally, all of the sections presented before show rather steep dipping of the thrusts (45° to 60°), either as directly displayed in the field or as can be deduced from section construction and deformation analysis within sediments. From our field work, northward thrusting has been locally evidenced all along the northern front zone of the range, i.e. from west to east, at locations N°: 10, 9, 8, 7, 1, 6, 5 and 2.

Yet, along the northern front of Tian Shan, the sedimentary series of the basin are not always thrusted by the range basement as described above. In some valleys, the Jurassic series can be continuously followed from the basin to the mountain interior. The Jurassic sediments are unconformably deposited and preserved on top of the range basement, in the contact zone. During our field work, such configuration has been analyzed at several locations (cf. Figure 4-1) and examples of unconformity type contact between basement units and sedimentary series of the Jungar basin will be illustrated, along different studied sections or locations, as follows.

4.2.1 Houxia east

The Houxia valley is an east striking small valley located close to the Urumqi He valley, in the southern part of the map of the studied area (Figure 4-1 and Figure 4-5, N°15). There, a thick series of Jurassic detrital sediments is preserved at rather high altitude within internal parts of the range (Figure 4-5). The northern boundary contact of this Jurassic small "basin" is pretty well exposed along the western side of the main Urumqi He valley (Figure 4-15). While Carboniferous metamorphic rocks display steep ancient fabric, the Jurassic sedimentary layers are only slightly tilted to the south (Figure 4-15). The interpreted picture of Figure 4-16 shows a clear unconformable stratigraphic contact in-between the Jurassic series and the underlying Carboniferous basement units. Here, the unconformity contact presents an orientation roughly parallel to the one of the bedding within the Jurassic sedimentary pile (Figure 4-15).

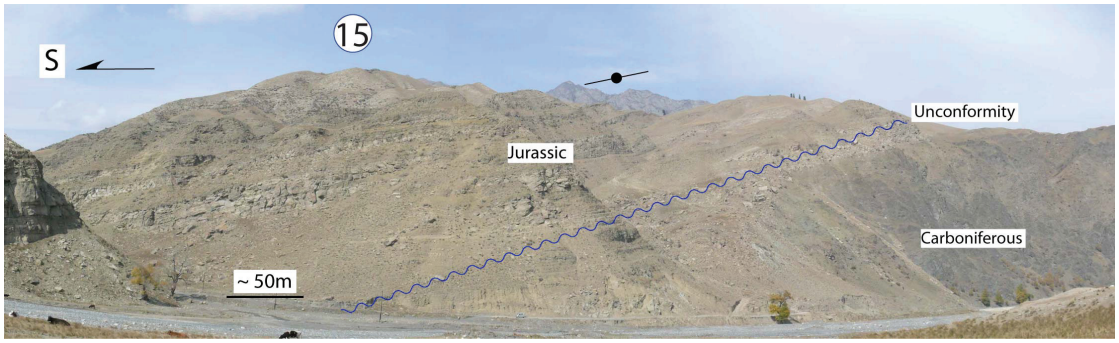

Figure 4-15. *Jurassic sediments unconformably deposited on top of the Carboniferous basement rocks at the northern margin of the Houxia basin preserved at rather high altitude within the range interiors.*

4.2.2 Changji He

This section is located ~20 km west to the Toutun He (Figure 4-1, N°16). In the geological map, along the northern contact zone between the Jurassic sediments and the Paleozoic basement, Triassic sediment specially outcrop in this area (Figure 4-5, N°16). In this piedmont area, the Jurassic sequences dip northwards stably with about

20-30° (Figure 4-5). In the field observation to the south, typical purple Triassic mudstone layers outcrop along a small valley (Figure 1-13). The dip-angle is about 20° towards northeast, which is different general east-west trending direction in the basin sediments. Its gentle dip-angle and the direction indicate the Triassic here seems weakly deformed during Cenozoic (Figure 4-16).

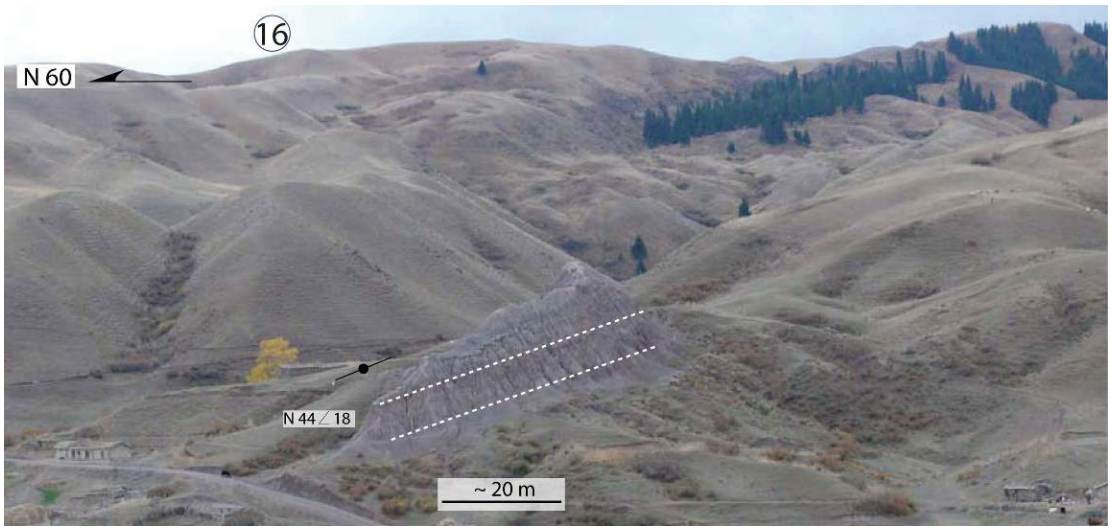

Figure 4-16. *Purple Triassic sediments with northeastward gentle dip angle in the contact area between the Paleozoic basement and the Mesozoic basin sediments. The location of photo 16 see Figure 4-17 and Figure 4-5.*

In the section scale (Figure 4-17), Paleozoic basement locate to south of the Triassic sequences. Our field work and the geological map show not obvious structure deformation between the Mesozoic sediments and the Paleozoic basement. North basinward, the dipping-angles of the Mesozoic series increase slowly northwards and form a kink fold near the Cretaceous series. If the thrust front in the northern Tiansahn prolong parallels along the mountain strike from Jingou He and Taxi He to this section (Figure 4-1), the "front" along this section is characterized by an unconformity without obvious structure deformation (Figure 4-17). This section suggests that the contact zone between the basement and the basin are not continuously separated by an obvious thrust fault.

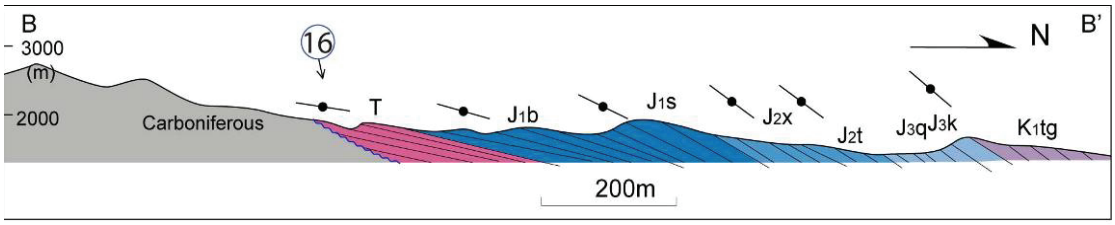

Figure 4-17. *Geological cross-section along the valley of the Chanji He. Location see Figure 4-1 and Figure 4-5.*

4.2.3 Hutubi He

The detailed structural observations along Hutubi He valley has been described in Chapter 3. This river flows down from the southern mountain and through the Hutubi city to the north (Figure 4-1 and Figure 4-2). Along this river, the northern sediments form an anticline, where the core consists of Middle-Lower Jurassic. Its southern limb dips 20-30 ° southwards, while the dipping-angle of the northern limb is gentle close the core and increase to ~60° within the Cenozoic series. This asymmetric geometry probably indicates the northern-propagation thrust fault in of the basement (Burchfiel et al., 1999). To south of this anticline, a paired syncline formed with Cretaceous series in the core. The southern limb of this syncline is characterized by stable northward dipping-angle about 20° in ~ 10 km to the south. In the southern end of this section (Figure 4-2), the Jurassic sediments sub-horizontal deposit on the Carboniferous turbitites without deformation, while the Paleozoic basement are with vertical fabrics (Figure 4-18, Figure 4-2, N°17).

These location correspond the northern front of Tian Shan, such as Jingou He and Taxi He (Figure 4-1 and Figure 4-2). The sub-horizontal Jurassic deposed on the mountain basement and the very gentle dipping-angle in Jurassic sediments in the contact area suggest that no significant tectonic contact between the basin and the mountain basement at “front”.

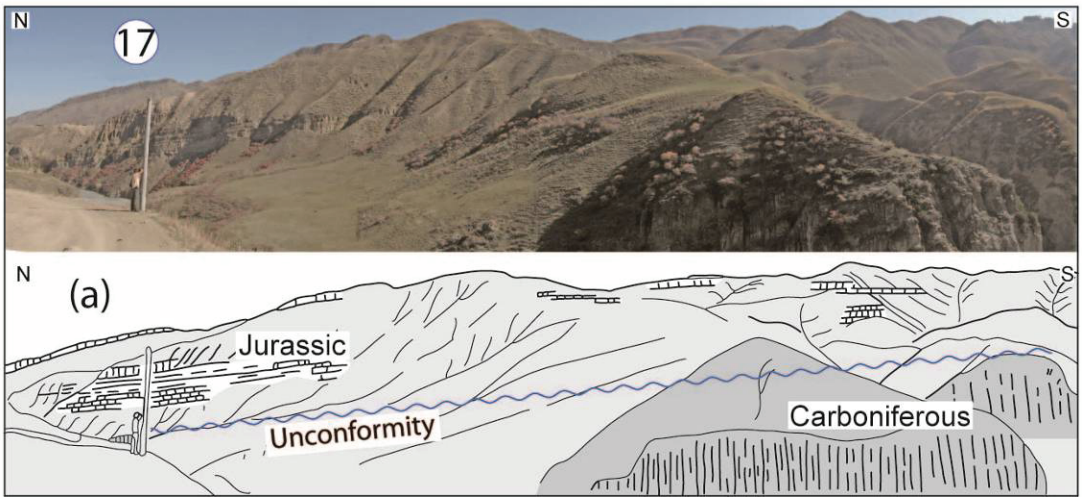

Figure 4-18. *Jurassic sediments unconformably overlie on the carboniferous basement. See Figure 4-1, N°17 for the location.*

4.2.4 Tugulu He

About 10 km west to Hutubi He, a minor valley incise the contact zone between the Lower Jurassic and the Paleozoic basement (Figure 4-1 and Figure 4-2 N°17).

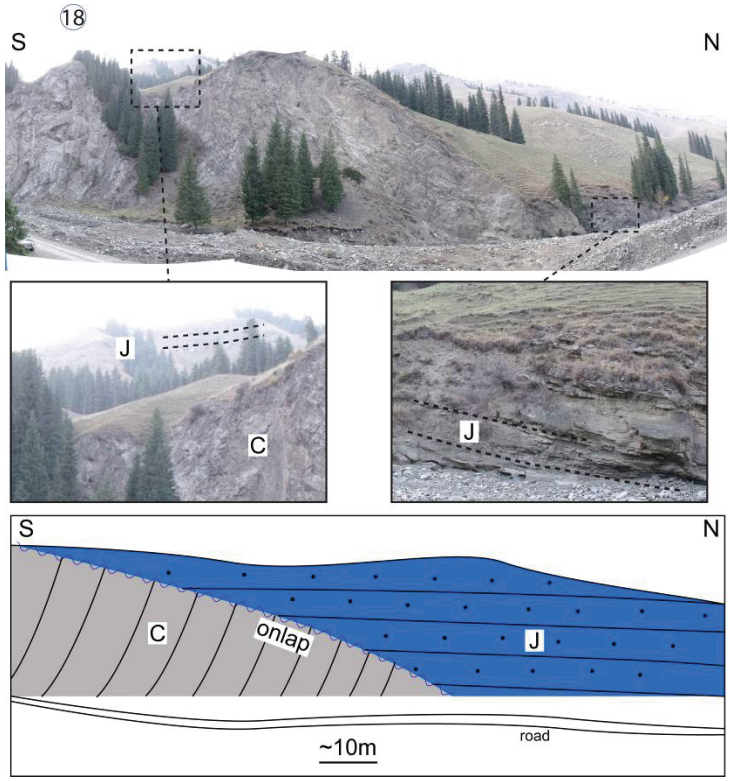

Figure 4-19. *The Jurassic series onlaps the Carboniferous basement without visible Cenozoic deformation. See Figure 4-1, N°18 for the location.*

This outcrop present well deformed Paleozoic basement with vertical fabrics. However, the Lower Jurassic sandstone deposit sub-horizontally to north side of the Paleozoic basement. Moreover, the Jurassic could be observed overlying on the basement (Figure 4-19). This structure presents an “onlap” sedimentary structure and it probably indicate a Mesozoic Paleo-relief (see Chapter 3). This structure is similar with above mentioned Hutubi He section, which also indicates not obvious deformation along the contact zone between the Paleozoic basement and the Jurassic sediments.

4.2.5 Dabaiyanggou

About 20 km westward to the Taxi He section, Lower Jurassic sediments are located adjacent to the Paleozoic basement. A north-south trending fault offsets the contact line between the Jurassic sediments and the Paleozoic basement (Figure 4-2). To the east, it is characterized by a thrust fault (e.g. Taxi He, Figure 4-2 N°1).

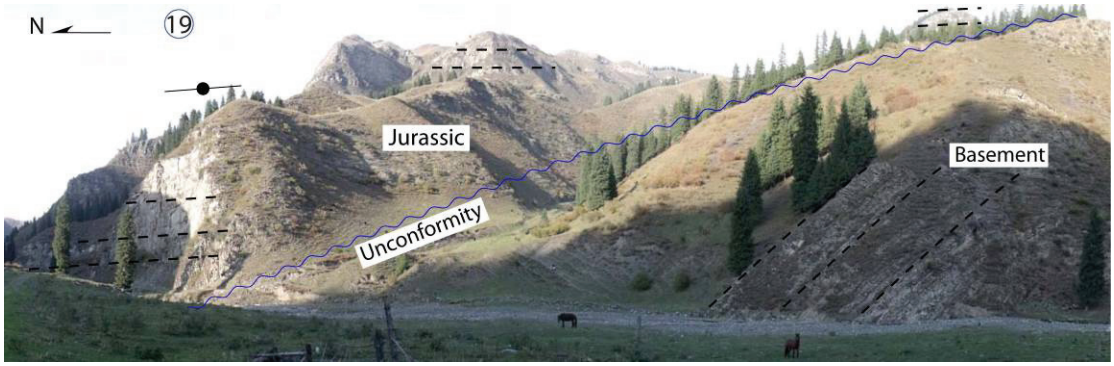

Figure 4-20. *Jurassic sediments sub-horizontally deposit on the steep basement. On the top of the southern basement, the Jurassic strata are horizontal extent southward to the mountain interior.*

To the west, along the Dabaiyanggou valley, thick white sandstone Jurassic layers show about 5° dipping northwards (Figure 4-20; Figure 4-2, N°19). In the right and southern part of this photo, the basement is composed by thin turbitites layers dipping ~60° northwards. Moreover, the sub-horizontal Jurassic sediments have been observed on the top of the basement. Therefore, the ‘onlap’ structure is showed here as well as the Tugulu He section (Figure 4-19). The contact zone between the basement and the sediments is indicated by the low topography minor valley (Figure

4-20). This structure of unconformity in contact area indicates no obvious deformation between the basement and the basin sediments.

4.2.6 Wusu

Along the northern piedmont of Tian Shan, the Tuositai anticline is the main structure feature, which shows high topography as well (Figure 4-1 and Figure 4-21).

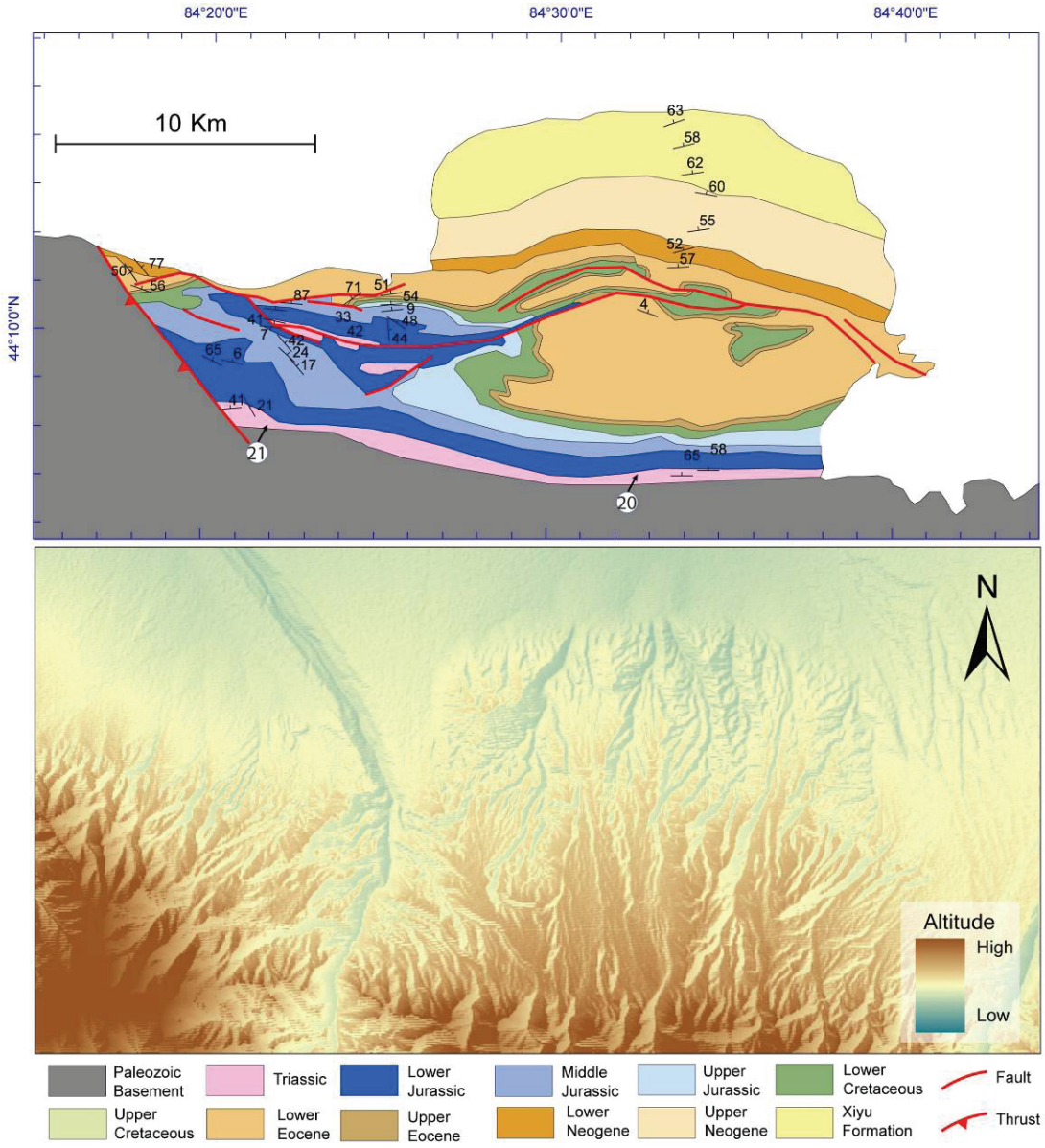

Figure 4-21. *Geological map (b) DEM of the Tuositai anticline in the Wusu area.*

The Tuositai anticline has a northern limb dipping 60° in Cenozoic series and a

southern limb characterized by ~ 10 km syncline (Figure 4-21). The syncline is most coved by Quaternary terraces in the field, excepting a narrow fold and two fault developed within it. The detailed structure of this area is presented by seismic and gravity measurements in Chapter 5. In the southern end of the basin sediments, Mesozoic series of Jurassic and Triassic outcrop adjacent to the Paleozoic basement. Field observations are carried out along the northern margin of basement and two outcrops are presented as follows (Wusu east and Wusu west).

Wusu east section is located at the southern end of the Tuositai anticline (Figure 4-21, N°20). As showed in the photo, the Jurassic sediments containing with coal layer dip northward with ~30 ° (Figure 4-22). Paleozoic basement is observed at the left hand in the photo (Figure 4-22). This characteristic of monocline in the sediments indicate that no significant movement between the Mesozoic Jurassic and the Paleozoic basement.

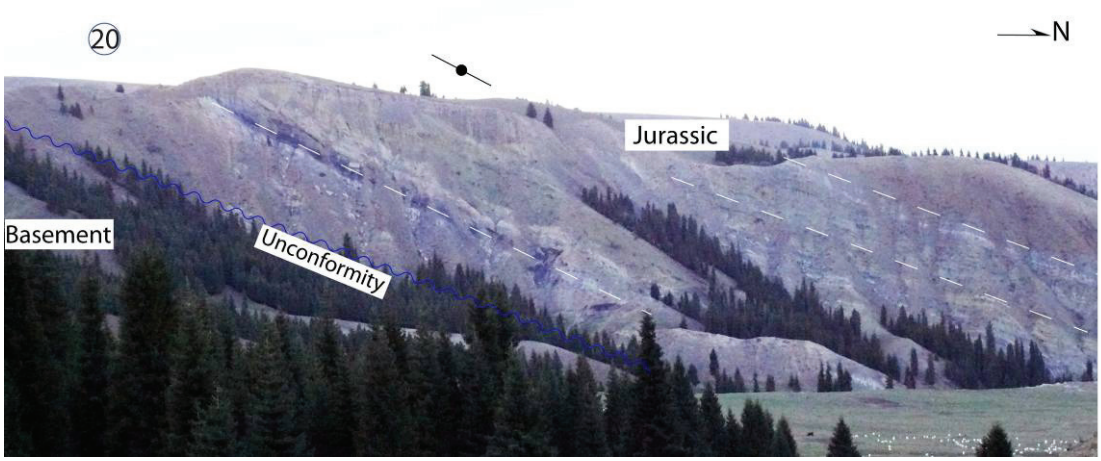

Figure 4-22. *Jurassic sediments deposit on the basement with gentle northward dip angle at Wusu East.*

About 15 km west to the Wusu east section, similar structure is observed in the Wusu west section. As showed in the photo (Figure 4-1 and Figure 4-21, N°21), Jurassic sediments deposit on the carboniferous basement without obvious deformation. The basement is dark in color and with vertical fabrics, while the Jurassic consist of white and yellow sandstone (Figure 4-23). The dip angle in the sediments is about 20° northwards (Figure 4-23). Further north, red and green

Cretaceous sediments are sub-horizontal in the back view of the photo. It suggests the weak deformation along the northern margin of the Paleozoic basement within the basin area.

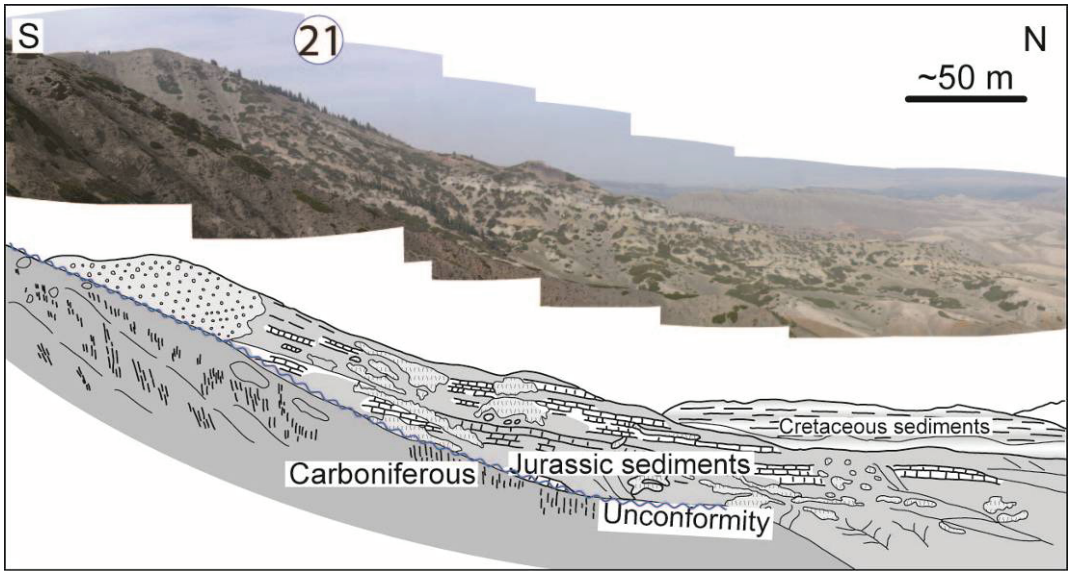

Figure 4-23. *Jurassic series overlie on the Paleozoic basement with a monocline towards north at the southern end of Wusu area.*

4.3 Fold contact

Previous studies show the thrust and the unconformity contacts between the mountain basement and the Mesozoic sediments. However, the two kinds of structures along the northern piedmont of Tian Shan indicates different deformation characteristics. For the first one, the basement thrust on the basin sediments and the sediment layers always show a local drag fold. In contrast, the second, i.e. unconformity, suggests very weak deformation between the mountain basement and the basin. Therefore, a kind of transition structure is necessary for the two structure types. In fact, folds in the contact zone have been observed in several sections along the northern front of Tian Shan. These folds are characterized by faults developed in the underlain basement. However, they does not cut the sediments and not thrust on the basin sediments yet. Therefore, the amplitude of deformation in the fold structure is between the faults and the unconformity contact. This kind of fold contact probably plays the role of the transition zone of the previous structures. From our field work,

two examples of fold contact are presented here, i.e. the Manasi He (C-C') and the Qingshui He (D-D').

4.3.1 Manasi He

The study of the Manasi He section focused on the southern part of the contact zone between the Paleozoic basement and the basin sediments (Figure 4-1, C-C').

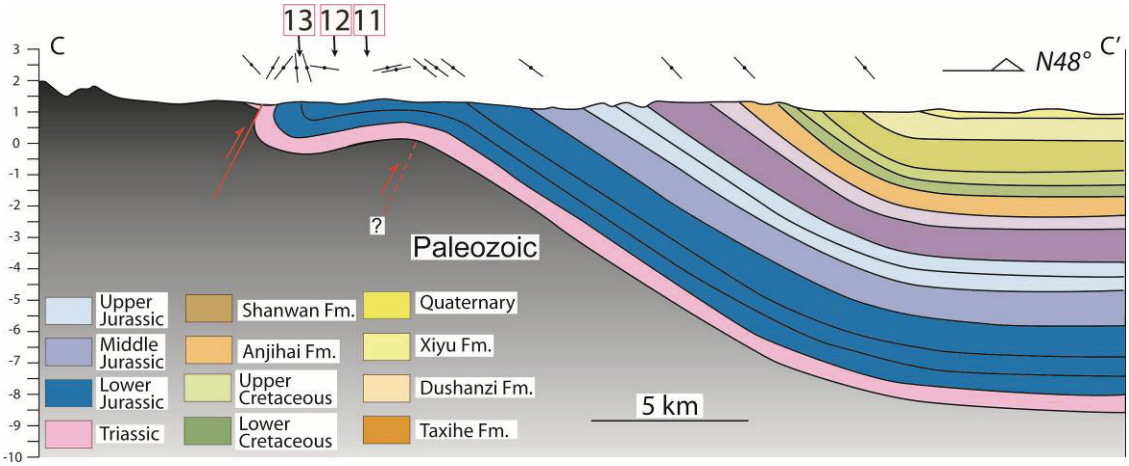

Figure 4-24. *Geological cross-section along Manasi He.*

The northern most of this section is characterized by a nomocline within the Cenozoic and Mesozoic series, dipping northward 40-60°. To the southern, the dip angels in Lower Jurassic decrease and then become southward with ~15° (Figure 4-24). This turning in dip-angles build an anticline with lower Jurassic in the core (Figure 4-24 and Figure 4-25a). The dipping-angel within the southern limb of this anticline turns into vertical and overturned in ~3 km southwards (Figure 4-25b and c). Further south, the purple Triassic mudstones show overturned as Jurassic series (Figure 4-25 c). Moreover, the thrust of basement rock on the Triassic has not been observed on the surface. Instead, Triassic becomes normal dip northwards and deposed directly on the Paleozoic basement with unconformity (Figure 4-24). At the most end of this section, the Triassic sediments dip northwards with ~ 50°. This rapid change from northern overturned to southern normal Triassic is less than 1 km distance, suggesting a fold and probably a fault here.

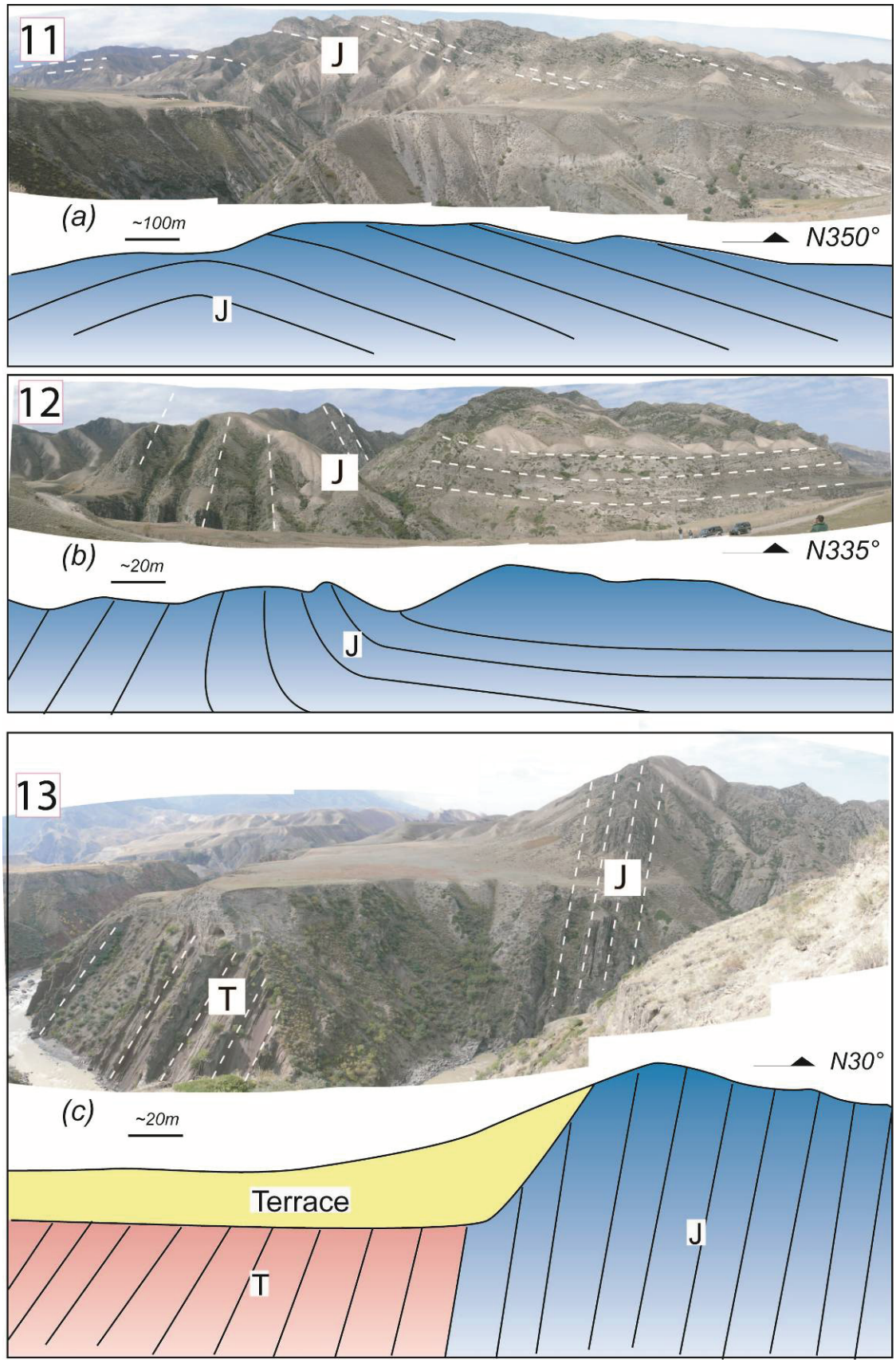

Figure 4-25 *(a) A gentle anticline in Jurassic. (b) Rapid change of the dip angles in Jurassic. (c) Sub-vertical contact between Jurassic and Triassic.*

Nevertheless, the net faulting lag should be small, as the Triassic strata deposit on the hangingall yet. The geometry here shows a fold with a limited fault along the contact zone between the basement and the sediments. In contrast, in the fault contact case, the basement thrust on the basin sediments and the overlying sediments of the hangwall have been eroded, suggesting more net slips. This kind of the fold contact is less deformed than thrust fault ones but more than unconformity ones as presented above. Therefore, it could be an important transition structure along the northern piedmont of Tian Shan.

4.3.2 Qingshui He

The Qingshui He section is located ~ 13 km west to the Manasi He section (Figure 4-1, D-D').

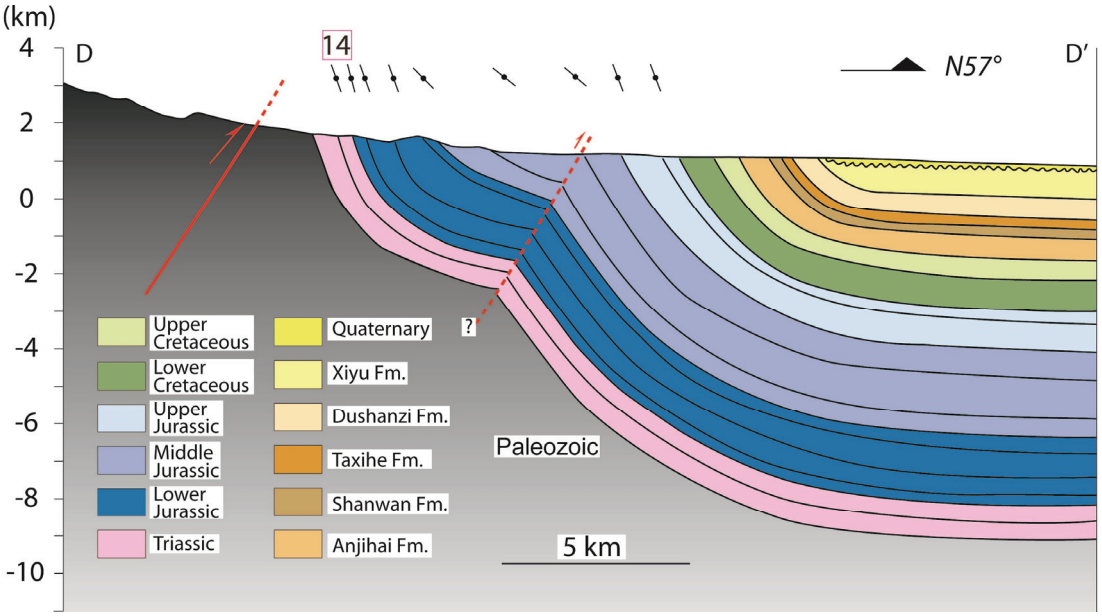

Figure 4-26. *Geological cross-section along Qingshui He. The southernmost basin sediments show a monocline but without any visible relative movement with respect to the Paleozoic basement.*

The geometry of the Qingshui He section is similar with the Manasi one. The northern part shows a monocline, including Eocene to Jurassic sediments. The dip angles change from steep 50-70° in the north to 20-30° in the south, building a kink fold. The southern limb of the kink fold dips about 25° close to the core but increase

southwardly closed to the basement (Figure 4-26). The basal Jurassic competent conglomerates layers dip northward ~ 70° at the southern this section (Figure 4-26). This steep Meszoic form the southern limb of a syncline with deformation showing a kink fold in the contact zone (Figure 4-26).

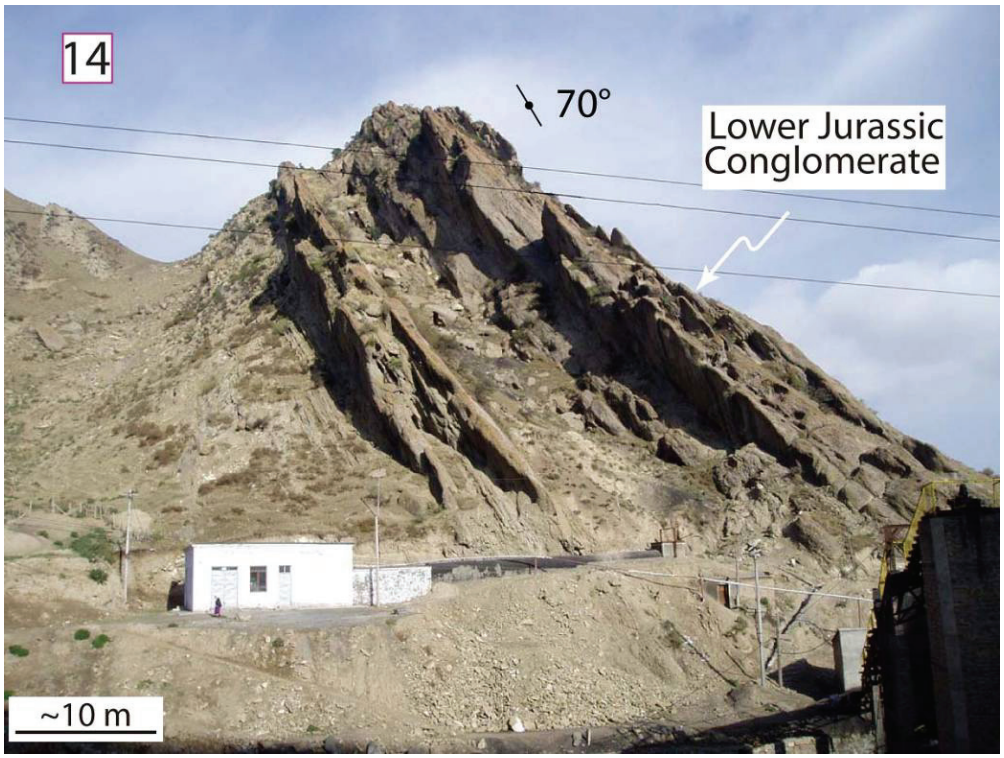

Figure 4-27. *Jurassic conglomerates show steep northward dip-angle along the Qingshui He section.*

4.4 Backthrust contact

Backthrust are the faults with contrast direction comparing with most forward thrust in the foreland thrust belt. They are common in the strongly deformed fold-and-thrust belts (Coward et al., 1988; Pfiffner et al., 2000; Kapp et al., 2005; Marquer et al., 2006). However, this type of tectonic has been only observed in the interior of the Tian Shan, but has not been discovered in the northern piedmont of Tian Shan during our field trips. Two locations of backthrust contact between the basement and the sediments are presented as follows: Houxia West and Hutubi He South, locations N°22 and 23 (Figure 4-1).

4.4.1 Houxia West

In the interior of the Mountain, Jurassic sediments overlie on the mountain basement with ~2000-2300m high altitude in Houxia area (Figure 4-5). The Jurassic series are good marks to record the deformation process during Mesozoic and Cenozoic. The Houxia West section is located 3 km west to the Urumuqi He along a minor vallay flowing from northern to southern (Figure 4-1 and Figure 4-5, N°22).

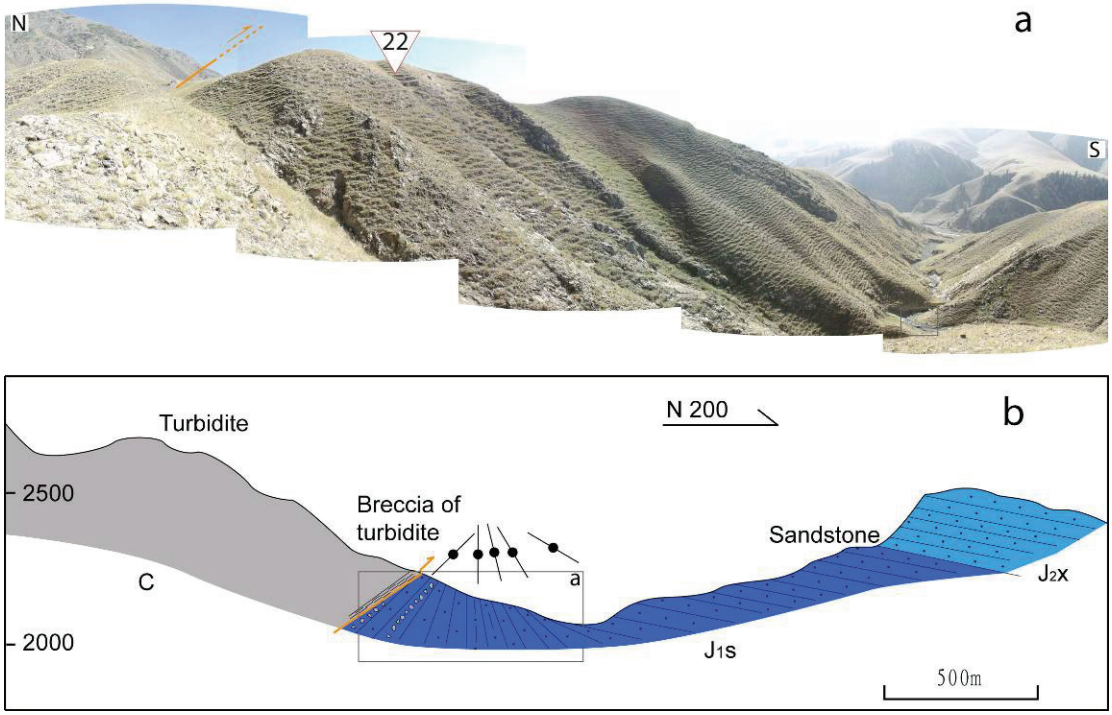

Figure 4-28. *The Carboniferous basement thrust southward on the Jurassic sediments. Sedimentary breccias, with clasts of Carboniferous basement rocks, have been locally found at the bottom of the Jurassic series.*

The Jurassic sediments consist of sandstones and interbed mudstones, with dip angle ~ 35° in the southern part of this section (Figure 4-28). Jurassic layers become steeper and overtured closed to the basement. Moreover, some sedimentary briccas, consisting of basement coarse anglar clasts, have been observed close to the basement. The sedimentary breccias in the Jurassic series indicate a range marginal facies, suggesting here is the ancient Mesozoic piedmont of the Mountain (see Chapter 3). Briefly state, the basement thrust southward on the basin of the interior of Tian Shan

by a thrust fault. The feature of the backthrust is similar with forward thrust contact in the northern piedmont of Tian Shan, where the sediments show a drag fold and rapid change of dip angles in ~ 500m close to the fault (Figure 4-28).

4.4.2 Hutubi He South

In the southern part of the Hutubi He, Jurassic sediments widespread overlie the Paleozoic basement (Figure 4-2). Within the Jurassic cover, basement outcrops along the southern of the Hutubi He. A southward thrust is drawn between the Jurassic cover in the south and the middle buck of basement in the north (Figure 1 and Figure 4-5, N°23).

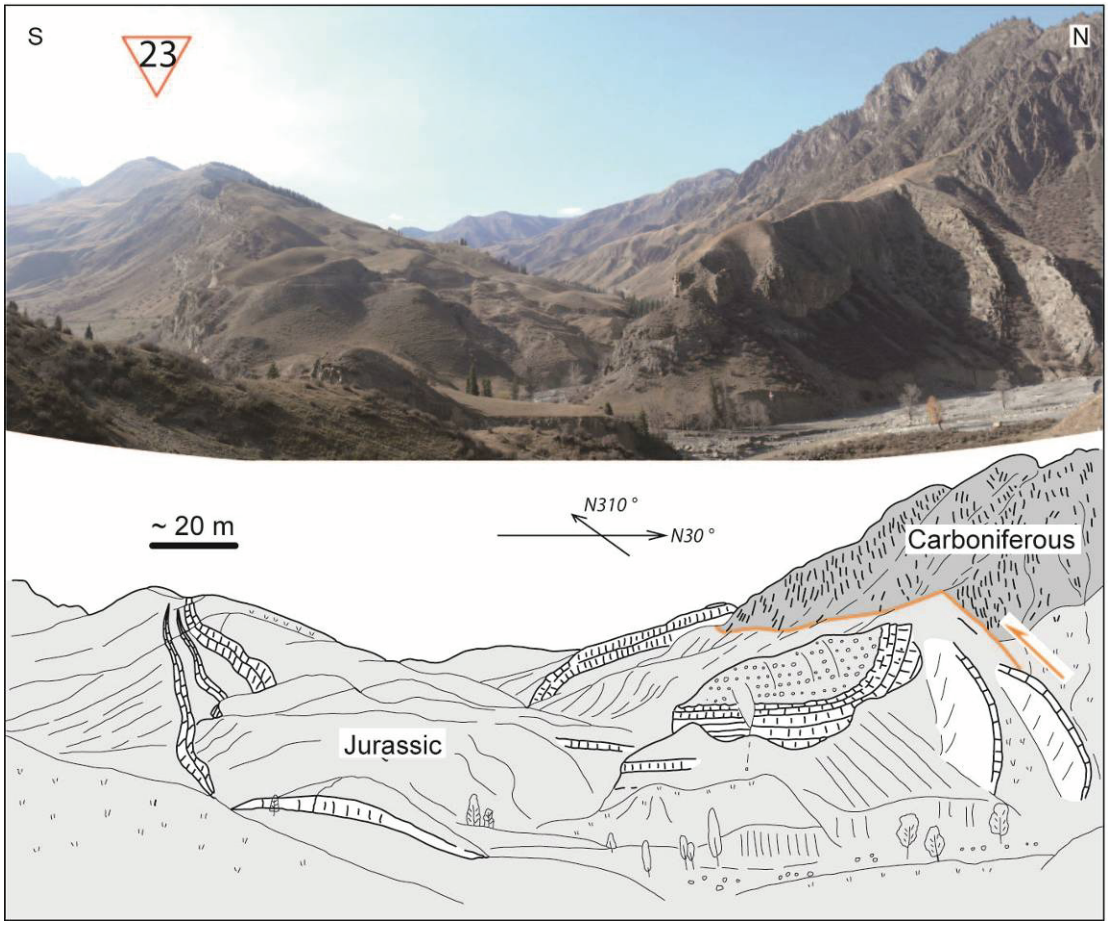

Figure 4-29. *To the south of the Hutubi He valley, the Carboniferous basement thrusts on the Jurassic sediments. However, the fault disappears to the west and the Jurassic sediments directly deposit on the basement with weak "kink" type folding.*

In field, the basement with vertical fabrics show vertical fabrics and the Jurassic sediments are overturned dipping northward adjacent to the contact (Figure 4-29). About 200m to south, the sediment layers turn to normal and dip northward ~ 30°. It forms a drag fold closed to the backthrust as previous forward thrust or backthrust. However in the back view, the fault disappears to the west and the Jurassic sediments deposit on the basement with weak "kink" type folding (Figure 4-29). This rapid lateral change of faults to less deformed fold suggests limited net slip along the fault. This lateral variation of deformation is very popular in the northern piedmont of Tian Shan in different scales. Moreover, the kink fold to the west of this location also indicates that the fold-contact in-between the basement and the sediments is located in the interior of mountain as well.

4.5 Discussion

The structural observations along the northern piedmont of Tian Shan are presented above with four distinguishable contact types, thrust, unconformity, folding and backthrust. The backthrust contact has been only observed in the interior of the Tian Shan mountain and rare seen in the southern of the Junggar foreland basin. However, several important structure problems are raised. Firstly, did décollement develop as backthrust in the zone of unconformity contact? Secondly, what is the contribution of the Mesozoic relief to the present Tian Shan topograpy? Thirdly, what is the mechanism of the deformation along the front of the Tian Shan.

4.5.1 Backthrust in the northern piedmont of Tian Shan

The backthrusts play important role in the deformation processes in the contract faults and thrust belts. They can absorb an important amount of shortening during the deformation, which is important to study the shortening amount (Coward et al., 1988; Pfiffner et al., 2000; Kapp et al., 2005; Marquer et al., 2006). Backthrust faults were proposed in the northern piedmont of Tian Shan to explain the importance of

shortening in the foreland Junggar basin (He et al., 2005). The Jurassic coal and Tertiary evaporates, such as gypsum, are often considered as layers of backthrust décollement (Deng et al., 1999; Chen et al., 2007; Dong et al., 2007; Lu et al., 2007). In the northern Tian Shan front, the basin sediments mainly consist of Mesozoic sediments, therefore, the Jurassic coal beds will be discussed below.

The well deformed coal bed is presented in the Toutun He West section (N° 6 in Figure 4-1). The coal bed is well deformed with cleavage and sandwiched by the overturned sandstone adjacent to the northward thrust (Figure 4-6). However, the sandstones are not deformed at all, suggesting the coal layer is rather easy to deform with deformation. Therefore, the backthrust, if existed, should be active at coal layers at first.

Carefully observations are taken out in the northern piedmont of Tian Shan. In the Tugulu He area (No. 24 in Figure 4-1), the Jurassic sandstone dips gentle northward with ~15° and this stratigraphic slope extends several kilometers northwards and southwards (Figure 4-30).

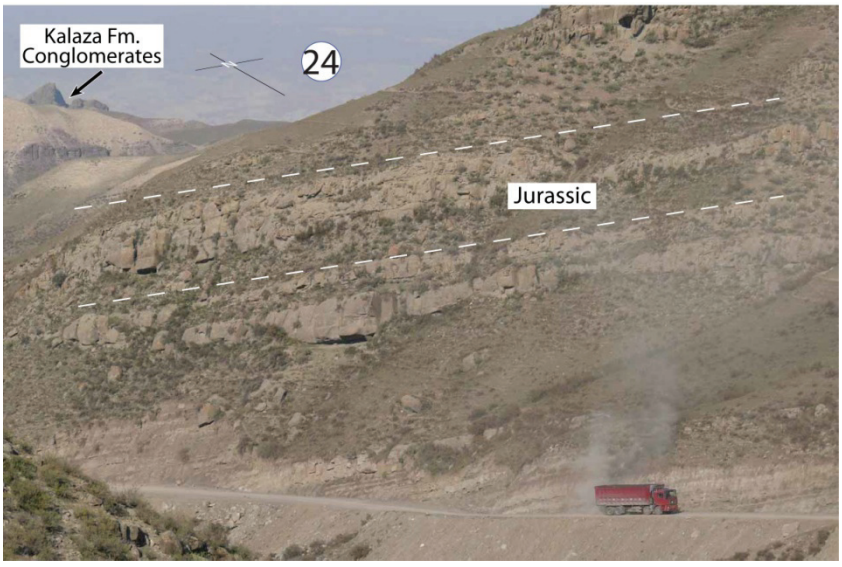

Figure 4-30. *Gentle northward dipping Jurassic sandstone extends northwards and southwards several kilometers.*

Moreover, the observed coal bed is interbedded with the Jurassic sandstone, where the vertical fractures indicate there is not horizontal shearing movement (Figure 4-31, No. 25 in Figure 4-1). Compared with the deformed coal bed adjacent to

a fault in Toutun He West section, this undeformed coal bed indicates there is no décollement movement in the contact zone in the northern piedmont of Tian Shan. In other words, the deformation just focuses on the thrusting area and the unconformity contact zone is without significant deformation.

Figure 4-31. *Coal bed inbedded in Jurassic sandstone. The vertical fractures indicate no horizontal movement.*

4.5.2 The effect of Mesozoic paleo-relief on the Cenozoic deformation

The geological and tectonic evidences illustrated in Chapter 3 show that the present Tian Shan may be importantly inherited from the Mesozoic relief. It is thus questionable for the importance of the Cenozoic deformation of the northern Tian Shan due to the India-Asia collision. Two thrust models are proposed in Figure 4-32. The first one concerns the horizontal basin bottom and another concerns the inclined basin basement with onalp sedimentary structure. The former one produces an important net slip and big shortening when the basement thrusts on the sedimentary cover (Figure 4-32a). In contrast, the latter produces less relative displacement (Figure 4-32b). For example, the Houxia West section shows that this section is located at the ancient Mesozoic Tinashan piedmont and activated during Cenozoic (Figure 4-1, N°22, Figure 4-28). A part of the present topography should be the influence of the Mesozoic mountains as shown in the second model (Figure 4-32).

This Mesozoic relief effect should be taken into account for the evaluation of the amplitude of the Cenozoic deformation of the modern Tian Shan due to the India-Asia collision.

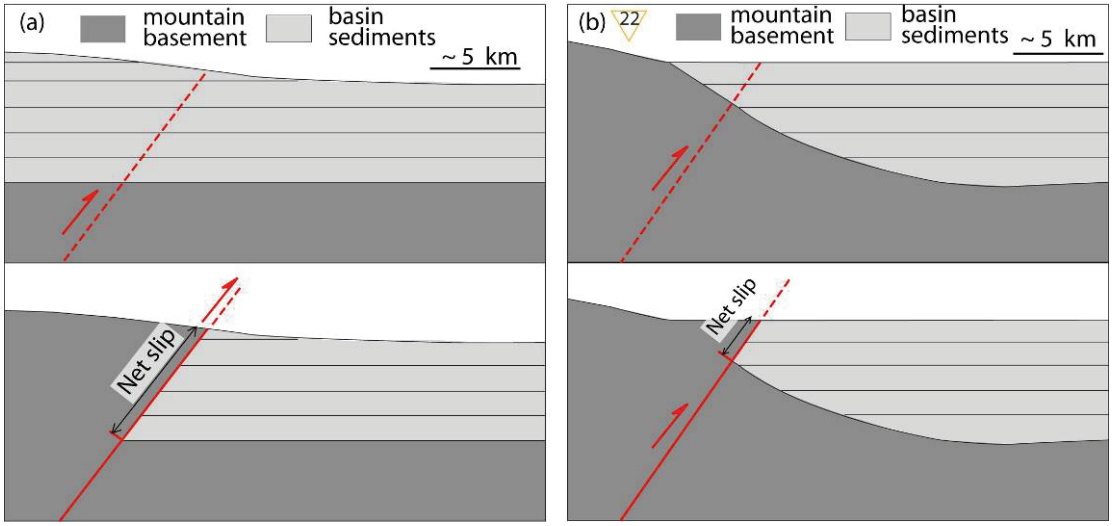

Figure 4-32. *(a) The thrusting of the basement on the sedimentary cover produces an important net slip in the horizontal base of basin. (b) The thrusting of the basement on the sedimentary cover produces less net slip in an onlapping contact in a high Paleo-relief area. See the example of N° 22 in Figure 4-1.*

4.2.3 Mechanism of the deformation along the northern Tian Shan

Three main structural types of the contact in the northern piedmont of Tian Shan have been identified, thrust, unconformity and fold. These structures are marked by the originally horizontal Mesozoic and Cenozoic sediments. It is difficult to distinguish the Paleozoic deformation style of the basement during subduction and collision processes. However, the field observations in the basement reveal some characteristics during their Cenozoic deformation.

Along the Urumuqi He, the Carboniferous basement consists of turbidites. They are well deformed by many parallel joints and faults, where quartz veins show reverse faulting steps (Figure 4-1, N°26, Figure 4-33a and a'). Moreover, in the south of the Taixi He valley, the basement shows some high-angle reversed faults. Quartz veins

are grinded into powders during the fault movement (Figure 4-1, N°27, Figure 4-33). These powders deposit on the surface by about 4 cm in thickness, suggesting that the fault is still active now. These structural characteristics show that the basement is deformed as a kind of rigid blocks with faults and joints. This deformation of block can be also observed in larger scales.

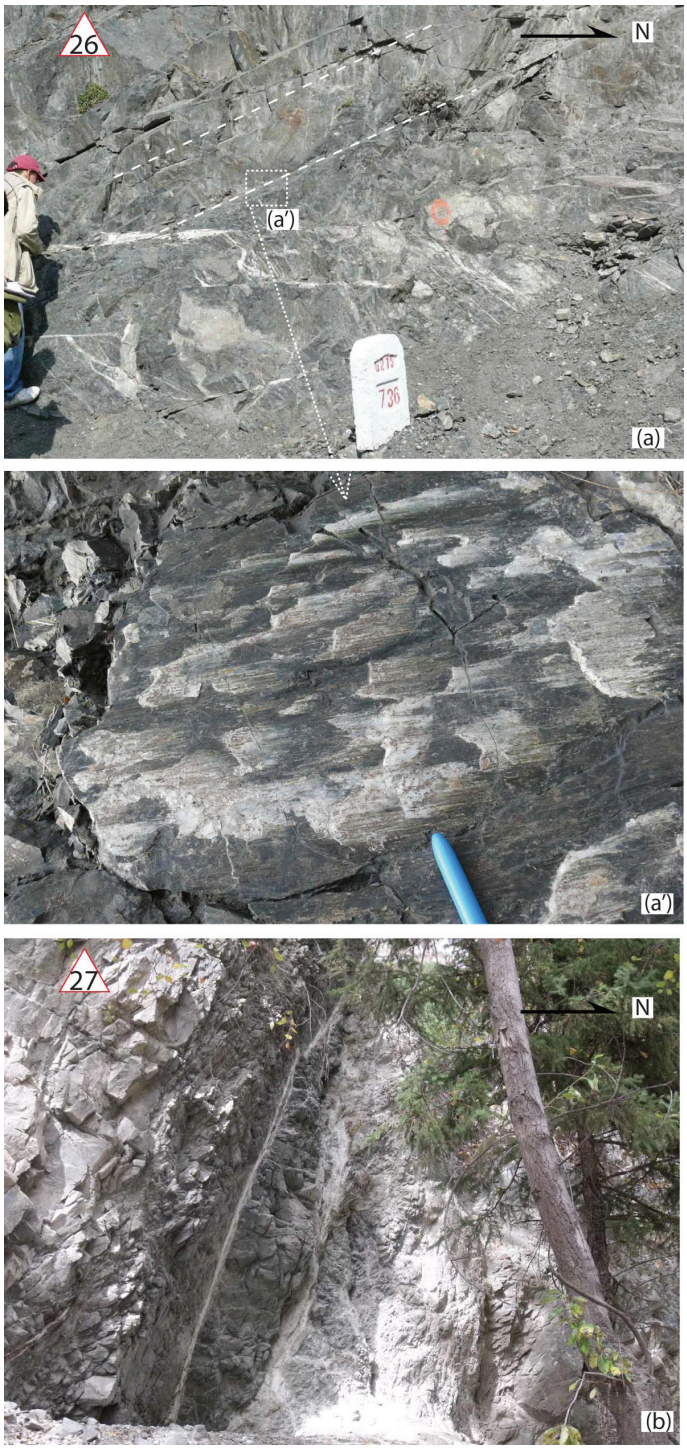

Figure 4-33. *(a) Joints and faults in Carboniferous turbidites show the deformed*

basement as blocks. (a') Faulting steps in quartz veins on the surface of faults. (c) Quartz veins were grinded into powders along the faults.

Four section sketches are constructed based on field observations in a ~100 km-wide zone along the northern front of Tian Shan from Manasi He to Hutubi He (Figure 4-34).

These four sections are spatially controlled by three reverse faults from south to north, F1, F2 and F3, respectively. The F1 fault in the mountain interior is presented in the Chinese geological maps (XJGB, 1993). Others faults in the basin are observed in field or inferred from the geometry of their overlay anticlines. In the western part, the southern fault (F1) is located in the basement that can be easily identified by published geological maps. In the eastern section (Sections c and d in Figure 4-30), F1 is marked on the contact between the basement and Jurassic sediments. Basinwards, the fault F2 is limited in the basement and did not cut the sedimentary cover (Sections a and b in Figure 4-34).

Although this fault can be well observed on the surface in the Taxi He section (Section c in Figure 4-30), it is disappeared in Section d with very gentle dipping northwards without deformation. The fault F3 in basement is inferred from the anticline of the sediments. This fault is better developed in the eastern two sections c and d (Figure 4-34). By the geometry of the sedimentary cover, it seems clear that the sedimentary structures of the basin layers are controlled by these three faults in the basement. These faults are sub-parallel with the front of the mountain and separated by a sub-equal interval of 15-20 km (Figure 4-34).

The basement is therefore cut by these faults into 15-20 km-wide blocks northwards and these blocks of the basement thrust with each other by faults between them. The faults show often a lateral component of net slip, where an obvious thrust disappears laterally.

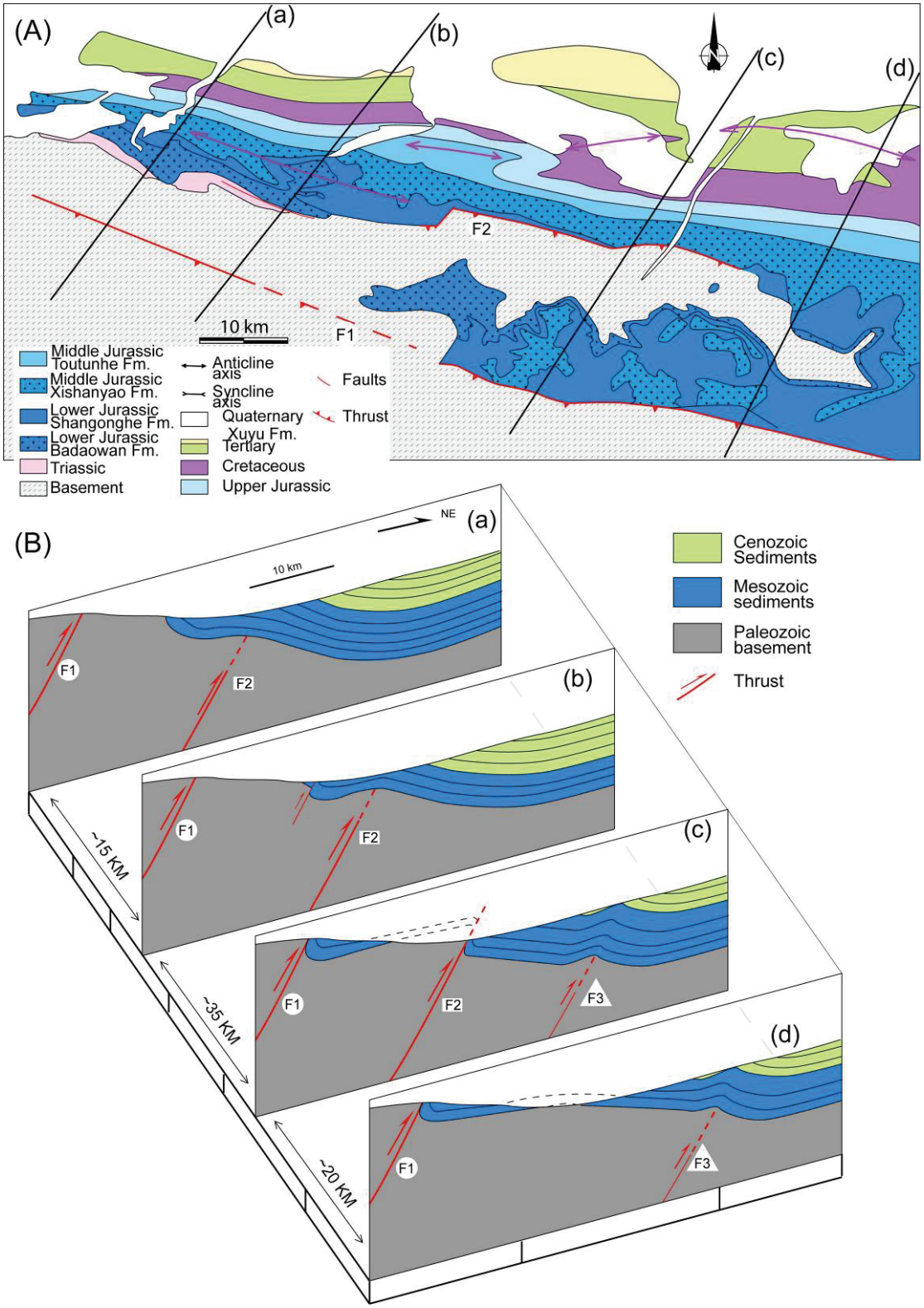

Figure 4-34. *Sketches diagram show the lateral variation mechanism of deformation. (A) Geological map of the northern front zone between the Manasi He and the Hutubi He (map position see Figure 4-1). (B) Four sections along the northern front of Tian Shan.*

These above characteristics are observed not only in the tens-kilometer scale, but also in kilometer scale and even in outcrops. The faults can turn laterally into a gentle fold in a short distance to the later side (Figure 4-35). An example of this fault is presented in southern Hutubi backthrust fault (Figure 4-1, Figure 4-26, *N° 23*). This shows that the fault displacement is limited because it is constrained by continuous sediments in lateral side.

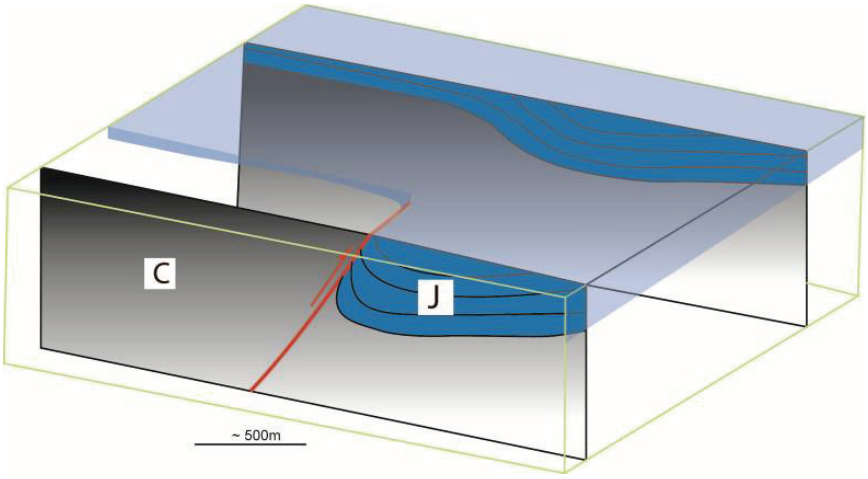

Figure 4-35. *Sketch diagram shows the lateral structural variation. This example can be seen in the southern Hutubi (Figure 4-1, N° 23).*

For the same reason, the lateral structural variation along the northern front of Tian Shan indicates that the northward thrusting movement in the frontal contact zone should be limited (Figure 4-36). The boundary between the mountain basement and the basin sediments does not show a clear thrust belt as often illustrated by a front of maturated range-basin (e.g. Pyrenees, Barrier 2002; Muñoz, 1992; Teixell, 1998; Vergés, 1999). The fault contact in the front often becomes a fold extending laterally or unconformity contact. This structural variation suggests that the deformation and the faulting are establishing and will be reinforced due to the future ongoing deformation by India-Asia collision. However, the shortening could be absorbed by fault-and-thrust belt in the foreland basin as well. The next chapter will focus on the basin structure by filed observation, seismic profile, drilled well and gravimetric measurement, and then on the estimation of Cenozoic deformation in the northern piedmont of Tian Shan.

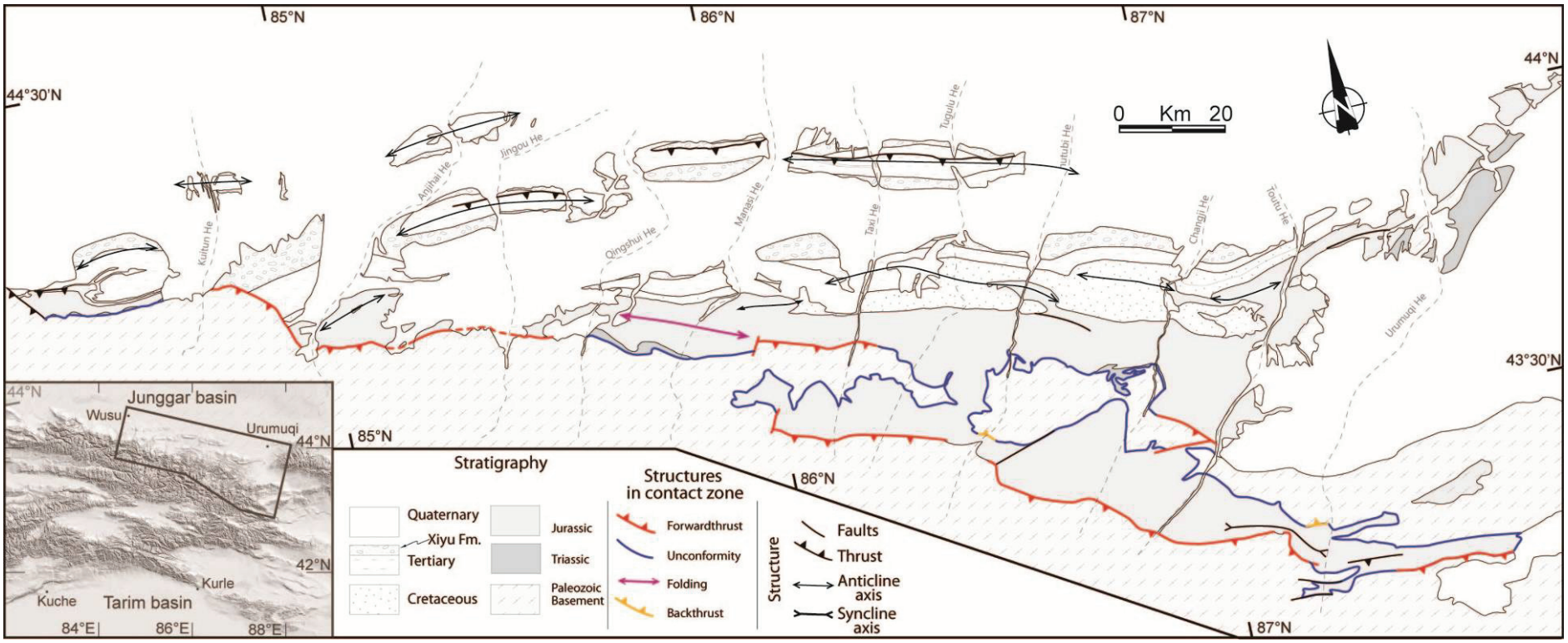

Figure 4-36. *The structural geological map of the northern piedmont of Tian Shan. The frontal structures of thrust, fold, unconformity and backthrust are marked by red, blue, violet and orange colored symbols, respectively*

Chapter 5

Regional geological sections along the north piedmont of Tian Shan and quantification of the Cenozoic deformation

Chapter 4 has presented the characteristics of highly variable structural styles of the contacts between the range basement and Junggar basin cover along the northern Tian Shan, indicating that the Cenozoic deformation is rather weak in the contact zone in-between the basement and the basin. Moreover, the thrust faults developed in the piedmont turn rapidly into kink folds, and then die out laterally. However, important amounts of Cenozoic deformation may have been absorbed by folds and thrust belts in the Junggar foreland basin. To quantify shortening and to understand how the deformation is distributed in the fold-and-thrust belt in the basin, large-scale geological sections have been constructed by integrating field observations, gravity measurements, available seismic profiles and drilled wells. To illustrate the structure of the whole northern Tian Shan piedmont and show the lateral distribution of deformation along the range, four sections have been chosen from east to west in this study, i.e. Hutubi He, Qingshui He, Jingou He and Wusu section (Figure 5-1).

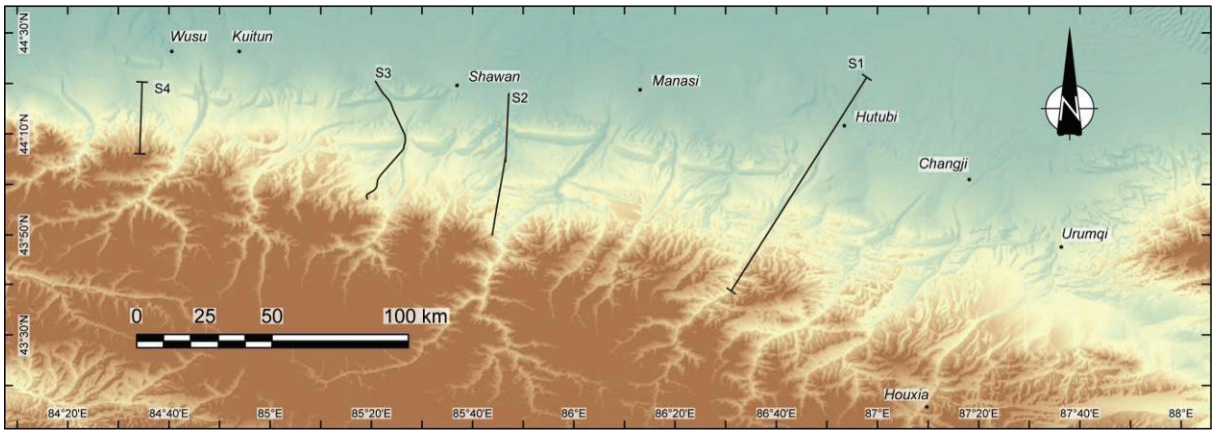

Figure 5-1. *Location of the four sections chosen to illustrate the deformation in the northern piedmont of Tian Shan. S1: Hutubi He section; S2: Qingshui He section; S3: Jingou He section; S4: Wusu section.*

5.1 Approach of the construction of regional geological sections

The principal aim of this study is to estimate the Cenozoic deformation in the northern piedmont of Tian Shan. To realize it, the first step is to recognize geological structures and then make geological sections from the front of the range to the basin and from the surface to the substratum of the basin. The following three complementary methods have been applied to the construction of geological sections.

(1) Surface structural observations

The field observations can provide the important information on tectonic structure, stratigraphic geometry, kinematics of the deformation, as well as key structural measurements needed for a good reconstruction of the cross-sections. A good geological section may be constructed where the geological outcrops are relatively continuous. However, it is not the case for the northern piedmont of Tian Shan. The high rate erosion produces thick Quaternary deposits that cover the majority of the basin surface and prevent the continuous surface observations (e.g. Figure 4-9). This is reason why seismic profiles have been used to complete the gaps. Moreover, the seismic profile may offer more information on the structure variation in the depth.

(2) Seismic profile

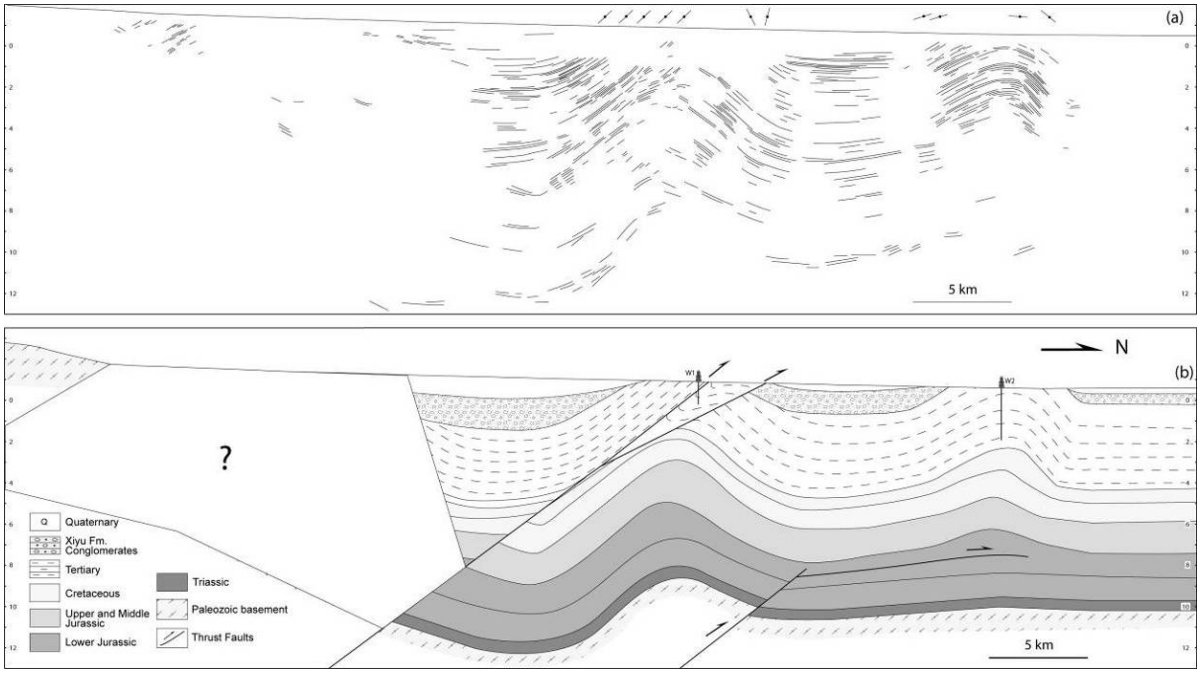

Figure 5-2. *(a) Uninterpreted line drawing of the seismic profile along the Jingou River section presented with the structural data measured on the field. (b) Interpretation of the seismic profile. The southern part of the profil remains unclear. It is then noteworthy that gravimetric data is the only way to propose reliable bulk geometry.*

As the Junggar basin is a hydrocarbon-producing basin, numerous seismic profiles are fortunately available in our study zone. Seismic reflectors have been well identified, presenting the main interfaces within the sediments and allowing defining the structure of the basin, even better with the surface structural observations (the right part of Figure 5-2);

However, for different reasons, such as the deformed strata making sightless of the seismic method, or the economic reason, the seismic profiles are sometimes absent, especially, in the range-basin contact zone (Figure 5-2), that makes some difficulties on the structural interpretations of this zone and, consequently, leads misunderstanding of the deformation mechanism. To ensure the reality of the constructed geological sections, the gravity method has been complementary applied as well in this study.

(3) Gravity measurement

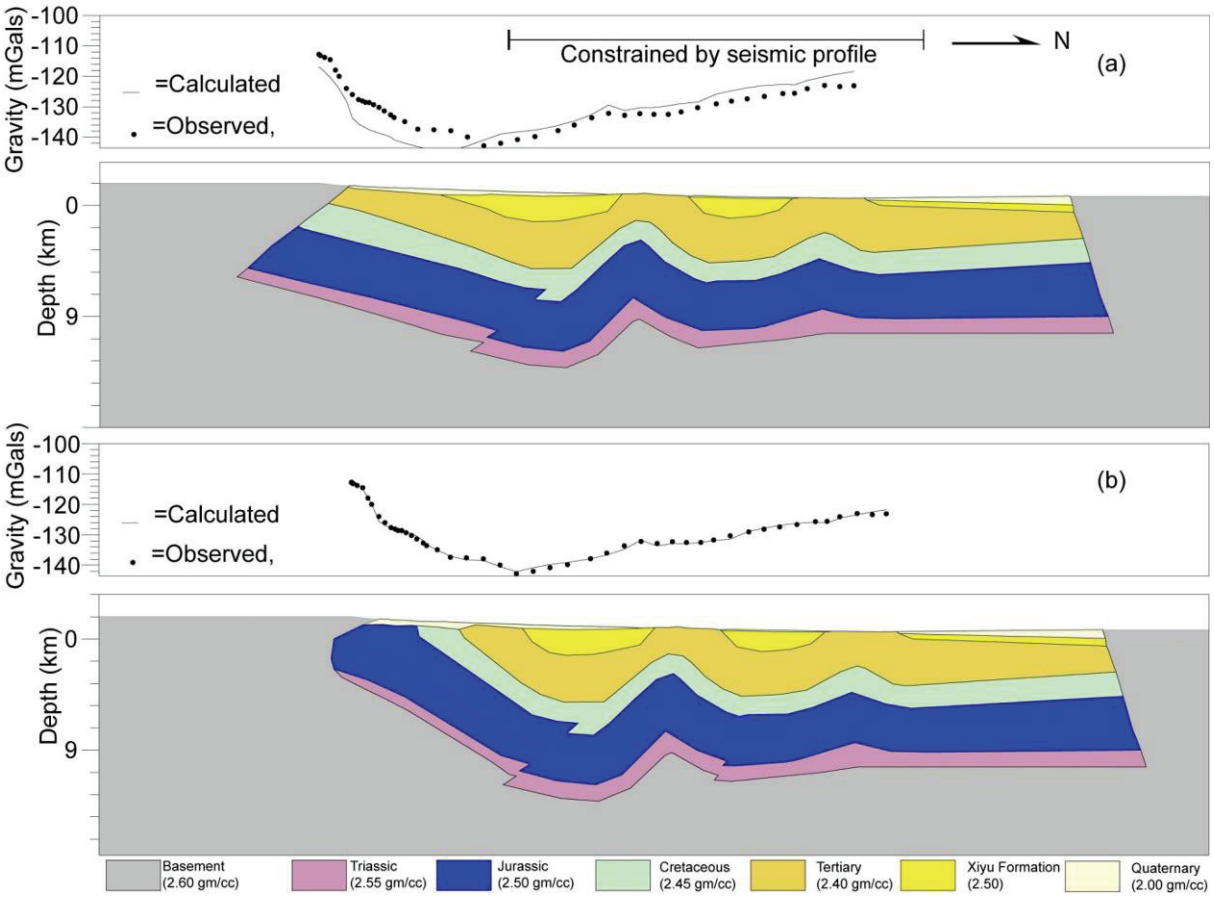

Figure 5-3. *An example to illustrate the importance of gravity method in the interpretation of geological section. (a) 2D gravity model computed after integration of geological and seismic data; (b) alternative model fitting to the gravity anomalies.*

Figures 5-2 and 5-3 present a good example for the utility and efficiency of the gravity method. The left part of Figure 5-2 shows a blind zone for both seismic method (inclined and/or strongly deformation) and surface observations (Quaternary cover), this blank space may be structurally interpreted by two distinguishable types of contact between the range basement and sedimentary cover: (1) thrusting of the range basement on the weakly or no deformed strata with a rather large faulting displacement (Figure 5-3a); (2) thrusting of the

range basement on the overturned strata with a rather small faulting displacement (Figure 5-3b). The interpretation of the gravity measurements carried out along this profile favorites the second model with better fit between the gravity anomalies and modeling (Figure 5-3), that presents also a good certainty to the construction of the geological section.

According to above experiences, gravity measurements have been systematically carried out along all four sections. Moreover, field observations, seismic profiles and available drilled wells have been integrated into the construction of their 2-D geological sections.

Time to depth conversion has been computed for seismic profiles. Gravity measurements have been carried out along these sections with a CG-5 gravimeter. These gravity data in each station are treated as Bouguer anomaly and modeled with GM-SYS of Geosoft. For details of the data processing on seismic reflections and gravity measurements, please see Appendixes 1 and 2, respectively.

5.2 Geological sections

Integrating all available field (structural and geological) and subsurface (seismic, gravity and drilled well) data, four 2-D geological sections have been constructed and presented in following.

5.1.1 Jingou He Section

The Jingou He section is located to the west of the Shawan city and along the Jingou He (Figure 5-4). It crosses two anticlines in the north and the contact zone in-between the Tian Shan basement and basin in the south. The northernmost anticline is named the Anjihai anticline, which is characterized by gently dipping symmetric limbs (about 15°). It exposes the coarse-grained Xiyu and Dushanzi formations (Figure 5-4). The seismic profile running along the anticlinal reveals a smooth, rather symmetric subsurface structure favoring with detachment-driven folding and the finite shortening is ~1.55km (He et al., 2005; Daëron et al., 2007). Moreover, faults lie in the depth and do not attain to the surface or shallow subsurface.

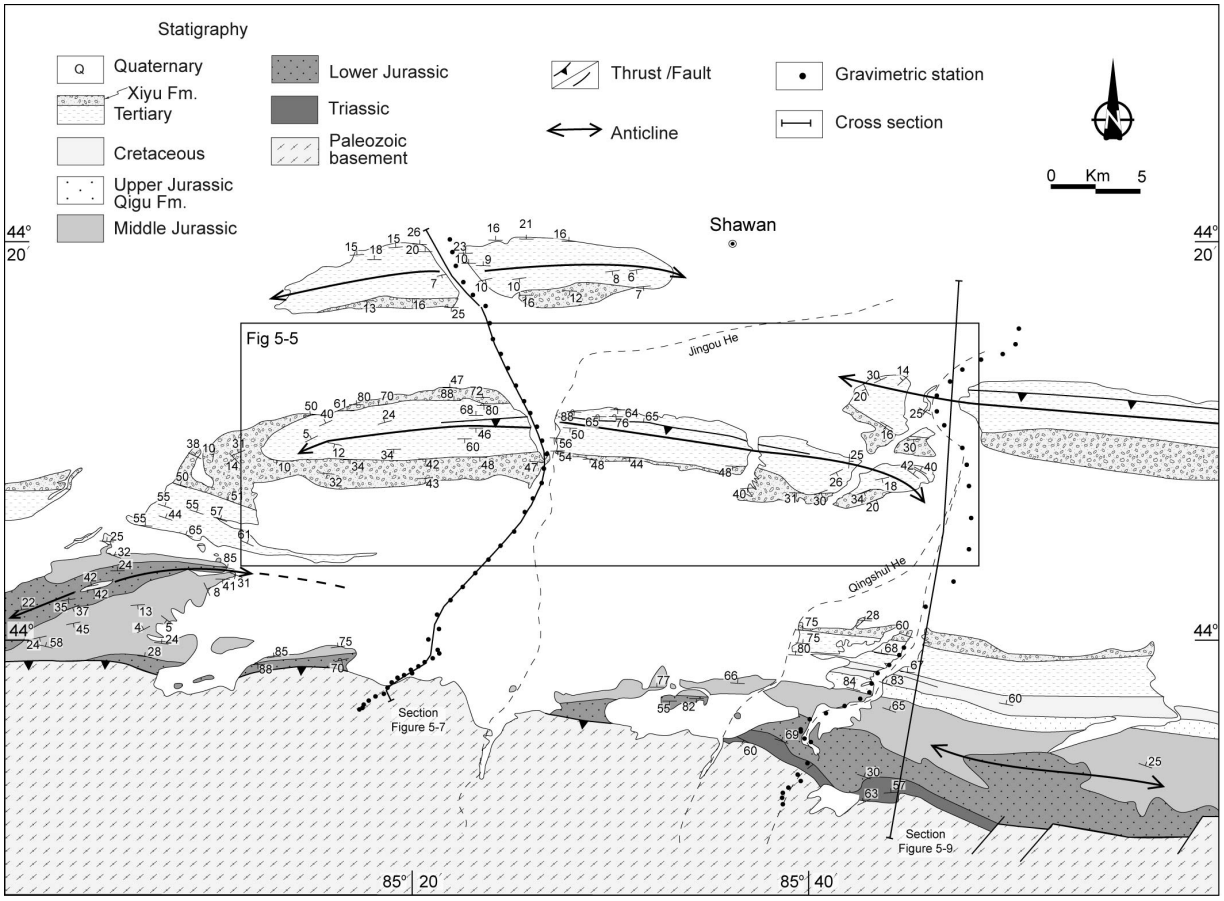

Figure 5-4. *Geological map of the Jingou He and Qingshui He areas with locations of seismic profiles and gravity stations.*

The southern anticline concerns the Huoerguosi anticline (Figure 5-4, Figure 5-5), which presents a clear asymmetric geometry with northward thrusts. In the outcrop-scale, the core of this anticline is well deformed (Figure 5-6). Two thrusts can be identified by field observations and satellite image. The southern one is illustrated by the thrusting of the greenish Anjihai formation on the redish Shawan formation (Figure 5-6). The upper unit of the thrust, to the southern Anjihai formation, shows a monocline, while the northern Shawan formation presents an asymmetric anticline. The southern limb dips southwards with about 30 degrees, but the northern limb is vertical or even overturned. In the northern limb, the Shawan formation is on contact with the sub-vertical greenish Taixihe formation. To the west, the motion along this thrust reduced rapidly, and two kilometers further west of the river it displays only the Shawan formation. Further north, about 50 m-thick Dushanzi formation thrusts on Quaternary terraces by the northward thrust fault (Figure 5-6). It is difficult to precisely estimate the net slips of these two faults. However, the compressive displacements along these faults could be limited because of following reasons. Firstly, these thrust faults are quite superficial and only located in the Cenozoic series, the underlain Mesozoic strata are not

thrust on the surface. Secondly, the faults are rapidly disappeared from the surface eastwards and westwards (Figure 5-5). For example, the Anjihai formation, located and well developed in the central part of the Huoerguosi anticline, is pinched out to both west and east sides, suggesting that the net slip of these fault decreases rapidly. Finally, but not the least, the eastern and western ends of this anticline show very gentle dips like the edge of a dome (Figure 5-4; Figure 5-5), indicating a small amount of deformation here. Therefore, the net fault slip in the central part of the anticline should be limited. Moreover, this fault does not exceed 10 km laterally neither westwards nor eastwards. This characteristic of the Huoerguosi anticline corresponds to the typical basin structure along the northern Tian Shan (Chapter 4).

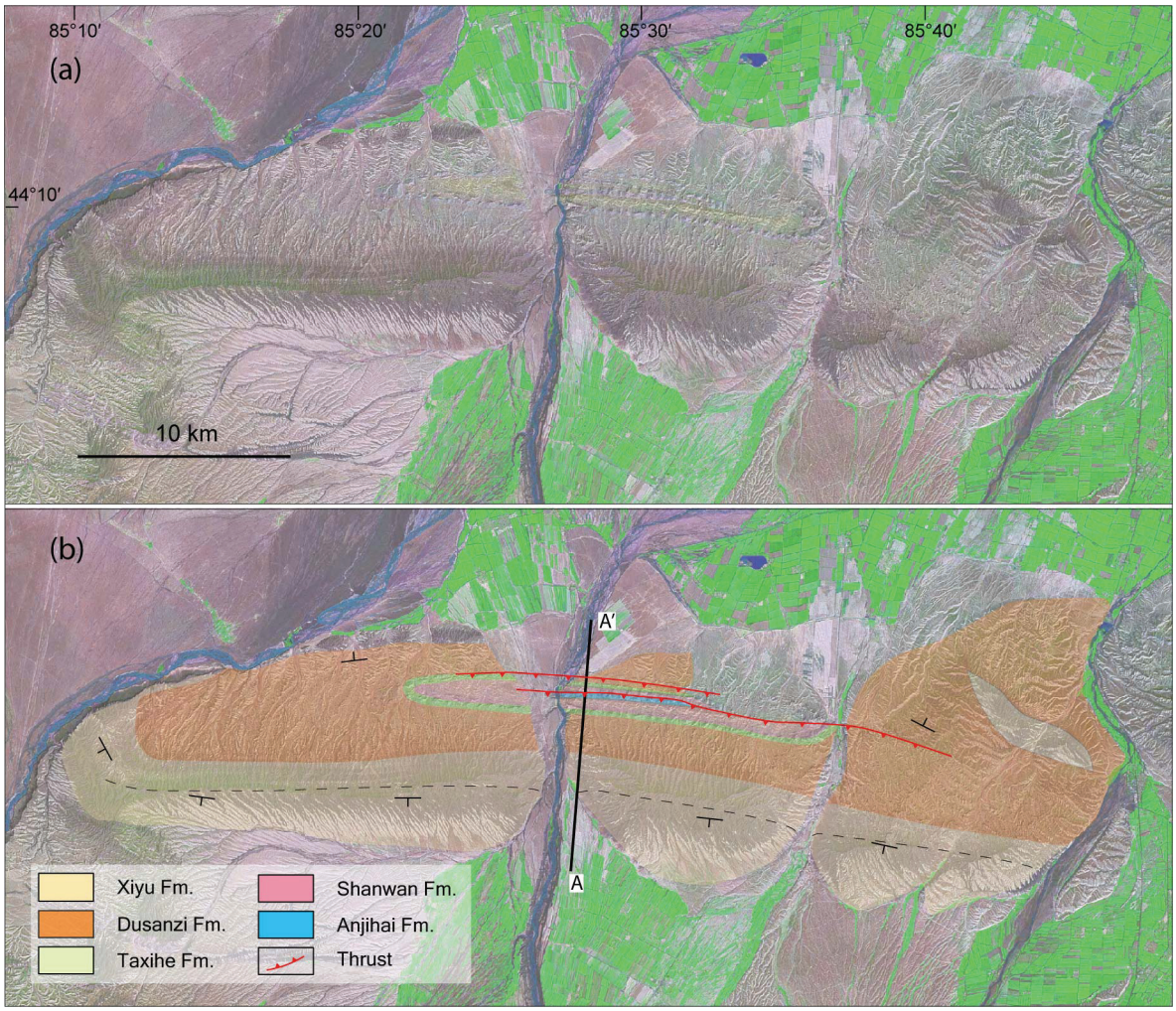

Figure 5-5. (a) Landsat TM image and (b) geologic interpretative map showing the Huoerguosi anticline along the Jingou He. See Figure 5-4 for its location.

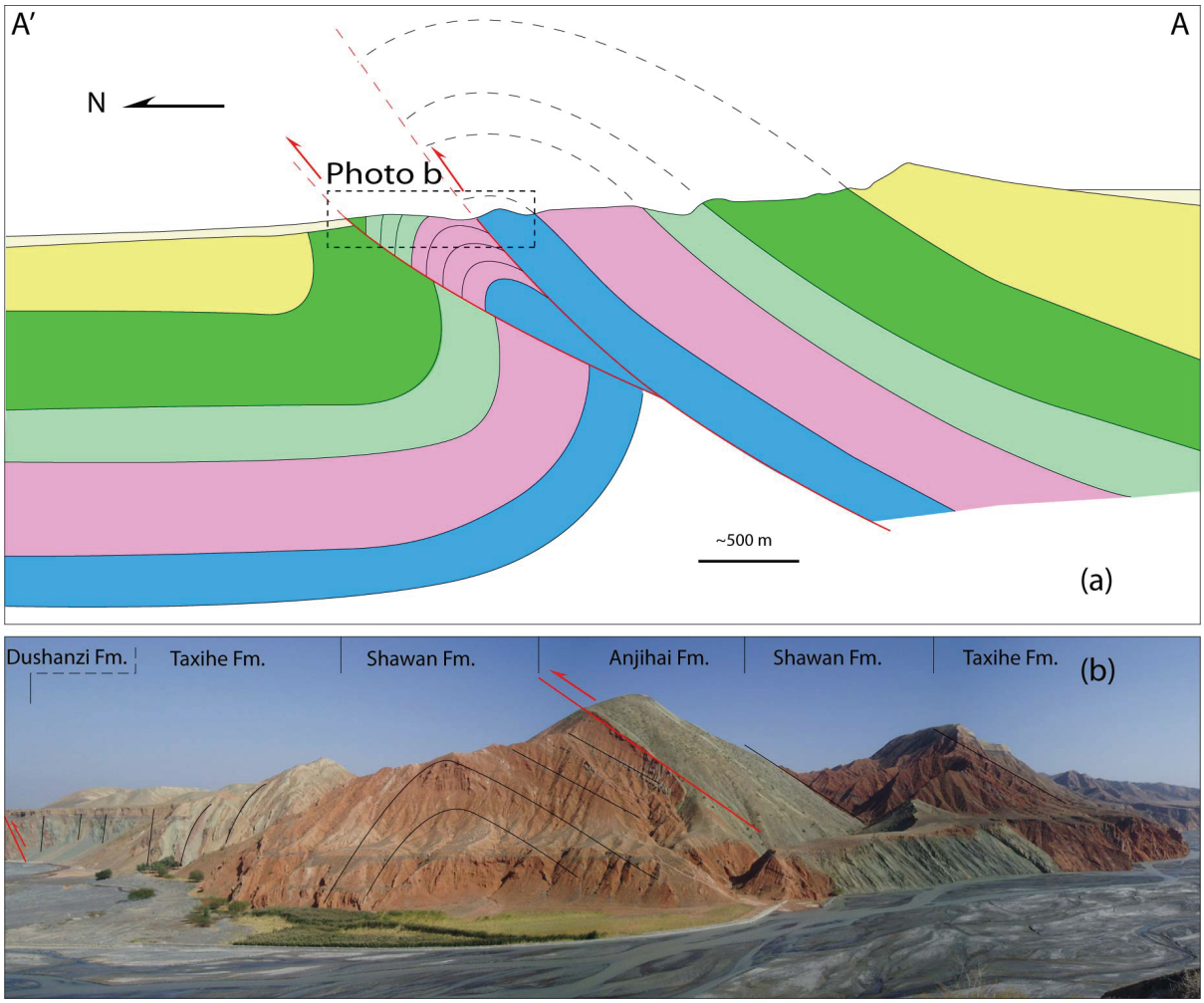

Figure 5-6. *(a) Interpreted section of the Huoerguosi anticline from Figure 5-5 and (b) the photo of its central part showing the anticline hinge complicated by thrust faults.*

As mentioned in Approach Section, because of the widespread Quaternary deposits, that can sometimes been several hundred of meters thick in the northern piedmont, the deep structure cannot be continuously observed on the surface from the front of Tian Shan to the basin (Figure 5-4). Gravity measurements have been therefore carried out and existed seismic profiles have been interpreted along this section (Figure 5-4).

Time to depth conversion of the seismic profiles has been computed along this section using velocities estimated from corresponding lithological facies. The geological map and observed stratigraphic geometry are integrated into the interpretation of this profile (Figure 5-7). Gravity measurements were carried out along the seismic profile and prolonged further south into the range (Figure 5-8).

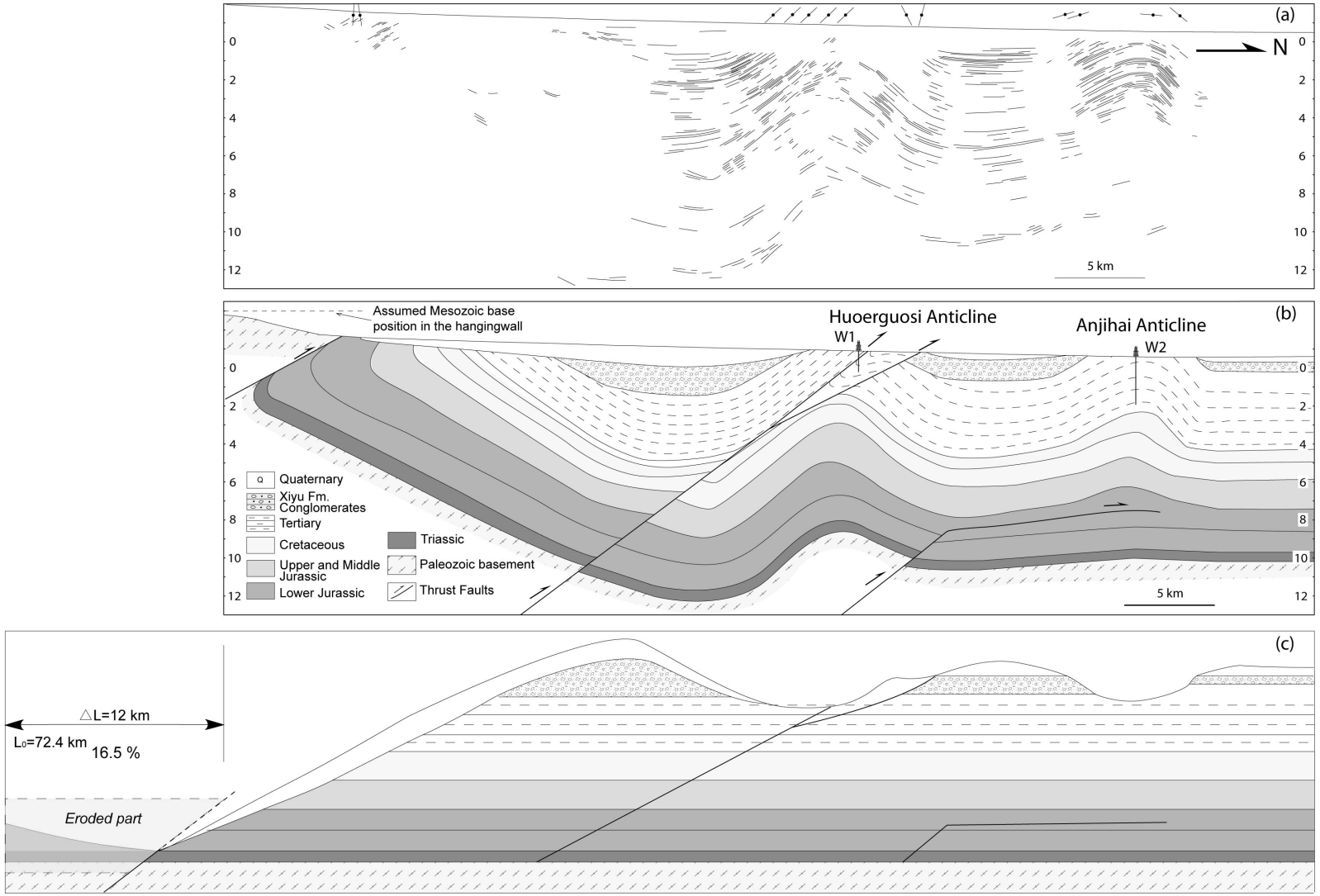

Figure 5-7. *(a) Linedrawing of the seismic profile along the Jingou He section associated with formation limits and dip angles on the field. (b) Interpretation of the seismic profile. (c) the restored section along Jingou He.*

The Anjihai anticline presents as a detachment fault in seismic reflection profile. Gravity profile does not show obvious anomaly here, because of the weak deformation and weak contrast in density within the whole Cenozoic series. Nevertheless, the Huoerguosi anticline position shows positive anomaly along the gravimetric profile, indicating an upward movement of deeper and denser rocks by folding and/or faulting. In seismic profiles, Tertiary strata are well deformed with two northward thrusts, which are also visible on the surface (Figure 5-6). Under these two thrusts, a fault-propagation fold is developed in the lower Mesozoic series (Figure 5-7b). A thrust fault cuts the northern limb and probably connects the Anjihai anticline by underlain the detachment fault (Figure 5-7). Two thrusting faults visible on the surface could be prolonged untile to the basement (Figure 5-7). However, the net slip should be limited, because this fault cannot be observed in another parallel seismic profile located 5 km to east (Li et al., 2010b). In the southern part of the seismic profile, reflectors are not clear for unknown reasons (Figure 5-7a). The structural section is only constrained by surface observations and the gravity data. Five kilometers west to the section, Jurassic layers show an overturned structure close to the mountain basement (Figure 4-10). Gravimetric profile shows higher positive anomaly values on the thrust with respect to that of the normal stratigraphic contact (Figure 5-8). Moreover, the positive anomaly here is less bounced than the model with basement in the footwall in the 2D forward model (Figure 5-8). It suggests that less dense Mesozoic sediments underlay the contact and show an overturned synform in the front of the thrust.

The restored cross-section has been constructed by integrating data from the geological profile (Figure 5-7c). As discussed above, the shortening in the Cenozoic series is limited as shown by the rapid decrease of lateral deformation in the Huoerguosi anticline, though It is difficult to precisely estimate the shortening. Once more, the Jurassic strata can be used as a mark layer of deformation. The main deformed part of this section is concentrated on the second fold-and-fault belt and the thrust contact between the mountain and the basin (Figure 5-7b). All the layers are restored to their initial horizontal geometry, and the thickness and lengths are reserved (Figure 5-7c). The bottom of the eroded Mesozoic level was assumed about 3000m on the mountain basement. This assumption is based on field observations in the southern Manasi area, where the Jurassic sediments horizontally deposed about 2500 to 3000m over on the mountain basement. The Jurassic series that could extend 40 km westwards to the Jingou He at the approximately same altitude was eroded at the actual section. The comparison between the geological section and the restored one indicates an about 12 km of shortening on this 72.4 km-long profile, taking the Jurassic layers as the

marker. Therefore, the shortening rate on this section is about 16.5%.

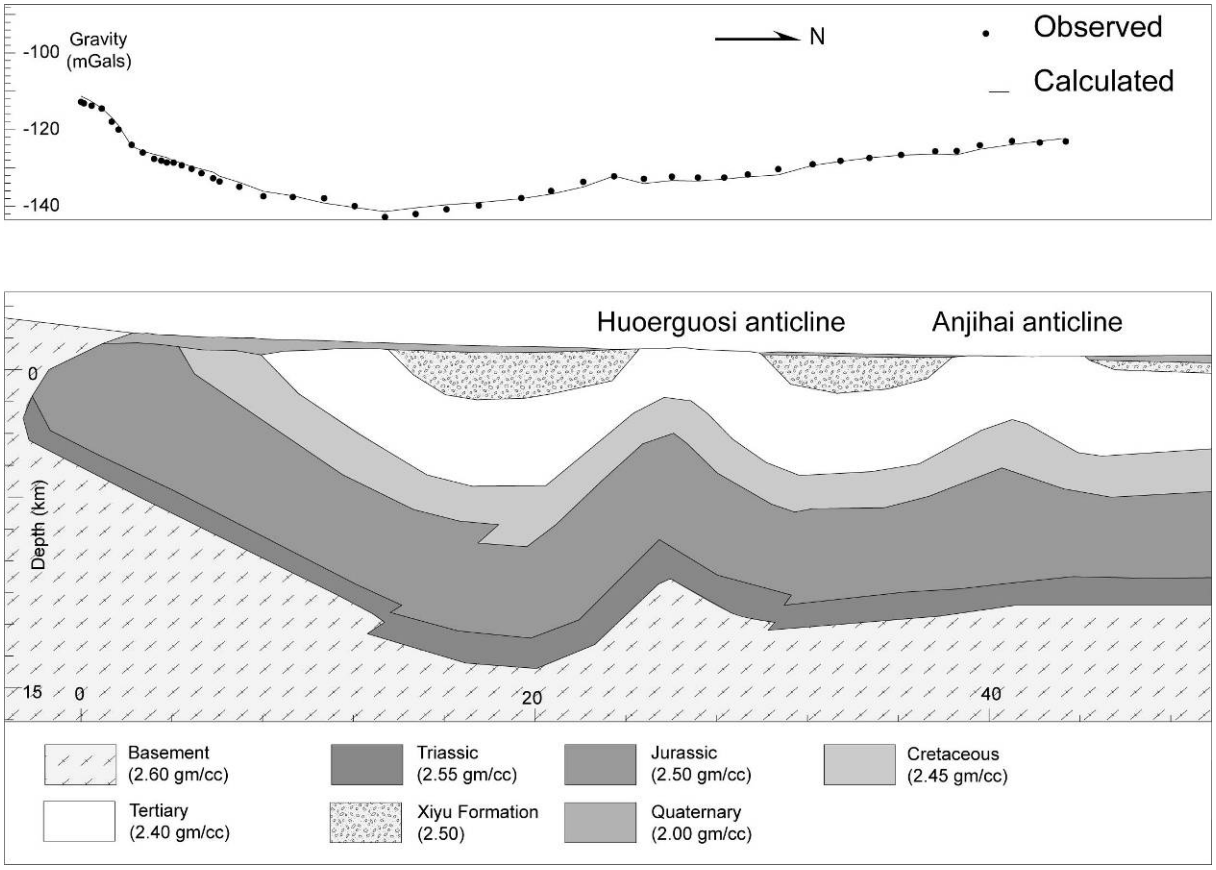

Figure 5-8. *Bouguer anomalies modeling along the Jingou He section. In the upper panel, the natural gravity data has been fitted to Bouguer anomaly data using densities indicated in the figure legends to construct the structural section.*

5.2.2 Qingshui He section

The Qingshui He section is located about 25km to east of the Jingouhe section (Figure 5-4). This section crosses the contact between the basement and the Junggar basin sediments in the south and two anticlines in the north (Figure 5-4). The northern one, namely the Manasi anticline, is similar with the Huoerguosi anticline in structure. Its southern limb dips about 45° southwards, while the northern limb dips steeply to the north or even overturned. A south-dipping thrust cuts the northern limb of this anticline. To south of the Manasi anticline, this section passes beside the eastern end of the Huoerguosi anticline. Farther south, the Cenozoic to Mesozoic series compose a monocline dipping about 60° northwards. It passes beside the western end of an anticline in Jurassic series. The Jurassic and Triassic sediments deposed on Paleozoic basement by stratigraphic contract dipping 60 to 70° north (Figure 5-4).

Gravity measurements have been carried out along this river, where, moreover, a seismic

profile is available. The seismic profile of Figure 5-9 shows the Manasi anticline with faults and the Tertiary series in the core. Below the faults, Mesozoic series forms a very gentle and asymmetric anticline. The northern limb is sub-horizontal and the southern limb dips 15° southwards, probably indicating a north-dipping thrust toward to south (Figure 5-9). However, this fault stops in the basement and doesn't attain to the basin sediments, which show a gentle anticline instead. To south of the Manasi anticline, a pair of small wavelength syncline-anticline is presented, extending until to in the eastern end of Huerguosi anticline where the deformation is weak with respect to its central part (Figure 5-4). The southern part of this section is characterized by a gentle anticline in Jurassic sediments (Figure 5-4). The contact is characterized by a fold of the Mesozoic basement without visible thrust fault in the field. Figure 5-10 presents the gravity measurements corresponding the seismic profile shows consistent geological interpretations.

A restored cross-section has been constructed by integrating data from the geological profile. The space-continuous Jurassic strata can be also used as a mark of deformation. The main deformed part of this section concentrates on gentle folds in the northern part and the fold contact between the mountain and the basin. All the layers are restored to their initial horizontal geometry, and the thickness and lengths are reserved (Figure 5-9). The bottom of the eroded Mesozoic level was also assumed 3000m over the mountain basement. The same argument has be used to this assumption, the Jurassic sediments horizontally deposed about 2500 to 3000m over the mountain basement according to the field observations in the southern Manasi area. The Jurassic could extend 15 km westwards to the Manasi He section with the approximately same altitude. The results show a shortening of ~6 km along this 63.1 km-long profile,taking the Jurassic layers as the marker. Therefore, the shorting rate is about 9.5% on this section.

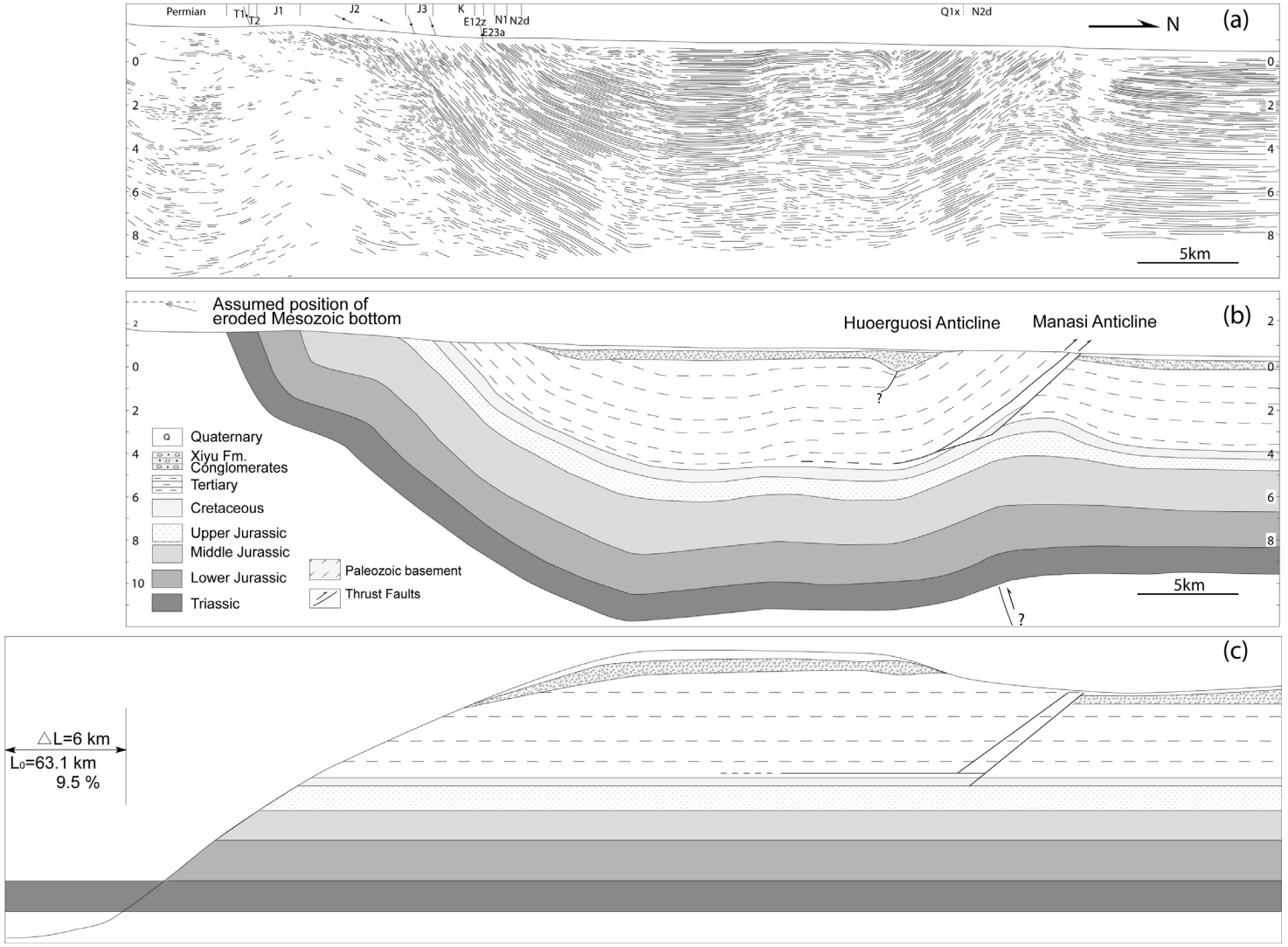

Figure 5-9. *(a) Linedrawing of the seismic profile along the Qingshui He section associated with geological formation limits and dip angles measured on the surface. (b) Interpretation of seismic profile. (c) Restored section along the Qingshui He.*

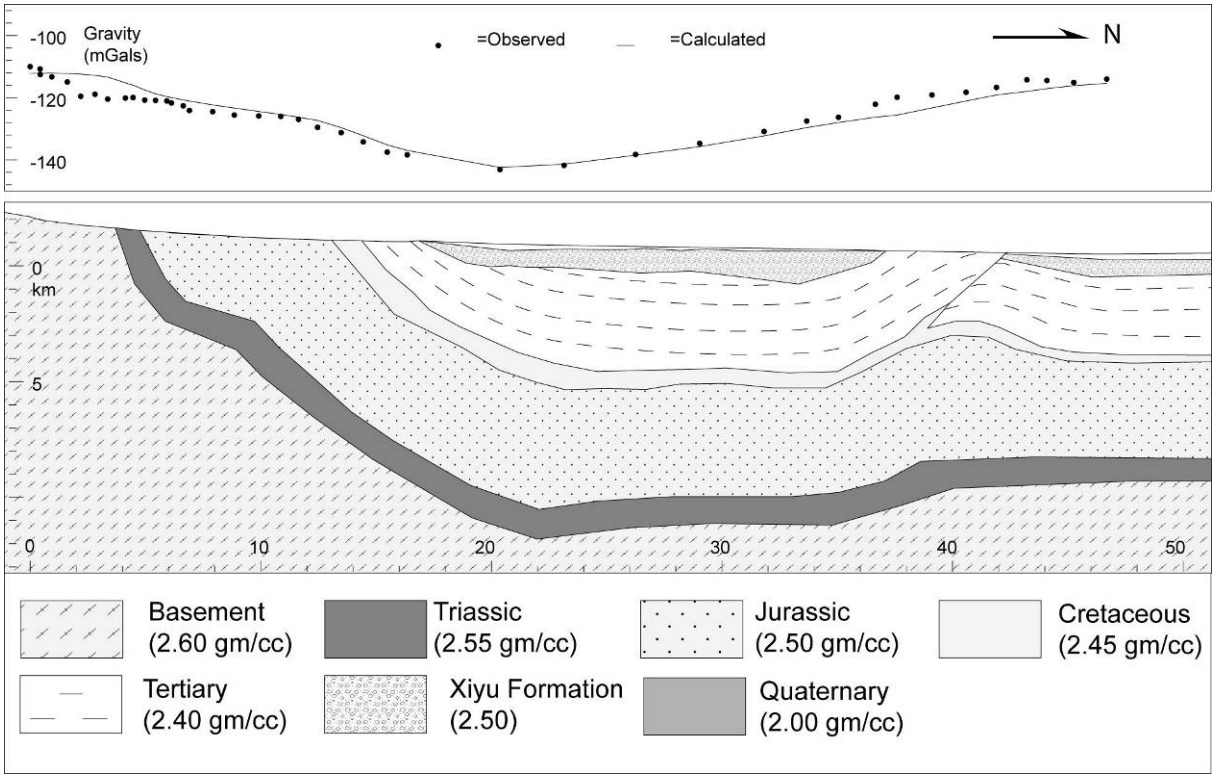

Figure 5-10. *Modeling of Bouguer anomalies along the Qingshui He section. In the upper panel, natural gravity data has been fitted to Bouguer anomaly data using densities indicated in the figure legend to construct structural section.*

5.2.3 Hutubi He section

Hutubi He flows northeastwards to the Junggar basin. It sub-perpendicularly cuts the structures of the fold-and-thrust belt in the northern piedmont of Tian Shan. Structural observations have been carried out in the southern part of this section. A seismic reflection profile is available for its northern part while gravity measurements have been carried out to complement the profile at the vicinity of the basement along the river (Figure 5-11).

To the north of the Hutubi He area, an anticline, namely the Tugulu anticline, can be observed to the west of the river (Figure 5-11). Its southern flank dips ~35 to 50° southwards, and the northern flank shows 45 to 60° northward dipping. The dip angle increases near the core and is even overturned due to the motion over a S-dipping thrust (Figure 5-11). While this anticline not extend eastward on map view, there covered by recent deposits, the seismic profile along the river shows similar structures at depth highlighting its lateral equivalent (Figure 5-12). The net slip of the thrust appears smaller than the outcropping west Tugulu anticline, evidenced by the lack of steep or overturned layers. The gravimetric profile also presented negative anomaly, indicating the fault and the anticline (Figure 5-13). The core of

the anticline is composed of the Cenozoic Dushanzi formation along the river, while older Anjihai formation presents in the central of Tugulu anticline.

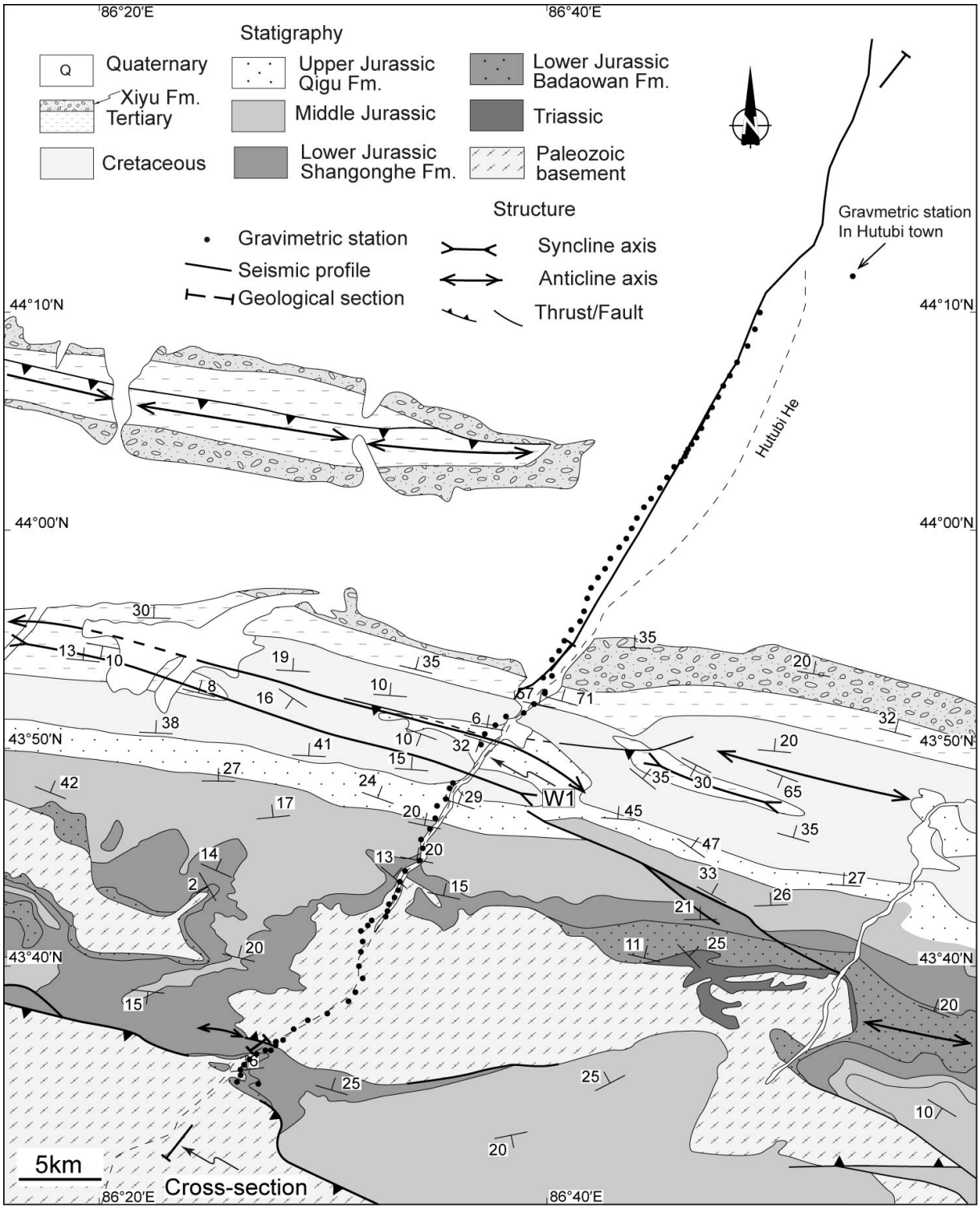

Figure 5-11. *Geological map of the Hutubi He area, with the locations of the seismic profile and the gravimetric stations.*

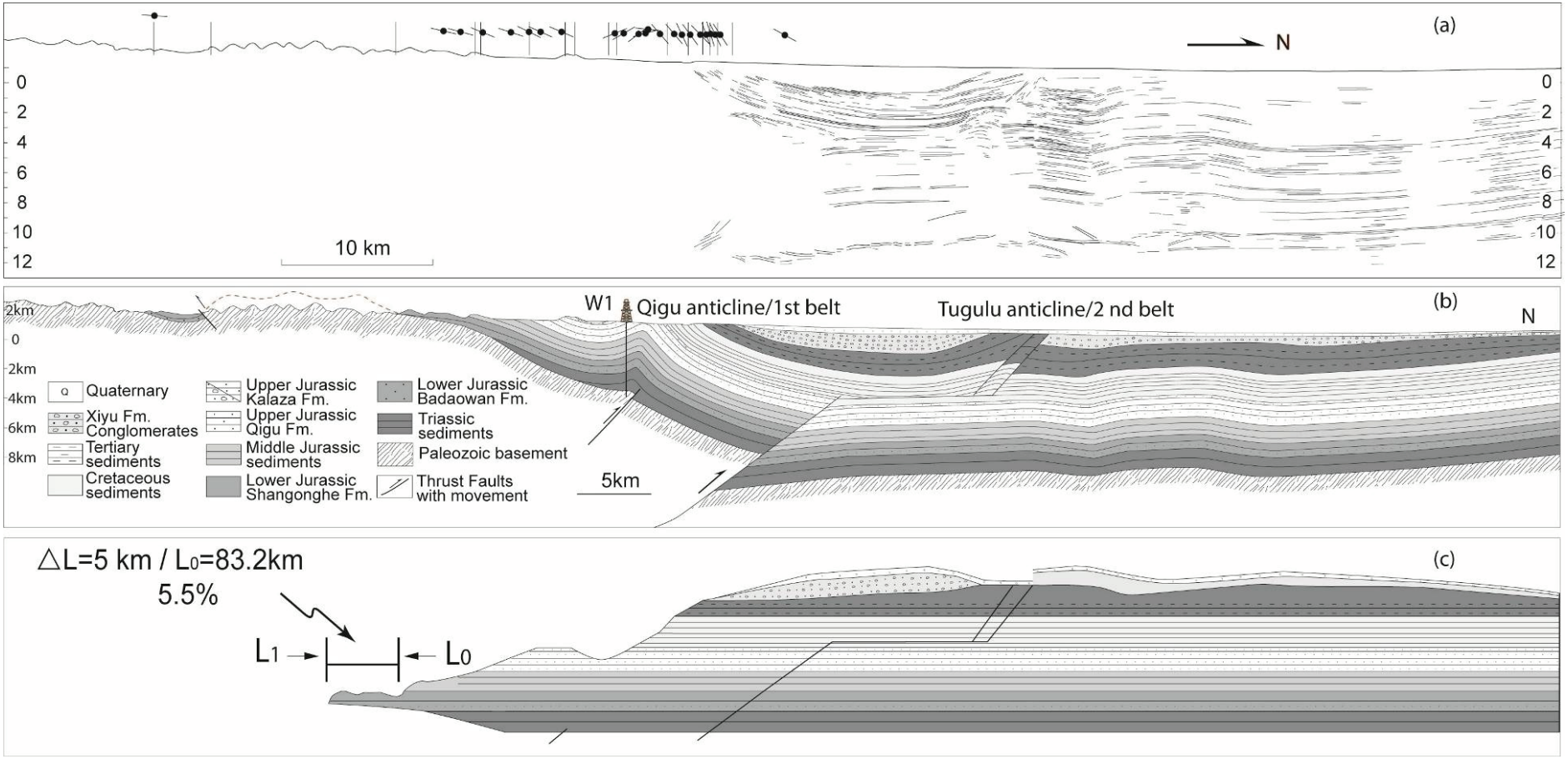

Figure 5-12. *(a) Linedrawing of the seismic profile along Hutubi He section (b) Interpretation of seismic profile. (c) Restored section along the Hutubi He, taking the Jurassic layers as marker.*

To the southern part of this section, Cenozoic to Mesozoic rocks uniformly dip to the north with an intermediate dip (~ 40 to 60°; Figure 5-11). It composes the northern flank of a second anticline farther south (Figure 5-12). This anticline is a gentle upright fold associated with a syncline in the south with only very limited thrust development. Further south, entering within the inner parts of the range (basement), sub-horizontal Lower Jurassic strata directly lie on the top of the Carboniferous units (Figure 4-15). In addition, a southward backthrust of basement rocks above Jurassic sediments can be observed to the south of the section, but the net slip must be limited as it rapidly dies out and the fault laterally transforms westwards to a kink fold (Figure 5-11 and Figure 5-12). The gravity profile along the southern part of the section shows positive anomalies in the anticline position (Figure 5-13). Bouguer anomaly modeling stops while entering the basement area because of the major influence of the steep topography in both sides of the valley.

Restored cross-sections has been constructed by integrating data from both geophysical and field data. The Jurassic strata can be continuously followed from the basin to the top of the basement. Therefore, they can be used as a continuous marker of deformation. A calculation for the initial length of the section has been made from the northernmost part of the section to the first outcrops of the Paleozoic basement (Figure 5-12). The main deformed part of this section concentrates on the two main fold-and-fault structures. All the layers are restored to their initial horizontal geometry and thickness and lengths are reserved (Figure 5-12). The comparison of two sections shows a shortening of about 5 km along this 83.2 km-long profile, taking the Jurassic layers as marker indicating a shortening rate is about 6 %.

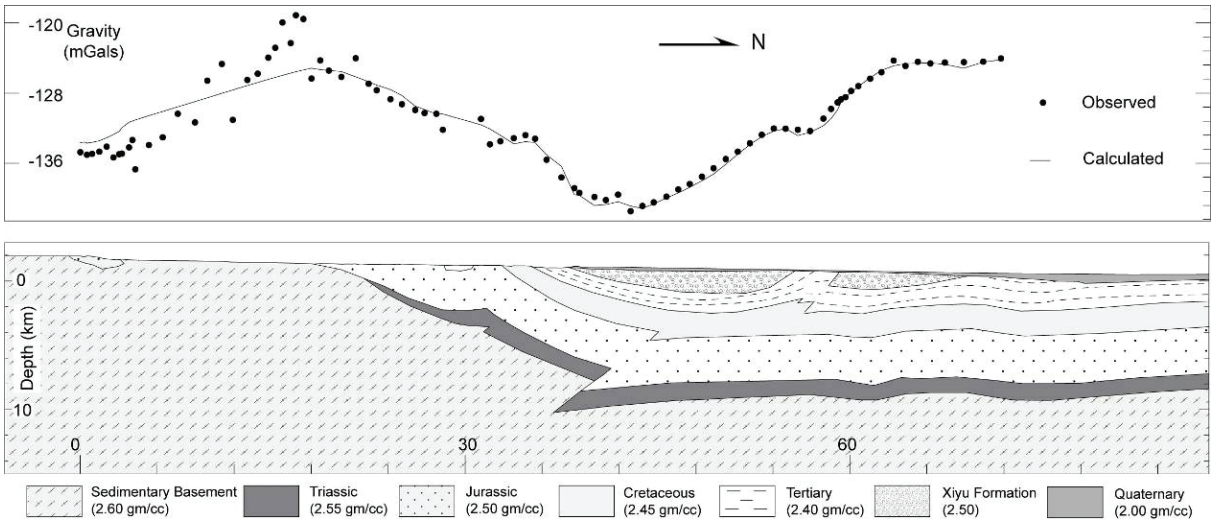

Figure 5-13. *Modeling of Bouguer anomalies along the Qingshui He section. In the upper panel, natural gravity data has been fitted to Bouguer anomaly data using densities indicated in the figure legend to construct structural section.*

5.2.4 Wusu section

The Wusu section is located southeast to the Wusu city, the westmost of the study area (Figure 5-14). In the field, the northern part of the section is characterized by monoclinal layers, composed of Cenozoic sediments dipping about 60° northwards (Figure 5-14). Further south, a large wavelength syncline is present involving some faults and small-scaled folds (Figure 5-14). A geological section has been built up integrating field surface observations, seismic profile and drilled wells (Figure 5-14). This section has been strengthened by gravity measurements and 2D forward modeling realized along the main road.

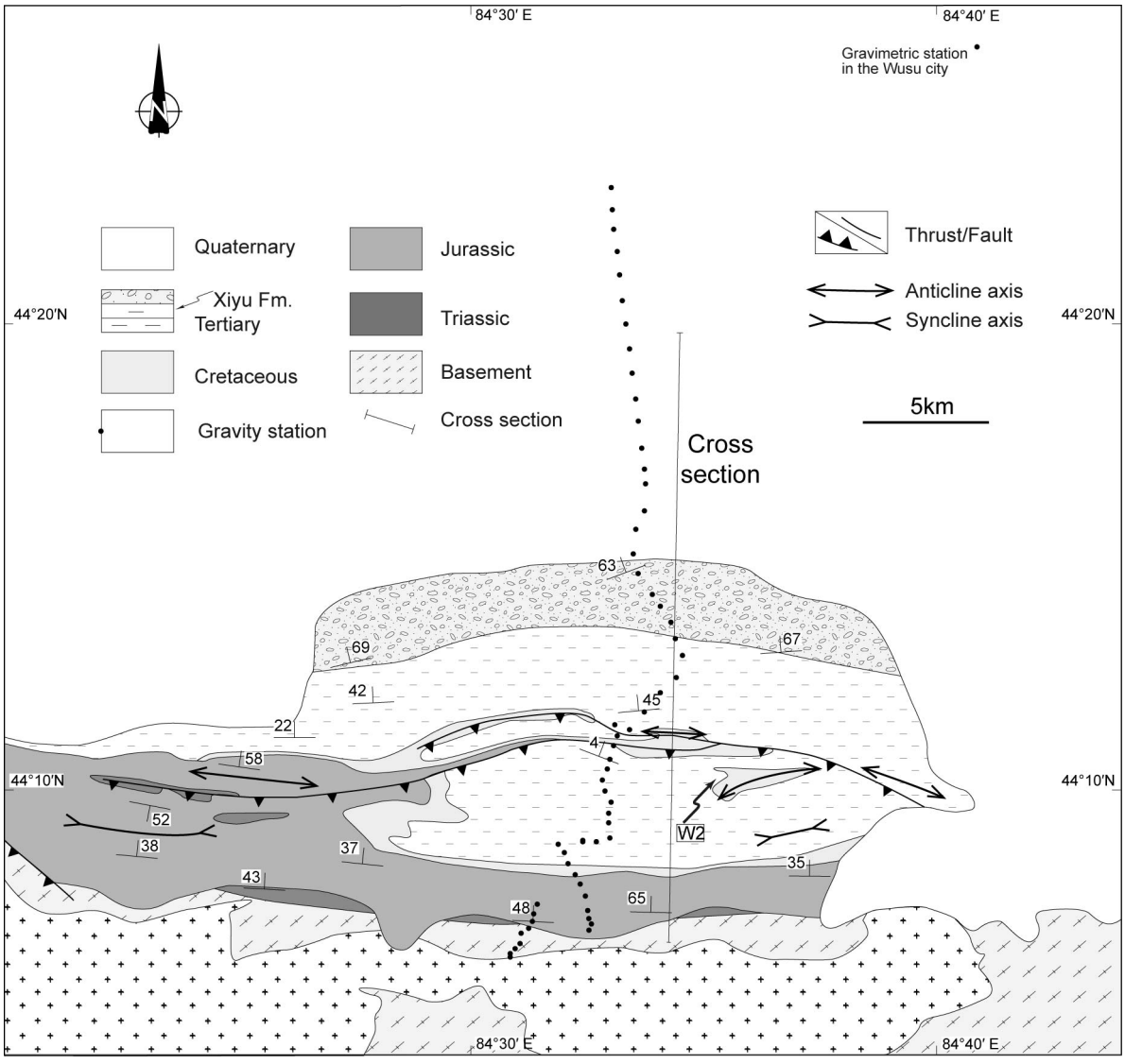

Figure 5-14. *Geological map of the Wusu area. Shown are the locations of the seismic profile and the gravimetric stations.*

In the Wusu area, the total thickness of the preserved Jurassic strata is reduced to about 1km according to drilled wells. Both seismic profile and gravimetric measurements show a

horizontal stratigraphic geometry for the northernmost part of this section without obvious deformation (Figure 5-14, Figure 5-16 and Figure 5-16). Moving southwardly, conformingly with the Hutubi He and other sections, the first-order structure of the Mesozoic-Cenozoic series displays a 40-60° northward dipping monocline (Figure 5-16 and Figure 5-15). Continuously to the south, the stratification becomes sub-horizontal and the structure of the sedimentary series displays as a large hinge fold. As drawn on the geological map, thrust faults are visible in the field in this segment. However, seismic data do not show any extend of the faults to depth into the Mesozoic series, indicating a limited thrust displacement along the faults. In the southernmost part of the Wusu section, sediments are directly covering basement units with a 20 to 40˚ diping northwards. As a whole, the structure of this section show a trishear fault-propagation fold, which indicates a thrust fault northwards in the deep basement (Figure 5-16 and Figure 5-16).

Taking the lower Jurassic as marker, the similar calculation on the balanced cross-section shows that the shortening is about 2.0 km on the 20.4 km-long profile (Figure 6-16b). Minor deformation recognized in the field is neglected, such as the two south dipping reverse faults that do not extend to depth on the seismic reflection profile. The shortening rate calculated along this section is then of the order of 9.8%.

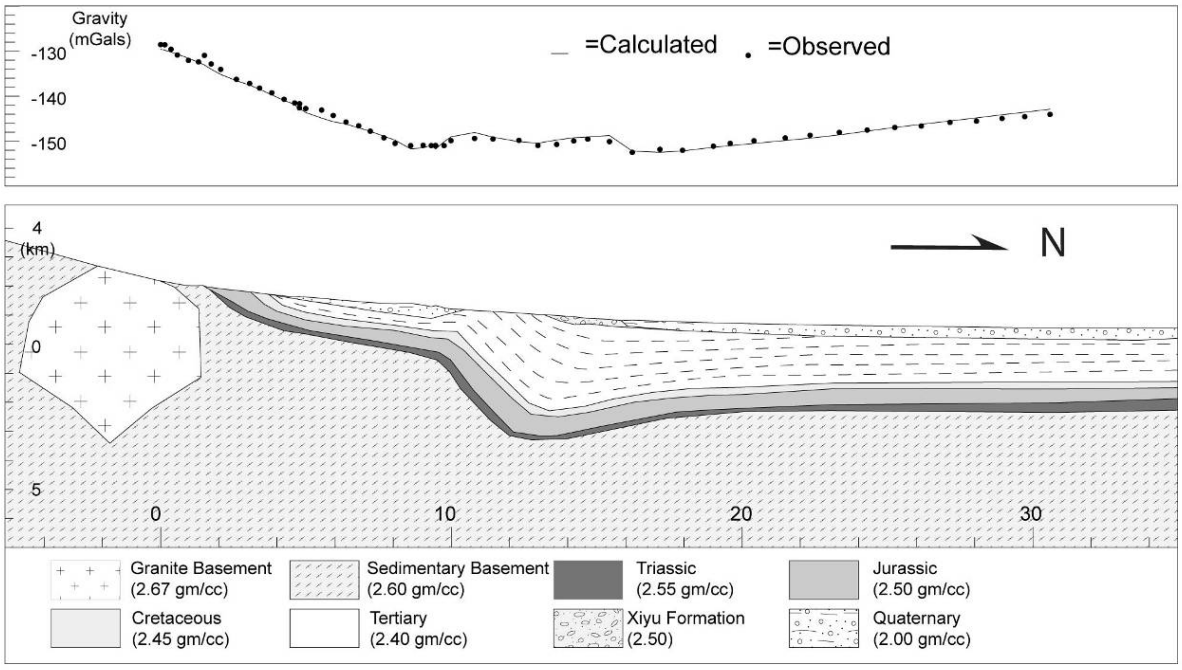

Figure 5-15. *Modeling of Bouguer anomalies along the Wusu section. In the upper panel, natural gravity data has been fitted to Bouguer anomaly data using densities indicated in the figure legend to construct structural section.*

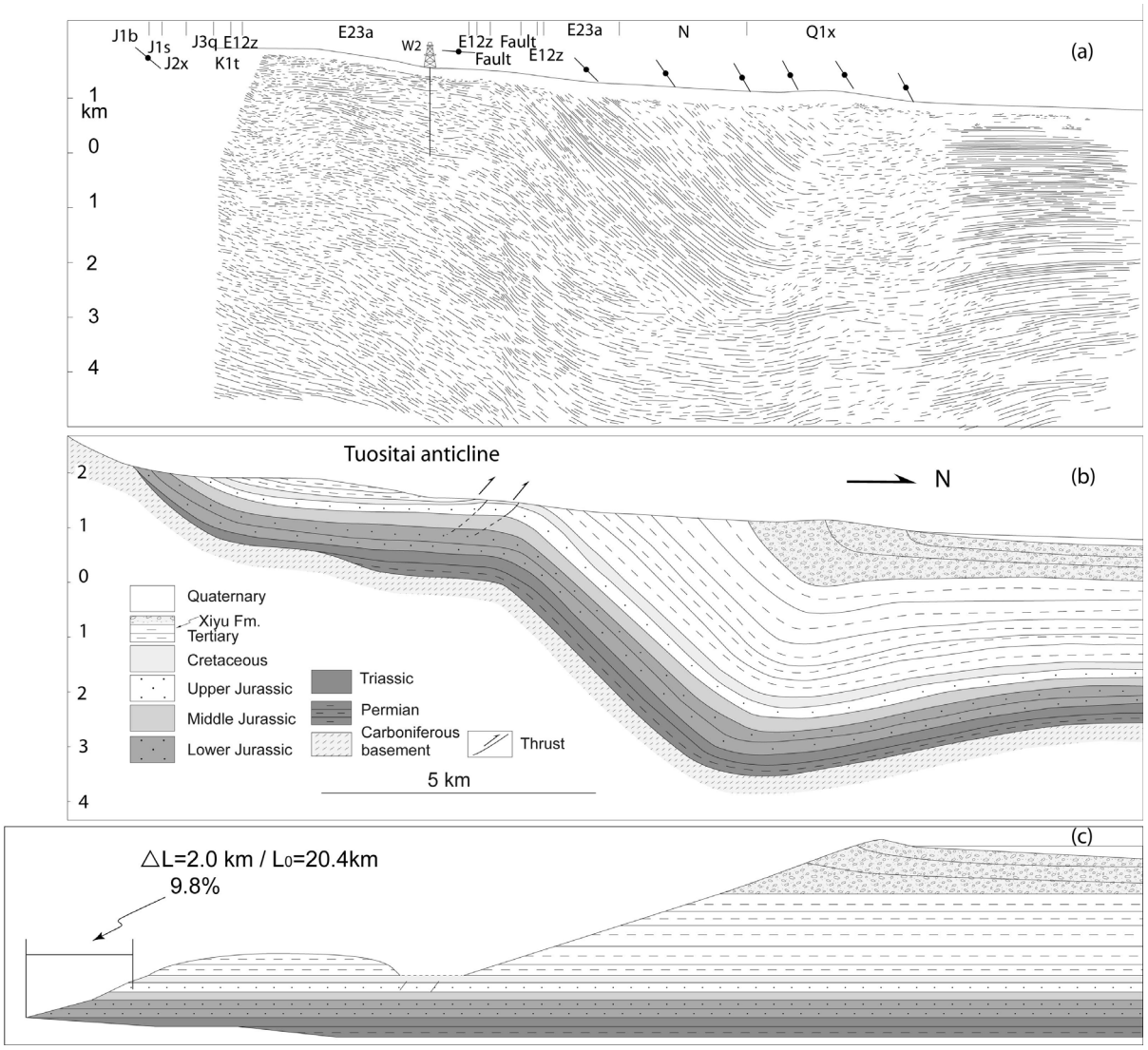

Figure 5-16. *(a) Linedrawing of the seismic profile along Wusu section associated with dip angle field measurements of (b) Interpretation of seismic profile. (c) Restored section along the Wusu section. Note the impressive thickness of the so called Xiyu formation here clearly displaying growth strata geometry*

.

5.3 Discussion

5.3.1 Mechanism of deformation in the northern piedmont of Tiansahn

(a) Is the northern Tian Shan characterized by a structural front?

The structure of the northern Tian Shan range has been carefully observed in the field. These observations together with structural measurements have been complemented with an important set of drilling well and geophysical data including seismic profiles and gravity measurements. Intracontinental orogens, such as the the Pyrenean mountain ranges and Canadian Rocky mountain, are often characterized by main frontal structures that concentrate most of the strain and most account for the overall shortening. Unlike this traditional view of a mature range front, the northern front of Tian Shan is characterized by a variety of structures within the contact with the Junggar basin, including thrust fault contact, kink fold contact and even still preserved unconformity, sedimentary contact.

First, thrust fault type contact between the basement and the Junggar basin sediments can be observed in several places, such as Taixi He, Jingou He and Kuitun He sections. Second, kink fold type contact with normal steep dip angle in sediments are located in Qingshui He and Manasi He sections. Last, sedimentary type contact with sub-horizontal unconformity between strongly deformed basement and overlying sediments without obvious deformation are widespread over the study area and mainly observed to the south of Hutubi He and Wusu sections. These three types of contracts between the Tian Shan basement and the Junggar basin sediments are displayed laterally along the northern front of the mountain belt (Figure 5-17). These types mostly depend on the local deformation intensity (local shortening) which fastly evolve laterally. Such local variations of shortening gives rise to the different structural geometry along the front of the northern Tian Shan, such as thrust to sedimentary contact from strong to weak deformation intensity.

These rather rapid lateral variations are also strongly suggested by Bouguer anomaly map in the northern piedmont of Tian Shan highlighting strong unexpected lateral gradient (Figure 5-18). Along a single structure, at this local scale, a clear range front can not be pointed out as deformation is distributed over a rather large orogen-parallel stripe where overall shortening

may reasonably been the same. The northern Tian Shan, while characterized by a spectacular orogenic front corresponding more or less to boundary between the basement rocks and the Junggar sediments is, to date, devoid of a clear structural front. The most probable reason may be due to the immaturity of the belt, tectonically reversed during the Neogene and as seen in the previous chapter from an existing relief.

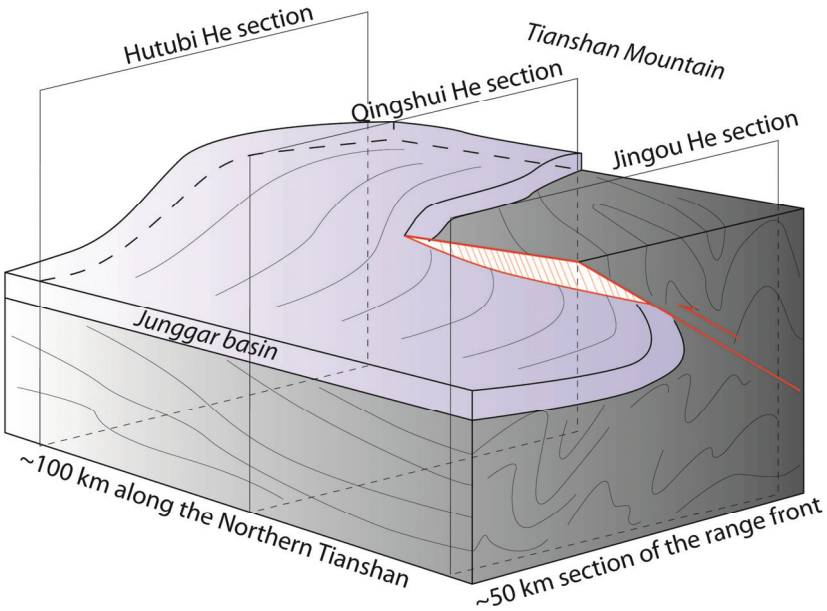

Figure 5-17. *Conceptual structural sketch showing how, on a rather local scale (~100km along the range), the structure may principally vary from a thrust to a unconformity through a fold observed at Jingou He, Qingshui He and Hutubi He between the basement and the Junggar sediments, respectively.*

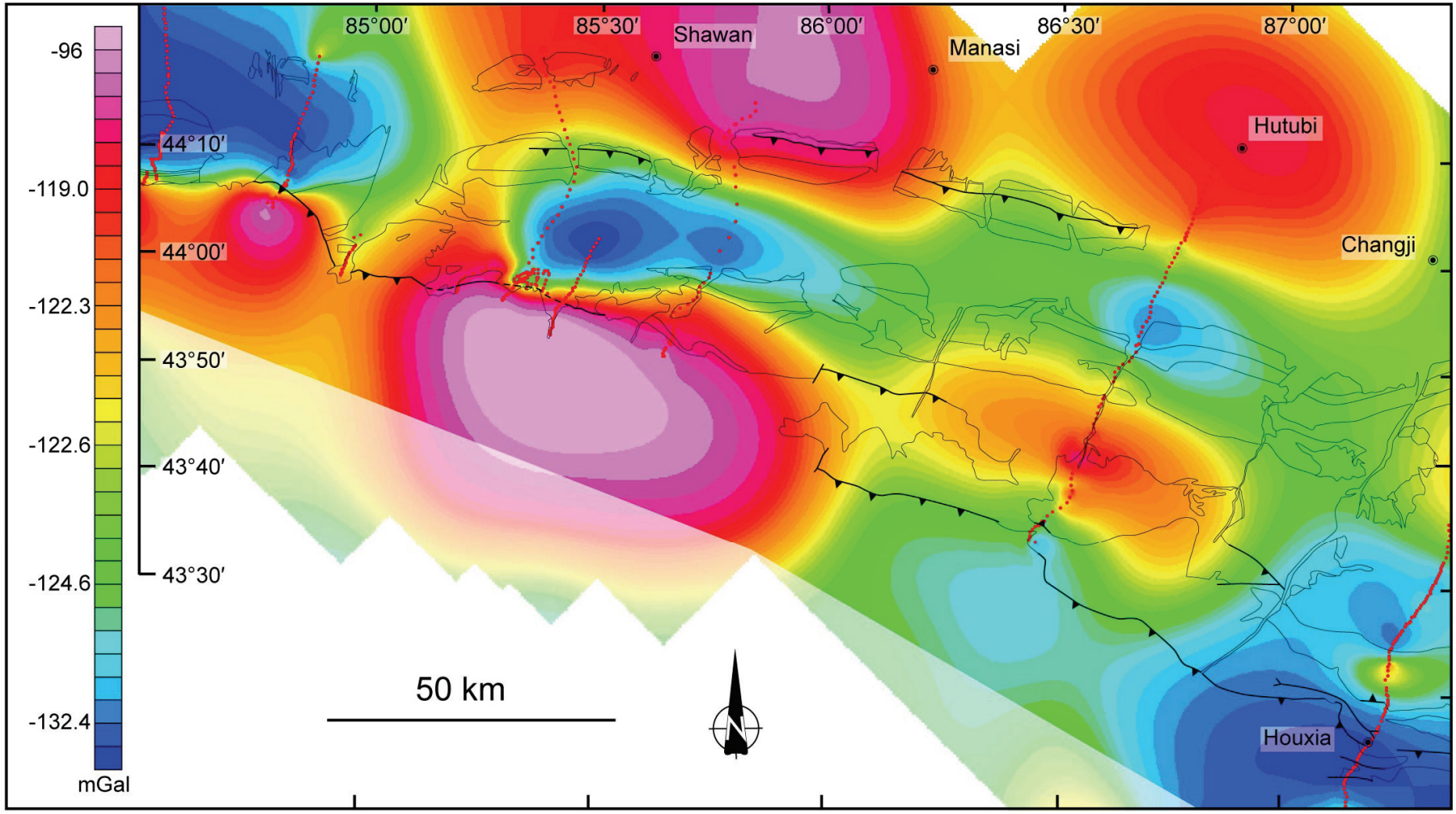

Figure 5-18. Bouguer anomaly map in the northern piedmond of Tian Shan with locations of gravity stations (red dots). Major geological limits are drawn. See Figure 4-1 for details of geological boundaries.

(b) The structure of the fold-and-thrust belt in the basin

Since the Junggar region has been widely investigated for oil and gas resources, seismic profiles and drilled wells are particularly abundant. These data together with field observations, structural studies permitted to settle the overall geometry of the fold-and-thrust belt developed along the Tian Shan range into the front zone (Avouac et al., 1993; Fu et al., 2003; Deng et al., 1996; Burchfiel et al., 1999; Molnar, 2004; He et al., 2005; Li et al., 2010b; Lu et al., 2010). The southernmost fold belt is located in the north of the basement–basin contact, such as the Qigu and the Qingshui He anticlines. Theses folds are basement-involved with gentle asymmetric anticlines. This belt is not well developed along the Jingou He and Kuitun He sections, where the contract is characterized by large-displacement thrust fault. In contrast, this first southern fold belt is well displayed along Manasi He, Hutubi He and Changji He in the east part of the study area where the southern contacts are less deformed. Therefore, this first southern fold belt is probably well deformed when the contact is less shortened, while it is weak deformed when the contact area absorbed the mainly shortening.

The second fold belt is mainly a fault-bend fold belt. The mechanisms to produce this fold require a décollement zone in Jurassic layers, such as coal layer or marls, with emerging ramps often observed in the field as a thin-skin deformation or deduced from the seismic profiles (Burchfiel et al., 1999; He et al., 2005). However, this fault-bend fold is accompanied and visibly controlled by basement fault at depth, such as the Huoerguosi anticline along Jingou He. This fault of rather high angle in basement reaches a flat décollement zone in the Mesozoic series and propagates northwards.

The third fold belt is composed, for example, by the Dushanzi and the Anjihai anticlines along the Kuitun He and Jingou He, respectively. The Dushanzi anticline is a fault-bend fold and the Anjihai anticline is a detachment fold. The basement is not involved in the deformation here (Daëron et al., 2007).

Fault-propagation fold accounts for most of the shortening in the first fold belt, while these faults are located in the Paleozoic basement. For the two fold belts in the north, the critical mechanism problem is where the faults come from. One model concerns the detachment in the basal Jurassic with ramps located in the second and third fold belts (Deng et al., 2000; Figure 5-19a). Based on our geological sections, an alternative deformation and propagation model is proposed (Figure 5-19b). It is characterized by: 1) the basement is deformed as rigid blocks; 2) no large-movement décollement in the basin; 3) the shortening is limited in the northern "front" and in the foreland basin as well.

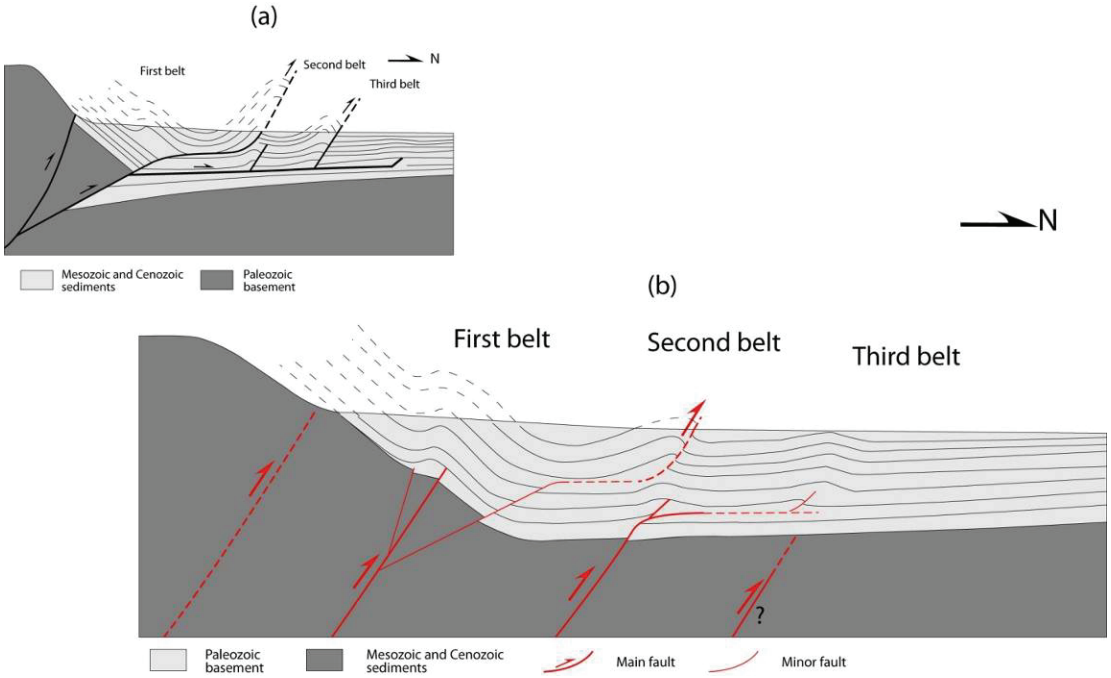

Figure 5-19. *(a) Sketch diagram proposed prior to this study for the northern of Tian Shan. A main décollement zone at the base of Jurassic layers accounts for a rather large shortening involving a main intrabasement blind fault (after Deng et al., 1999). (b) Model proposed in this study where deformation, still gentle is localized over pre-existing basement structures whose reactivation deforms the sedimentary cover. Deformation and slip over these faults may be captured by decollement zones.*

5.3.2 The shortening in the foreland thrust-and-fold belt

Shortening estimates have been previously calculated for most of the anticlines in

the northern Tian Shan foreland from seismic data (Deng et al., 1991; Molnar et al., 1994; Deng et al., 1996; Burchfiel et al., 1999; Deng et al., 2000; Wang et al., 2004; Daëron et al., 2007; Charreau et al., 2008). However, these local shortening values, rather high for individual structures in these three fold belts, could not be simply summed up to reach the total account of shortening for the whole fold-and-thrust belt (Table 5-1), because of not only the laterally variation of the structures (Burchfiel et al., 1999), but also the different deformation characteristics in depth. For example, the shortenings in the northernmost (third) and second thrust belts, which is mostly calculated with Cenozoic layers, could not summed up with that in the southernmost (first) thrust belt, which is calculated with Mesozoic layers. Moreover, theses studies are most concept model-driven rather than data model-driven (Avouac et al., 1993; Burchfiel et al., 1999). Therefore, in this study, lower Jurassic strata as a marker are restored and are used to calculate the regional shortening.

South belt			Middle belt			North belt		
Qigu anticline	~6.2 km ~5.5 km	B D1	Huoerguosi anticline	~10 km	C	Dushanzi anticline	2.12-2.35	B M
Nan'anjihai anticline	>4.2 km ~ 5 km	D1 L	Manasi anticline	~6.5 km	D1		~2.9	D1
Tuostain anticline	~ 4.6-5 km	B	Tugulu anticline	~6.0 km ~5.5 km	Y B M	Anjihai anticline	~1.5	D2 L D3

B: Burchfiel et al., 1999; D1: Deng et al., 2000; L: Li et al., 2010; C: Charreau et al., 2008
Y: Yang et al., 1996; M: Molnar et al., 1994; D2: Daëron et al., 2007; D3: Deng et al., 1991

Table 5-1. *Shortening estimates of anticlines in the northern piedmont of Tian Shan (Lu et al., 2010).*

Besides the deformation of the three successive fold belts in the foreland basin, the shortening is also located in the intramountain basin areas as presented in Chapter 4. However, this fault varies to an unconformity contact along strike suggesting a various and limited displacement. In fact, along the northern piedmont of Tian Shan, relatively important shortenings in the contact zone between the range and the basin can be only observed in the Junggar southern thrusting faults of the Kuitun He and Jingou He sections. Other sections did not show obvious fault in the contact zones, and Jurassic sediments can be continuously followed from the basin to the inner parts

of Tian Shan.

In summary, the comparison of geological sections with their corresponding restored ones shows shortenings of 12 km (16.5%), 6 km (9.5%), 5 km (6%) and 2 km (9.8%) for the Jingou He, Qingshui He, Hutubi He and Wusu He sections, respectively. This data are fairly weak with respect to the well developed foreland basin. However, though these estimates, deriving from multidisciplinary yet consistent studies, are rather accurate for the foreland basin, the total shortening in the front zone or event the whole intercontinental range may be highly underestimated as the main intrabasement thrust and, more generally, the deformation in the basement remain unexplored.

Chapter 6

General discussions, conclusions and perspectives

The current high relief of the Tian Shan range is traditionally considered as a far-field consequence of India-Asia collision (e.g. Tapponnier and Molnar, 1977; Avouac et al., 1993) which is responsible for the tectonic reactivation of the Paleozoic range (Avouac et al., 1993; Hendrix et al., 1994). Propagation of the deformation to the north and inception of the reactivation throughout the Tian Shan area is still a matter of debate. Based on numerous and multidisciplinary observations, the effective onset of deformation seems, in any case, younger than 25 Ma, leading some authors to suggest high rates of deformation (Avouac et al., 1993; Molnar and Ghose, 2000; Charreau et al., 2008; Lu et al., 2010). Field works carried out during the last 3 years in this PhD thesis all along the northern piedmont of Tian Shan show rather weak deformation in the piedmont and conversely point out the existence of a significant Mesozoic paleo-relief. To better understand the evolution of the northern piedmont of the Tian Shan, a brief review of new data acquired in this study will firstly be exposed in this chapter. Then, a synthetic analysis is made to discuss the main results. Finally, general conclusions on this work will be exposed as well as some ideas on the future research needed on this topic.

6.1 Persistence and contribution of a Mesozoic paleo-relief

Basement rocks encountered in the Tian Shan range carry unambiguous traces for a long-lived subduction, accretion and collision history during Paleozoic times and several sutures have been described as well as major shear zones of various geometry and kinematics (Windley et al., 1990; Gao et al., 1998; Xiao et al., 2004; Charvet et al., 2007; Wang et al., 2007). The present-day topography of the Tian Shan is traditionally related to the Neogene intracontinental reactivation of such main inherited structures within the Tian Shan range (Tapponnier and Molnar, 1977; Avouac et al., 1993). Mesozoic history of the northern Tian Shan is characterized by thick continental sediments deposits. Despite this period remains widely unexplored, it appears devoid of any major deformational event. This study along the northern

piedmont of Tian Shan, however, unambiguously demonstrates new and clear field evidences for the existence of a significant Mesozoic relief before the Neogene uplifting. The Jurassic series are mostly characterized by thick coarse-grained continental deposits. Within intramountain basins, sedimentary breccias carrying a significant contribution of Carboniferous basement clasts characterise the base of the series, arguing for the presence of a rather proximal paleo-relief of basement rocks along the range front and the occurrence of proximal intramountain basins. In parallel, while a major thrust system is traditionally evoked between Junggar basin deposits and the basement units, some of the studied sections show unconformable deposit of Triassic to Jurassic sediments overlying deformed basement rocks with a continuous extend of sedimentary series from basin to the top range. Some of sections clearly show "onlap" type deposits of Jurassic clastic sediments on top of the Paleozoic basement that was thus significantly sloping down to the north at that time. These results are strengthened by the attitude of the geological outlines of lower Mesozoic series that clearly display regional onlaps at map-scale. A major paleo-relief along the northern Tian Shan is thus progressively sealed during, at least, a part of Mesozoic times, and particularly during Triassic and Lower Jurassic times (Figure 3-8a).

At the outcrop scale, the "onlap" architecture reveals local drastic paleo-elevation difference of at least of 100-150m for some hectometers horizontal distance (see example in the Hutubi He area). At a larger scale (50 km), the thickness difference of Jurassic sediments reaches around 1300 m between the outcropping series along the Tian Shan and drill well data basinward (Figure 3-5 in Chapter 3). In addition, while the entire Mesozoic sedimentary sequence is preserved within the basin, from Triassic to Cretaceous, Triassic to Middle Jurassic strata are missing within most interior parts of the range. No major internal deformation is observed within the sedimentary series and layers of Mesozoic sediments remain almost parallel in the northern Tian Shan piedmont. These latter features argue for the existence of a relatively high relief during Early Jurassic time and its progressive infilling, or covering during Mesozoic times (See chapter 3 for detail arguments). This paleo-elevation difference of 1300m

indicates a minimum for the relative altitude of the Tian Shan early Mesozoic paleo-relief.

This major result from this thesis work is in agreement with published indirect studies that emphasized a probable Mesozoic relief located within the present day basement range. Firstly, Mesozoic paleocurrent indicators highlight northward sediments transport along the southern Junggar basin flanks and southward transport along the north Tarim basin area (Hendrix et al., 1992; Li et al., 2004). Secondly, due to the agglomeration of "terranes" from different origin during Paleozoic times, the basement of Tian Shan is made of several contrasted lithologies (Windly et al., 1990; Gao et al., 1998; Wang et al., 2007). Clastics, and in particular sandstone deposits can thus be tied to specific source terranes within the Tian Shan basement complex. The mineralogical composition of sandstone layers is different in the southern Junggar and north Tarim basins, indicating that a Mesozoic Tian Shan mountain was most probably separating the two basins (Hendrix et al., 2000). Thirdly, the apatite fission-track cooling ages reported by recent studies suggest the unroofing of Tian Shan during Mesozoic (Dumitru et al., 2001; Guo et al., 2007; Zhang et al., 2007; Wang et al., 2009; Jolivet et al., in press). At last, isopach maps show that the Mesozoic series in the southern Junggar and northern Tarim basins are thicker on both sides of the Tian Shan range (Gu, 1994), indicating that an ancestral Mesozoic Tian Shan would be present and i) was the source of sediments, ii) controlled the sedimentation location in the adjacent basins and iii) the range was roughly striking parallel to the current one.

Thus, field observations and large-scale map analyses done in this study argue for i) the persistence of a paleo-relief from early Mesozoic times and during Triassic and Jurassic times and ii) relief "infilling" by a continuous clastic sedimentation, with no deformation and/or vertical movement associated with, during that period. From this and from available sedimentological data, the following scenario may be proposed for the Mesozoic relief evolution along the northern piedmont of Tian Shan. During Middle Jurassic times, clastic sediments conformably deposited on top of the Lower

Jurassic strata within the basin, while they progressively deposited onlap of the Paleozoic basement toward the mountain interior (Figure 3-8a). Middle Jurassic deposits extend to a larger area with respect to the Lower Jurassic and the paleo-relief latitudinal extension was certainly less important during Middle Jurassic than that during Triassic/Early Jurassic (Figure 3-8b). During the latest Jurassic to Early Cretaceous, conglomerates and breccias deposited onto the Middle Jurassic sediments with a weak angular discordance. These conglomerates are geographically confined along the front of Tian Shan and this particular formation becomes laterally finer, toward the basin. This behaves as very thick alluvial fans deposited downwards from a major relief rising in the south, as the ones currently deposited along the modern Tian Shan range, with limited northward transport of sediments (Figure 3-8c).

This study brings the first and numerous field-based observations that unambiguously demonstrate the persistence of a major paleo-relief during Mesozoic times that is currently passively integrated into the modern Tian Shan. As shown here, the altitude difference for this Mesozoic paleo-relief can be computed to a minimum of 1300 m for a horizontal distance of 50 km along the northern Tian Shan piedmont. Consequently, a preexisting relief must be considered when studying either tectonic or geomorphological Cenozoic evolution of the Tian Shan. Indeed, both the shortening amount over the main structures of the front and fold-and-thrust belt and the bulk Tian Shan modern topography are traditionally assigned to its Cenozoic reactivation but results from this study show that these must be reduced.

6.2 The immature fold-and-thrust belt of the northern front of Tian Shan

6.2.1 Analysis of the range-basin contacts

As shown before field analysis shows that remnants of unconformable Mesozoic deposits over the Paleozoic basement, rather high in the range, are still preserved along the northern Tian Shan (Figure 6-1).

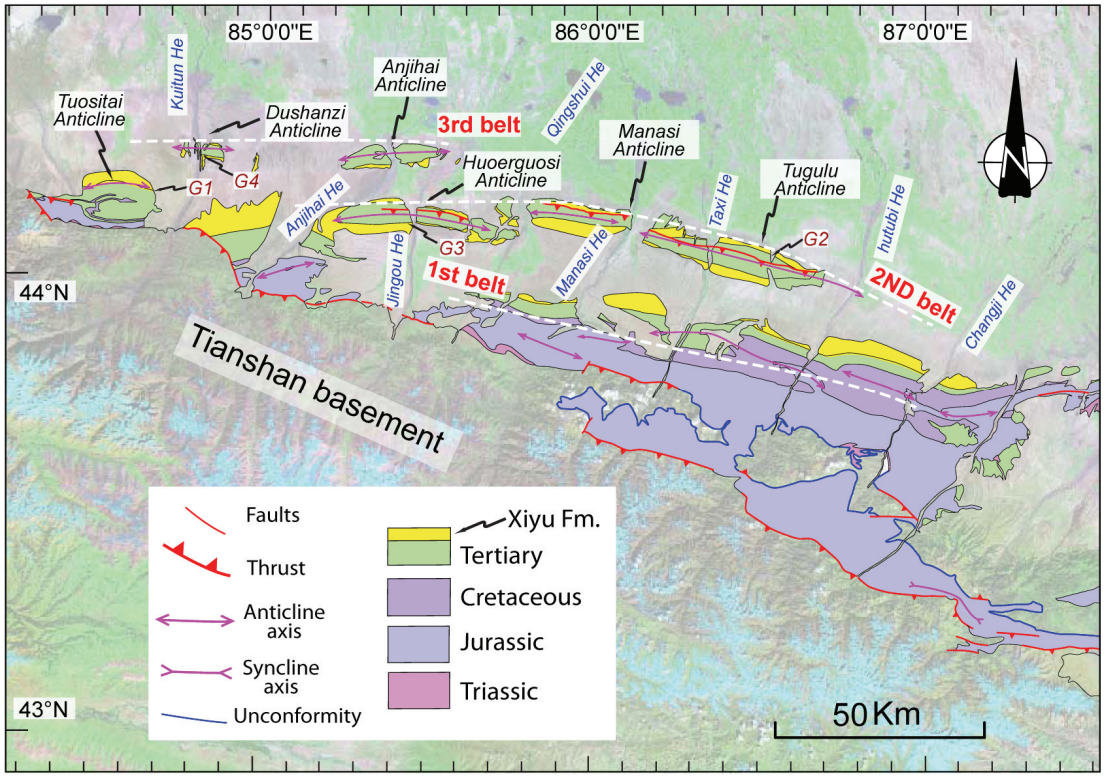

Figure 6-1. *The geological map of the northern piedmont of Tian Shan with Satellite image. G1-G3 indicat the locations of magnetostratigraphy studies of growth strata (Charreatu et al., 2005; 2008; Lu et al., 2010) and G4 indicat the manetostratigraphy study of Xiyu formation (Charrea et al., 2007).*

Structural analysis held in this thesis has also proven particularly instructive for analyzing the contact between the Tian Shan basement and the Junggar basin. In brief, three types of contact can be recognized among the several studied sections and outcrops and the two corresponding end-members can be defined as i) unambiguous northward thrust faulting of the Paleozoic basement units on the sedimentary series of the Junggar basin and, conversely, ii) pure unconformity contact of the clastic sediments above the basement and structural continuous extension of the layers from basin toward the range uplands. Such continuous unconformity basal contact in-between the mountain basement and the basin sediments argues for no significant deformation along those corresponding segments of the range front (Figure 4-35 in Chapter 4, Figure 5-17 in chapter 5). Between the two end-members, intermediate case of front deformation results in fold development; these folds display as large

scale chevron type folds which geometry itself evolves from gentle upright fold to strongly asymmetric kink fold and ultimately to thrust fault (Figure 6-1 and Figure 4-1 in Chapter 4). Moreover, the different types of contacts show rapid lateral variations along strike (e.g. Figure 4-35 in Chapter 4). Consequently, shortening accumulated over front thrust faults must be weak as these faults rapidly turn into folds, along the strike, within about 10 km distance (Figure 4-35 in Chapter 4). In the northern Tian Shan, the outcropping basement rocks generally display steep to vertical fabrics and appear as more mechanically competent with respect to Junggar sediments; they are faulted and comprise a significant amount of joints (Figure 4-33 in Chapter 4). This kind of deformation is well illustrated in the trishear fault propagation folding (Figure 1-8 in Chapter 1). These observed structural characteristics of a giving structure that presents rapid lateral evolution argue for an overall weak deformation, during Cenozoic, along the northern front of the range and suggests a relative immaturity of the orogenic fold-and-thrust belt.

Such character is a first order difference from other intracontinental mountain ranges, such as French Pyrenees piedmont. This latter intracontinental collision range has been extensively studied and the deformation pattern observed at surface can be quite well linked with the deep crustal-scale structure which has been imaged through geophysical investigations (Roure et al., 1989; Teixell et al., 1998). In the Pyrenees (Figure 1-3a), the range basement is separated from the Aquitaine basin by the northward North Pyrenean thrust (Sibuet et al., 2004). The basement thrusts northwards and the Aquitaine sediments are deeply buried under the thrusting fault (Figure 1-3b), as illustrated by the corresponding ECORS deep seismic profile (Roure et al., 1989; Figure 6-2a). This structure suggests that the northern piedmont of Pyrenees is characterized by i) a large amount of shortening, ii) strain and displacement very localized at crustal-scale, concentrating on few main structures along the front range and iii) a cylindrical character of the deformation pattern in the piedmont with main structures extending on several tens of kilometers along the range front. As such, the structure of the northern piedmont of Tian Shan presents a different

nature with respect to the Pyrenean front (c.f. Figure 1-3b, Figure 6-2a and b).

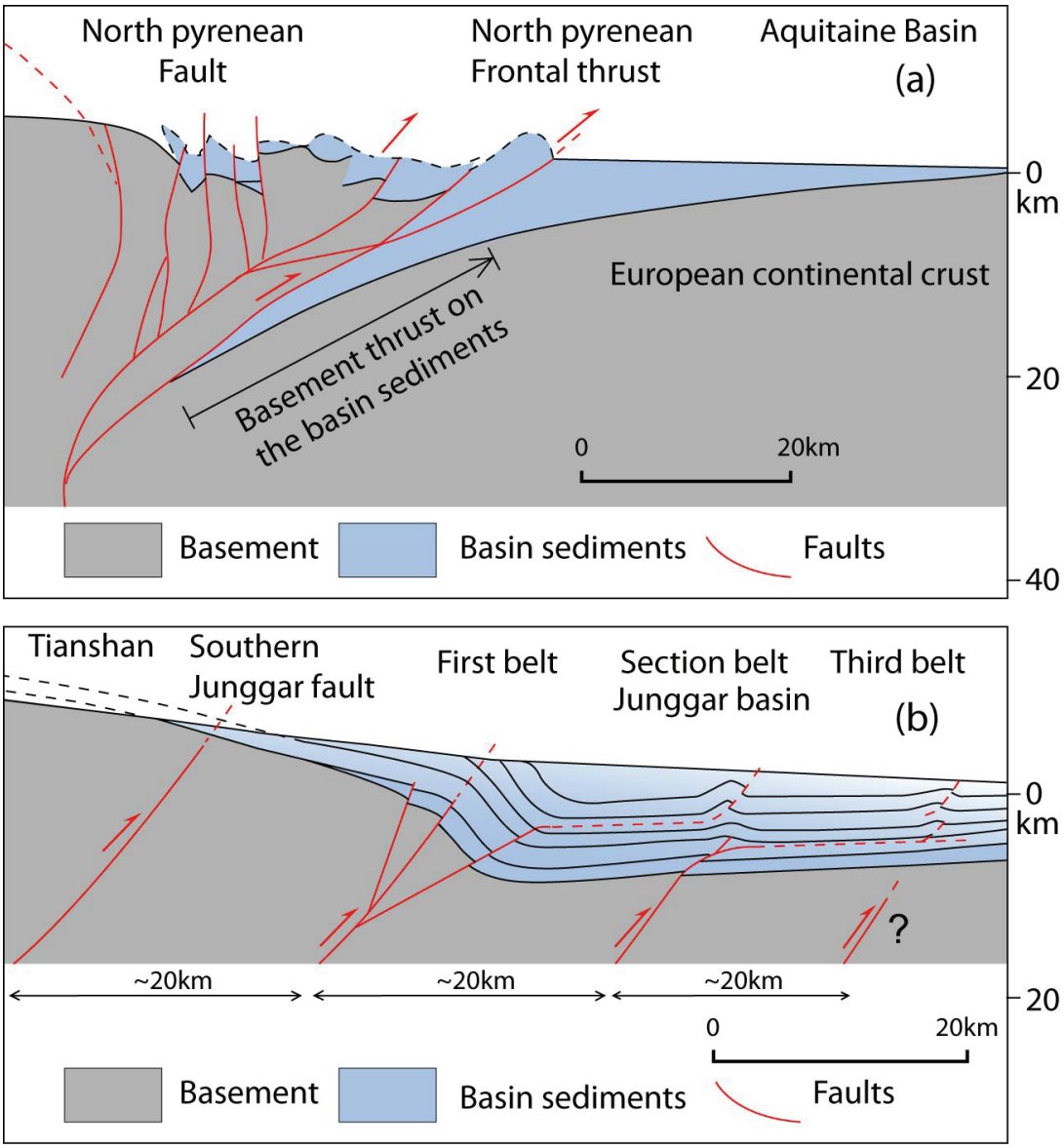

Figure 6-2. *(a) Crust scale geological section interpreted from the ECORS seismic profile in the northern piedmont of Pyrenees (Roure et al., 1989; Sibuet et al., 2004). (b) Interpreted section of the northern piedmont of Tian Shan; finite deformation is rather weak and the structural front of the range could not strictly be defined and localized in that case. As discussed in the text, conversely with the case of the Pyrenees, the deformation is not (yet) localized along a major crust scale structure but would better be distributed over several basement reverse faults.*

In Tian Shan, the Jurassic sediments can be continuously followed, from the basin to the interior of Tian Shan, along several sections (e.g. the Hutubi section in Figure

5-12; Figure 6-2b). The deep structure of the northern Tian Shan does not present any northward thrusting fault crossing over the crust, from Moho to the surface, as the northern Pyrenean front does. Instead, the structure of the middle and lower crust show sub-horizontal attitude in the northern piedmont of Tian Shan (Zhao et al., 2003). This feature can also be shown on deep seismic profiles crossing the northern Tian Shan fold-and-thrust belt (Lu et al., 2000; Xu et al., 2002; Zhao et al., 2003; Wang et al., 2004).

6.2.2 Deformation pattern within the fold-and-thrust belt

Integrating data from field observations, gravity measurements, seismic profiles and drilled wells several “regional scale” sections have been built crossing over the northern front and piedmont of the Tian Shan, within the foreland basin of the range. The Mesozoic-Cenozoic series, with low mechanical competence, overlie on the basement and certain parts of the series can be used to constrain the deformation as a mark layer along the studied cross sections. Three rows of fold-an-thrust belts are recognized in the southern of Junggar foreland basin with strikes roughly parallel to the Tian Shan mountain range (Figure 6-1; Figure 4-1) and showing different structural styles.

The first southern belt is well developed and exposed in the east of the study area, such as along the Hutubi He and Chanji He valleys where a rather large anticline is mapped (Figure 6-1). The structure of this belt has been proposed to develop above a major thrust fault which is limited to depth as it only involves the basement and does not cut through the sedimentary cover (Deng et al., 1996; Burchfiel et al., 1999; Deng et al., 2000; Lu et al., 2007). However, such fold belt structure does not extend westwardly: instead, in the Jingou He area, for instance, the sedimentary series displays a single north gently dipping monocline showing that the above mentioned basement thrust must die out laterally, along strike of the range front. This feature is compatible with field observations made along the front zone of the northern Tian Shan, which highlight quick lateral transitions of deformation pattern. Besides,

shortening of the foreland fold-and-thrust belt, along the Jingou He section, is accommodated by another northward reverse fault which developed further south of the monocline (Figure 6-1; Figure 4-1). This latter thrust fault could hardly be considered as the prolongation of the blind thrust as described above as it does not extend in the same prolongation and, in turn, it also laterally dies out eastwardly (Figure 6-1; Figure 4-1).

The second and middle belt, displays as a series of parallel and inline anticlines developed in the Mesozoic to Cenozoic series of the basin: the Huoerguosi anticline along the Jingou He, the Manasi anticline along the Manasi He and the Tugulu anticline along the Taixi He (Figure 6-1; Figure 4-1). These anticlines are often interpreted as fault-bend fold (Deng et al., 2000; Charreau et al., 2008)

At surface, the third and northernmost belt is solely composed of two inline anticlines striking ~east-west. The Anjihai anticline displays as a typical right detachment fold with gentle dipping angle (~ 30°) in the south and north limbs (Figure 5-4; Figure 6-1). Similarly, ~30 km to the west, the Dushanzi anticline shows gentle dip-angle in the southern limb but a reverse fault cut across the northern limb of the fold in that case.

At the first order, the whole of the Cenozoic fold-and-thrust belt, displays only limited shortening, structures marking strong deformation, such as recumbent fold, overlapping nappes, duplex or thick overturned sedimentary series, have never been observed along the northern Tian Shan. They have certainly not yet been developed within the basin cover, at that stage of the Cenozoic deformation history. The total shortening calculated from the four studied regional-scale cross sections reach a maximum of ~12km in the study area of northern Tian Shan, for ~70 km long sections.

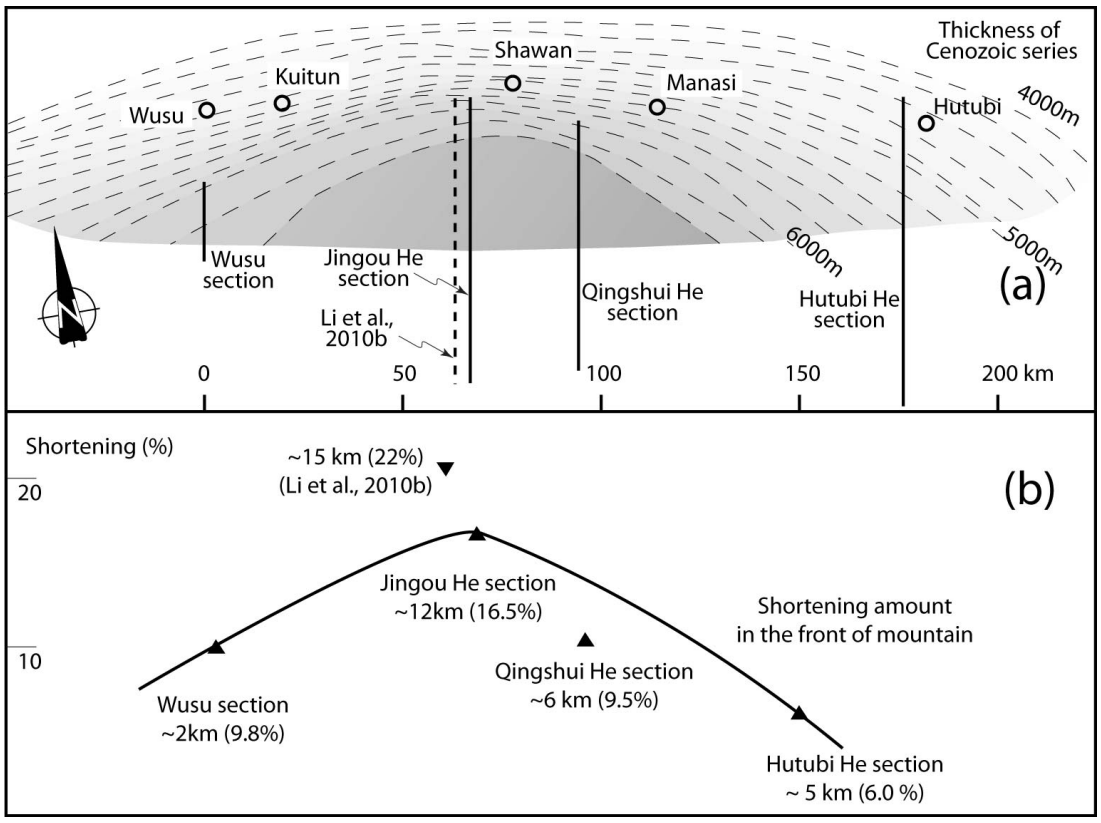

Figure 6-3. *(a) Contour map of the Cenozoic sedimentary thickness in the northern piedmont of Tian Shan and with the locations of four sections. (b) Diagram of shortening amount and rate for four studied sections along the northern piedmont of Tian Shan.*

Structural analysis highlights clear uncylindrical pattern of the deformation within the fold-and-thrust belt. Indeed, along strike of the structures – i.e. east to east-southeast striking – the three fold belts present a series of repeated structural culminations, where local shortening is locally at maximum, flanked by less shortened areas that, finally, vanish to the lateral ends within ~ 15-20 km (Figure 5-19 in Chapter 5; Figure 6-1). Moreover, the total shortening amount presents high lateral variations. From west to east, the geological sections display shortening amounts of: 2, 12, 6 and 5 km for the Wusu section, the Jingou He section, the Qingshui He section and the Hutubi He section, respectively (Figure 6-3). If the total length of each section is measured from the front of mountains to the end of topographic slope (i.e. to the zero topographic gradient), the corresponding deformation amount has been calculated for each section varying from a minimum of 6% to a maximum of 16.5%

(Figure 6-3). A similar study has been carried out and consistent results have been obtained for the Jingou He, i.e. ~15 km of shortening and 22% of shortening amount (Li et al., 2010b). Figure 6-3 presents these shortening rates obtained from the four sections compared with the contour map of the Cenozoic sedimentary thickness in the study area. The variation of the shortening rate is correlated with the lateral thickness variation of Cenozoic sediments. In particular, the Jingou He section, with a maximal shortening amount of 16.5%, corresponds to the thickest deposit zone for Cenozoic sediments. Shortening amount decreases eastwards and westwards, while the thickness decreases in the same manner. This suggests that the shortening amount would control location of the maximum subsidence, along the northern front of Tian Shan, during Cenozoic.

6.2.3 Which tectonic model could apply for Cenozoic north Tian Shan deformation?

Different types of models have been proposed to explain the development and mechanisms of deformation through the foreland fold-and-thrust belt of northern Tian Shan. As shown on figure 6-4, the first model type is characterized by a rather large movement along a main frontal crust-scale thrust. This movement is propagated forward through a horizontal décollement localized at the bottom or within the sedimentary series and a significant amount of shortening is thus accommodated within the two frontal external belts (Figure 6-4a). In the particular case of northern Tian Shan, this décollement is assumed to be localized in the basal part of the Mesozoic sedimentary series and it merges, to the south, with a main front thrust system at the basement/sediments boundary (Avouac et al., 1993; Burchfiel et al., 1999; Deng et al., 2000; Charreau et al., 2008; Lu et al., 2010). Such tectonic model induces a great displacement either i) along the frontal main thrusts, ii) over the flat décollement and through one or the other external belt or iii) both (see Figure 26b in Avouac et al., 1993). An alternative model has also been proposed with the development of duplex structures in the basement units, just below the range “front”

(Figure 6-4b). In this model, shortening is accommodated in the fold-and-thrust belt through a flat décollement and associated shortening across the two external belts (He et al., 2005). This shortening is smaller in this model than in the previous one and a consequent part of the shortening imposes by the numerous basement duplex is accommodated by large movement localized along a backthrust system developed within the north dipping sedimentary series, parallel to the layers orientation and emerging along the range front (Figure 6-4b; He et al., 2005).

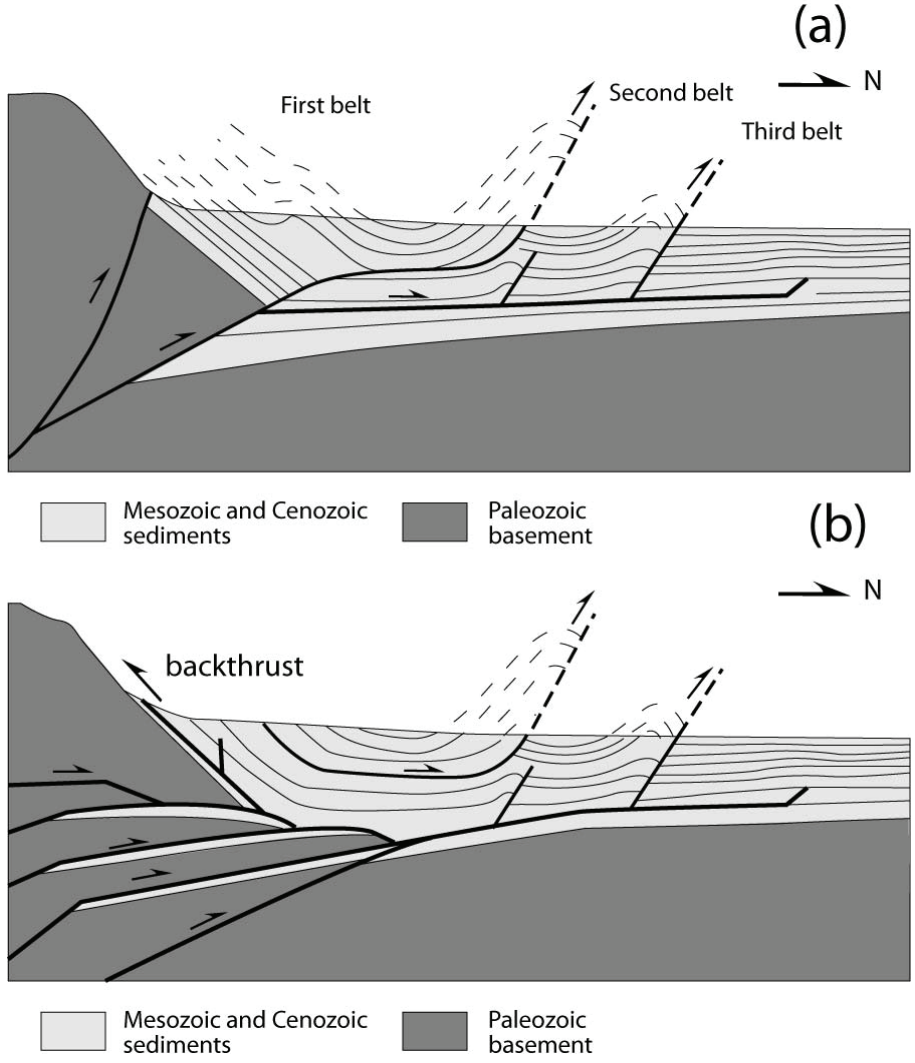

Figure 6-4. *Models of deformation within a foreland fold-and-thrust belt with: (a) movement along a main frontal, crust scale thrust transmitted through a décollement structure within the sedimentary series and large movements in the frontal external belts (Modify after Deng et al., 2000), (b) construction of duplex type structures within the basement, below the range front. Shortening of the fold-and-thrust belt is*

accommodated by an horizontal décollement and more limited movement in the external belts in that case but large movement along a backthrust developed parallel with the sedimentary layers (Modify after He et al., 2005).

However, as discussed below, structural analyses and observations made during this thesis work do not allow applying one or the other of these two proposed tectonic models.

First, the present study highlights a rather limited deformation of the northern Tian Shan fold-and-thrust belt, if compared with what would previously be admitted. Based on combined geological and geophysical data, four regional scale sections have been built. The maximum shortening amount calculated across the belts is of 12 km along the Jingou He section, which is 16.5% shortening for a 72.4 km initial section length. Other sections show 2 km (9.8% shortening for 20.4 km initial section length), 6 km (9.5% shortening for 63.1 km initial length) and ~5 km (6.0% for 83.2 km initial length) in the Wusu, Qingshui He and Hutubi He sections, respectively. The nature front contact in-between the basement and the basin sediments has been taken into account for these calculations as, for instance, in the Hutubi He section where the Jurassic series can be followed from the basin to the Mountain interior, which is an important marker for deformation analysis and restoration. These results highlight very small shortening amount within the foreland fold-and thrust belt in the southern Junggar basin and, as a whole, this first order feature is not compatible with one or the other of the two proposed models implying rather large net shortening amount through the front of the northern Tian Shan and the fold-and-thrust belt.

Second, both above presented models, and in particular the first one (see Figure 6-4a) imply a significant shortening through one or the other of the external belts and, thus, rather large movement along the corresponding thrusts emerging within these belts (Figure 6-4a and b). However, the present study shows that these folds of the basin display as uncylindrical folding. As discussed in chapter 5 (Figure 5-2), such as the Huoerguosi anticline along Jingou He: the limits of Cenozoic series in the two limbs forms ellipses shapes in map view and closed to the two sides of the

fold, along strike. A reverse fault, located in the central part of the anticline, thus rapidly disappears eastwards and westwards sides from the centre. Therefore, the net movement along such thrust fault must be limited and the deformation in the fold laterally dies out, along strike, in ~ 15-20 km distance. Other folds of the second belt – Manasi anticline and Tugulu anticline – are similar in geometry and the associated local shortening amount is also limited for the same reason. In the third fold belt, the width of the Anjihai and of the Dushanzi anticline is about 20 km and 10 km, respectively. The gentle dip angles of the strata on the two limbs and their uncylindrical geometry suggest these folds are also only weakly deformed. Uncylindrical folding within the fold-and-thrust belt clearly shows only weak shortening. As the surface deformation rise from the "basal" basin flat décollement (Figure 6-4a and b), the weak deformation indicates that the movement along this décollement must also be limited, which is not compatible with, at least the first of the models previously proposed.

Third, shortening within the fold-and-thrust belt can be accommodated by significant movement along a backthrust system, as proposed in the second of the models. These backthrusts would localize either within the base of the sedimentary series or along the basement/sediments contact itself (Figure 6-4b). However, among the overall study sections and outcrops visited for this work, backthrust movement has never been observed within the Mesozoic sedimentary series. Coal layers are the weakest layers of the Mesozoic sedimentary series which is the more represented along the contact interface with the basement units, all along the range piedmont. This feature is particularly well expressed where frontal northward thrust occurred: underlying and overturned sediments present a big internal deformation contrats in between these coal layers and the others interstratified coarse clastic sediments. Yet, coal layers located close to the front area where a monocline structure of the sedimentary series is observed are undeformed (see Figure 4-31). These segments of the piedmont where the development of a duplex system could be assumed, to depth, do not show the backthrust systems conditioning this tectonic model (Figure 6-4b).

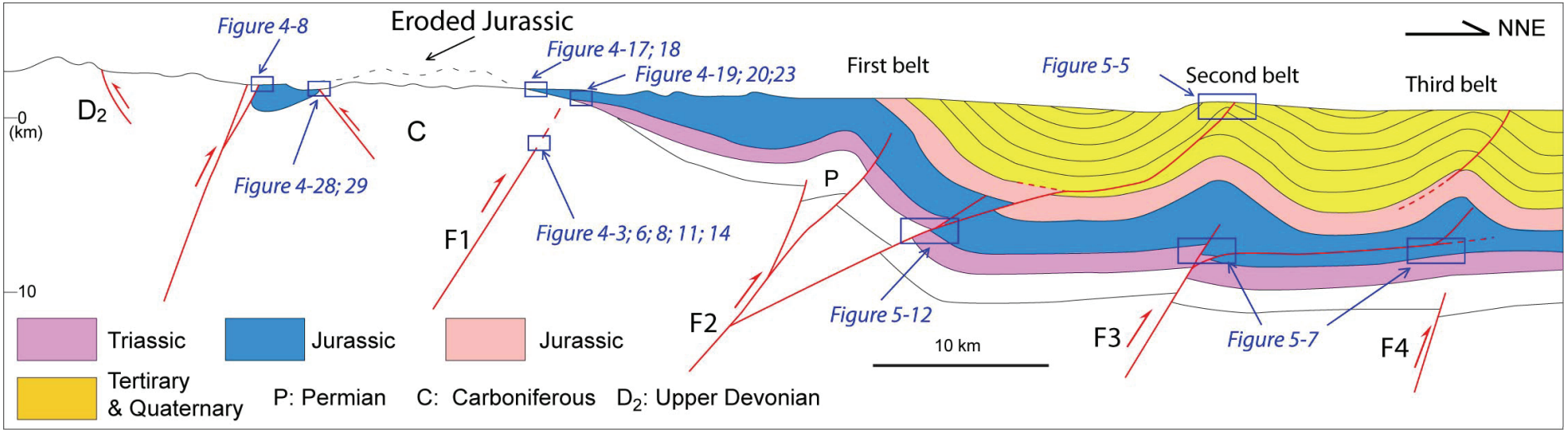

Figure 6-5. *Sketch diagram of the structure and developing model for the northern Tian Shan. Numbers indicate the faults in the basement (modify after Qi et al., 2007).*

Fourth, regional sections, integrated with seismic interpretation and gravity modeling, suggest that, in addition to their folding, some reverse movement affected the Jurassic layers in depth. Along the Jingou He section, the steep basement fault cut the Jurassic layers in the middle segment of the section (Figure 5-7). Moreover, a steep thrust crosses and offset the basal surface of the basin (Figure 5-12). These structures questioned the previously proposed models showing large regional flat décollement in Mesozoic series within, the foreland Junggar basin (Figure 6-4a and b).

Thereby, tectonic models implying large total shortening amounts for the belts, large thrust movements within the external belts and/or significant backthrust movements along the front of the range are almost inapplicable to the case of northern Tian Shan.

By consequence, an alternative model for development of the deformation within the fold-and-thrust belt can be proposed from the present work study. Summarizing principal observations and interpretations, a "model" cross section can be drawn for the north Tian Shan piedmont, as displayed on Figure 6-5. From south to north this one can be detailed as follows: Jurassic sediment unconformably deposed on the basement and can border with reverse faults in the mountain interior, such as along the Toutun He section (Figure 4-5, Figure 6-5) and in the Houxia valley (Figure 4-18, Figure 6-5) . Going north, in some places, the Jurassic series can be continuously followed on top of the interior mountain basement units (cf. Hutubi section; Figure 5-9; Figure 6-5), while Jurassic sediments have been eroded in other sections (e.g. Jingou He section; Figure 5-4, Figure 6-5). Along the basement/basin boundary, either thrust fault or unconformity contact are observed along the northern front of the mountain (Figure 6-5). Northward, deformation rises from the basement faults and propagates into the basin. Geophysical data highlight that the basement thrust may exist below the sedimentary cover. Yet, movement along these faults is limited to the base of the sediments and only rarely crosses over the entire series. Movements along flat décollements are limited in the sediments and only developed for propagating

local shortening between the main faults of the basement and the belts (Figure 6-5). As well displayed on study sections and on Figure 6-5, basement blocks are separated by important inverse faults with an interval distance of ~15-20 km (Figure 4-34; Figure Figure 6-5; and see Qi et al., 2007). Almost the same interval distance can be measured in between the three fold belts in the foreland basin of Junggar and we propose that the location of these belts could be driven by the one of underlying basement faults which would play an important role in the deformation propagation process. This feature is compatible with the mechanical behavior of basement units: indeed, field study in mountain interior suggests that the basement is principally made of competent rocks and that few localized main structures cut these basement units into rigid blocks. This new image of the mechanisms driving deformation within the north Tian Shan fold-and-thrust belt is highly compatible with a schematic model published by Lacombe and Mouthereau, 2002 for the foreland tectonics of ranges (Figure 6-6a). Their model display deep detachment tectonics in forelands of orogen as recognized in Taiwan or western Alps belts (Lacombe and Mouthereau, 2002). Basement shortening in forelands are accommodated at the scale of the upper crust, which requires that it is partially decoupled from the deeper lithosphere levels by a crustal detachment (Figure 6-6a). This detachment presumably occurs along the midcrustal, thermally weakened brittle-ductile transition. In the previous exampled belts, the detachment ramps toward the surface into a shallow detachment and propagates far away from the orogen. However, in the northern front of Tian Shan, present-day microseismicity shows a hypocentral depth-distribution between 5 and 35 km, with a peak at 20 km (Wang et al., 2004). The nowadays geothermal gradient follows a “modern type” gradient of ~ 22°C/km suggested by borehole (Hendrix et al., 1994). At a depth of ~20 km, a weakened brittle-ductile transition zone may be concerned with the temperature of about 440°C and the pressure about 500Mpa (27 MPa/km) (Horii and Nemat-Nasser 1986; Byerlee 1968). In our model (Figure 6-6b), the main detachment would be located ~15-20 km in depth and ramps to surface in the foreland. These ramp faults cut basement into rigid blocks which have also been

evidenced by field observations and well displayed on geological sections. The basin sediments couple with the sectoried basement in the first southernmost fold belt. While in the second and third belts, the sediments decouple with basement by some shallow décollements (Figure 6-6b). In these two models, the first one show large displacement along the front of the mountain and numerous faults rise from the deep detachment to surface, suggesting amount of shortening in the front. However, in northern piedmont of Tian Shan, large displacement fault is absent in the front, and only two or three ramp faults rise from the deep detachment fault. This characteristic confirms that the fold-and-thrust belt in the northern piedmont of Tian Shan is fairly weakly deformed than the examples in the first model, such as Taiwan, western Alps, Pyrenees belts.

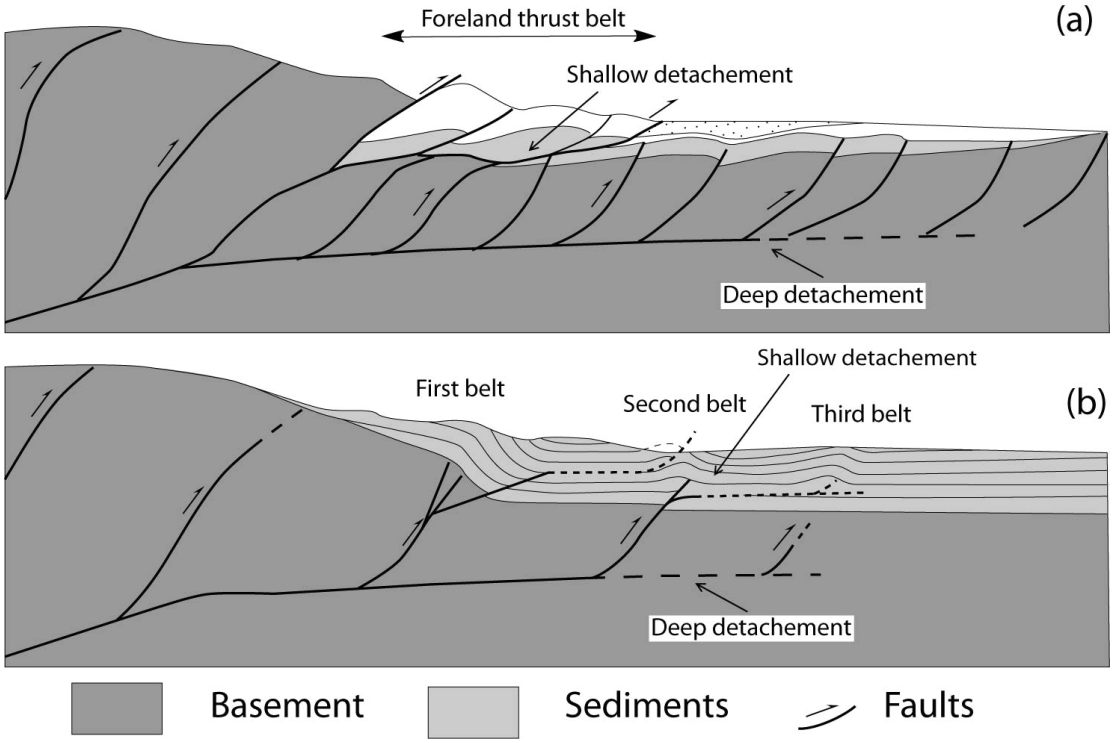

Figure 6-6. *(a) Schematic model of superimposed shallow and deep detachment tectonics in orogen forelands of (Lacombe and Mouthereau, 2002). (b) Adaptation of this scheme to the Tian Shan structure.*

6.2.4 Structural characteristics of an immature fold-and-thrust belt

Front of a collision orogens are commonly characterized by fold-and-thrust belts, which is critical to establish the relationship between the range and the adjacent foreland basin (Davis et al., 1983; Dahlen et al., 1984; Vann et al., 1986; Tozer et al., 2006; Lacombe et al., 2007). Strongly deformed orogens, such as Pyrenees, Canadian Rocky Mountains present highly folded foreland basins and fold-and-thrust belts, with important front thrusts developed between the range basement and the adjacent foreland basins, deep décollements as well as recumbent folds, duplex and nappes (Price, 1981, 2001; Teixell, 1998). Contrarily, this study highlights that the Cenozoic shortening is very limited in front of the northern Tian Shan range, in comparison with these others intracontinental collision ranges (Price, 1981, 2001; Teixell, 1998). In comparison to these well known examples which can be considered as mature front of collision orogens, the active northern Tian Shan fold-and-thrust belt can be regarded as an 'immature' range front structure. The characteristics of an immature fold-and-thrust belt and relative front range can thus be drawn, from the example of the northern Tian Shan piedmont, as follows:

- First, Shortening within the belts developed within the foreland basin is rather small. Thus, movements along the potential frontal thrusts associated with these folds are limited. This limited shortening indicates that the inception of deformation is young or that the rate is low,

- Second, resulting from the preceding point, deformation pattern displays as very uncylindrical through the fold-and-thrust belt,

- Third, no backthrust developed within or at the base of the sedimentary series in front of the range, which would be the result of a young, weak deformation. This is a structural feature that may initiate and amplify later on during the evolution of the deformation process in piedmont areas,

- Fourth, as discussed above, no backthrust movement and limited thrust movement within the belts indicate limited development of a potential horizontal

décollement structure within the sedimentary series. A regional décollement would be associated with more localized deformation, along a crust-scale structure, in front of the range; such décollement can propagate much shortening deformation, in the basin area, which is commonly developed in more strongly deformed orogen front, such as Canadian Rocky mountains (Debelmas et al., 2008; Figure 1-4b),

- Finally, Localization of the belts could be controlled by the location of basement deep thrusts which would imply the characteristic distance separating these belts (the same mean distance than in-between the thrust faults visible within the range interiors). It indicates that deformation of the basement is distributed over a large band in front of the range, with several reverse faults active in the interior parts of the range and below the foreland basin sediments. This characteristic is contrasted with more strongly and mature collision range fronts where deformation in the basement levels is better localized along a main front thrust structure that likely cross over the entire continental crust (e.g. northern front of Pyrenees; Teixell, 1998).

The immature character of the northern Tian Shan could be explained by several reasons as follows. First, the far-effect of India-Asia collision decreased by a progressive northward propagation of deformation (Tapponnier and Molnar, 1977; Tapponnier et al., 2001). The northern Tian Shan piedmont may be almost considered as the northern end of this far field compression. Geodetic measurements in central area show the total shortening rate between longitudes 81°E and 85°E is only 4.7±1.5 mm/year. Eastwards, this rate decreases to <1 mm/year between longitudes 86°E and 87°E (Abdrakhmatov et al., 1996; Wang et al., 2001). Second, the southern piedmont of the Tian Shan may have 20-40 km of crustal shortening with a horizontal shortening strain amount of 20-30% during the late Cenozoic (Yin et al., 1998). The net horizontal shortening through the Tian Shan area could thus be accommodated by southern foreland fold-and-thrust belt. Deep seismic profiles cross the whole Tian Shan show the Tarim block is bended and subducted under the Tian Shan, while the Junggar block is much less deformed showing a flat geometry (Zhao et al., 2003). This indicates that the northern piedmont may have experienced less deformation than

the southern one. Third, several estimations of Cenozoic shortening in the interior of the Tian Shan have been estimated across Tian Shan, i.e. 80 km (Allen et al., 1994), 100 km (Molnar and Tapponnier, 1975), 124±30 km (Avouac et al., 1993), and 330 ±760 km (Chen et al., 1991). Despite the important difference among these values, the basement of the interior mountain could absorb a large part of the total shortening.

Finally, the northern piedmont of Tian Shan is active, evidenced by seismicity studies (Molnar et Deng, 1984, Avouac et al., 1993; Deng et al., 1996; Ghose et al., 1998; Wang et al., 2004). The shortening in north-south direction will be ongoing with the continuously northward displacement of India plate, therefore, the northern piedmont of Tian Shan will be more and more developed and become a mature fold-and-thrust belt.

6.3 Deformation timing and shortening rate in the northern piedmont of Tian Shan

The northward propagation of the deformation and precise timing of the Tian Shan Cenozoic reactivation have been largely questioned during last decades (Avouac et al., 1993; Hendrix et al., 1994; Métivier and Gaudemer 1997; Abdrakhmatov et al., 2001). To estimate the onset of the Cenozoic range uplifting and the deposition of sediments, several geochronological methods have been applied in both northern and southern Tian Shan flanks, such as fission tracks, magnetostratigraphy, and results become more and more available (Zhou et al., 1997; Yin et al., 1998; Sun et al., 2004; 2007; 2009; Charreau et al., 2005; 2007; Ji et al., 2008; Charreau et al., 2009). Meanwhile, some current strain rates in this area have also recently published by GPS kinematical studies (Wang et al., 2001; Niu et al., 2007; Yang et al., 2008). After discussing how those data can be used to determine the onset timing of the Cenozoic foreland deformation, the shortening amounts calculated for the present study area will be confronted to the deformation rates estimated and accepted for the northern piedmont of Tian Shan though the uncertainties would be relatively large due to the important discrepancies of estimations coming from different methods. Such analysis

is still important to better understand the deformation processes in front of the Tian Shan or for intracontinental collision settings, in general. In future works, much more detailed and multidisciplinary work needs, therefore, to be reinforced.

6.3.1 Onset timing of Cenozoic foreland deformation

The timing of deformation in the northern piedmont of Tian Shan is evidenced by the development of fold-and-thrust belts, unconformities and growth strata. Age determinations for these particular structures are often approached using sedimentary sequence, fission tracks and magnetostratigraphy. Here are briefly summarized the recent results.

A 400-m-thick Latest Jurassic coarse conglomerates and breccias unconformably overlay on the early Jurassic series indicating a significant deformation and/or uplift of the ancient Tian Shan during Latest Mesozoic (Chapter 3; Hendrix, 2000; Dumitru et al., 2001; Jolivet et al., in press). However, these conglomerates are wedging rapidly out and are only deposited in the piedmont of mountains. The dip angle difference between the conglomerate series and underlying layers is less than 5°, the deformation seems, therefore, very weak at that time. Moreover, in the basin cover, the Cretaceous through Neogene sedimentary series are mostly parallel and display conformable contacts, suggesting that no significant deformation occurred during that time interval (Burchfiel et al., 1999; Bullen et al., 2001; Bullen et al., 2003; Sobel et al., 2006). It seems that the deformation didn't propagate to the interior of the foreland basin at least until Neogene.

By extrapolating the current shortening rate derived from GPS measurements to the past and assuming that the total shortening rate across the western Tian Shan is around 200 km, Abdrakhmatov et al., (1996) suggested that most of Tian Shan was constructed during the past 10 Ma. By comparing cumulative crustal shortening across Tian Shan with current deformation rates, Avouac et al. (1993) estimated that the initiation of the deformation began at 16 +22/-9 Ma. According to the calculated mass accumulation rates in the Junggar basin, Métivier and Gaudemer (1997) placed

the beginning of the major uplift at 16 Ma. Their analyses show that the accumulation rate has been accelerated at around 5 Ma, which could indicate an acceleration of the Tian Shan uplift at that time. In situ apatite fission-track analyses from sediments exposed in both north and south of Tian Shan suggest that the unroofing of the Tian Shan began ca. 24–25 Ma (Hendrix et al., 1994; Dumitru et al., 2001). More and more recent fission track results seem confirming this age for the onset of Tian Shan topographic reactivation (Guo et al., 2006; Zhang et al., 2007; Wang et al., 2009; Jolivet et al., in press). This commonly accepted age for the reactivation and new uplift of the Tian Shan range relief may relate to the onset time of the deformation within the foreland fold-and-thrust belt. However, front deformation along the range is not obligatory directly linked with the uplift of the range interiors.

An alternative method for estimating the onset age of shortening within the foreland fold-and-thrust belts consists in analyzing the growth strata structures developed within foreland basins. In northern Tian Shan, growth strata structures are particularly well expressed through within the Xiyu conglomerates formation (Xu et al., 1992) such as in the Tuositai anticline, the southernmost fold belt along Wusu section, at the bottom of the Xiyu formation (Lu et al., 2010; Figure 6-1, G1). However, age of this series along this section is not available up to now. Yet, about 10 km east to the Tuositai anticline, the sedimentary boundary between the Dushanzi formation and Xiyu conglomerate has been magnetostratigraphically dated at 4.8 Ma in the Dushanzi anticline along Kuitun He (Charreau et al., 2005; Figure 6-1, G4). This 4.8-Ma-old boundary is located ~ 10 km northward to the basal Xiyu conglomerate of the Tuositai anticline. Assuming the northward propagating rates of 3.9 mm/yr (Charreau et al., 2009), the Xiyu conglomerate limit of ~10 km southwards should be about 2.5 Ma older, in other words, the age of the growth strata extrapolated at the basal Xiyu conglomerate, in the Tuositai anticline, could be about 7.3 Ma. This may suggest that the study area experienced a tectonic forcing starting at that time. In the middle and second fold belt, Charreau et al., (2008) have identified growth strata in the Huoerguosi anticline (Figure 6-1, G3) by seismic profiles along the Jingou He

and estimated its age at ~10 Ma by the magnetostratigraphic study and stratigraphic correlation. In the same second fold belt, but about 70 km to the east, two magnetostratigraphic results have been reported for the Tugulu anticline (Figure 6-1, G2). Li et al. (2010a) proposed that the sediment accumulation rates increase at ~ 4 Ma and that growth strata of the Xiyu formation started ~2 Ma ago, which provides a minimum age for folding here. Another study by Lu et al. (2010) also reported the same acceleration of sediment-accumulation rate at ~4 Ma. Moreover, the age of growth strata in the upper Taxi He formation is estimated at about 6 Ma. The significant dispersion in age even for the growth strata from folds of the same belt (at lateral distance of ~70 km (Figure 6-1), confirms the heterogeneous and uncylindrical pattern of the deformation along the northern piedmont of Tian Shan.

In summary, several growth strata marking tectonic movements have been identified and dated directly and indirectly along three sections. Two of them have been studied in the same Taxi He section, one is estimated at 2 Ma and another at 6 Ma, suggesting that multiphase tectonic forcing could have taken place along the northern Piedmont of Tian Shan. Three oldest ages of growth strata observed in these sections are about 10 Ma in the Huoerguosi anticline along the Jingou He section, 7.3 Ma at the Tuositai anticline along the Wusu section and 6 Ma at the Tugulu anticline along the Taxi He section. It is worthy to notice the age of growth strata in the Huoerguosi anticline located in the middle fold belt is about 3 Ma older than that of the Tuositai anticline located in the southernmost fold belt, but ~ 70 km westwards. As shown in this study, the southernmost belt is absent in the Jingou He section. These laterally heterogeneous ages of growth strata indicate that the deformation within the southern Junggar basin do not propagate parallel with respect to the front range, in other words, folds from the same fold belts may not be necessarily developped simultaneously.

It should be noticed here that most ages mentioned above come from growth strata analysis made on the surface. It is still possible that other growth strata structures may be masked by younger sedimentary cover and unexposed due to the

weak deformation.

6.3.2 Qualitative shortening rates

The deformation rate is a key parameter to study processes of the uplifting of Tian Shan and the deformation of its foreland basin. Several rather heterogeneous rates have recently been proposed, based on different methods. Geodetic survey shows a deformation rate of ~5 mm/yr across the range and at the longitude of the Jingou He area (Reigber et al., 2001; Wang et al., 2001; Niu et al., 2007; Yang et al., 2008). However, Inferred from theoretical modeling and geological investigations, the deformation rate ranges from about 1 to 3 mm/yr (Avouac et al., 1993; Molnar et al., 1994; Charreau et al., 2008).

If two extreme oldest ages of growth strata may be considered as the possible range of the earliest tectonic forcing in the south Junggar basin, i.e. 10 Ma and 6 Ma, the deformation rate in this study area may be estimated as well according to the shortening amounts observed along four geological sections (Table 6-1).

		Shortening rate (*mm/yr*)	
Section	**Shortening** (*km*)	for **6 Ma** onset Age	for **10 *Ma*** onset Age
Jingou He	12	2	1.2
Qingshui He	6	1	0.6
Hutubi He	5	0.8	0.5
Wusu	2	0.3	0.2

Table 6-1. *The shortening rates calculated with different onset ages.*

The higher values of these estimations (0.3-2 mm/y) seem quite consistent with those estimated by other methods (1-3 mm/y). However, the difference between the lowest values from this study and other methods is a factor of 5. This may question if the shortening in some sections, such as Wusu, would be underestimated by this study. In fact, these geological sections are essentially estimated with seismic profiles and Jurassic sediments as marker layer. Moreover, geological structures in this area are

relatively simple. If there were an error on the restoration of geological section and an underestimation on the shortening, it would not be as important as a factor of 5. If the estimated results in Table 6-1 are qualitatively admitted, one of conclusions can be made is that the deformation rates are laterally variable as we observed for the contact types along the piedmont and ages of growth strata along the fold belts.

Based on the shortening amounts estimated in this study and on the above mentioned deformation rates defined by other methods we can calculate the tectonic onseting age of deformation within the north Tian Shan foreland. Taking the extreme values of deformation rate, i.e. 1 and 3 mm/yr, the minimum and maximum possible deformation onset time can be estimated for the four studied sections of this study, in the northern piedmont of Tian Shan (Table 6-2).

		Onset Age (*Ma*)	
Section	**Shortening** (*km*)	for **1** ***mm/yr*** shortening rate	for **3** ***mm/yr*** shortening rate
Jingou He	12	12	4
Qingshui He	6	6	2
Hutubi He	5	5	1.7
Wusu	2	2	0.7

Table 6-2. *The onset age of deformation calculated with different shortening rates.*

The calculated results show a relative late deformation onset age. The maximal age is about 12 Ma for the Jingou He section when a shortening rate of 1 mm/y is applied, even only 4 Ma when 3 mm/y applied.

Two possibilities may be proposed to explain the late estimated ages, assuming the shortening has been well estimated. (1) the deformation rate estimated by GPS measurements is temporary for a very recent and short period and it could not be representative of the whole deformation history since the last reactivation of the Tian Shan, saying that the deformation rate should be lower than the actual one; (2) The deformation rate estimated by the growth strata study may varies from 1 to 3 mm/y.

These deformation rates, corresponding to the tectonic events, may be discrete instead of continuous. In other words, these rates present an intensive deformation nature only for a short period. After such intensive deformation period when the growth strata formed, the deformation rate may decrease. If so, the initial deformation onset time may be earlier than the results presented in Table 6-2. (3) as the shortening has been estimated only from the geological section of the basin cover, the deformation onset time of in the basin may be significantly delayed with respect to that in the mountain range (cf. ~25 Ma for uplifting estimated by fission tracks).

It is worthy to notice that the calculated onset times are very heterogeneous, even qualitatively. This may indicate that the deformation may start at different times, even for folds owning to the same row of fold belt. For instance, the Jingou He and Taxi He anticlines, located both in the middle fold belt, show onset ages of 12 and 6 Ma, respectively (Figure 6-1). These folds are isolated and do not connect each other in the depth. This may reveal that these folds seem having spatial relationship (equidistance to the front of the range), but are not coeval. As illustrated for the contact zone which displays rapid lateral variation of contact types, the deformation in the basin is also highly uncylindrical and also variable in time. Once more, this character indicates that the deformation in the northern fold-and-thrust belt has not been well developed, yet, and the study area is experiencing the beginning of a foreland deformation process. As discussed above, the appearance of three fold belts parallel to the Paleozoic structure may be just related to basement thrust that could be inherited Paleozoic structures.

In summary, according to relatively comprehensive study (detailed field observation, geophysical investigation, drilled well, etc…), small amounts of shortening in the basin cover of Junggar have been calculated from restored geological sections. Considering previous studies on geochronology, kinematic motion from the study area, the first obvious conclusion made is that the deformation is highly variable along the strike of the range in age of the tectonic onsetting, deformation rate and amount. This may emphasis again the immature nature of the northern piedmont of Tian Shan as an

orogenic belt and the ongoing process of foreland basin development in south Junggar.

6.4 Influences of inherited structures and paleo-relief on the development of Cenozoic Tian Shan

6.4.1 Influence of the Mesozoic paleo-relief

In the northern piedmont of Tian Shan, marginal sedimentary breccias and coarse conglomerates were deposited in Jurassic series (Figure 3-3 in Chapter 3). The Jurassic "onlap" structure has also been deduced in the front of modern Tian Shan from the present field analysis, as illustrated in Figure 3-6. These characteristics indicate that a significant relief existed during Mesozoic times. The range piedmont was certainly located close and along the northern modern Tian Shan front during latest Jurassic, early Cretaceous times as the Kalaza sedimentary breccias locate along the present northern front of the modern mountain, along a N100-110° strike (see Chapter 3). Moreover, some locations described in this thesis work display the Paleozoic basement units thrusting over overturned Jurassic sedimentary breccias, such as in the Houxia section (Figure 4-26a). Such observation suggests that, at local scale, the Mesozoic paleo-relief may have controlled the location of the Cenozoic thrust faults, as illustrated on Figure 6-7. Indeed, analysis of these coarse sedimentary breccias highlighted i) erosion of the Paleozoic basement units and ii) a very limited transport of those clastic sediments, both features underlining the location of foothills during Mesozoic times (Figure 6-7a and Figure 3-6). On the other hand, structural observations made such as in the Houxia valley clearly shows that Cenozoic deformation could have localize exactly along those paleo-foothills as illustrated on figure 6-7b (Figure 3-4). In that case, Cenozoic Tian Shan "front" structures may be influenced by the piedmont of the Mesozoic paleo-relief. However, while segments where Jurassic series deformed during Cenozoic shortening, the northern Tian Shan front also displays continuous Mesozoic series and preserved onlap type structures

(Figure 3-6) which highlight, conversely, only poor control of the paleo-relief structure on the location of Cenozoic deformation (cf. Hutubi He section illustrated in Figure 6-7b and Figure 3-6).

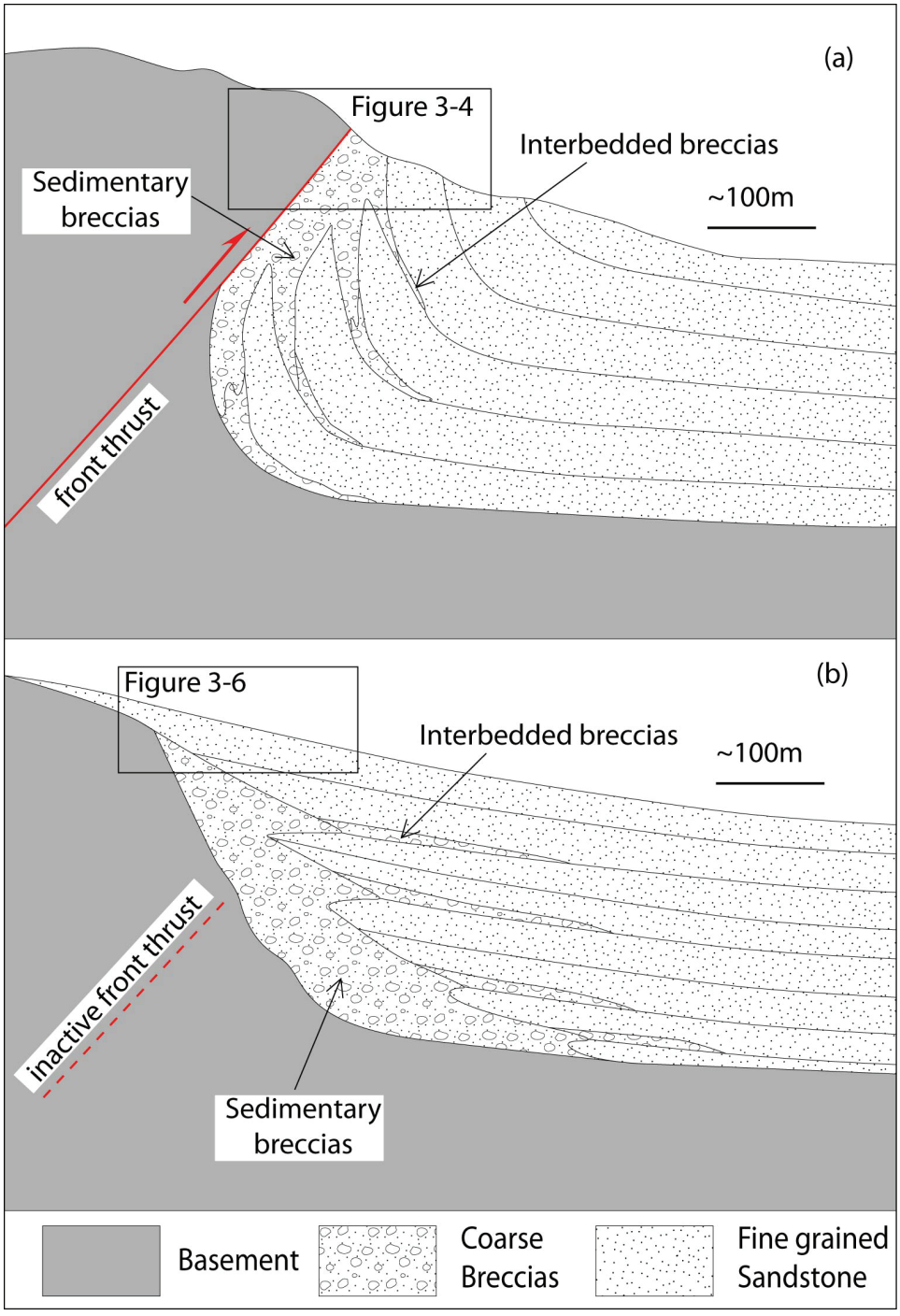

Figure 6-7. (a) An active Cenozoic thrust between the Paleozoic basement and the Jurassic sedimentary breccias. (b) inactive Cenozoic "front" of the northern Tian Shan.

Besides, several previous studies, such as Avouac et al. (1993), Burchfiel et al. (1999) and Deng et al. (2000), have suggested that a significant displacement has occurred along the thrust of the northern front of Tian Shan, assuming that the mountain basement rises from the deep basal basin (~10 km in depth) and thrusts onto the sediments. However, evidences for the persistence of a Mesozoic paleo-relief indicate the mountain basement was shallowly buried or located at a similar altitude with sediments along the Mesozoic front (Figure 6-7b). Therefore, the thrust between the mountain basement and the basin sediments could be much less important with respect to the previous estimation with rather small accounts of slip, such as observed in Houxia section (Figure 3-4 and Figure 4-28). Therefore, the deformations in the front, even though thrust contacts can be sometimes observed between the mountain basement and the basin sediments, are less important than that estimated by previous studies because of the neglect of the paleo-relief in Tian Shan front.

6.4.2 Influence of the Paleozoic structure

The importance of inherited structures in the geological evolution of Tian Shan has been pointed out by numerous studies (Molnar et al., 1973; Molnar and Tapponnier, 1975; Hendrix et al., 1992; Dumitru et al., 2001; Sobel et al., 2001; Wang et al., 2009; Jolivet et al., in press). For instance, earthquake analyses show that location of the current deformation can be related, to some extent, to the one of ancient structures (Molnar et al., 1973; Molnar and Tapponnier, 1975). With only few exceptions, most authors consider that the Tian Shan Cenozoic activity is related to the reactivation of crust structures inherited from the Paleozoic collision (Allen et al., 1993; Avouac et al., 1993; Hendrix et al., 1994; Yin et al., 1998; Allen et al., 1999; Dumitru et al., 2001). Yet, up to now, only poor discussion have been exposed and details for such a reactivation are often lacking.

Recent statistic studies on the Quaternary deformation show that the current maximum shortening axis in Tian Shan area is sub-horizontal and strike ~ N0° (Holt

et al., 1995; Holt, 2000; Kreemer et al., 2003); in other words, the resulting structural must strike at about N90°. On the other hand, in the study area, the major Paleozoic shear zones, in the interior of the range, strike about N105-110° (Figure 6-8; Carroll, 1990; Charvet et al., 2007; Gao et al., 1998; Shu et al., 2004; Kröner, 2007; Wang et al., 2007; 2008). These shear zones display high-dipping angles and dextral strike-slip movements until, at least, late Permian (Wang et al., 2008; Shu et al., 2010).

If considering deformation pattern of the basement units in the study area: the chapter 4 of this thesis show that the basement units are faulted and clearly separated into blocks with an interval of 15 to 20 km wide (Figure 4-34 and Figure 5-19). Field observations show that localized brittle deformation within basement rocks cut across the pervasive ductile structures lasting from the Paleozoic evolution of the range; few indicators – e.g. fault planes and tension gashes – also point out that basement units most probably behave as brittle and rather strong blocks, within the upper crust level, during Cenozoic intracontinental reactivation of the range. In addition, this study highlights that the Cenozoic shortening in front of the range results in very uncylindrical deformation pattern and presents strong lateral variations of the nature of the structures developed along-strike. Yet, analysis of the resulting structural map clearly shows that the brittle thrust developed within the mountain interiors, along the boundary in between basement rocks and Mesozoic sediments, can often be continuously extended in strike of an ancient, inherited basement shear zone. Rectangle zone A in the central part of Figure 6-8 particularly well highlight such configuration; the corresponding ductile shear zone is located to the north of the major North Tian Shan Fault (NTF) and was active as a strike-slip shear zone during Permian (Wang et al., 2006; Charvet et al., 2007).

If considering now the deformation pattern through the fold-and-thrust belts:

i) in the eastern part of the study area, from Urumqi to Shawan, fold axes and thrust faults developed within the foreland sedimentary series also show a N100-110° mean striking orientation, sub-parallel with respect to the inherited Paleozoic structure (Figure 6-8). The southernmost fold belt is characterized by basement-involved

structure. The basement is “cut” by reverse faults into rigid blocks (Figure 6-5) with also a parallel strike. It must be pointed out here that the thrusts developed within the interior parts of the range, within basement units, but also the ones observed within the foreland fold-and-thrust belts systematically display very steep dip angles. This feature, which is a rather peculiar one for the orientation attitude of reverse faults, may certainly be influenced by the orientation of the Paleozoic structures (shear zones or more penetrative steep cleavage developed within basement rocks).

ii) Conversely, in the north-western part of the study area, from Anjihai to Wusu, the northernmost anticline belt shows E-W striking axes (see Anjihai and Dushanzi anticlines; Figure 6-8). This orientation is well consistent with the one of the maximum shortening axis direction deduced from Quaternary structures analysis, as exposed above. Within that particular area, i.e. west of the study area and rather far from the range “front”, 10° to 20° angle difference can be measured in between the Paleozoic structure and the fold axis orientation, which contrast with the rest of the studied fold-and-thrust belt. It is noteworthy that this feature coincides with parts of the foreland basin where Cenozoic sediments are the thickest along the study area of the northern Tian Shan piedmont (Figure 6-8). The change in fold orientations is progressive in-between the eastern and western parts of the study area which also corresponds to a progressive variation of the Cenozoic sediments thickness (Figure 6-8). Indeed, in the easternmost part, Jurassic series outcrops directly at surface while the same series is buried in depth (~10 km), below Cenozoic strata, in the western area (Figure 6-8). As the difference in fold orientations looks correlated with the thickness variation of the Cenozoic sediments in between the eastern and western parts of the study area, we propose that the Cenozoic sedimentary pile may act as a decoupling layer. Yet, where the sedimentary thickness is the less important, in the eastern part of the basin as well as all along the range front, orientation of the structures observed at surface seems controlled by the one of the underlying basement structures, inherited from the Paleozoic tectonic history; shortening deformation of the cover may thus be coupled with the basement-involved structure in that case.

Conversely, where the sedimentary thickness is the more important, in the western part of the basin, orientation of the structures (i.e. folds and thrust faults) only depends on the maximum shortening orientation; orientation of the inherited Paleozoic structures seem not to have any control in that case as they are deeply buried below the Cenozoic sediments much certainly acting as a decoupling layer in that case.

From the all above discussed points, this study shows that the localization of the Cenozoic deformation – and in particular the location and orientation of reverse faults and folding – must be controlled, in most part of the study area, by Paleozoic inherited structures, including crust scale ductile shear zone as well as more penetrative ductile deformation. On the other hand, Cenozoic sedimentary series may act as a decoupling layer where they display the thickest deposits. Structures east-west mean striking is thus solely controlled by the one of the regional north-south striking maximum shortening direction in that case.

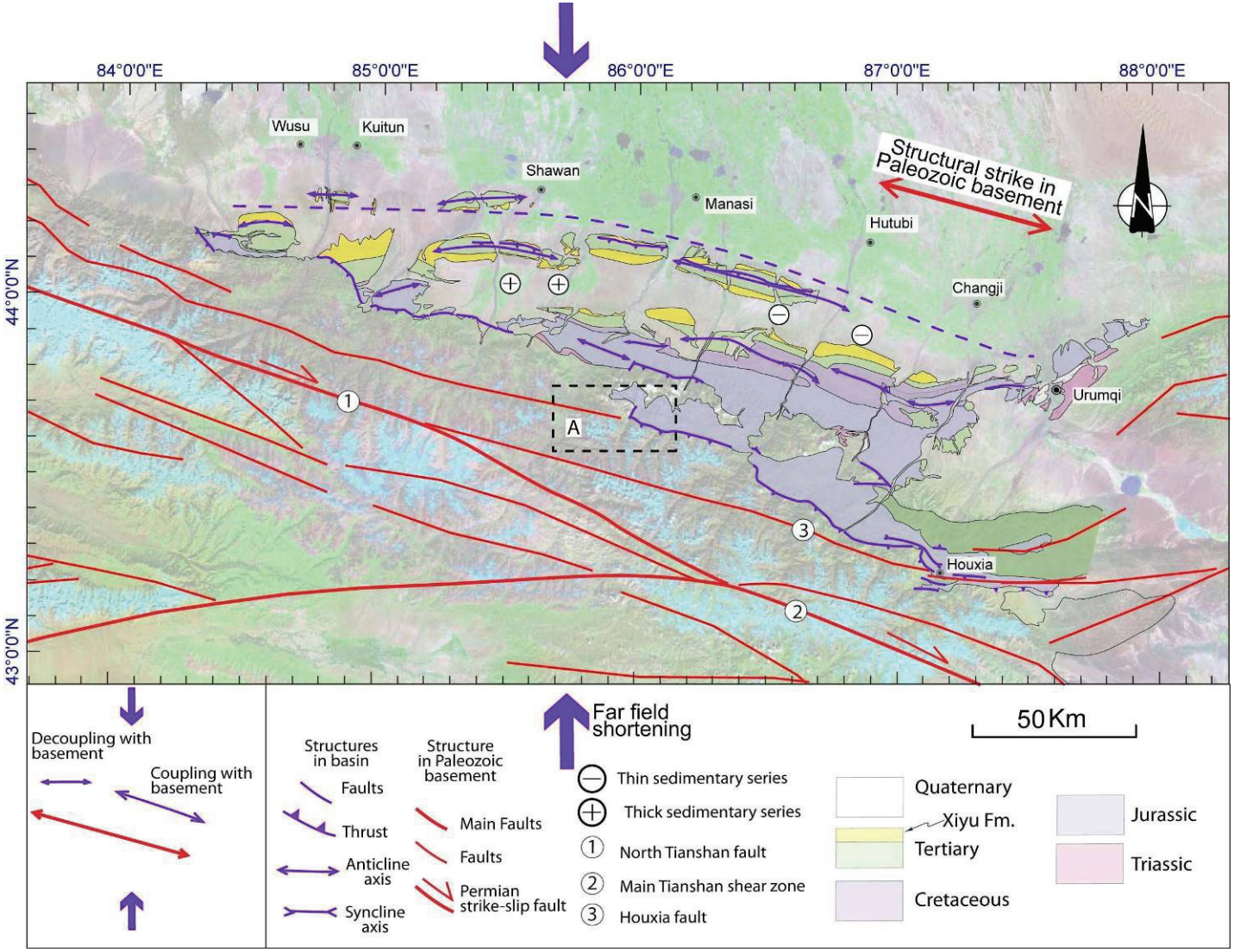

Figure 6-8. *Geological map of the northern piedmont of Tian Shan, with comparision of the location and orientation of the Paleozoic and Cenozoic structures.*

6.5 Conclusions

The Tian Shan mountain range, located in the northwest of China, has experienced successive tectonic events. The most attention has been, up to now, concentrated on the Paleozoic subduction-collision related block accretion of the range and its Cenozoic reactivation. Its contrasted topography and obvious fold-and-thrust belts along its piedmont have attracted attention of geoscientists since several decades and the ongoing deformation of the northern piedmont of Tian Shan offers an ideal natural laboratory to study the active mountain building. Moreover, the obtained results concerning the deformation amount, rate and mechanism are still in debate, in order to better understand the uplifting process and the deformation mechanism of Cenozoic Tian Shan, we have carried out a multidisciplinary study along its the northern piedmont from Urumqi to Wusu areas integrating detailed structural observations on the field as well as subsurface data including seismic profiles, gravity measurements and drilled wells. The main conclusions of this study can be made as follows:

(a) About the "immature" northern front of Tian Shan

The observations along the range-basin contacts show variable structural types between the basement range and the basin sediments, i.e. fault, fold and unconformity that admits rapid lateral evolution. The basin structure is mainly characterised by discrete and uncylindrical folds in the Meso-Cenozoic series. By integrating all available data, restored geological sections show rather weak shortening amounts ranging from 12 km (16.5%) to 5 km (6%) for the Jingou He and the Hutubi He sections, respectively. Above observations argue that the deformation should be weak with a significant lateral variations along the northern piedmont of Tian Shan.

In the depth, the structure of the basement is characterised by parallel high-angle-dipping thrusts characterised by a rather steady 15-20 km wide periodicity. No any low-angle and important amplitude thrust (nappe) neither backthrust has been observed in the northern piedmont of Tian Shan despite previous interpretations (Avouac et al., 1993; Burchfiel et al., 1999; Deng et al., 2000). Moreover, only few-kilometre-scaled décollements have been identified within the basin.

Assuming the modern shortening rate is 1-3 mm/yr, suggested by the geodetic surveying and geological investigations (Avouac et al., 1993; Molnar et al., 1994; Wang et al., 2001; Niu

et al., 2007; Charreau et al., 2008; Yang et al., 2008) and admitting the shortening amount obtained from this study, the oldest deformation onset age may be extrapolated to about 12 Ma (for about 12 km in shortening) among four studied geological sections. This result may be representative for the northern Tian Shan piedmont as these sections are extended about 170km east-westwards. Therefore, this representative onset age of modern deformation may indicate the northern piedmont is "young" with respect to onset age of unroofing age of Tian Shan (~25 Ma by fission tracks; e.g. Hendrix et al., 1994; Dumitru et al., 2001; Jolivet et al., in press).

Comparing to well-developed fold-and-thrust-belts in other ranges, such as Pyrenees (France) or Rocky Mountains (Canada), the features of the surface and deep structures, weak deformation and "younger" age may characterise the northern piedmont of Tian Shan as an immature orogenic front. As this area is still experiencing characterised by the ongoing India-Eurasia convergence, and the deformation rate is relatively high, the deformation will, therefore, become stronger and its 'maturity' will be, consequently, better and quickly developed.

(b) Consequences of Mesozoic Paleo-relief in present Tian Shan

Our study clearly has evidenced, at different encasing scales, the existence of a major Mesozoic paleo-relief along the northern Tian Shan range. A minimal difference of relative altitudes of about 1300m has been estimated between the basin and the mountain range based on the thickness variation and onlap sedimentary structure of the lower Jurassic series. The concept that the far-effect of the collision India-Asia is the only responsible for the present topography of the Tian Shan should be, therefore, questioned. In other words, the Mesozoic paleorelief has probably influenced the present Tian Shan topography. The Cenozoic uplifting of Tian Shan, due to the India-Asia collision, may be therefore reduced.

(c) Mechanism of the deformation in the northern "front"

Field observations and restored geological sections suggest rather weak deformation in the northern piedmont of Tian Shan. The basement on the surface is deformed by joints or steep faults and is appears to behaviour as rigid blocks. Large-scaled sections show that the basement is cut into rigid blocks with a roughly periodic interval of ~15-20 km. As the

overlying sediments are sub-horizontal, the basement should be weakly deformed though some joints and minor faults have been observed within it. Moreover, in the contact zones, all visible tectonic contacts are of reverse faults. Regional detachment, proposed in previous studies (Avouac et al., 1993; Burchfiel et al., 1999; Deng et al., 2000) with large movement has yet not been traced in the study area. Therefore, the deformation in the northern piedmont of Tian Shan is most probably controlled by the basement structures, which are mostly characterized by the steep dipping reverse faults.

A tentative model has been proposed for the deformation mechanism in the northern piedmont of Tian Shan. The reverse fault features are separated by ~15-20 km suggests that these reverse faults may be considered as ramps and be produced by a deep detachment fault. This detachment may be located about 15-20 km in the depth where it is localised below the traditional depth of brittle-ductile transition zone (Wang et al., 2004). In the upper and more brittle zone, the basement may be cut by reverse faults into rigid internally unstrained blocks. The northward compressive deformation is mainly propagated by the relative movement among these blocks. These reverse faults, visible in the contact zone and into the basement range have mainly deformed the basin cover and produced the fold belts in the basin. This model is significantly different from previous proposed ones: large detachment of the basin cover with respect to the basement.

(d) Paleozoic inherited structures on the present Tian Shan

Cenozoic structures, such as fold axes of thrust traces in the southern Junggar basin presents a general N90° strike in the western study area where the series are characterized by thick Cenozoic cover. To the East, with an extent of ~130 km in distance along the range Cenozoic cover disappears and Mesozoic rocks directly crops out. There, structure strikes are consistently N 100-110° and appear parallel to the main Paleozoic shear zones in the northern Tian Shan with strike direction around N100-110° as well. Some of these Paleozoic shear zones have been rejuvenated during Cenozoic and deform the basin sediments along this direction when the sedimentary cover in thin. However, to the West, where sedimentary cover is rather thick with ~5 km of Cenozoic series, direction of the structures, while probably linked to the same reactivation at depth, are rather orthogonal to the main shortening direction (i.e. N90°) and appears as newly formed. The Dushanzi and Anjihai anticlines show east-west orientated strikes by a difference of about 10-20° with respect to the Paleozoic structure. It indicates that the basin cover in the western study zone may be decoupled with the basement

structure and the far-effect of the north-south compression probably plays a main role here.

6.6 Perspectives

Though this study has made progresses in the understanding of the Cenozoic evolution of the northern piedmont of Tian Shan, such as the role of far-effect of India-Asia collision on the present topography of Tian Shan, the process and mechanism of deformation along its northern piedmont of Tian Shan Cenozoic, onset age of tectonic forcing in the Junggar basins, etc., several essential problems still remain unclear.

(a) Relationship between Paleozoic Inherited and Cenozoic structures

The control of the Paleozoic structure on the Cenozoic one seems having been demonstrated, but still qualitatively. Much detailed work is need in geometrical relationship, relative kinematic movements, and active age constrain both the Paleozoic and Cenozoic faults are necessary to clarify their relationships.

(b) The 3D modelling of the southern Junggar basin

Though four geological sections have built up from the basin to the range along the northern piedmont of Tian Shan, the observations still remain discrete, especially because of highly lateral variations of deformation style, rate and shortening the 3D modelling will help to better reveal structural characteristics of the study zone and understand the deformation mechanism. Furthermore, this work may also allow estimating the sedimentary volume, understanding the foreland basin processing, and, consequently, probably erosion and uplifting history of Tian Shan.

(C) Cenozoic evolution of the southern piedmont of Tian Shan

The northern piedmont of Tian Shan has been characterised as an immature orogenic belt. Its southern piedmont seems having undergone stronger Cenozoic deformation suggested by previous studies (e.g. Yin et al., 1998). However, what are the characteristics of the front in the southern piedmont? What is the difference between the northern and southern piedmont in

deformation? Much more field works are needed to answer these critical questions and to understand the deformation propagation of due to the collision India-Asia and the Cenozoic uplifting history of Tian Shan.

References

A

Abdrakhmatov, K.Y., Aldazhanov, S.A., Hager, B.H., Hamburger, M.W., Herring, T.A., Kalabaev, K.B., Makarov, V.I., Molnar, P., Panasyuk, S.V., Prilepin, M.T., Reilinger, R.E., Sadybakasov, I.S., Souter, B.J., Trapeznikov, Y.A., Tsurkov, V.Y., and Zubovich, A.V., 1996, Relatively recent construction of the Tien Shan inferred from GPS measurements of present-day crustal deformation rates: Nature, v. 384, 450-453.

Aitchison, J.C., Davis, A.M., Badengzhu, and Luo, H., 2002, New constraints on the India- Asia collision: the Lower Miocene Gangrinboche conglomerates, Yarlung Tsangpo suture zone, SE Tibet: Journal of Asian Earth Sciences, v. 21, 251-263.

Allen, M.B., Windley, B.F., Zhang, C., Zhao, Z.Y. and Wang, G.R., 1991, Basin Evolution within and Adjacent to the Tien-Shan Range, NW China: J. Geol. Soc. London, v. 148, 369-378.

Allen, M.B., Windley, B.F., and Zhang, C., 1993, Palaeozoic collisional tectonics and magmatism of the Chinese Tien Shan, central Asia: Tectonophysics, v. 220, 89-115.

Allen, M., Windley, B., and Zhang, C., 1994, Cenozoic tectonics in the Urumgi-Korla region of the Chinese Tien Shan: Geologische Rundschau, v. 83, 406-416.

Allen, M.B., Vincent, S.J., and Wheeler, P.J., 1999, Late Cenozoic tectonics of the Kepingtage thrust zone: Interactions of the Tien Shan and Tarim Basin, northwest China: Tectonics, v. 18, 639-654.

Allmendinger, R.W., and Shaw, J.H., 2000, Estimation of fault propagation distance from fold shape: Implications for earthquake hazard assessment: Geology, v. 28, 1099-1102.

Arthaud, F., and M. Séguret, 1981, Les structures pyrénéennes du Languedoc et du Golfe du Lion (Sud de la France): Bull. Soc. Geol. Fr., v. 7, 51-63.

Avouac, J.-P. and Peltzer, G., 1993, Active tectonics in southern Xinjiang, China : Analysis of terrace riser and normal fault scarp degradation along the Hotan-Qira Fault system: Journal of Geophysical Research, v. 98 : 21773-21807.

Avouac, J.-P., and Tapponnier, P., 1993, Kinematic model of active deformation in central

Asia: Geophys. Res. Lett., v. 20, 895-898.

Avouac, J.-P., Tapponnier, P., Bai, M., You, H., and Wang, G., 1993, Active Thrusting and Folding Along the Northern Tien-Shan and Late Cenozoic Rotation of the Tarim Relative to Dzungaria and Kazakhstan: Journal of Geophysical Research-Solid Earth, v. 98, 6755-6804.

Avouac, J.-P., and DeWever, P., 2002, Himalaya-Tibet - Le choc des continents, CNRS Editions, 191 p.

B

Barrier, L., 2002, Ineractions deformation-sedimentation dans les systems compressifs supra-crustaux, exemples naturels et modélisation analogique [Ph.D Thesis]: Paris, Université de Rennes 1.

Beck, R.A., Burbank, D.W., Sercombe, W.J., Riley, G.W., Barndt, J., Berry, J.R., Afzal, J., Asrar, M.K., Herman, J., Metje, J., Cheema, A., Shafique, N.A., Lawrence, R.D., and Khan, M.A., 1995, Stratigraphic evidence for an early collision between India and Asia: Nature, v. 373, 55-58.

Besse, J., Courtillot, V., Pozzi, J.P., Westphal, M., and Zhou, Y.X., 1984, Palaeomagnetic estimates of crustal shortening in the Himalayan thrusts and Zangbo suture: Nature, v. 311, 621-626.

Bullen, M.E., Burbank, D.W., Garver, and J.I., and Abdrakhmatov, K.Y., 2001, Late Cenozoic tectonic evolution of the northwestern Tien Shan: New age estimates for the initiation of mountain building: Geological Society of America Bulletin, v. 113, 1544-1559.

Bullen, M.E., Burbank, D.W., and Garver, J.I., 2003, Building the Northern Tien Shan: Integrated thermal, structural, and topographic constraints: Journal of Geology, v. 111, 149-165.

Burchfiel, B.C., Tectonics of Noncollisional regimes, the modern Andes and theMesozoic cordilleran Orogen of the Western United States in: Geophysics study committee, 1990, Continental tectonics, Washington, D.C.

Burchfiel, B.C., Brown, E.T., Deng, Q.D., Feng, X.Y., Li, J., Molnar, P., Shi, J.B., Wu, Z.M., and You, H.C., 1999, Crustal shortening on the margins of the Tien Shan, Xinjiang, China: International Geology Review, v. 41, 665-700.

Byerlee, J.D., 1968, Brittle-Ductile Transition in Rocks: J. Geophys. Res., v. 73,

4741-4750.

C

Calcagno, P., Lazarre, J., Courrioux, G., and Ledru, P., 2007, 3D geometric modelling of an external orogenic domain: a case history from the western Alps (massif de Morges, Pelvoux): Bulletin de la Société Géologique de France, v. 178, 263-274.

Cao, R.L., Zhu, S.H., Zhu, X.K., Guan, Y.B., 1992, Plate and terrane tectonics of Northern Xinjiang, in: Tu, G.Z. eds, New Improvement of Solid Geosciences in Northern Xinjiang, Science Press, Beijing, 11-26.

Carroll, A.R., 1990, Junggar basin, northwest China: trapped Late Paleozoic ocean: Tectonophysics, v. 181, 1-14.

Carroll, A.R., Graham, S.A. and Smith, M.E., 2010, Walled sedimentary basins of China: Basin Res., v. 22, 17-32.

Charreau, J., Chen, Y., Gilder, S., Dominguez, S., Avouac, J.-P., Sen, S., Sun, D.J., Li, Y.G., and Wang, W.M., 2005, Magnetostratigraphy and rock magnetism of the Neogene Kuitun He section (northwest China): implications for Late Cenozoic uplift of the Tian Shan mountains: Earth and Planetary Science Letters, v. 230, 177-192.

Charreau, J., Avouac, J.-P., Chen, Y., Dominguez, S., and Gilder, S., 2008, Miocene to present kinematics of fault-bend folding across the Huerguosi anticline, northern Tian Shan (China), derived from structural, seismic, and magnetostratigraphic data: Geology, v. 36, 871-874.

Charreau, J., Chen, Y., Gilder, S., Barrier, L., Dominguez, S., Augier, R., Sen, S., Avouac, J.-P., Gallaud, A., Graveleau, F., Wang, Q.C., 2009, Neogene uplift of the Tian Shan Mountains observed in the magnetic record of the Jingou River section (northwest China): Tectonics, v. 28.

Charreau, J., Gumiaux, C., Avouac, J.-P., Augier, R., Chen, Y., Barrier, L., Gilder, S., Dominguez, S., Charles, N., and Wang, Q., 2009, The Neogene Xiyu Formation, a diachronous prograding gravel wedge at front of the Tian Shan: Climatic and tectonic implications: Earth and Planetary Science Letters, v. 287, 298-310.

Charvet, J., Shu, L.S., and Laurent-Charvet, S., 2007, Paleozoic structural and geodynamic evolution of eastern Tian Shan (NW China): welding of the Tarim and Junggar plates: Episodes, v. 30, 162-186.

Chen, C.M., Lu, H.F., Jia, D., Cai, D.S., and Wu, S.M., 1999, Closing history of the

southern Tian Shan oceanic basin, western China: an oblique collisional orogeny: Tectonophysics, v. 302, 23-40.

Chen, S.P., Qi, J.F., Yu, F.S., Yang, Q., 2007, Deformation characteristics in the southern margin of the Junggar basin and theire controlling factors: Acta Geologica Sinica, 81, 151-157.

Chen, Y., Cogne, J.P., Courtillot, V., Tapponnier, P., and Zhu, X.Y., 1993, Cretaceous Paleomagnetic Results from Western Tibet and Tectonic Implications: Journal of Geophysical Research-Solid Earth, v. 98, 17981-17999.

Choukroune, P., and Séguret, M., Tectonics of the Pyrenees, role of gravity and compression, in: De Jong K.A. and Schölten, Gravity and Tectonics, John Wiley, New York, 1973, 141-156.

Coleman, R.G., 1989, Continental Growth of Northwest China: Tectonics, v. 8, 621-635.

Cosgrove, J.W. and Ameen, M.S. 2000, Forced folds and Fractures: Geological Society, London, Special Publications, v. 169.

Coward, M.P., Kidd, W.S.F., Yun, P., Shackleton, R.M., and Hu, Z., 1988, The Structure of the 1985 Tibet Geotraverse, Lhasa to Golmud: Philosophical Transactions of the Royal Society of London. Series A, Mathematical and Physical Sciences, v. 327, 307-333.

D

Daëron, M., Avouac, J.-P., and Charreau, J., 2007, Modeling the shortening history of a fault tip fold using structural and geomorphic records of deformation: Journal of Geophysical Research-Solid Earth, v. 112.

Dahlen, F.A., Suppe, J., and Davis, D., 1984, Mechanics of Fold-and-Thrust Belts and Accretionary Wedges: Cohesive Coulomb Theory: J. Geophys. Res., v. 89, 10087-10101.

Dahlstrom, C.D.A., 1969, Balanced cross sections: Canadian Journal of Earth Sciences, v. 6, 743-757.

Dahlstrom, C.D.A., 1990, Geometric constraints derived from the law of conservation of volume and applied to evolutionary models for detachment folding: American Association of Petroleum Geologists Bulletin, v. 74: 336-344.

Davis, D., Suppe, J., and Dahlen, F.A., 1983, Mechanics of Fold-and-Thrust belts and accretionary wedges: Journal of Geophysical Research, v. 88, 1153-1172.

De Donatis, M., 2001, Three-Dimensional Visualization of the Neogene Structures of an External Sector of the Northern Apennines, Italy: AAPG Bulletin, v. 85, 419-431.

Debelmas, J., Mascle, G., and Basile, C., 2008, Les Grandes Structures Géologiques : Dunod, Paris, 322 p.

Deng, Q.D., Feng, X.Y., You, H.C., Zhang, P.Z., Zhang, Y., Li, J., Wu, Z.M., Xu, X.W., Yang, X.P., and Zhang, H.W., 1991, The characteristic of deformation and mechanism of Dushanzi-Anjihai active reverse fault-fold zone in the northern flank of theTian Shan Mountains: Beijing, Seismology Press.

Deng, Q.D., Zhang P.Z., Xu X.W., Yang X.P., Peng S.Z., 1996. Paleoseismology of the northern piedmont of Tian Shan Mountains, northwestern China: J. Geophys. Res., v. 101, 5895-5920.

Deng, Q.D., Feng, X.Y., Zhang, P.Z., Xu, X.W., Yang, X.P., Peng, S.Z., and Li, J., 2000, ActiveTectonics of theTian Shan Mountains: Beijing, Seismology Press, 399 p.

Deramond, J., Souquet, P., Fondecave-Wallez, M. J. and Specht, M., 1993, Relationships between thrust tectonics and sequence stratigraphy surfaces in foredeep: model and examples from the Pyrenees (Cretaceous-Eocene, France, Spain), in: Williams G. D. and Dobb, A., eds, Tectonics and seismic sequence stratigraphy, Geological Society of London Special Publications, v. 71: 193-219.

Dewey, J.F., 1965, Nature and origin of kink-bands: Tectonophysics, v. 1, 459-494.

Dewey, J.F. and Bird, J.M., 1970, Mountain belts and the new global tectonics: Journal of Geophysical Research, v. 75, 2625-2647.

Dong, C. Q., Sun, Z.M., Hong, T.Y., 2007, Identification of the detachments in the foreland fold-thrust belt in southern margin of Junggar basin: Petroleum Geology and Experiment, v. 12.

Du, Z.L., 2007, Tectonic and thermal evolution of the Jurassic hydrocarbon source rock in the piedmont basins of the Chinese Tian Shan [Ph.D Thesis]: Beijing, Institute of Geology and Geophysics, Chinese Academy of Sciences.

Dumitru, T.A., Zhou, D., Chang, E.Z., Graham, S.A., Hendrix, M.S., Sobel, E.R., and Carroll, A.R., 2001, Uplift, exhumation, and deformation in the Chinese Tian Shan, in: Hendrix, M.S., and Davis, G.A., eds., Paleozoic and Mesozoic tectonic evolution of central Asia: From continental assembly to intracontinental deformation: Boulder: Colorado, Geological Society of America Memoirs, v. 194, 71-99.

E, F

English, J.M. and Johnston, S.T., 2004, The Laramide orogeny: What were the driving forces? International Geology Review, v. 46, 833-838.

Erslev, E.A., Holdaway, S.M., O'Meara, S.A., Jurista, B., and Selvig, B., 2004, Laramide minor faulting in the Colorado Front Range: New Mexico bureau of geology & Mineral resources, bulletin, v. 160, 181-203.

Faill, R.T., 1973, Kink band folding. Valley and Ridge province, Pennsylvania: Geological Society of America Bulletin, v. 84, 1289–1314.

Fernandez, O., Munoz, J.A., Arbues, P., Falivene, O., and Marzo, M., 2004, Three-dimensional reconstruction of geological surfaces: An example of growth strata and turbidite systems from the Ainsa basin (Pyrenees, Spain): AAPG Bulletin, v.88, 1049-1068.

Fu, B., Lin, A., Kano, K.-i., Maruyama, T., and Guo, J., 2003, Quaternary folding of the eastern Tian Shan, northwest China: Tectonophysics, v. 369, 79-101.

G

Gallaud, A., 2008, Interaction Orogenèse – Climat – Erosion en Asie Centrale durant le Cénozoïque : L'impact de la surrection de la chaîne du Tian Shan sur le climat dans le bassin du Junggar [Ph.D Thesis]: Orléans, Université d'Orléans.

Gao, J., He, G., Li, M., Xiao, X., Tang, Y., Wang, J., Zhao, M., 1995, The mineralogy, petrology, metamorphic P-T-D-t trajectory and exhumation mechanism of blueschists, south Tian Shan, northwest China: Tectonophysics, v. 250, 151-168.

Gao, J., Li, M.S., Xiao, X.C., Tang, Y.Q., and He, G.Q., 1998, Paleozoic tectonic evolution of the Tian Shan Orogen, northwestern China: Tectonophysics, v. 287, 213-231.

Garzanti, E., 2007, Comment on "When and where did India and Asia collide?" by Jonathan C. Aitchison, Jason R. Ali, and Aileen M. Davis: Journal of Geophysical Research, v. 113.

Ghose, S., Hamburger, M.W., and Ammon, C.J., 1998, Source parameters of moderate-sized earthquakes in the Tien Shan, central Asia from regional moment tensor inversion: Geophys. Res. Lett., v. 25, 3181-3184.

Gomez, F., M. Barazangi, and W. Beauchamp, 2000, Role of the Atlas Mountains

northwest Africa) within the African-Eurasian plateboundary zone: Geology, 28, 769-864.

Graham, S.A., Hendrix, M.S., Wang, L.B., and Carroll, A.R., 1993, Collisional successor basins of western China: Impact of tectonic inheritance on sand composition: Geological Society of America Bulletin, v. 105, 323-344.

Guan, S.W., Li, B.L., He, D.F., Wang, X., Suppe, J., Lei, G.L., 1994, Late Cenozoic Active Fold-and-thrust belts in the southern and northern flanks of Tian Shan: Acta Geologica Sinica, v. 6, 725-744.

Gu, J., 1994, Depositional facies and petroleum: Petroleum exploration of Tarim basin: Beijing, Petroleum Industry Press, 310 p.

Guo, Z.J., Zhang Z.C., Wu C.D., Fang S.H., Zhang R., 2006, The Mesozoic and Cenozoic exhumation history of Tian Shan and comparative studies to the Junggar and Altai Mountains: Acta geologica Sinica, v. 1, 1-15.

H

Han, B.F., He, G.Q. and Wang, S., 1999, Postcollisional mantle-derived magmatism, underplating and implications for basement of the Junggar Basin: Sci. China. Ser. D, v. 42, 113-119.

Hardy, S. and Ford M, 1997, Numerical modeling of trishear fault propagation folding: Tectonics, v. 16, 841-854.

Harrison, T.M., Copeland, P., Kidd, W.S.F., and Yin, A.N., 1992, Raising Tibet: Science, v. 255, 1663-1670.

He, D., Suppe, J., Yang, G., and Huang, S., 2005, Guidebook for field trip in south and north Tian Shan foreland basin, Xinjiang Uygur Autonomous Region, China: International conference on the thery and application of fault-related folding in foreland basins, 1-78.

Hendrix, M.S., Graham, S.A., Carroll, A.R., Sobel, E.R., Mcknight, C.L., Schulein, B.J., and Wang, Z.X., 1992, Sedimentary Record and Climatic Implications of Recurrent Deformation in the Tian-Shan - Evidence from Mesozoic Strata of the North Tarim, South Junggar, and Turpan Basins, Northwest China: Geological Society of America Bulletin, v. 104, 53-79.

Hendrix, M.S., Dumitru, T.A. and Graham, S.A., 1994, Late Oligocene Early Miocene Unroofing in the Chinese Tien-Shan - an Early Effect of the India-Asia Collision:

Geology, v. 22, 487-490.

Hendrix, M.S., 2000, Evolution of Mesozoic sandstone compositions, southern Junggar, northern Tarim, and western Turpan basins, northwest China: A detrital record of the ancestral Tian Shan: J. Sed. Res., v. 70, 520-532.

Hinze, W.J., Braile, L.W., Keller, G.R., Lidiak, E.G., Models for midcontinent Tectonism. in: Geophysics study committee, 1990, Continental tectonics, Washington, D.C.

Holt, W.E., Li, M., and Haines, A.J., 1995, Earthquake strain rates and instantaneous relative motions within central and eastern Asia: Geophysical Journal International, v. 122, 569-593.

Holt, W.E., 2000, Velocity field in Asia inferred from Quaternary fault slip rates and Global Positioning System observations: Journal of Geophysical Research, v. 105, 19185-19209.

Horii, H., and Nemat-Nasser, S., 1986, Brittle Failure in Compression: Splitting, Faulting and Brittle-Ductile Transition: Philosophical Transactions of the Royal Society of London. Series A, Mathematical and Physical Sciences, v. 319, 337-374.

Huang, B., Piper, J.D.A., Peng, S., Liu, T., Li, Z., Wang, Q., and Zhu, R., 2006, Magnetostratigraphic study of the Kuche Depression, Tarim Basin, and Cenozoic uplift of the Tian Shan Range, Western China: Earth and Planetary Science Letters, v. 251, 346-364.

Huang, T.K., 1949, Briefly geological presentation of Xinjiang Province, 9, Xinjiang.

Huang, T.K., 1978, An outline of the tectonics characteristics of China: Eclogae Geologicae Helvetiae, v. 71, 611-635.

J, K

Jacobshagen, V., Ğörler, K., Giese, P., 1988, Geodynamic evolution of the Atlas System (Morocco) in Post Paleozoic times, In: Jacobshagen, V., eds, The Atlas System of Morocco: Springer, Berlin, 481–499.

Jahn, B.-M., Griffin, W.L., and Windley, B., 2000, Continental growth in the Phanerozoic: Evidence from Central Asia: Tectonophysics, v. 328.

Jahn, B.-M., 2004a, The Central Asian Orogenic Belt and growth of the continental crust in the Phanerozoic: Geological Society, London, Special Publications, v. 226, 73-100.

Jahn, B.-M., Windley, B., Natal'in, B., and Dobretsov, N., 2004b, Phanerozoic continental

growth in Central Asia: Journal of Asian Earth Sciences, v. 23, 599-603.

Ji, J., Luo, P., White, P., Jiang, H., Gao, L., and Ding, Z., 2008, Episodic uplift of the Tian Shan Mountains since the late Oligocene constrained by magnetostratigraphy of the Jingou River section, in the southern margin of the Junggar Basin, China: J. Geophys. Res., v. 113.

Jia, C.Z., Tectonic Characteristics and Petroleum, Tarim Basin, China, Beijing: Petroleum Industry Press, 1997, 438 p.

Jolivet, M., Dominguez, S., Charreau, J., Chen, Y., Avouac, J.-P., Li, Y.A., Wang, Q.C., Mesozoic and Cenozoic tectonic history of the Central Chinese Tian Shan: Reactivated tectonic structures and active deformation: tectonics, in press.

Kapp, P., Yin, A., Harrison, T.M., and Ding, L., 2005, Cretaceous-Tertiary shortening, basin development, and volcanism in central Tibet: Geological Society of America Bulletin, v. 117, 865-878.

Konopelko, D., Biske, G., Seltmann, R., Eklund, O., Belyatsky, B., 2007, Hercynian post-collisional A-type granites of the Kokshaal Range, Southern Tien Shan, Kyrgyzstan: Lithos, v. 97, 140-160.

Kreemer, C., Holt, W.E., and Haines, A.J., 2003, An integrated global model of present-day plate motions and plate boundary deformation: Geophysical Journal International, v. 154, 8-34.

Kröner, A, Windley, B.F., Badarch, G., Tomurtogoo, O., Hegner, E., Jahn, B.M., Gruschka, S., Khain, E.V., Demoux, A., Wingate, M.T., 2007, Accretionary growth and crust-formation in the central Asian Orogenic Belt and comparison with the Arabian-Nubian shield, in: Hatcher Jr., R.D., Carlson, M.P., McBride, J.H., Martinez Catalan, J.R. eds, 4-D framework of continental crust, Geological Society of America Memoir 200, 181–209 p.

Kröner, A., Hegner, E., Lehmann, B., Heinhorst, J., Wingate, M.T.D., Liu, D.Y., Ermelov, P., 2008, Palaeozoic arc magmatism in the Central Asian Orogenic Belt of Kazakhstan: Shrimo zircon ages and whole-rock Nd isotopic systematic: Journal of Asian Earth Sciences, v. 32, 118-130.

L

Lacombe, O., Lavé, J., Roure, F., and Vergés, J., 2007, Thrust Belts and Foreland Basins : Springer.

Lacombe, O., and Mouthereau, F., 2002, Basement-involved shortening and deep detachment tectonics in forelands of orogens: Insights from recent collision belts (Taiwan, Western Alps, Pyrenees): Tectonics, v. 21.

Laurent-Charvet, S., Charvet, J., Shu, L.S., Ma, R.S. and Lu, H.F., 2002, Palaeozoic late collisional strike-slip deformations in Tian Shan and Altay, eastern Xinjiang, NW China: Terra Nova, v. 14, 249-256.

Laurent-Charvet, S., 2001, Accrétions continentales en Asie centro-orientale : évolution géodynamique etstructurale du Tian Shan et du Junggar oriental (nord-ouest Chine) au Paléozoïque [Ph.D Thesis]: University of Orléans, Orléans, France.

Laville, E., Pique, A., Amrhar, M., Charroud, M., 2004, A restatement of the Mesozoic Atlasic Rifting (Morocco): Journal of African Earth Sciences, v. 38, 145–153.

Li, C., Dupont-Nivet, G., and Guo, Z., 2010a, Magnetostratigraphy of the Northern Tian Shan foreland, Taxi He section, China: Basin Research, in press.

Li, C., Guo, Z., and Dupont-Nivet, G., 2010b, Late Cenozoic tectonic deformation across the northern foreland of the Chinese Tian Shan: Journal of Asian Earth Sciences, in Press.

Li, Z., Song, W.J., Peng, S.T., Wang, D.X. and Zhang, Z.P., 2004, Mesozoic-Cenozoic tectonic relationships between the Kuqa subbasin and Tian Shan, northwest China: constraints from depositional records, Sed. Geol., v. 172, 223-249.

Li, Z. and Peng S., 2010, Detrital zircon geochronology and its provenance implications: responses to Jurassic through Neogene basin-range interactions along northern margin of the Tarim Basin, Northwest China: Basin Res., v.22, 126-138.

Li, Z.W., Roecker, S., Li, Z., Wei, B., Wang, H., Schelochkov, G., Bragin, V., 2009, Tomographic image of the crust and upper mantle beneath the western Tien Shan from the MANAS broadband deployment: Possible evidence for lithospheric delamination: Tectonophysics, v. 477, 49-57.

Liu, H.F., Liang, H.S., Cai, L.G., Xia, Y.P., Liu, L.Q., Evolution and strucutral style of Tian Shan and Adjacent Basins, Northwestern China: Earth Science-Journal of China University of Geosciences, v. 6, 727-741.

Lu, D., Li, Q., Gao, R., Li, Y., Li, D., Liu, W., and Zhang, Z., 2000, A deep seismic sounding profile across the Tian Shan Mountains: Chinese Science Bulletin, v. 45, 2100-2107.

Lu, H.F., Wang, S.L., Jia, C.Z., 2007, The mechanism of the southern Junggar Cenozoic thrusts: Earth Science Frontiers, v. 14, 168-174.

Lu, H.H, Burbank, D.W., Li, Y.L., and Liu, Y.M., 2010, Late Cenozoic structural and stratigraphic evolution of the northern Chinese Tian Shan foreland: Basin Research, v. 22, 249-269.

M

Ma, R.S., Wang, C.F., Ye, S.F., 1993, Tectonic framework crustal evolution of Eastern Tian Shan Mountains: Publishing House of Nanjing University, Nanjing, 225 p.

Marquer, D., Calcagno, P., Barfety, J.-C., and Baudin, T., 2006, 3D Modeling and Kinematics of the External Zone of the French Western Alps (Belledonne and Grand Châtelard Massifs, Maurienne Valley, Savoie): Eclogae Geologicae Helvetiae, v. 99, 211-222.

Martelet, G., Calcagno, P., Gumiaux, C., Truffert, C., Bitri, A., Gapais, D., and Brun, J.P., 2004, Integrated 3D geophysical and geological modelling of the Hercynian Suture Zone in the Champtoceaux area (south Brittany, France): Tectonophysics, v. 382, 117-128.

Maxelon, M., and Mancktelow, N.S., 2005, Three-dimensional geometry and tectonostratigraphy of the Pennine zone, Central Alps, Switzerland and Northern Italy: Earth-Science Reviews, v. 71, 171-227.

Métivier, F., and Gaudemer, Y., 1997, Mass transfer between eastern Tien Shan and adjacent basins (central Asia): constraints on regional tectonics and topography: Geophysical Journal International, v. 128, 1-17.

Missenard, Y., 2006. Le relief des Atlas Marocains : contribution des processus asthénosphe´riques et du raccourcissement crustal, aspects chronologiques. [Ph.D thesis]: Université de Cergy Pontoise, France, 236 p.

Missenard, Y., Taki, Z., Frizon de Lamotte, D. et al., 2007, Tectonic styles in the Marrakesh High Atlas (Morocco): the role of heritage and mechanical stratigraphy: J. Afr. Earth Sci., v. 48, 247–266.

Mitra, S., 1990, Fault-Propagation Folds: Geometry, Kinematic Evolution, and Hydrocarbon Traps: AAPG Bulletin, v. 74, 921-945.

Molnar, P., Fitch, T.J., and Wu, F.T., 1973, Fault plane solutions of shallow earthquakes and contemporary tectonics in Asia: Earth and Planetary Science Letters, v. 19, 101-112.

Molnar, P., and Tapponnier, P., 1975, Cenozoic Tectonics of Asia: Effects of Continental

Collision: Features of recent continental tectonics in Asia can be interpreted as results of the India-Eurasia collision: Science, v. 189, 419-428.

Molnar P. and Qidong D., 1984, Faulting associated with large earthquakes and the average rate of deformation in central and eastern Asia: Journal of Geophysical Research, v. 89, 6203–6227.

Molnar, P., 1988, Continental tectonics in the aftermath of plate tectonics: Nature, v. 335, 131-137.

Molnar, P., Brown, E.T., Burchfiel, B.C., Qidong, D., Xianyue, F., Jun, L., Raisbeck, G.M., Jianbang, S., Zhangming, W., Yiou, F., and Huichuan, Y., 1994, Quaternary Climate-Change and the Formation of River Terraces across Growing Anticlines on the North Flank of the Tien-Shan, China: Journal of Geology, v.102, 583-602.

Molnar, P. and Ghose S., 2000, Seismic moments of major earthquakes and the rate of shortening across the Tien Shan: Geophys. Res. Lett., v. 27, 2377-2380.

Molnar, P., 2004, Late cenozoic increasein accumulation rates of terrestrial sediment, How Might Climate Change Have Affected Erosion Rates: Annu. Rev. Earth Planet. Sci., v. 32, 67-89.

Muñoz, J.A., 1992. Evolution of a continental collision belt: Ecors-Pyrenees crustal balanced cross-section, in: McClay, K.R., eds, Thrust tectonics, Chapman&Hall, Londaon, 235-246.

Narr, W. and Suppe, J., 1993, Kinematics of basement-involved compressive structures: American Journal of Science, v. 294, 302-360.

Nelson, M.R., McCaffrey, R., Molnar, P., 1987, Source parameters for eleven earthquakes in the Tien Shan, central Asia: Determined by P and SH waveform inversion: Journal of Geophysical Research, v. 92, 12629-12648.

Niu, Z.J., You, X.Z., and Yang, S.M., 2007, Analysis of contempoary crustal deformation characteristics with GPS data of Tian Shan mountain: Journal of geodesy and Geodynamcis, v. 27, 1-9.

Novoa, E., Mount, V. and Suppe, J., 1998, Map-view interference of monoclinal folds: Journal of Structural Geology, v. 20, 339-353.

N, P, Q

Paterson, M.S. and Weiss, L.E., 1966, Experimental Deformation and Folding in Phyllite: Geological Society of America Bulletin, v. 77, 343-374.

Patriat, P., and Achache, J., 1984, India-Eurasia collision chronology has implications for crustal shortening and driving mechanism of plates: Nature, v. 311, 615-621.

Pfiffner, O.A., Ellis, S., and Beaumont, C., 2000, Collision tectonics in the Swiss Alps: Insight from geodynamic modeling: Tectonics, v. 19, 1065-1094.

Poblet, J., McClay, K., Storti, F. and Munz, J.A., 1997, Geometries of syntectonic sediments associated with single-layer detachment folds: Journal of Structural Geology, v. 19, 369-381.

Pozzi, J.-P., and Feinberg, H., 1991, Paleomagnetism in the Tajikistan: continental shortening of European margin in the Pamirs during Indian Eurasian collision: Earth and Planetary Science Letters, v. 103, 365-378.

Price, R.A., 1981, The Cordilleran foreland thrust and fold belt in the southern Canadian Rocky Mountains: Geological Society, London, Special Publications, v. 9, 427- 448.

Price, R.A., 2001, An evaluation of models for the kinematic evolution of thrust and fold belts: structural analysis of a transverse fault zone in the Front Ranges of the Canadian Rockies north of Banff, Alberta: Journal of Structural Geology, v. 23, 1079-1088.

Putz, M., Stüwe, K., Jessell, M., and Calcagno, P., 2006, Three-dimensional model and late stage warping of the Plattengneis Shear Zone in the Eastern Alps: Tectonophysics, v. 412, 87-103.

Qi, J.F., Chen, S.P., Yang, Q., Yu, F.S., 2008, Characteristics of tectonic deformation within transitional belt between the Junggar Basin and teh northern Tian Shan Mountain: Oil&Gas geology, v. 29, 252-282.

R

Reigber, C., Michel, G.W., Galas, R., Angermann, D., Klotz, J., Chen, J.Y., Papschev, A.,Arslanov, R., Tzurkov, V.E., and Ishanov, M.C., 2001, New space geodetic constraints on the distribution of deformation in Central Asia: Earth and Planetary Science Letters, v. 191, 157-165.

Rich, J.L., 1943, Mechanics of low-angle overthrust faulting as illustrated by Cumberland thrust block, Virginia: American Association of Petroleum Geologists Bulletin, v. 118, 1584-1596.

Roure, F., Chouckroune, P., Berastegui, X., Muñoz, J.A., Villien, A., Matheron, P., Bareyt, M., Seguret, M., Camara, P. and Deramond, J., 1989, ECORS deep sismic data and

balanced cross sections: geometric constraints on the evolutio of the Pyrenees: Tectonics, v. 8, 41-50.

Rowley, D.B., 1996, Age of initiation of collision between India and Asia: A review of stratigraphic data: Earth and Planetary Science Letters, v. 145, 1-13.

Rowley, D.B., 1998, Minimum age of initiation of collision between India and Asia north of Everest based on the subsidence history of the Zhepure Mountain section: J. Geol. v. 106, 229–235.

S

Schuchert, C., 1925, Significance of taconic orogeny: GSA Bulletin, v. 36, 343-350.

Sébrier, M., Siame, L., Zouine, M., Winter, T., Missenard, Y., Leturmy, P., 2006, Active tectonics in the Moroccan High Atlas: Comptes Rendus Géoscience, v. 338, 65–79.

Sengör, A.M.C., 1991, Plate tectonics and orogenic research after 25 years: Synopsis of a Tethyan perspective: Tectonophysics, v. 187, 315-330, 337-344.

Sengör,, A.M.C., Natalin, B.A., and Burtman, V.S., 1993, Evolution of the Altaid Tectonic Collage and Paleozoic Crustal Growth in Eurasia: Nature, v. 364, 299-307.

Sengör,, A.M.C., and Natal'in, B.A., 1996, Turkic –type orogeny and its role in the making of the continental crust: Annual Review of Earth and Planetary Sciences, v. 24, 263-337.

Shaw, J.H., Connors, C., Suppe, J., 2003, Seismic interpretation of contractional Fault-related folds, An AAPG Seismic Atlas: American Association of Petroleum Geologists Bulletin.

Shu, L., Yu, J., Charvet, J., Laurent-Charvet, S., Sang, H., and Zhang, R., 2004, Geological, geochronological and geochemical features of granulites in the Eastern Tian Shan, NW China: Journal of Asian Earth Sciences, v. 24, 25-41.

Shu, L.S., Deng, X.L., Zhu, W.B., Ma, D.S., and Xiao, W.J., 2010, Precambrian tectonic evolution of the Tarim Block, NW China: new geochronological insights from the Quruqtagh domain: Journal of Asian Earth Sciences, In Press.

Sibuet, J.-C., Srivastava, S.P., and Spakman, W., 2004, Pyrenean orogeny and plate kinematics: J. Geophys. Res., v. 109.

Sobel, E.R., and Dumitru, T.A., 1997, Thrusting and exhumation around the margins of the western Tarim basin during the India-Asia collision: Journal of Geophysical Research-Solid Earth, v. 102, 5043-5063.

Sobel, E.R., Oskin, M., Burbank, D., and Mikolaichuk, A., 2006, Exhumation of basement-cored uplifts: Example of the Kyrgyz Range quantified with apatite fission track thermochronology: Tectonics, v. 25, 70-81.

Specht, M., 1989, Tectonique de chevauchement le long du profil ECORS-Pyrénées: Modèle d'évolution de prisme d'accrétion continental [Ph.D Thesis]: Université de Bretagne occidentale, France, 353 p.

Stearns, D.W., 1964, Macrofracture patterns on Teton anticline N.W. Montana (abstract) (Eos): Transactions of the American Geophysical Union, v. 45, 107.

Stewart, K.G. and Alvarez, W., 1991, Mobile-hinge kinking in layered rocks and models Journal of Structural Geology, 13, 243-259.

Sun, J., Zhu, R., and Bowler, J., 2004, Timing of the Tian Shan Mountains uplift constrained by magnetostratigraphic analysis of molasse deposits: Earth and Planetary Science Letters, v. 219, 239-253.

Sun, J.M., Xu, Q.H., and Huang, B.C., 2007, Late Cenozoic magnetochronology and paleoenvironmental changes in the northern foreland basin of the Tian Shan Mountains: Journal of Geophysical Research-Solid Earth, v. 112.

Suppe, J., 1983. Geometry and kinematics of fault-bend folding: American journal of science, v. 283: 634-721.

Suppe, J. and Medwedeff, D., 1990, Geometry and kinematics of fault-propagation folding: Eclogae Geologicae Helvetiae, 83: 409-454.

Suppe, J., Connors, C.D. and Zhang, Y.K., 2004, Shear fault-bend folding, In: McClay, K.R., eds, Thrust Tectonics, American Association of Petroleum Geologists, Memoir 82, 303–323.

T

Tapponnier, P., and Molnar, P., 1977, Active Faulting and Tectonics in China: Journal of Geophysical Research, v. 82, 2905-2932.

Tapponnier, P., and Molnar, P., 1979, Active faulting and Cenozoic tectonics of the Tien shan, mongolia, and baykal regions: J. Geophys. Res., v. 84, 3425-3459.

Tapponnier, P., Peltzer, G., Le Dain, A.Y., Armijo, R., and Cobbold, P., 1982, Propagating extrusion tectonics in Asia: New insights from simple experiments with plasticine: Geology, v. 10, 611-616.

Tapponnier, P., Peltzer, G., Armijo, R., 1986, On the mechainics of the collision between

India Asia, In: Coward, M.P., Ries, A.C., eds, Collision Tectionics, Geological Society London Specical Publication, v. 19, 115-157.

Tapponnier, P., Meyer, B., Avouac, J.-P., Peltzer, G., Gaudemer, Y., Guo, S., Xiang, H., Yin, K., Chen, Z., Cai, S., and Dai, H., 1990, Active thrusting and folding in the Qilian Shan, and decoupling between upper crust and mantle in northeastern Tibet: Earth and Planetary Science Letters, v. 97, 387-403.

Tapponnier, P., 2001, Oblique Stepwise Rise and Growth of the Tibet Plateau: Science, v. 294, 1671-1677.

Teixell, A., 1998, Crustal structure and orogenic material budget in the west central Pyrenees: Tectonics, v. 17, 395-406.

Teixell, A., Arboleya, M.-L., Julivert, M., Charroud, M., 2003, Tectonic shortening and topography in the central High Atlas. Tectonics, v. 22, doi:10.1029/2002TC00146.

Tozer, R., Butler, R., Chiappini, M., Corrado, S., Mazzoli, S., and Speranza, F., 2006, Testing thrust tectonic models at mountain fronts: where has the displacement gone? Journal of the Geological Society, v. 163, 1-14.

V, W

Valdiya, K.S., Himalaya: Emergence and evolution, Universities Press Vann, I.R., Graham, R.H., and Hayward, A.B., 1986, The Structure of Mountain Fronts: Journal of Structural Geology, v. 8, 215-227.

Wang, B, Faure M, Cluzel, D., Shu, L.S., Charvet J., Meffre S., Ma Q., 2006, Late Paleozoic tectonic evolution of the northern West Chinese Tian Shan Belt: Geodinamica Acta, v. 19, 227–237.

Wang, B. Chen, Y., Zhan, S., Shu, L.S., Faure, M., Cluzel, D., Charvet, J. and Laurent-Charvet, S., 2007, Primary Carboniferous and Permian paleomagnetic results from the Yili Block (NW China) and their implications on the geodynamic evolution of Chinese Tian Shan Belt: Earth Planet. Sci. Lett., v. 263, 288-308.

Wang, B., Shu, L.S., Cluzel, D., Faure, M., and Charvet, J., 2007, Geochemical constraints on Carboniferous volcanic rocks of the Yili Block (Xinjiang, NW China): Implication for the tectonic evolution of Western Tian Shan: Journal of Asian Earth Sciences, v. 29, 148-159.

Wang, B., Faure, M., Shu, L.S., Cluzel, D., Charvet, J., De Jong, K., and Chen, Y., 2008, Paleozoic tectonic evolution of the Yili Block, western Chinese Tian Shan: Bulletin

De La Société Géologique De France, v. 179, 483-490.

Wang, B.Y., Lang, Z.J., Li, X.D., Qu, X., Li, T., Huang, C., Cui, X., 1994, Comprehensive survey of geological sections in the west Tian Shan of Xinjiang, China: Science Publishing House, Beijing, 202 p.

Wang, C.Y., Yang Z.E., Luo, H. and Mooney, W.D., 2004, Crustal structure of the northern margin of the eastern Tien Shan, China, and its tectonic implications for the 1906 M similar to 7.7 Manas earthquake: Earth and Planetary Science Letters, v. 223, 187-202.

Wang, Q., Zhang, P.Z., Freymueller, J.T., Bilham, R., Larson, K.M., Lai, X., You, X.Z., Niu, Z.J., Wu, J.C., Li, Y.X., Liu, J.N., Yang, Z.Q., and Chen, Q.Z., 2001, Present-day crustal deformation in China constrained by global positioning system measurements: Science, v. 294, 574-577.

Wang, Q. C., Li S. J. and Du z. L., 2009, Differential uplift of the Chinese Tian Shan since the Cretaceous: constraints from sedimentary petrography and apatite fission-track dating: Int. J. Earth Sci., 98, 1341-1363.

Wang, X.W., Wang, X.W., Ma, Y.S., 2005, Analysis of the fold-thrust zone in the southern Junggar Basin, northwestern China: Earth Science Frontiers, 12, 411-421.

Watson, M.P., Hayward, A.B., Parkinson, D.N., and Zhang, Z.M., 1987, Plate tectonic history, basin development and petroleum source rock deposition onshore China: Marine and Petroleum Geology, v. 4, 205-225.

Windley, B.F., Allen, M.B., Zhang, C., Zhao, Z.Y., and Wang, G.R., 1990, Paleozoic Accretion and Cenozoic Redeformation of the Chinese Tien-Shan-Range, Central-Asia: Geology, v. 18, 128-131.

Windley, B.F., Alexeiev, D., Xiao, W.J., Kroner, A., and Badarch, G., 2007, Tectonic models for accretion of the Central Asian Orogenic Belt: Journal of the Geological Society, v. 164, 31-47.

X, Y

XBGMR. (1993). – Regional geology of Xinjiang Uygur autonomy region.– Geological Memoirs, Ser. 1, No. 32, Map Scale 1: 1,500,000, Geological Publishing House, Beijing, 1-841.

Xiao, W.J., Zhang, L.C., Qin, K.Z., Sun, S., and Li, J.L., 2004, Paleozoic accretionary and collisional tectonics of the Eastern Tian Shan (China): Implications for the

continental growth of Central Asia: American Journal of Science, v. 304, 370-395.

Xiao, X.C., Tang, Y.Q., Feng, Y.M., Zhu, B., Li, J., Zhao, M., 1992, The tectonic evolution of North Xinjiang its adjacent regions: Geol. Pub. House, Beijing, 190 p.

Xu, C.M., He, X.S., Wu, X.Z. and Yao, X.Y., 1992, Structure analysis and petroleum exploration prospect of Tostai area in Juggar Basin: Xinjiang Petrol. Geol., v. 13, 197-205.

Xu, Y., Liu, F.T., Liu, J.H., and Chen, H., 2002, Crust and upper mantle structure beneath western China from P wave travel time tomography: Journal of Geophysical Research-Solid Earth, v. 107.

Yang, S.M., Li, J., Wang, Q., 2008, The deformation pattern and fault rate in the Tian Shan Mountains inferred from GPS observations: Science in China D (Earth Sciences). v. 51, 1064-1080.

Yin, A., Nie, S., Craig, P., Harrison, T.M., Ryerson, F.J., Qian, X.L., and Yang, G., 1998, Late Cenozoic tectonic evolution of the southern Chinese Tian Shan: Tectonics, v. 17, 1-27.

Yin, A., and Harrison, T.M., 2000, Geologic Evolution of the Himalayan-Tibetan Orogen: Annual Revue of Earth Planetary Science, v. 28, 211-280.

Yin, A., 2010, Cenozoic tectonic evolution of Asia: A preliminary synthesis: Tectonophysics, v. 488, 293-325.

Yin, A., Nie, S., Craig, P., Harrison, T.M., Ryerson, F.J., Qian, X.L., and Yang, G., 1998, Late Cenozoic tectonic evolution of the southern Chinese Tian Shan: Tectonics, v.17, 1-27.

Z

Zhang, Z.C., Guo, Z. J., Wu, C.D., Fang, S.H., 2007, Thermal history of the Jurassic strata in the Northern Tian Shan and its geological significance, revealed by apatite fission-track and vitrinite-relfectance analysis: Acta Petrologica Sinica, v. 23, 1683-1695.

Zhao, J.M., Liu, G.D., Lu, Z.X., Zhang, X.K., and Zhao, G.Z., 2003, Lithospheric structure and dynamic processes of the Tian Shan orogenic belt and the Junggar basin: Tectonophysics, v. 376, 199-239.

Zhou, D., 1997, Studies in the tectonics of China: Extensional tectonics of the northern margin of the South China Sea; amalgamation and uplift of the Tian Shan; and wedge

extrusion model for the Altyn Tagh fault [Ph.D. thesis]: Stanford, California, Stanford University.

Zhu, B., Kidd, W.S.F., Rowley, D.B., Currie, B.S., Shafique, N., 2005, Age of initiation of the India–Asia collision in the east-central Himalaya: J. Geol., v. 113, 265–285.

Appendixes

Appendix 1. Interpretation of seismic data

The seismic method is by far the most important geophysical technique in terms of expenditures and number of geophysicists involved. Its predominance is due to high accuracy, high resolution, and great penetration (Telford et al., 1990). The basic technique of seismic exploration consists of generating seismic waves and measuring the time required for the waves to travel from the sources to a series of geophones, usually disposed along a straight line directed toward the source. From a knowledge of traveltimes and the velocity of the waves, one attempts to reconstruct the paths of the seismic waves. Structural information is derived principally from paths that fall into two main categories: headwave (refracted) paths, in which the principal portion of the path is along the interface between two rock layers and hence is approximately horizontal, and reflected paths, in which the wave travels downward initially and at some point is reflected back to the surface, the overall path being essentially vertical (Figure A-1). For the both types of path, the traveltimes depend on the physical properties of the rocks and the altitudes of the beds. The goal of seismic exploration is to deduce information about the rocks, especially about the attitudes of the beds, from the observed arrival times and from variation in amplitude, frequency, phase, and wave shape. In this thesis, we focus on the seismic reflection.

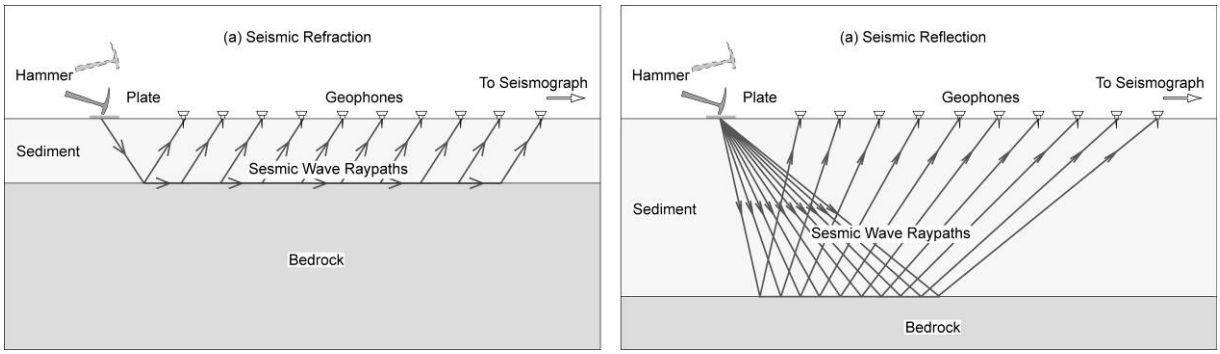

Figure A-1. *Seismic refraction model, (b) seismic reflection model (Modified from USGS website).*

Seismic methods are widespread used in variety domains. The mainly goal is exploring for petroleum: the locations for exploratory wells rarely are made without seismic information. Seismic methods are also important in orogenic structures study, such as ECORS (Etude Continentale et Océanique par Réflexion et réfraction Sismiques) in Pyrenees (Roure et al., 1989; ECORS Pyrenees Team, 1988), ECORS-CROP in the Alps (Bayer et al., 1987; Schmid and Kissling, 2000) and COCORP profile in Rocky Mountains (Allmendinger, et al., 1982; Brewer et al., 1982). Seismic profiles are widespread used in foreland fold-and-thrust belt (e.g.

Bally et al., 1966; Tozer et al., 2006; McClelland and Oldow, 2004).

The original profiles are come from some Chinese petrol companies. In this study, we concentrate in the interpretation of seismic profiles. About 200 drilled well are come from some source. These seismic profiles were well treated by commercial processes, such as stack, migration and noise attenuation. They present the two-way travel reflection times in y-axis. So it has to translate the two-way time to depth.

Local stacking velocities derived from the reflection survey are used for the conversion of seismic wave travel times into depths. Moreover it provides an indication of the lithology of a rock or, in some cases, the nature of the pore fluids contained within it. Several methods are used for the conversion of the time sections to depth.

Firstly, it could be treated in Adobe software Photoshop with another plugin, namely seismic plugin by Jay Lieske (1998). It is software that works within Photoshop 5 or 6 to depth-correction and unfold scanned seismic reflection profiles. One channel in photoshop of filled gray presents the velocity of a seismic profile. The values in the gray channel must be in the range of a byte, 0…255. The values in the channel could associate with real velocities by arbitrary factor. For example, if we choose a pixel value of 40 to represent the seismic velocity of air (2000 m/s one-way) then pixels with a value of 50 represent 2500 m/s, 100 represent 5000 m/s, etc. Finally, the original image will be pushed off or up by rubbersheeting each column according to the velocity model channel.

Secondly, original seismic profile could be converted to depth by “DIY” computer programmers. For example, Matlab could be easily used for bitmap treating. Every pixel is calculated and relocated to their real vertical depth according to velocities. All the pixels locate in their really depth in the seismic profile (Shengli Wang, personal communication).

Finally, time profiles are converted to depth by the first methods when they are with simpler velocities structure. In contrast, some profiles are complex to describe by different velocities by blocks, which are treated by the second methods.

References

Telford, W.L., Geldart, L.P. and Sheriff, R.E. (1990), Applied geophysics, 2nd ed: Cambridge university press, 790 p.

Allmendinger, R.W., Brewer, J.A., Brown, L.D., Kaufman, S., Oliver, J.E., and Houston, R.S., 1982, COCORP profiling across the Rocky Mountain Front in southern Wyoming, Part 2:

Precambrian basement structure and its influence on Laramide deformation: Geological Society of America Bulletin, v. 93, 1253-1263.

Bally, A.W., Gordy, P.L., and Stewart, G.A., 1966, Structure, seismic data, and orogenic evolution of southern Canadian Rocky Mountains: Bulletin of Canadian Petroleum Geology, v. 14, 337-381.

Bayer, R., et al., Group of the Alpes ECORS-CROP Profil, 1987, Premièrs résultats de la traversée des Alpes occidentales par sismique reflexion verticale (Programme ECORS-CROP). C.R. Ac. Sc. Paris. t.305, sII, 1461-1570.

BREWER, J.A., ALLMENDINGER, R.W., BROWN, L.D., OLIVER, J.E., and KAUFMAN, S., 1982, COCORP profiling across the Rocky Mountain Front in southern Wyoming, Part 1: Laramide structure: Geological Society of America Bulletin, v. 93, 1242-1252.

ECORS Pyrenees Team, 1988, The ECORS deep reflection seismic survey across the Pyrenees: Nature, v. 331, 508-511.

Liu, B.J., Shen, J., Zhang, X.K., Chen, Y., Fang, S.M., Song, H.P., Feng, S.Y., Zhao, C.B., 2007, The crust structures and tectonics of Ürumqi depression revealed by deep seismic reflection profile in the northern margin of Tian Shan mountains, Chinese J. Geophys., v. 50, 1464～1472.

McClelland, W.C., and Oldow, J.S., 2004, Displacement transfer between thick- and thin-skinned décollement systems in the central North American Cordillera: Geological Society, London, Special Publications, v. 227, 177-195.

Roure, F., Choukroune, P., Berastegui, X., Munoz, J.A., Villien, A., Matheron, P., Bareyt, M., Seguret, M., Camara, P., and Deramond, J., 1989, Ecors deep seismic data and balanced cross sections: Geometric constraints on the evolution of the Pyrenees: Tectonics, v. 8, 41-50.

Schmid, S.M., and Kissling, E., 2000, The arc of the western Alps in the light of geophysical data on deep crustal structure: Tectonics, v. 19, 62-85.

Tozer, R., Butler, R., Chiappini, M., Corrado, S., Mazzoli, S., and Speranza, F., 2006, Testing thrust tectonic models at mountain fronts: where has the displacement gone? Journal of the Geological Society, v. 163, 1-14.

Appendix 2. Methodology of gravity data

2.1 Basic theory

The basis of the gravity survey method is Newton's Law of Gravitaion, which states that the force of attraction F between two masses $m_1 m_1$ and $m_2\, m_2$, whose dimensions are small with respect to the distance γ between them, is given by

$$F = \frac{G m_1 m_2}{\gamma^2}$$

where G is the Gravitational Constant

(6.676.67 × $10^{-11} m^3 kg^{-1} s^{-2}$6.67 × $10^{-11} m^3 kg^{-1} s^{-2}$).

Consider the gravitational attraction of a spherical, non-rotating, homogeneous Earth of mass M and radius R on a small mass m on its surface. It can be simply considered that the mass of a sphere acts as though it were concentrated at the centre of the sphere and by substitution in the last equation:

$$F = \frac{GM}{R^2} m = mg$$

Force is related to mass by acceleration and the term $g = GM/R^2 g = GM/R^2$ is known as the gravitational acceleration, namely gravity. The weight of the mass is given by mg.

On the Earth, gravity should be constant. However, the Earth's ellipsoidal shape, rotation, irregular surface relief and internal mass distribution cause gravity to vary over its surface.

The gravitational field is most usefully defined in terms of the Gravitational potential U:

$$U = \frac{GM}{r}$$

Whereas the gravitational acceleration g is a vector quantity, having both magnitude and direction, the gravitational potential U in any direction gives the component of gravity in that direction. The sea-level surface, or geoid, is the most easily recognized equipotential surface, which is everywhere horizontal, that is, at right angles to the direction of gravity. The shape of the Earth, determined by geodetic measurements and satellite tracking, is nearly spheroidal,

bulging at the equator and flattened at the poles. The term "reference spheroid" is an oblate ellipsoid that approximates the mean sea-level surface (geoid), with the land above it removed. This theoretical model was described by the International Union of Geodesy and Geophysics with a formula in 1930.

$$g_t = 978{,}049(1 + 0.005{,}2884 \sin^2 \emptyset - 0.000{,}005{,}9 \sin^2 2\emptyset$$

This formula has been superseded by the Geodetic Reference System 1967 (GRS67).

$$g_t = 978{,}031.846(1 + 0.005{,}278{,}895 \sin^2 \emptyset + 0.000{,}023{,}462 \sin^4 \emptyset) mGal$$

where $\emptyset$ is latitude.

Because of the excess mass in depth, the geoid and reference spherioid do not coincide and the local mass anomalies warp the geoid (Figure A-2a). The geoid is expedted to be warped upward under the continents because of attracting material above and downward over the ocean basins because of the low density of water (Figure A-2b). The deviation between the two surfaces is as much as 100m.

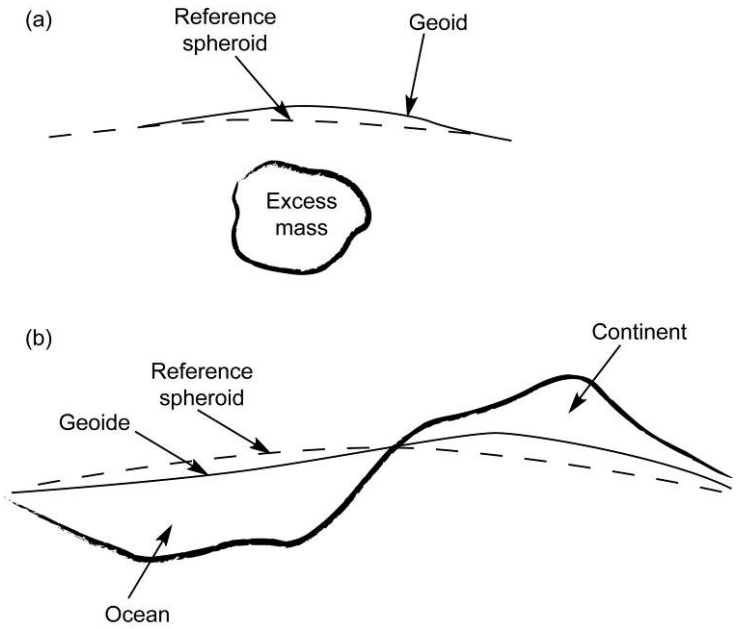

Figure A-2. *Reference spheroid and geoid. (a) Local excess mass warpe the geoid. (b) Continent and Ocean warp the geoid.*

2.2 Gravity anomalies of simple-structures

The gravitational attraction of a point mass m at a distance r from the mass and the

gravitational attraction Δg_r in the direction of the mass is given by $\Delta g_r = Gm/r^2$ from Newton's Law. The gravity anomaly Δg caused by the mass is $\Delta g_r = Gmcos\theta/r^2$ (Figure A-3).

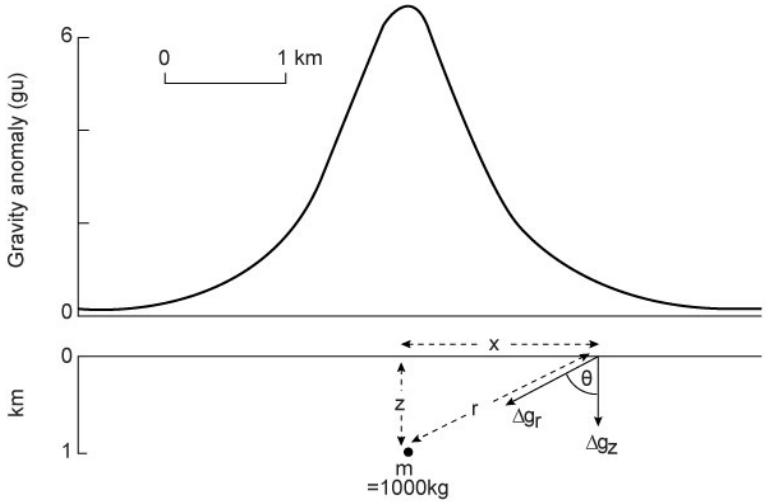

Figure A-3. *The gravity anomaly of a point mass or sphere.*

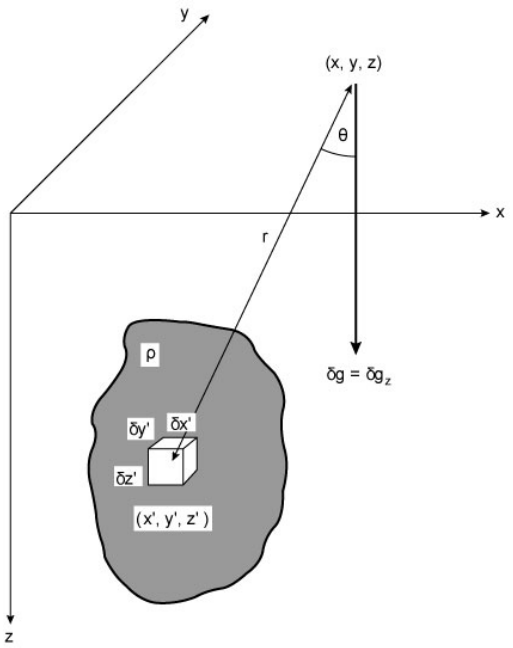

Figure A-4. *The gravity anomaly of an irregular shape.*

In general, the gravity anomaly of a body of any shape can be determined by summing the attractions of all the mass elements which make up the body (Figure A-4). Considering a small prismatic element of such a body of density ρ, the anomaly of whole body Δg is then found by summing all such elements which make up the body, then

$$\Delta g = \int\int\int G\rho \frac{(z'-z)}{r^3} dx'dy'dz'$$

Where $r = \sqrt{(x'-x)^2 + (y'-y)^2 + (z'-z)^2}$

Some forward models are presented here. For example, 1 km square with 0.07 gm/cc more in density could cause a 0.09 mGal anomaly in surface. The anomaly curve shows a symmetric curve below the denser mass. The anomaly increases when the square moves upward and decreases when it moves downward (Figure A-5).

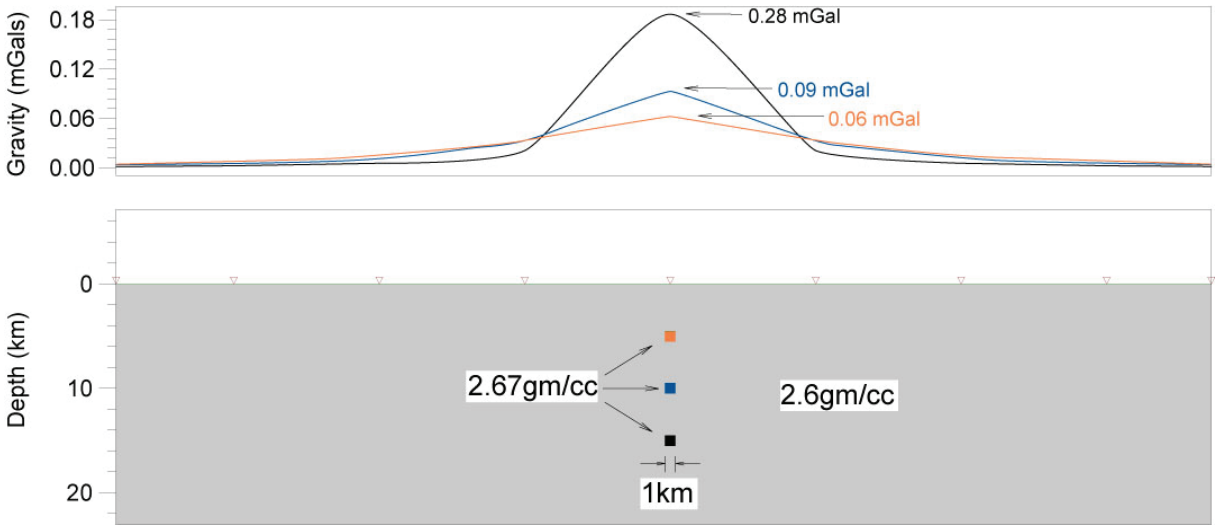

Figure A-5. *The gravity anomaly of an square with 1 km and 0.07 gm/cc density contrast.*

A fault could also cause the gravity anomaly in surface. For example, a fault reverse with one layer denser could cause a rotationally symmetric curve (Figure A-6). The lighter layer in this section also results in a similar model profile.

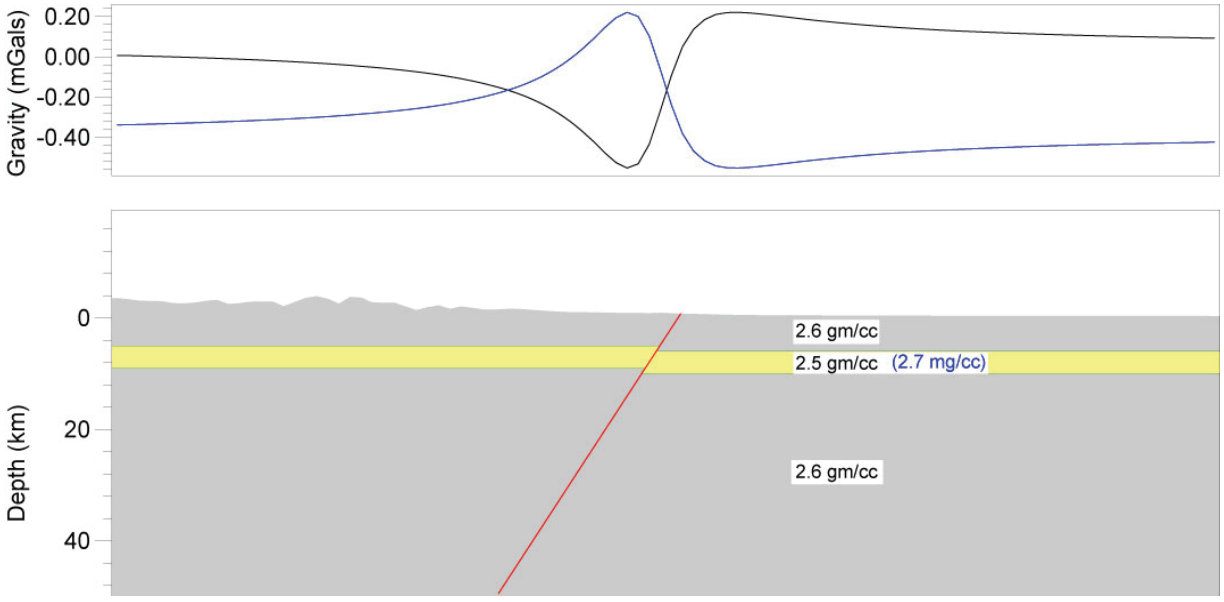

Figure A-6. *The gravity anomaly of a reserve fault, which cut off a less or more 0.1 gm/cc in density.*

The folds could be identified by the profile of the gravity anomaly. For example, a detachement fold with 0.1 mg/cc lighter in density and with 4 km wave length cause 1 mGal anomaly (Figure A-7).

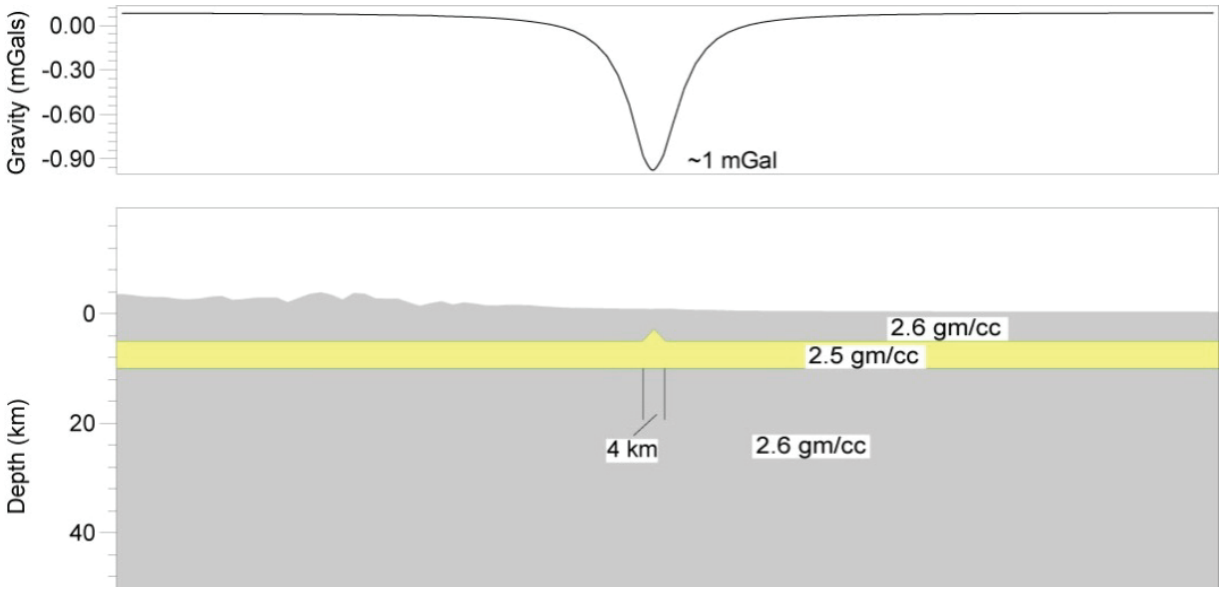

Figure A-7. *The gravity anomaly of a detachment fold, which cut off a less or more 0.1 gm/cc in density.*

Finally, the forward simple model of a foreland basin is constructed. We assume that the density of the basement it 2.6 gm/cc and the basin sediments is 2.4 gm/cc. The profile of the anomaly is controlled by the contract of the basin and basement. The anomaly increase to the mountain direction but decreased when the thickness of the basin increase (Figure A-8).

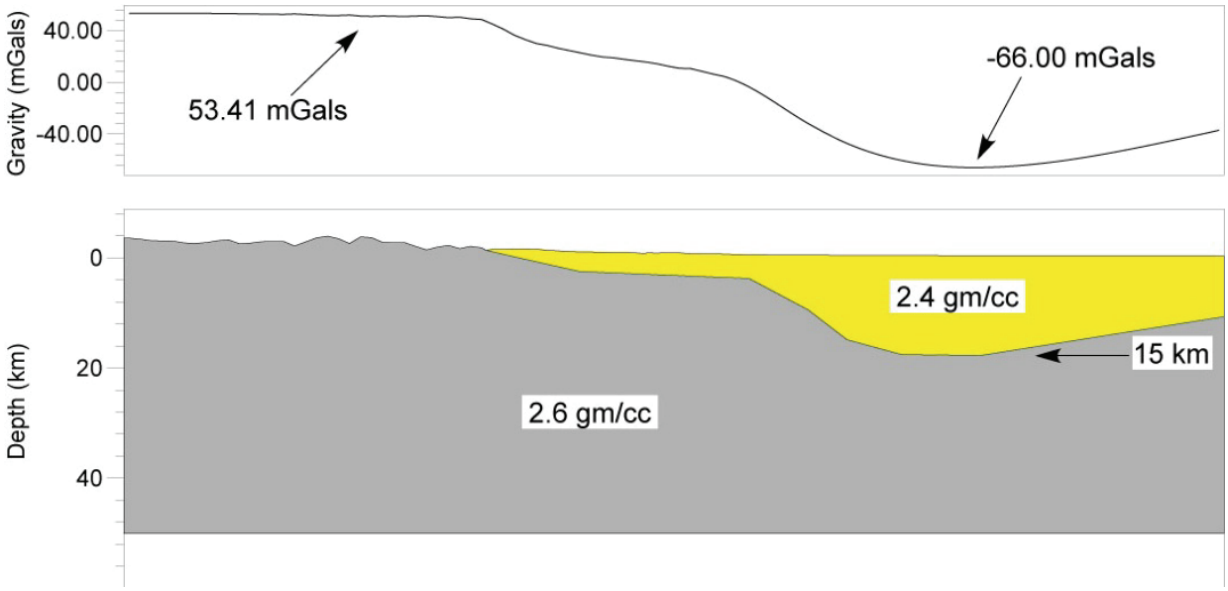

Figure A-8. *The gravity anomaly of a foreland basin (2.4 gm/cc) and a mountain basement.*

2.3 Density analysis

Gravity anomalies result from the difference in density, or density contrast, between a body of rock and its surroundings. The sign of the density contrast determines the sign of the gravity anomaly. Most common rock types have densities range from 1.60 and 3.20 Mgm^{-3}. The density of a rock is dependent on both its mineral composition and porosity.

Several methods are used to determine the densities in the northern piedmont of Tian Shan. The direct measurements on rock samples is the common way, which is usually necessary to measure several tens of samples of each particular rock type in order to obtain a reliable mean density and variance. Moreover there are some indirect methods, providing a mean density of a particular rock unit which may be internally quite variable. They are measured in boreholes, Nettleton's method of density determination, and also by the P-wave velocities of rocks.

We carried out the direct measurement by electronic balance (

Figure **A-9**). The rocky samples are dried in a baker during 12 hours. They are then weighted on the balance and obtain the value in air g_{dry}. After that, they are weighted in water g_{w1}. They are placed in a dry plate about 30 minutes and weighted wet on the balance g_{wet} then weighted in water g_{w2}. Finally, two type of the densities can be calculated, the dry and the wet.

$$Density\ dry = g_{dry}/(g_{dry} - g_{w1})$$

$$Density\ dry = g_{dry}/(g_{dry} - g_{w1})$$

However, the Cenzoic are the sandstone and mudstone without well compression. They would dissolve in water. We measured their volumes in a measuring cup and the density will be:

$$Density\ dry = g_{dry}/V$$

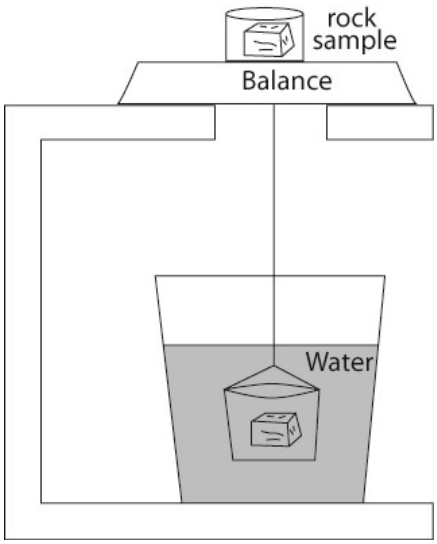

Figure A-9. *Cartoon shows the direct measurement of rock densities with.*

Nettleton's method of density determination involves taking gravity observations over a small isolated topographic prominence. Field data are reduced using a series of different densities for the Bouguer and terrain corrections (Figure A-10).The density value that yields a Bouguer anomaly with the least correlation (positive or negative) with the topography is taken to represent the density of the prominence. The method is useful in that no borehole or mineshaft is required, and a mean density of the material forming the prominence is provided. A disadvantage of the method is that isolated relief features may be formed of anomalous materials which are not representative of the area in general.

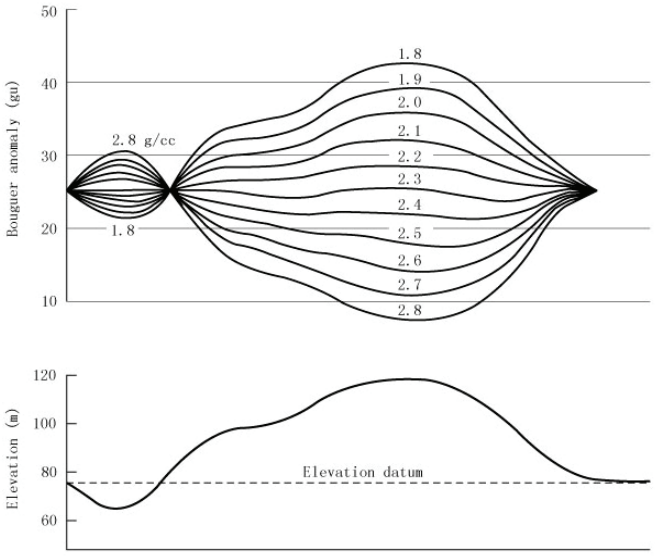

Figure A-10. *Nettleton's method of density determination over an isolated topographic feature.The profile corresponding to a value of 2.3 gm/cc shows least correlation with topography so this density is taken to represent the density of the feature (Kearey et al., 2002).*

Densities are also provided from the P-wave velocities of rocks obtained in seismic surveys. P-wave velocities are related with various rock densities by empirical velocity-density formulas (Gardner et al., 1974; Birch 1960; 1961; Christensen and Fountain 1975; Figure A-11). Nafe and Drake (1963) suggested that velocities estimated from seismic are probably no more accurate than about $\pm 0.10\ g/cc$. However, this is the only method available for the estimation of sensibilities of deeply buried rock units which cannot be sampled.

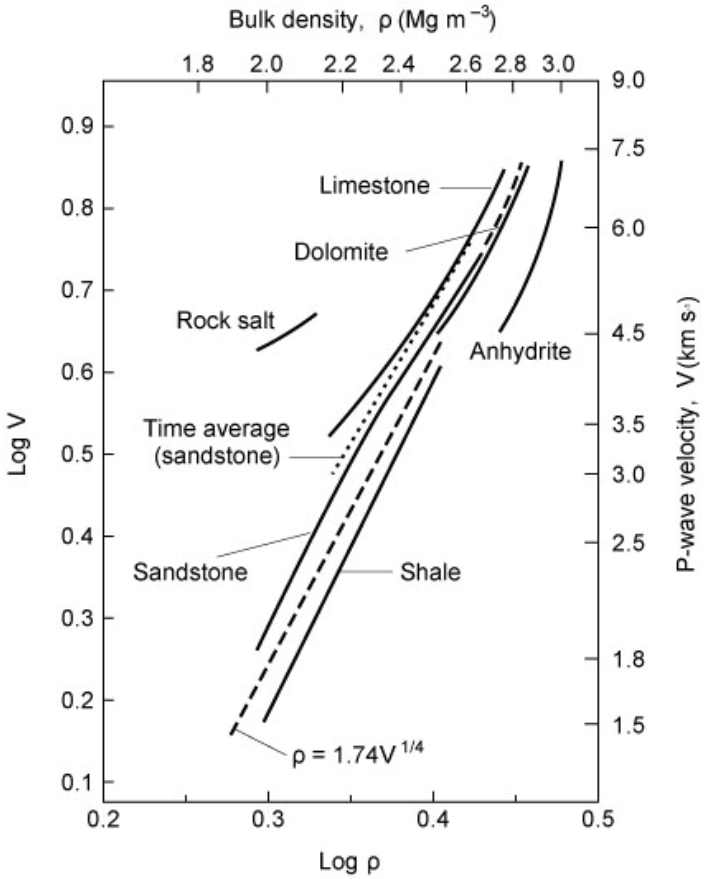

Figure A-11. *Logarithm of P-wave velocity against density for various rock types, show the best-fitting linear relationship between density and log velocity (after Gardner et al., 1974).*

Number	Lithology	Age	W1	W2	W3	W4	W5	W6	**D1**	D2
Cen3a	microconglomates	Cenozoic	0.1652	0.4306	0.4919	0.7569	0.6103	0.4913	**2.24**	1.48
Cen5	marnes silt	Cenozoic	0.165	0.3674	0.4229	0.6251	0.5092	0.3752	**2.35**	2.15
Cen6	marnes silteuses	Cenozoic	0.1652	0.343	0.4814	0.6591	0.5601	0.3636	**2.26**	1.79
Cen7	sandstone carbonate	Cenozoic	0.1651	0.4863	0.5687	0.8892	0.6982	0.4949	**2.48**	2.33
Cen8	sandstone	Cenozoic	0.1652	0.4204	0.4861	0.7457	0.5905	0.4288	**2.44**	2.29
Cen1	Greenish sanstone	Cenozoic	*	0.2812	0.1602	0.2824	0.1631	0.2855	**2.30**	2.29
TS123/K	sandstone	Cretacous	*	0.1627	0.0968	0.1633	0.0988	0.1654	**2.44**	2.44
J3a	marnes	Jurassic	0.1651	0.5551	0.5725	0.9619	0.7249	0.5606	**2.56**	2.47
J4a	marnes	Jurassic	0.1651	0.3475	0.515	0.6973	0.5968	0.3564	**2.23**	2.01
J4b	marnes	Jurassic	0.1651	0.3669	0.4985	0.7002	0.578	0.3703	**2.54**	2.43
J3c(A)	medium sandstone	Jurassic	*	0.4211	0.2491	0.4249	0.2595	0.4348	**2.39**	2.40
J3c(B)	medium sandstone	Jurassic	*	0.4325	0.2565	0.436	0.2673	0.4468	**2.40**	2.40
J4b	red sandstone	Jurassic	*	0.4556	0.2754	0.4567	0.2784	0.4601	**2.51**	2.50
K130	sandstone	Jurassic	*	0.7333	0.451	0.7352	0.4531	0.7372	**2.58**	2.58
K148	sandstone	Jurassic	*	0.5139	0.2969	0.5183	0.3107	0.5319	**2.32**	2.32
T1	Marres	Triassic	0.165	0.5713	0.5849	0.9909	0.7579	0.619	**2.35**	0.01
T2a	conglomerate and gravel	Triassic	*	0.87	0.5277	0.8723	0.5329	0.8774	**2.52**	2.52
T2b	sandstone	Triassic	*	0.6728	0.4076	0.674	0.4107	0.6774	**2.52**	2.52
K146B	Puddingstone	Permian	*	0.6214	0.3744	0.6264	0.3859	0.6363	**2.46**	2.48
P1a	andsite	Permian	*	0.4168	0.2569	0.4174	0.2574	0.4181	**2.59**	2.59
P1c	volcanoclastite	Permian	*	0.2506	0.1561	0.2514	0.1569	0.2522	**2.62**	2.62
P2	red silsite	Permian	*	0.4041	0.2467	0.4049	0.2472	0.4058	**2.55**	2.54
P3	red sandstone	Permian	*	0.5456	0.3381	0.5469	0.3389	0.5477	**2.61**	2.61
K104	sandstone	Permian	*	0.5747	0.3523	0.5762	0.3536	0.5774	**2.56**	2.56
C1a	andésite massive	Carboniferous	*	1.0186	0.6499	1.0193	0.6502	1.0196	**2.75**	2.75
C1b	conglomerate of andsite	Carboniferous	*	0.657	0.4191	0.6578	0.4195	0.6583	**2.75**	2.75
C2	marbre	Carboniferous	*	0.731	0.4585	0.7321	0.4591	0.732	**2.67**	2.67
C3	Andsite	Carboniferous	*	0.5874	0.3644	0.5915	0.374	0.6021	**2.58**	2.57
C4	Andsite	Carboniferous	*	0.9455	0.5827	0.9466	0.583	0.947	**2.59**	2.59
K107	sandstone	Carboniferous	*	0.3388	0.2106	0.3399	0.2116	0.3414	**2.62**	2.60
K82	sandstone	Carboniferous	*	0.8335	0.5222	0.8346	0.5225	0.8355	**2.66**	2.66
K89	limestone	Carboniferous	*	0.6933	0.4264	0.694	0.4268	0.6967	**2.59**	2.56
K168	limestone	Carboniferous	*	0.7469	0.4697	0.7479	0.4699	0.7484	**2.68**	2.68
K137	sandstone	Cretacous	*	0.4069	0.251	0.4076	0.252	0.4084	**2.59**	2.60
K91	limestone	Carboniferous	*	0.5052	0.3052	0.5071	0.3091	0.5117	**2.50**	2.49

Table A-1. *The measurement data of density samples with balance.*

In this study, absolute densities are measured directly by electronic balance. Two methods are used to two types of samples: the incompact and the solid. For the first one, six values are obtained, weight of cup dry (W1), weight of samples dry with cup dry (W2), weight of cup and water (W3), weight of samples , cup and water (W4), weight of more water without sample (W5) and weight of samples wet, cup and water (W6).

D1=(W2-W1)/(W5-W3); D2=(W2-W1)/[W5-W3+(W6-W2)].

Secondly, for the solid sample, also six values are obtained without W1 in the Table A-1. They are weight of dry sample (W2), weight of sample in water (W3), weight of wet sample (W4), weight of wet sample in water (W5) and weight of wet sample after previous step (W6).

D1=W2/(W4-W3); D2= W2/(W6-W5).

Two results of density are calculated and compared to verify the effect of the porosity in measurement (D2). D1 is the original density result.

P-wave velocities are also used for determining rock densities (Table A-2). It is based on the formula:

$\rho(gm/cc) = 0.31V_p^{0.25}$ (from Gardner et al., 1974).

	seismic velocity	Density(gm/cc)
Q24	2500	2
Q1x	3600	2.4
N2d	3400	2.37
N1t	3500	2.38
N1s	3700	2.42
E23a	3150	2.32
E12z	4100	2.48
K2d	4750	2.57
K1tg	4230	2.5
J3	4300	2.51
J2	4300	2.51
J1	4500	2.54
T	4600	2.55
Basement	5000	2.61

Table A-2. *Densities of every formation obtained from Seismic P-velocities.*

The density of the northern Tian Shan has been studied in previous studies (В·И· Tchaikov, 1951; Li et al., 1958; Gao et al., 1958; Jiang et al., 1983; Zuo et al., 1999, Figure A-12). Those results were obtained by a great deal of measurements and they correspond to our measurement and velocity results.

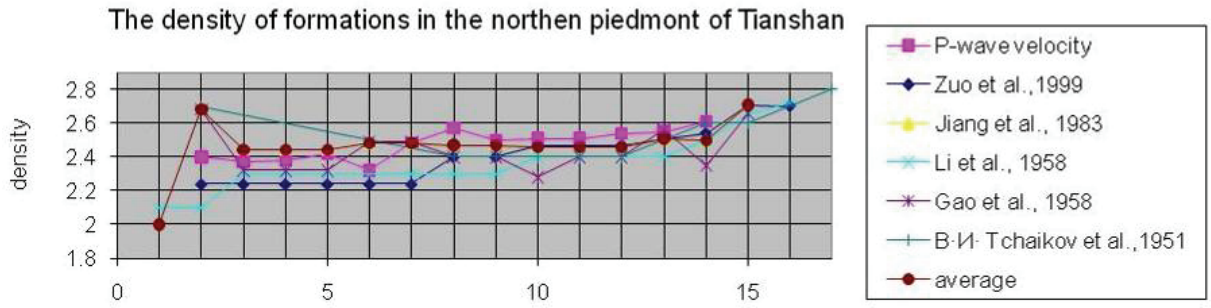

Figure A-12. *Density distribution from different resoures. 1 to 15 indicate Quaternary (1), Xiyu Fm. (2), Dushanzi Fm. (3) , Taxi He Fm. (4), Shawan Fm. (5), Anjihai Fm. (6), Ziniquanzi Fm. (7), Dongou Fm. (8), Tugulu Fm. (9), Upper Jurassic (10), Middle Jurassic (11), Lower Jurassic (12), Triassic (13), Permian (14), Carboniferous (15), Devonian (16) and crystal basement.*

Finally, the densities which are implied to gravity models are showed following (Table A-3). They are much simpler than really formation variation in density but show the characters of density variation in the southern Junggar area.

	Basement	Triassic	Jurassic	Cretaceous	Tertiary	Xiyu Fm.	Quternary
Densities (gm/cc)	2.6	2.55	2.5	2.45	2.4	2.5	2.0

Table A-3. *The densities of southern Junggar basin used for the following gravity modeling.*

2.4 Gravity measurement

2.4.1 Field measurements

The measurement is carried out by SCINTREX CG-5 (Figure A-13), the reading error is about 1 μGal. The error of 100 m in longitude or latitude could result in an error of 0.1 mGal in maximum. In contrast, the altitude variation is important to the gravity study, an error of 30 cm could cause the same error value.

Figure A-13. *Gravimeter of Scintrex CG-5.*

ProMark 3 RTK, a Post-processing differential GPS of Magellan®, has less than 10 cm in error with full of signal. It worked with a base fixed and the rover on the point to be surveyed (Figure A-14).

Before interpretation of the gravity data, all variations in the Earth's gravitational field which do not result from the differences of density in the underlying rocks are corrected, such as latitude correction, elevations correction and Tidal correction (details see Joly 2005; Kearey et al., 2002).

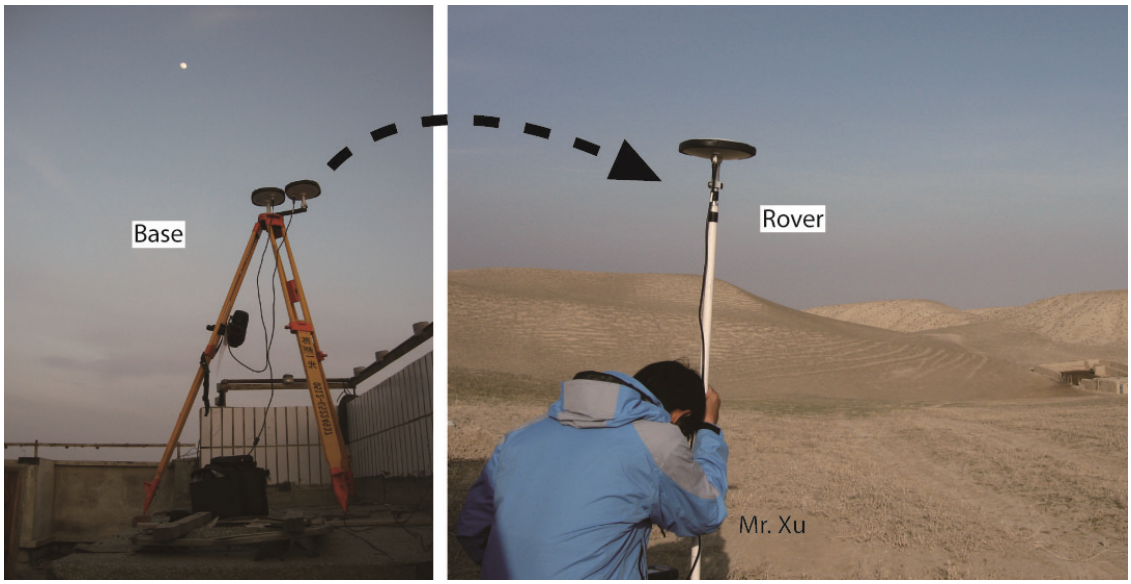

Figure A-14. *Post-Processing Surveying of GPS Promark 3 RTK.*

2.4.2 Crust-scale structure.

The crust-scale structure of Tian Shan has been studied by several methods, such as seismic topographic image (Xu et al., 2002; Li et al., 2009) or by deep seismic sounding (Lu et al., 2000; Wang et al., 2004; Zhao et al., 2003). Results show that the depth of Mono present a shift of 10 km from the Junggar basin to the Mountain area. In this study, these results are used to constrain the deep Moho surface, which have regional effect in gravity measurement.

In western part of the Mountain, the geometry of Moho is based on the deep seismic sounding result of Lu et al.(2000). This profile traversed Tian Shan along the Dushanzi and Kuitun road. It shows that Moho is offset by 10 km in the northern Tian Shan region, 62 km deep in the south while 52 km deep in the Moho beaneath the Tian Shan Mountain (Figure A-15). Following 2D forward models include the structure in depth. The upper mantle is 3.3 gm/cc, while 3.0 gm/cc in the lower crust. This deep profile is parallel to the Wusu section, Kuitun section and Jingouhe section.

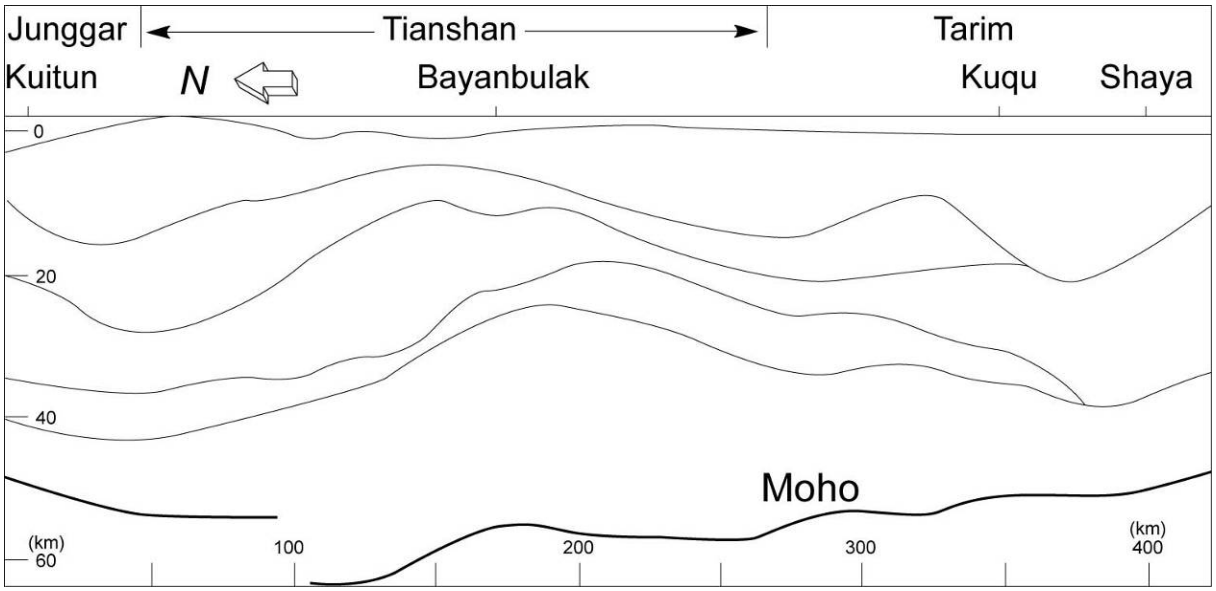

Figure A-15. S*chematic crustal structure along the Kuitun-Shaya profile in the Tian Shan area. The overstriking line indicates the Moho (after Lu et al., 2000).*

In the eastern part, the deep seismic reflection profile in the front of Tian Shan was published (Wang et al., 2004). This profile is along the Manasi He, about 20 km to the Qingshui He (Figure A-16). The offset of the Moho in the basin along this section is different with the Kuitun profile.

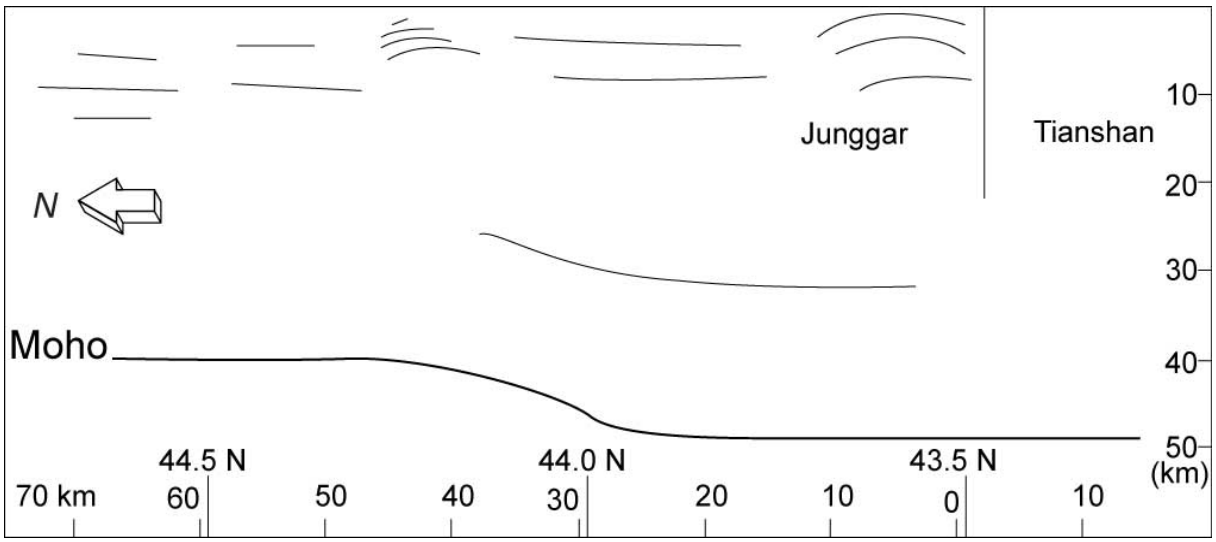

Figure A-16. *Sketch of the crustal structure in the northeastern Tian Shan margin along Manasi He (after Wang et al., 2004).*

References

В·И· Tchaikov, 1951, The southern margin of Junggar, 1951 gravity report.

Gao, X. and Xue, Y.X., 1958, Report of gravity and magnetic survey of Junggar basin

(Xiazijie-Manasi central profile).

Jiang, Y.D. et al., 1983, Bouguer anomaly map of Xinjiang (1/200,000,000).

Joly A., 2007, Relationships between plutons and lithospheric discontinuities, A multidisciplinary study of granitic plutons emplacement along the Sillon Houiller Fault (French Massif Central). contribution from structural, gravity, magnetics and AMS data for 3D modelings [PhD Thesis]: Université d'Orléans, Orléans, 307 p.

Kearey P., Brooks, M. and Hill Ian, An introduction to geophysical exploration, Third edition, 2002, Blackwell Science.

Li, Y.Z. et al, 1958, Report of Junngar gravity and magnetic reseach.

Nafe, J.E. and Drake, C.L., 1963, Physical properties of marine sediments. In: Hill,M.N. (ed.), The Sea,Vol. 3. Interscience Publishers, New York, 794–815.

Zuo, L.P., Li, T. and Tian, S.M., 1999, Superficial veiws on the ancient basement problem in Zhunger Basin: Geophysical prospecting for petroleum, v. 38, 112-117.

Appendix 3. Methods of 3D modeling

Traditionally in geology, both stratigraphic and structural analyses have been carried out in one or two dimensions. 3D geological models are usually achieved integrating surface, wells and seismic data. Due to the difficulty of collecting these data, reliable 3D models are generally realized by oil companies for exploration or production and by engineering companies for major infrastructural works, such as dams and tunnels. 3D models can improve, at different scale, our capability of understanding the geometry of complex geological settings: they also permit to compute volumes and parameterize geological data for further applications.

Recently, the 3D approach to geology has been applied to field data with interesting results following different work flows (Berra et al., 2008; Bistacchi et al., 2008; De Donatis, 2001; Dhont et al., 2005; Fernandez et al., 2004; Joly et al., 2008; Martelet et al., 2004; Tonini et al., 2008; Zanchi et al., 2009). Several commercial software were developed for 3D geological modeling. For example, Gocad (Geological Object Computer Aided Design) of CRPG; 3D Move by Midland Valley Exploration; Geomodeller by BRGM; Earthversion by Dynamic Graphics, Inc. and so on. Most of them are based on the interpolation in every point to construct boundary surfaces then in 3D volumes. In this chapiter, 3D modeling procedure is focused on work with 3D GeoModeller and Gocad.

The 3D Geomodeller is a software that take into account the limited shape and topology geological objects. This tool construct geological 3D model by complex implicit functions. To do this, it combines not only the available structural data on interfaces, but also data in depth (e.g., drilled wells, sections of geophysics). The algorithm is based on the interpolation of a scalar field defined in the space, the gradient in which is orthogonal to the orientations. The modeled interfaces are shows as isovalues of the interpolated field (Lajaunie et al., 1997). Geological body geometry is described by discretising reference isovalues. Faults are modelled by the same method of inserting discontinuities in the potential field(Calcagno et al., 2008).

Geostatistical methods

Geostastic method of Kriging allows estimating a field knowing spot values of a field by isovalues of potential-field. There are spatial correlations between a field and its derivatives.

So interfaces are finally represented as isolines in two dimension or isosurfaces in three dimensions by interpolation (Figure A-17).

Cubic covariance function of the potential field is used in this software. In practice, date is defined by varies methods as followings. An orientation is translated into three partial. Data polarity can complete the gradient of the potential field. If two points belong to the same interface, it indicates that the value of potential filed between these two points is zero.

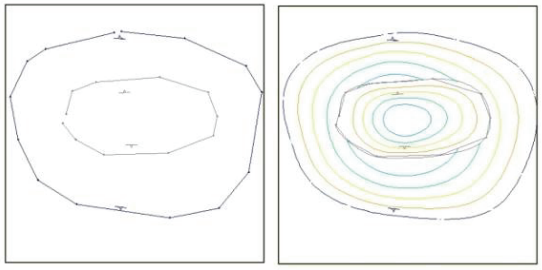

Figure A-17. *Principle of the potential-field interpolation method (in 2D). (a) An anticline mapped by two formations outlines and their dip measurements. (b) The geological formation modelled by the potential-field method.*

Faults are presented with a spatial function discontinuous in the system for cokriging, as a function of drift. Its value is 1 in one side of the fault and decrease to 0 on the other side depending on the distance to the fault and the distance along the fault. For example, if a translation is rigid, the function would be zero for one side and one for other side. Otherwise, if it is wished to model a gradual deformed fault, the function depends on its distance from the edge and along the fault (Figure A-18).

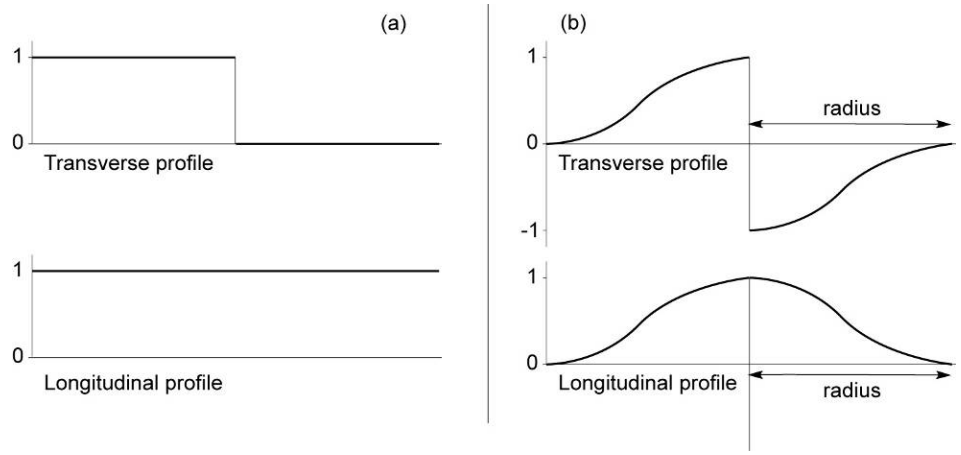

Figure A-18. *Graphical profiles of the drift function took into the cokriging equations to model the effect of offsets to geological formations across faults. (a) Infinite fault. The drift function is 1 on one side of the fault and 0 on the other side (transverse profile). The longitudinal profile shows that the fault is infinite. (b) Finite fault. The domain of fault was*

influenced in an ellipsoid. The drift function varies from 1 or −1 to 0 when moving away from the fault (transverse profile). Along the fault, the drift function decreases from the centre to the fault limits (longitudinal profile).

In real cases, it is rare that the interfaces are parallel or subparallel within a study area. It must interpolate these separately interfaces or groups of interfaces. It is reduced to interpolate as many potential fields there are distinct groups of interfaces intersecting. For example, modeling structures complexes such as folds or granitic intrusions, which can be modeled by surface elevation of the type z = f (x, y), n is only possible by the introduction of polarity on orientation data. We then define a series as a set of layers (formations) concordant and one uses a potential field series.

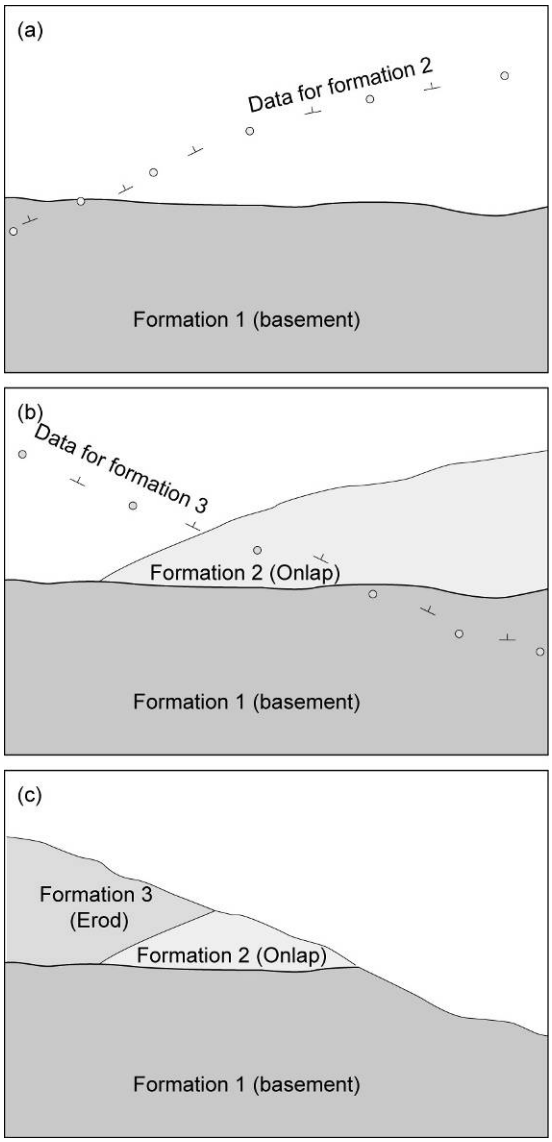

It remains to impose the rules specific to geology to determine the relationship between series and thereby solving the problems of contact between them. There are two rules: erosion (Erode) and deposit (onlap). Such rules can solve all situations encountered. The formations of a series of type onlap will only be deposited in the space left by the previous series. The formations of a series of type Erode will both erode existing series and settle. Erode combines two events: a sequence of erosion then a phase of deposition (Figure A-19)

Figure A-19. *(a) Formation 1 (basement) and potential field of Formation 2. (b) Interpolated Formation 2 by an Onlap relation and data for potential field of formation 3. (c) Interpolated formation 3 by an Erode relation.*

As reliable sections constructed in the southern Junggar basin, 3D modeling could be built in the the software of Geomodeller (BRGM). 3D modeling in the foreland basin could used to calculated the sediments volumes during different periods and show the variation

sedimentary and structural variations along the Tian Shan front. So far the 3D modeling is primary constructed along the Jingou He (Figure A-20). As more reginal sections to be built in the future, the whole fold-and-thrust belt in the foreland could be present in three dimension.

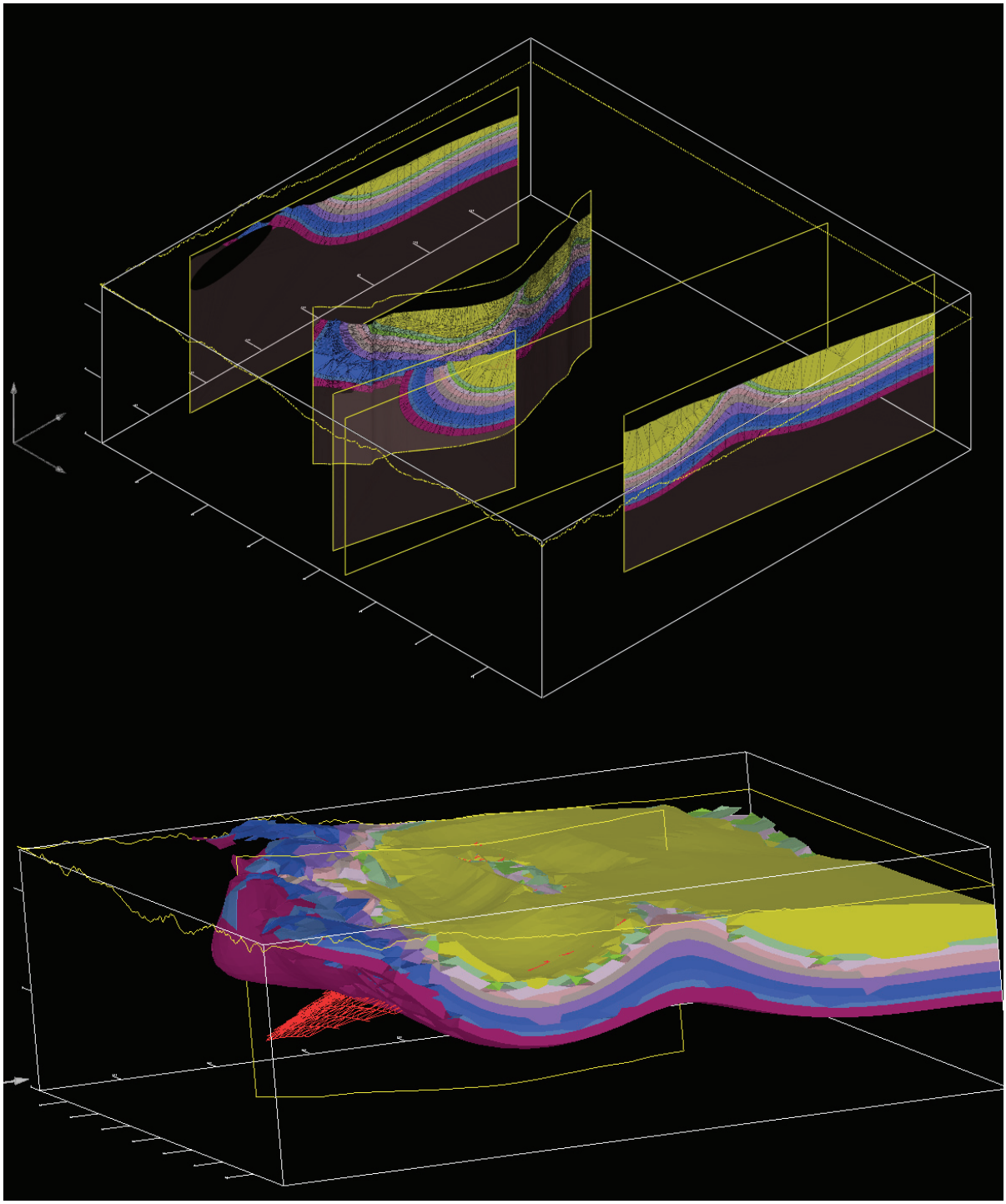

Figure A-20. *The 3D model in the southern Junggar basin, integrated by three north-south trending sections.*

References

Berra, F., Salvi, F., Zanchi, A., Avaro, A., Bonavera, M., and Sterlacchini, S., 2008, 3D reconstruction from surface data in complex geological settings: the example of a thrust stack in the Mesozoic cover of the Southern Alps (Italy): Geoinformatica, 1-15.

Bistacchi, A., Massironi, M., Dal Piaz, G.V., Dal Piaz, G., Monopoli, B., Schiavo, A., and Toffolon, G., 2008, 3D fold and fault reconstruction with an uncertainty model: An example from an Alpine tunnel case study: Computers & Geosciences, v. 34, 351-372.

De Donatis, M., 2001, Three-Dimensional Visualization of the Neogene Structures of an External Sector of the Northern Apennines, Italy: AAPG Bulletin, v. 85, 419-431.

Dhont, D., Luxey, P., and Chorowicz, J., 2005, 3-D modeling of geologic maps from surface data: AAPG Bulletin, v. 89, 1465-1474.

Fernandez, O., Munoz, J.A., Arbues, P., Falivene, O., and Marzo, M., 2004, Three-dimensional reconstruction of geological surfaces: An example of growth strata and turbidite systems from the Ainsa basin (Pyrenees, Spain): AAPG Bulletin, v. 88, 1049-1068.

Joly, A., Martelet, G., Chen, Y., and Faure, M., 2008, A multidisciplinary study of a syntectonic pluton close to a major lithospheric-scale fault - Relationships between the Montmarault granitic massif and the Sillon Houiller Fault in the Variscan French Massif Central: 2. Gravity, aeromagnetic investigations, and 3-D geologic modeling: Journal of Geophysical Research-Solid Earth, v. 113.

Martelet, G., Calcagno, P., Gumiaux, C., Truffert, C., Bitri, A., Gapais, D., and Brun, J.P., 2004, Integrated 3D geophysical and geological modelling of the Hercynian Suture Zone in the Champtoceaux area (south Brittany, France): Tectonophysics, v. 382, 117-128.

Tonini, A., Guastaldi, E., Massa, G., and Conti, P., 2008, 3D geo-mapping based on surface data for preliminary study of underground works: A case study in Val Topina (Central Italy): Engineering Geology, v. 99, p. 61-69.

Zanchi, A., Francesca, S., Stefano, Z., Simone, S., and Graziano, G., 2009, 3D reconstruction of complex geological bodies: Examples from the Alps: Computers & Geosciences, v. 35, 49-69.

Ke CHEN

Le piémont nord du Tian Shan : cas d'école d'un front de chaîne immature

La chaîne actuelle du Tian Shan (Asie centrale) est considérée comme une conséquence directe de la réactivation d'une ceinture orogénique du Paléozoïque due à la collision Inde-Asie, au Cénozoïque. Un travail détaillé a été réalisé le long du piémont nord de la chaîne en intégrant les observations géologiques de terrain, analyses structurales, profils sismiques, nouvelles mesures des anomalies gravimétriques et des données de forages.
Tout d'abord cette étude apporte de nouvelles preuves directes, à différentes échelles, sur l'existence d'un paléo-relief majeur le long du front nord du Tian Shan au cours du Mésozoïque, et plus particulièrement pendant le Jurassique. Deuxièmement, la quantité de raccourcissement calculée à travers cette ceinture de plis et chevauchements nord du Tian Shan est relativement faible et les structures reconnues le long du front de la chaîne présentent une hétérogénéité latérale forte. Ainsi, alors qu'un chevauchement du socle paléozoïque sur les séries sédimentaires mésozoïques et cénozoïques du bassin est remarquablement exposé le long de certaines vallées, d'autres sections montrent que les séries sédimentaires du Trias au Jurassique peuvent être suivies de manière continue, depuis le bassin jusque sur le toit du socle Paléozoïque où ils reposent en discordance relativement haut dans la chaîne. Quatre coupes géologiques ont été construites par l'intégration des données pluridisciplinaires acquises. La restauration de ces coupes montre que les taux de raccourcissement sont inférieurs à 20% et peuvent descendre à un minimum de 6%. Ces observations suggèrent que le piémont nord du Tian Shan est plutôt «jeune» et que la chaîne d'avant pays est encore à un stade primaire de son évolution tectonique. En d'autres termes, le piémont nord du Tian Shan peut être considéré comme un exemple type de front de chaîne immature.

Mots clés: Tian Shan, déformation, front, ceinture de chevauchements et de plis, basin d'avant-pays, immature.

The northern piedmont of Tian Shan: a case study of immature range front

The modern Tian Shan (Central Asia) is considered as a direct consequence of the reactivation of a Paleozoic orogenic belt due to the India – Asia collision, during Cenozoic times. A detailed work has been investigated along the northern piedmont of Tian Shan, integrating the field work, structural analysis, seismic profile data, gravity anomaly measurements and drilled wells. Firstly, this study brings new and direct evidences, at different scales, for the existence of a major paleo-relief along the northern Tian Shan range during Mesozoic, and particularly during Jurassic times. Secondly, the calculated shortening amount in the northern piedmont of Tian Shan is rather small and the structural pattern of its front is heterogeneous along-strike. While, thrusting of the Paleozoic basement on the Mesozoic or Cenozoic sedimentary series of the basin is remarkably exposed along several river valleys, other sections display continuous Triassic to Jurassic sedimentary series from the basin to the range where they unconformably overlie on the Carboniferous basement. Four cross-sections are made by integrating multi-method data, showing that shortening amounts are less than 20% and could be even until to 6%. This suggests that the Tian Shan intracontinental range is rather "young" and still at a primary stage of its tectonic evolution. In other words, its front may be considered as a typical example of an immature range front.

Key words: Tian Shan, deformation, front, fold-and-thrust belt, foreland basin, immature.

Institut des Sciences de la Terre d'Orléans
1A, rue Férolerie, 45071 ORLÉANS, France

Institute of Geology and Geophysics
Chinese Academy of Sciences, 100029 Beijing, China